

OVIDIU COTLET

BOSE-FERMI MIXTURES WITH ELECTRONS AND
POLARITONS

DISS. ETH NO. 26276

BOSE-FERMI MIXTURES WITH ELECTRONS
AND POLARITONS

A dissertation submitted to attain the degree of

DOCTOR OF SCIENCES of ETH ZURICH
(Dr. sc. ETH Zurich)

presented by

OVIDIU COTLET
Dipl., Eidgenössisches Polytechnikum

born on 14 June 1990
citizen of Romania

accepted on the recommendation of

Prof. Dr. A. Imamoglu, examiner
Prof. Dr. E. Demler, co-examiner
Prof. Dr. R. Schmidt, co-examiner

2019

To Remina

ABSTRACT

The work in this thesis lies at the interface between quantum optics and condensed matter physics, and deals primarily with strongly-interacting, degenerate mixtures of photons and electrons. More specifically, we consider solid state systems where photons hybridize with excitons (bound electron and hole pairs) to form coherent superpositions known as polaritons. This hybridization increases the scattering cross section between photons and electrons, leading to the emergence of novel, strongly correlated states of matter involving photons, which we investigate using the many-body techniques developed in condensed matter physics. Nevertheless, most of our work is more general and directly applies to the wider field of Bose-Fermi mixtures.

On the one hand we study the influence of electrons on photons. We show that, due to the strong interactions with electrons, the polaritons (or excitons) dress with a polarization cloud in the electron system and form new quasiparticles which we call polaron-polaritons, in analogy to the polaron quasiparticles in solid-state systems. This dressing changes the properties of the polariton quasiparticles dramatically. In addition to strongly increasing photon nonlinearities, we show that in certain regimes this dressing cloud makes polaritons respond to electric and magnetic fields as if they were charged.

Alternatively, electrons can also be dressed by fluctuations in the photonic system, to form new quasiparticles. We investigate how this dressing can induce a superconducting instability in the electron system, where electrons pair-up in Cooper pairs, by exchanging the polaritons in their dressing clouds. This could lead to the exciting possibility of turning superconductivity in semiconductor materials on and off using laser fields.

The work in this thesis establishes Bose-Fermi mixtures formed of itinerant electrons and excitons (or polaritons) as a promising platform for the investigation of many-body physics with photons. In addition to providing valuable explanations to puzzling experimental observations, it reports important theoretical advances such as analysis of striking electrical and magnetic field response of photonic excitations.

ZUSAMMENFASSUNG

Die in dieser Dissertation vorgestellte Arbeit befindet sich an der Schnittstelle zwischen der Quantenoptik und der Physik der kondensierten Materie und befasst sich vorwiegend mit stark wechselwirkenden, entarteten Mischungen aus Photonen und Elektronen. Insbesondere betrachten wir Systeme in denen Photonen mit Exzitonen (gebundene Zustände aus Elektron-Loch Paaren) kohärente Überlagerungen, sogenannte Polaritonen, bilden. Diese Hybridisierung erhöht den Streuquerschnitt zwischen Photonen und Elektronen und führt zu der Entstehung von neuartigen, stark korrelierten, photonischen Zuständen, welche wir mit Methoden der Vielteilchenphysik erforschen. Trotz der Fokussierung auf Halbleitermaterialien findet ein Großteil dieser Arbeit direkte Anwendung in der Beschreibung von Bose-Fermi Mischungen.

Wir betrachten zunächst den Einfluss von Elektronen auf Photonen. Wir zeigen, dass Polaritonen (oder Exzitonen) durch starke Wechselwirkungen mit Elektronen eine „Polarisationswolke“ im elektronischen System bilden und mit dieser „dekoriert“ werden. In Analogie zu der Polaronbildung in Festkörpern entstehen hierdurch neue Quasiteilchen, welche Polaron-Polaritonen genannt werden. Die Polarisationswolke verändert die Eigenschaften der Polaritonen drastisch. Zusätzlich zu stark erhöhten Photon-Nichtlinearitäten zeigen wir, dass neutrale Polaritonen durch ihre Dekoration auf elektrische und magnetische Felder reagieren können, als wären sie geladen.

Umgekehrt können auch Elektronen durch Fluktuationen im photonischen System dekoriert werden und neue Quasiteilchen bilden. Wir untersuchen, wie dieser Effekt eine supraleitende Instabilität in dem elektronischen System erzeugen kann. Der Austausch von dekorierenden Polaritonen ermöglicht es den Elektronen Cooper-Paare zu bilden. Dies eröffnet spannende Möglichkeiten Supraleitung in Halbleitermaterialen durch Laserlicht zu steuern.

Diese Arbeit etabliert Bose-Fermi Mischungen aus Elektronen und Exzitonen (oder Polaritonen) als vielversprechende Plattform für die Untersuchung der Vielteilchenphysik mit Photonen. Zusätzlich zu wertvollen Klärungen experimenteller Beobachtungen, werden auch wichtige theoretische Fortschritte, wie die Analyse der Wirkung von elektrischen und magnetischen Feldern auf optische Anregungen, dargelegt.

ACKNOWLEDGEMENTS

I would like to express my deepest gratitude to my Ph.D. advisor, Atac Imamoglu, for his constant support and encouragement. His enthusiasm and passion about physics have often been contagious. I am grateful that he gave me the opportunity to tackle very interesting and puzzling questions under his guidance. I would like to thank him for our (almost daily) discussions, which were crucial for my research. Nevertheless, I also enjoyed our numerous conversations about politics and other unrelated subjects.

I would also like to thank Eugene Demler for the discussions we had while he was at ETH but also for the many Skype discussions we had afterwards. His vast knowledge of condensed matter physics has been of crucial importance throughout my work.

I would also like to thank Richard Schmidt for his help and for the cordial discussions we had throughout my Ph.D. . His input has been critical for the majority of the phenomena studied in this thesis.

I would also like to thank my collaborators, especially Falko Pientka and Dominik Wild, for their numerous inputs and help.

I also want to thank my physics high-school teacher, Marilena Sibechi, for kindling my interest in physics.

I would also like to thank my colleagues. Special thanks go out to Meinrad, for his friendship and for forming the prestigious "Lunch @ 1 Group"; to Sina, for making any subject matter interesting; to Martin for the thought-provoking conversations; to Patrick for the poker evenings; to Ido, for his contrarian opinions; to Li Bing, for her positive attitude; to Alex, for his friendliness, as well as to all the other colleagues who made the time during the Ph.D. that much more interesting.

Last but not least, I would like to thank my family for their constant encouragement. I would like to thank especially Remina for her constant support, and my parents for always encouraging me to become a scientist.

CONTENTS

1	INTRODUCTION	1
1.1	Light-matter interactions	1
1.2	Excitons and exciton-polaritons	3
1.3	Electron-polariton Bose-Fermi mixture	4
1.4	Outline and contributions of this thesis	7
2	EXCITON-POLARITONS AND THEIR INTERACTIONS	11
2.1	Transition metal dichalcogenide monolayers	12
2.2	Exciton quasiparticle	15
2.2.1	Bare exciton-exciton interaction	17
2.3	Exciton-polaritons	18
2.4	Renormalization of interactions	21
2.4.1	Exciton-exciton interactions	23
2.4.2	Interaction of two polaritons	26
2.5	Conclusion	29
3	POLARON PHYSICS WITH LIGHT	31
3.1	Exciton-electron interaction	33
3.2	Fermi polarons	39
3.3	Fermi polaron polaritons	47
3.4	Bose-polaron polaritons	49
3.4.1	Weakly interacting polariton gas	49
3.4.2	Bose-polaron formation	52
3.4.3	Effective Bose-polaron model	55
3.5	Conclusion	56
4	POLARON INTERACTIONS	57
4.1	Many-body Green's functions	59
4.1.1	Green's function approach to the Fermi polaron problem	60
4.1.2	Feynman diagrams	65
4.2	Conserving approximation	66
4.2.1	Two-particle correlation functions	68
4.3	Exciton-polarons	70
4.4	Polaron polaritons	74

4.5	Polaron interactions	75
4.5.1	Interaction between Fermi-polaron polaritons	77
4.5.2	Interaction between Bose-polarons	79
4.6	Conclusion	80
5	FERMI-POLARONS IN INTERACTING FERMIONIC SYSTEMS	83
5.1	Low-energy degrees of freedom of a system of interacting electrons	84
5.1.1	Plasmons in the RPA limit	88
5.2	Fermi polarons in interacting Fermi liquid	89
5.3	Conclusion and outlook	91
6	ROTON STATES IN OPTICAL SPECTRA	93
6.1	Rotons	94
6.2	Roton states in doped semiconductor	95
6.2.1	Exciton Schroedinger equation	96
6.2.2	Results	97
6.2.3	Bethe-Salpeter equation	99
6.3	Backflow corrections	101
6.4	Fermi polaron quasiparticles	104
6.5	Experimental signatures of the roton minimum	106
6.6	Conclusion	108
7	POLARON TRANSPORT	111
7.1	Introduction	112
7.2	Heuristic derivation of polaron drag	115
7.2.1	Polaron drag in clean systems	115
7.2.2	Polaron drag in dirty systems	116
7.2.3	Semiclassical drag transconductivity	117
7.2.4	Reverse effect	117
7.2.5	Effective gauge field	118
7.2.6	Conclusion	119
7.2.7	Summary of results	120
7.3	Diagrammatic calculation of transconductivity using the conserving approximation	121
7.3.1	Attractive polaron quasiparticles	122
7.3.2	Low exciton density expansion	124
7.3.3	Evaluation of the vertex functions to zeroth order in n_x	127
7.3.4	Evaluation of transconductivity to first order in n_x	128

7.3.5	Transconductivity in terms of low-energy excitations	132
7.4	Transconductivity of polaron polaritons	134
7.5	Nonequilibrium effects	137
7.5.1	Boltzmann equation	139
7.5.2	Estimation of the friction forces from disorder and incoherent scattering with electrons	141
7.5.3	Equations of motion for polarons and polaritons	145
7.6	Magnetic field response of exciton polaritons	147
7.7	Conclusion and outlook	148
8	SUPERCONDUCTIVITY	149
8.1	Introduction	150
8.2	Electron-electron interactions mediated by polaritons	153
8.2.1	Bogolyubov transformation	154
8.2.2	Polariton softening	154
8.2.3	Electron-electron interaction	158
8.3	Renormalized Hamiltonian	160
8.3.1	Quasi particle approximation	161
8.3.2	A Debye energy for polaritons?	162
8.4	Superconductivity and Charge Density Waves	163
8.4.1	Superconductivity	164
8.4.2	Supersolid and Charge Density Waves	169
8.5	Materials suitable for reaching the strong coupling regime	170
8.6	Conclusion	172
9	SUMMARY AND OUTLOOK	175
A	APPENDIX	177
A.1	Effective attractive polaron propagator	177
A.2	Polaron dispersion for a drifting Fermi sea	179
A.3	Polaron transport using a variational approach	181
A.4	Polaron lifetime	184
A.4.1	Interaction between polarons and electrons	184
A.4.2	Polaron lifetime using Fermi's Golden Rule	185
A.4.3	Polaron lifetime from self energy	186
A.4.4	Polaron lifetime at finite exciton density	187
A.5	Relation between $\text{Im}\Sigma_{\text{int}}$ and $\text{Im}G_x$	189
A.5.1	Exciton density	191
A.6	Proof of Eq. (7.33) in main text	192
A.7	Migdal-Eliashberg theory	193

CONTENTS

A.8	Superconductivity	203
A.8.1	McMillan equation	204
A.8.2	Superconducting gap equation	205
A.8.3	Comparison to previous work	208

BIBLIOGRAPHY 209

NOTATION

FREQUENTLY USED SYMBOLS

$e_{\mathbf{k}}^{\dagger}$	electron creation operator
$h_{\mathbf{k}}^{\dagger}$	hole creation operator
$x_{\mathbf{k}}^{\dagger}$	(1s) exciton creation operator
$c_{\mathbf{k}}^{\dagger}$	cavity-photon creation operator
$a_{\mathbf{k}}^{\dagger}$	lower-polariton creation operator
$N_{e/x}$	electron/exciton number
$n_{e/x}$	electron/exciton density
m	electron mass
m_x	exciton mass
m_c	cavity-photon mass
$\xi_{\mathbf{k}}$	electron dispersion
$\omega_{\mathbf{k}}$	exciton dispersion
$v_{\mathbf{k}}$	cavity-photon dispersion
$\Omega_{l/u,\mathbf{k}}$	lower/upper polariton dispersion
$\Omega_{\mathbf{k}}$	lower polariton dispersion
g	light-matter (or exciton-photon) coupling strength
$V_{\mathbf{k}}$	Coulomb interaction
$v_{\mathbf{k}}$	exciton-electron interaction
$u_{\mathbf{k}}$	exciton-exciton interaction
χ	response function
T	T-matrix
$\Sigma(\dots)$	Self-energy
$G(\dots)$	time-ordered Green's function
$\mathcal{G}(\dots)$	imaginary time Green's function
Φ	Luttinger-Ward functional
$ \Theta\rangle$	Many-body ground state
$ \Theta_0\rangle$	Many-body ground state in absence of interactions

NOTATION

\mathcal{A}	quantization area
η	positive infinitesimal constant

INTRODUCTION

We provide a motivation for and an outline of the thesis. This thesis deals with systems where the properties of optical photons are strongly modified, allowing the realization of novel states of matter involving photons. More specifically we consider systems where optical photons interact strongly with two dimensional electron systems. We investigate both the modification of the photonic systems due to interactions with electrons as well as the converse effect of the modification of electron properties due to the interaction with photons. We discuss the interesting collective degrees of freedom that emerge due to the interplay between interactions, and the Bose and Fermi statistics.

1.1 LIGHT-MATTER INTERACTIONS

The differences between light and matter are quite fundamental. As we know from the standard model of particle physics, all physical phenomena that we encounter in our daily life can be explained by a handful of elementary particles. An insightful way to group all the particles in the Standard Model is in terms of their quantum statistics, which divides elementary particles into two fundamental groups: fermions and bosons. Except for the Higgs scalar boson, responsible for the emergence of the mass of particles, the other bosons are the gauge bosons, since they exist as a direct consequence of the local gauge symmetry of quantum field theory. These gauge bosons are the force carriers, and elementary particles can interact with each other by exchanging these bosons.

Photons are the gauge bosons of the electromagnetic field, and all electromagnetic phenomena can be explained through the kinematics and interactions of photons with charged particles. The study of these phenomena belongs to the field of quantum electrodynamics (QED). To keep track of these processes it is convenient to illustrate them pictorially using (Feynman) diagrams. The interaction between light and matter can be represented through the diagram on the left in Fig.1.1. The charge of the particle is the only quantity determining the probability amplitude for this process to take place. It is remarkable that any electromagnetic phenomenon can be formed from a combination of such vertices. For instance the Coulomb

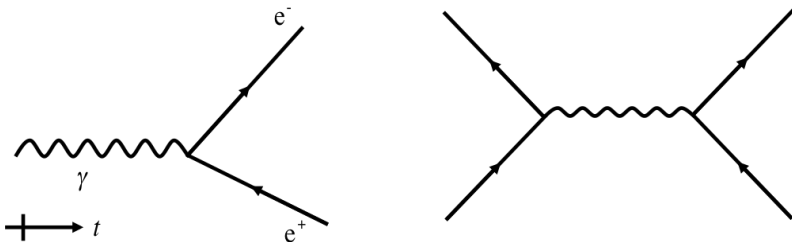


FIGURE 1.1: Left: elementary light-matter coupling vertex. Right: electron-electron Coulomb scattering mediated by photon exchange, formed by combining two vertices. The squiggly line is the photon propagator. It has no direction since the vertex stands for both absorption and emission of photons. The arrows are the electron propagators. Propagators denote the probability amplitude for a particle to move from a point in spacetime to another. We remark that only the topology of the diagram is fixed. We can stretch and rotate the diagram as we wish. For instance if we flip the light-matter coupling diagram horizontally we can see that it can also denote processes where an electron-positron pair annihilate to emit (and also absorb) a photon.

scattering between two electrons can be formed from two such vertices as shown in the right diagram in Fig.1.1.

For specificity let's focus on the interaction between optical photons and electrons, and let's look at a collection of photons in vacuum. They can either propagate freely, or create electron-positron pairs through the vertex Fig.1.1. However, the energy required to create pairs of matter-antimatter particles of mass m out of the vacuum is huge ($\Delta = 2mc^2$), many orders of magnitude larger than the energy of optical photons. According to Heisenberg's uncertainty principle, these pairs will only exist for an extremely short amount of time \hbar/Δ . This means that such interaction processes play virtually no role, leading to optical photons propagating indefinitely without interacting with each other, one of the defining characteristics of photons.

Fortunately, the situation changes drastically if we consider photons in condensed matter systems. These systems, where a macroscopic number of interacting particles are closely packed (the particles are "condensed", hence the nomenclature), can be quite complex. However, often they behave like a collection of weakly interacting particles with modified (or renormalized) properties, which are sometimes called quasiparticles to em-

phasize the difference from the underlying particles. In semiconductor materials the relevant degrees of freedom are (conduction-band) electron and (valence-band) hole quasiparticles, which are similar to the electron and positron elementary particles in vacuum. However, due to the renormalization introduced by the crystal lattice, these quasiparticles have different effective masses compared to their vacuum counterparts and the energy required to create electron-hole pairs can be comparable to the photon energy. This allows the study of QED physics in solid systems, in very different parameter regimes compared to vacuum. In particular it ensures that the properties of photons can be strongly modified due to the interactions with resonant interband electron-hole pair excitations. Moreover, the scattering process can be further enhanced due to the formation of bound states between the electron and the hole, as we discuss next.

1.2 EXCITONS AND EXCITON-POLARITONS

We emphasize that the light-matter vertex is local. On the other hand, the electron and hole quasiparticles in solid-state systems form plane waves that are delocalized over the whole quantization volume. This means that the light-matter coupling strength is extremely small due to the low probability for two particles in plane waves to find each other and interact with photons.

However, such a simple analysis does not take into account the fact that the electron and the hole created by the optical photon attract each other (by exchanging virtual photons, not necessarily optical) due to their opposite charges. Due to this attraction they form a tightly bound molecular state known as an exciton, similar to the hydrogen atom in vacuum. Clearly, the bound state formation strongly increases the probability that the two particles meet each other and interact with photons.

Diagrammatically, the emergence of the bound state can be represented through the repeated interaction between electrons and holes necessary to prevent the two particles from flying apart. It can be proven that in this perturbative approach based on diagrams the probability amplitude of a process corresponds to the sum of all the topologically distinct diagrams describing the process. Adding all the diagrams consisting of these repeated Coulomb interactions between the electron and the hole can be represented recursively in Fig.1.2. These vertex corrections lead to a renormalization of the light-matter vertex by a factor of about $\sqrt{\mathcal{V}/a^3}$, where a is the Bohr radius of the bound state.

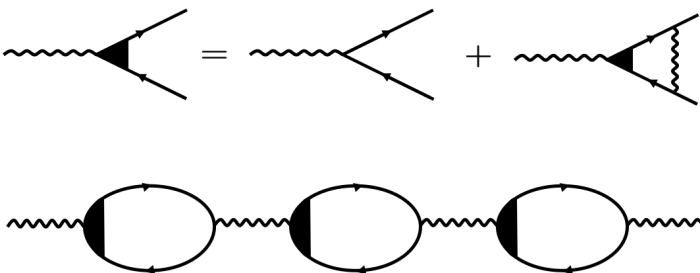


FIGURE 1.2: Upper panel: Vertex corrections due to exciton bound-state formation. Lower panel: one of the diagrams corresponding to the propagation of the polariton quasiparticle

The renormalization of interactions is closely related to the modification of the photon quasiparticle. The propagation of a photon in this system can be represented by diagrams such as those in Fig.1.2. We can see that the new quasiparticle, called exciton-polaritons will oscillate between being a photon or being an exciton, leading to the hybridization of photons and excitons into a new quasiparticle called exciton-polariton. In addition to strongly enhancing the electron-photon and photon-photon scattering, the coupling to excitons has the advantage of isolating the photons from the continuum formed of electron-hole pair excitations, an important ingredient for the existence of quasiparticles.

The strong renormalization of the light-matter interaction vertex opens the door towards the study of phenomena involving interacting photons.

1.3 ELECTRON-POLARITON BOSE-FERMI MIXTURE

We remark that the simple light-matter vertex directly explains most phenomena involving optical photons that we encounter in our everyday life, such as the light emission of the common light-bulb or the photon detection of our eyes, as well as most phenomena that are usually studied in the field of quantum optics. On the other hand, the simple Coulomb interaction vertex is enough to describe most phenomena in condensed matter systems, and most times, one can ignore the microscopic origin of this interaction. These vertices still treat light and matter very asymmetrically, consistent with the traditional view that photons can be absorbed or emitted by matter particles, as well as mediate interactions between them. In contrast, in this thesis, we will focus on some of the higher or-

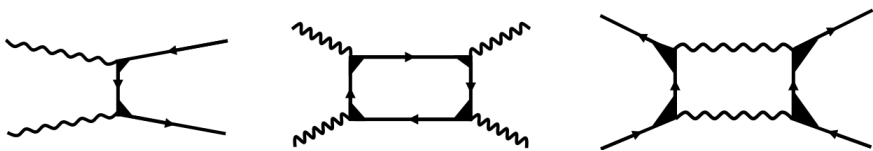


FIGURE 1.3: Electron-photon scattering (left), photon-photon scattering (middle), second-order electron-electron interaction (right)

der interactions that can be created starting from the light-matter coupling building block. These have been comparatively less studied both in either condensed matter or quantum optics and make us reevaluate some of the traditional assumptions about light.

More specifically, we are interested in scattering processes, i.e. processes where two particles exchange energy and momentum. Our analysis will rely on the Compton scattering vertex, which describes the scattering of an electron and a photon. This vertex can be formed from two elementary vertices, as shown in Fig.1.3 (including the vertex corrections due to the exciton formation). Intuitively, this is an electron-exchange interaction between an initial electron and a polariton, corresponding to the initial electron trading places with the electron dressing the polariton. Therefore, in this thesis we will be considering systems of strongly interacting exciton-polaritons (or simply excitons) and electrons. Since the strength of the light matter vertex is directly proportional to the inverse Bohr radius of the exciton, we will be working in monolayers of transition metal dichalcogenides (TMDs) which represent an ideal platform for studying such phenomena, due to the tightly bound exciton states, with Bohr radii of about a nanometer.

We will be following two main directions in this thesis. On the one hand we will be concerned with understanding the effect of electrons on polaritons and the resulting quasiparticles and collective states that emerge as a result of the dressing of the photon. For instance the electron dressing of polaritons can result in significant polariton-polariton interactions. We present one such diagram in Fig.1.3, which is formed by two electron-polariton vertices, and describes photon-photon scattering mediated by exchange of electrons and/or holes. This photon-photon scattering vertex has been at the basis of the burgeoning field of quantum fluids of light, which required the fruitful integration of concepts from quantum optics and condensed matter physics and led to a wealth of novel physical phenomena due to the interplay between dissipation, the lightness of the polariton

quasiparticles and strong interactions [1]. Note that this vertex does not require the presence of any conduction-band electrons in the system (they are created by the photons). However, as we will show in this work, the presence of electrons can open up new possibilities for the modification of the photon quasiparticles, for instance leading to much stronger nonlinearities than the vertex in Fig.1.3.

On the other hand we also investigate the effect of photons on electrons and how photons can be used to control the properties of electrons. For instance in Fig.1.3 we show how the electron-polariton scattering vertex can mediate higher-order interactions between electrons. Generally, this second order vertex is neglected since it is much smaller than the direct Coulomb vertex presented in Fig.1.1. However, by shining strong lasers in the system we can create a coherent polariton population, in some particular mode. Doing a mean-field approximation, which diagrammatically corresponds to replacing one of the photon propagators with a c-number corresponding to the number of photons in the system, one can see that the electron-electron scattering vertex in Fig.1.3 becomes very similar to the initial Coulomb interaction vertex in Fig.1.1. Crucially, the strength of this vertex is increased by a factor proportional to the number of photons, which can make this vertex comparable in strength to the initial vertex. This shows how strong optical pumping can lead to significant modifications of the electron quasiparticles, allowing the optical control of the electron properties.

This system of interacting electrons and polaritons (or excitons) can be considered as an example of a class of condensed-matter system referred to as Bose-Fermi mixtures. Such systems exhibit a rich phenomenology, since interaction effects compete with the Bose-enhancement and Pauli-blocking due to the statistics of the particles. Although such systems have been studied in ultracold atomic, there are still many open problems left to be investigated. In many of the phenomena that we investigate in this thesis, the photonic part of the polaritons does not play a fundamental role, and our results represent important contributions to the burgeoning field of Bose-Fermi mixtures. On the other hand, some results are system-specific and emerge due to the special properties of light, such as their ultra-small mass (we will discuss how photons "acquire" a mass) and the non-equilibrium nature of photonic excitations.

1.4 OUTLINE AND CONTRIBUTIONS OF THIS THESIS

Below we give a brief outline of the thesis, emphasizing the novel contributions that it makes.

We begin Chapter 2 with a brief overview of the monolayer TMD systems that we will investigate. We then introduce the exciton and exciton-polariton quasiparticles, and discuss the interactions between them. This allows us to move on to the first important contribution of this thesis, which concerns the renormalization of the interactions of the polariton quasiparticles. It is well known that the bare interaction between quasiparticles is usually not directly measurable. For instance, if a repulsive interaction is strong enough, particles will avoid each other in order to decrease their potential energy, resulting in an effective renormalization of their interaction. Remarkably, we find that this renormalization process is strongly suppressed in polaritons, due to their small mass, which makes it too costly for polaritons to avoid each other. This result can have important implications for the field of interacting photons. More specifically, we predict that in order to increase interactions between polaritons, one should focus on increasing the light matter coupling strength or the range of the interactions, instead of focusing solely on increasing the strength of the bare photon-photon scattering.

In Chapter 3 we introduce the hybrid Bose-Fermi mixture of electrons and (exciton)polaritons, which is at the basis of the work in this thesis. We focus on regimes where the exciton-electron interaction is strong enough to lead to the formation of bound states between excitons and electrons known as trions. The second important contribution relates to the study of the density-imbalanced regime where the density of electrons is much larger than the exciton or polaritons. Considering first the case of excitons interacting with electrons, we show that the relevant degrees of freedom in this system can be interpreted using the framework of mobile quantum impurities, and that the optical excitations in TMDs are collective states that we call exciton-polarons [2], in analogy to the Fermi-polaron quasiparticles studied in ultracold atomic gases [3–5], which in turn are related to the polaron quasiparticles in solid state systems first investigated by Landau [6]. These excitations correspond to excitons dressed by polarization waves in the electron-system. This novel interpretation is in stark contrast to the traditional view that the optical spectra of doped semiconductors are dominated by trions and excitons. Then, we consider the regime where the light-matter coupling is strong enough to lead to the formation

of polaritons and show that polaritons can couple to the exciton-polaron states to form ultra-low mass polaron quasiparticles, that we call polaron-polaritons.

We end Chapter 3 by considering the opposite regime where the polariton density is much larger than the density of electrons, which represents the third important contribution of this thesis. We discuss the dressing of electrons with the excitations in the polariton system to form new quasi-particles known as Bose-polarons [7–9]. We discover that the peculiar dispersion of polaritons, which changes from an ultralow mass parabolic dispersion at momenta smaller than the photon momentum to a sizable mass parabolic dispersion at momenta larger than the photon momentum, has important consequences for the Bose-polaron formation. Since this photon momentum is much smaller than the other momentum scales in the problem, this effectively gives a gap (or mass) to excitations. This allows us to analyze the effects of incompressible states on polaron formation. Remarkably, we find that the gap, instead of suppressing the polaron dressing, can actually increase it, providing a tuning knob in this respect.

While the theoretical investigations in Chapter 3 are based on a simple wavefunction approach [3], in Chapter 4 we introduce the concept of many-body Green’s functions [10] which allow us to go beyond the limitations of the wavefunction approach in Chapter 3. We also introduce the important concept of conserving approximations, first discussed by Baym and Kadanoff [11]. Then, using a conserving approximation, we derive for the first time the diagrams corresponding to the interaction between polaron quasiparticles, which represents the fourth important contribution of this thesis. We find two main contributions. One stems from the exchange of excitations between polarons. The other, less commonly studied contribution, comes from the composite nature of the polarons. Leaving a detailed calculation of these interaction diagrams for later work, we estimate the strength of the second contribution on the polaron-polariton quasiparticles. In this scenario, the second contribution comes because the dressing of a polariton modifies the electron system, such that when another polariton is added its dressing is slightly suppressed. We show that the polaron dressing can increase significantly the polariton interactions, a fact corroborated by corresponding experimental results [12].

On the other hand, for the Bose-polaron quasiparticles that we introduced in Chapter 3, we expect that the diagrams corresponding to exchange of excitations will be the dominant one. We calculate these interactions and show that the excitation gap in the polariton system strongly

increases these interactions, a fact that could be used to create optically induced attractive interactions between electrons and eventually to induce a superconducting phase transition in the electron system.

The derivations in Chapter 3 and 4 completely neglect the interactions between electrons, mainly because of the difficulty of including them properly. In Chapter 5 we present another method that can be used to solve many-body problems in general and the polaron problem in the presence of interacting fermions in particular, which represents the fifth important contribution of this thesis. This method, based on determining the approximate creation operator of the quasiparticles, combines the simplicity and transparency of the wavefunction method with the advantages of the Green's function method, and allows us to include the effect of the long-range electron-electron interactions on the polaron formation, going beyond the often used Hartree-Fock or random phase approximation.

The analysis in the previous chapters treats excitons as rigid objects, completely neglecting the internal structure of the exciton. In Chapter 6 we reevaluate this approximation and discuss the modification of the exciton internal structure due to the repulsive interaction with electrons in the same valley [13], and represents the sixth important contribution of this thesis. We show that this interaction can lead to the development of a roton-like minimum in the exciton dispersion (i.e. the dispersion minimum is shifted to a finite momentum), similar to the roton states in superfluid ^4He [14]. We find indirect evidence of such states in the photoluminescence spectra, introducing a novel explanation for the puzzling difference between absorption and emission spectra in TMDs.

In chapter 7 we continue investigating the electron-polariton Bose-Fermi mixture in the density imbalanced regime where the polariton density is much smaller than the electron density. In this chapter we investigate the response of polaron-polaritons to an applied electric field on the electron system [15], which represents the seventh important contribution of this thesis. Remarkably, we show that in certain regimes the neutral polaron-polaritons respond to the electric field as if they were charged. Most importantly, this non-perturbative, zero temperature Coulomb drag effect is fundamentally different from the most common drag effects that are usually weak and vanish at zero temperature. It is also very different from the drag of molecular states such as trions, for this reason we call this polaron drag. In fact, we find that the best explanation of this effect is that the electron motion creates an effective gauge field for the polaritons, not unlike the electron motion creates a magnetic field. Indeed we find a very

general relationship between the velocity of electrons, the mass renormalization of the polaron quasiparticles and the strength of the effective gauge field. We also discuss the effect of magnetic fields applied to the electron system and the consequences due to the non-equilibrium nature of the polariton system. The calculations in this chapter is based on a conserving diagrammatic calculation of the full frequency-dependent transconductivity, and they represent an important addition to the field of non-perturbative Coulomb drag [16]. At the same time our results suggest novel ways for manipulating photons using low-frequency electric and magnetic fields or for the optical manipulation of the transport properties of electrons.

In Chapter 8 we consider a slightly different Bose-Fermi mixture, where polaritons and electrons interact repulsively, and therefore there is no trion bound state. While in previous chapters we considered collective phenomena where interactions led to the development of short-ranged order in the system, in this chapter we discuss the long-range ordered states that can exist due to interactions in this hybrid Bose Fermi mixture. We find that fluctuations in the polariton system can mediate attractive interactions between electrons, leading to a superconducting instability. Similarly, excitations in the electron system can mediate attractive interactions between polaritons, that can lead to the development of roton states, and eventually could lead to the emergence of a supersolid state. In contrast to the previous chapters where we focused either on the effect of the electron system on the polaritons or vice-versa, in this scenario we find it important to treat these interactions simultaneously. Remarkably, we find that the development of the roton minimum contributes towards the robustness of the superconducting state, and we find that the superconducting critical temperature is highest in the proximity of the supersolid transition. This represents the eighth and final contribution of this thesis.

The work in this thesis is closely connected to recent experimental work in optically probed transition metal dichalcogenene monolayers, and can be used to explain the features of the experimetanl data in these systems. On the other hand it also reports theoretical proposals for novel phenomena and their analysis using the techniques of many-body physics. It establishes electron-polariton Bose-Fermi mixtures as promising platforms for the exploration of collective phenomena involving optical photons.

2

EXCITON-POLARITONS AND THEIR INTERACTIONS

We present the material system that we investigate in this thesis and discuss the formation of the exciton and exciton-polariton quasiparticles. We then focus on the interactions between quasiparticles, and discuss how strong interactions are usually renormalized to much weaker values. Remarkably, the light photon mass can prohibit this renormalization, forcing particles to interact more strongly, and leading to larger measurable effects of interactions.

As we already mentioned in the introduction, one of the main goals of this thesis is to establish Bose-Fermi mixtures of polaritons and electrons as a fertile platform for the investigations of many-body physics involving photons. Although in most regimes, photons can be treated as very weakly interacting particles, we have argued that in semiconductor materials, photons can be made resonant with bound interband electron-hole pairs, known as excitons, which leads to a sizable renormalization of the light-matter coupling. This in turn opens the door to studying phenomena with strongly interacting photons.

The exciton binding energy is often a good measure of the strength of the interactions in the material and therefore of the robustness of the various interacting states that we can hope to create. For this reason, in the rest of this thesis we will mainly consider monolayers of transition metal dichalcogenides (TMDs) presented in Fig.2.1, which exhibit very large binding energies of the order of 0.5eV. Therefore, after a brief introduction to TMDs, we discuss the exciton states that can be created in these material. We also discuss how, by embedding the monolayer in a distributed Bragg-reflector (DBR) cavity, the light-matter coupling can be further increased. This can lead to the hybridization of excitons and photons and the formation of polaritons.

After these preliminaries, we begin the original work in this thesis by discussing the (short-ranged) interactions between exciton and exciton-polariton quasiparticles and introducing the concept of interaction renormalization, which we will also encounter often in this thesis. Although bare interactions between quasiparticles can be substantial, they can often have little measurable effect. One example is when interactions are so

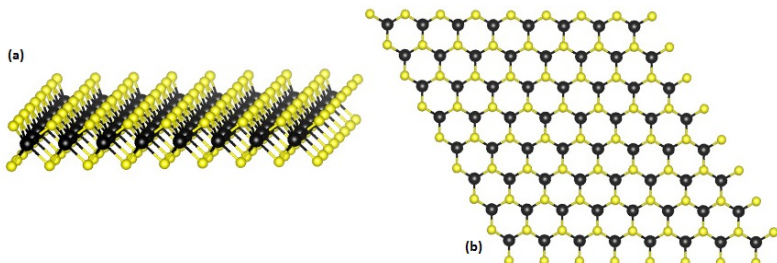


FIGURE 2.1: Monolayer transition metal dichalcogenide. M atoms are in black. X atoms are in yellow. Image courtesy of Wikipedia.

strong that particles would prefer to avoid each other and pay a small kinetic energy cost, rather than coming close enough to feel the interactions. We investigate this renormalization of interactions, by solving the problem of two interacting particles (excitons or polaritons). Our main finding is that, in contrast to excitons, polaritons cannot avoid each other so efficiently because of the small photon mass. This can lead to larger measurable effects of the interactions in polariton systems. This is quite remarkable, since polaritons interact only through their excitonic component and it often assumed that polariton interactions must therefore be smaller.

This chapter is organized as follows. We give a brief introduction to TMDs in Sec.2.1, we discuss the exciton quasiparticles in Sec.2.2. In Sec.2.3 we evaluate the photon-exciton coupling and discuss the formation of polaritons. Then, in Sec.2.4 we discuss the exciton and exciton-polariton interactions and their renormalization. We conclude this chapter with Sec.2.5.

2.1 TRANSITION METAL DICHALCOGENIDE MONOLAYERS

In order to make photons interact strongly we rely on the renormalization of the light-matter coupling due to exciton formation. For this reason we want to work with materials with strongly bound excitons. Over the past few years, monolayers of semiconducting transition metal dichalcogenides (TMDs) have emerged as promising candidates in this respect, since they support tightly bound excitons with binding energies of several hundred meV. Moreover, the charge carrier density of TMDs can be readily tuned with electrostatic gates, allowing facile creation of two-dimensional electron systems, the second component of our Bose-Fermi mixture. It is further possible to modify the properties of TMDs by stacking them with

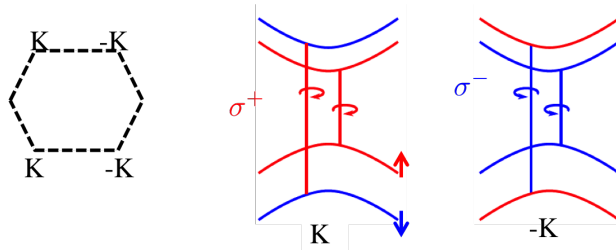


FIGURE 2.2: Left: first Brillouin zone of MoSe₂. Right: TMD band structure in the proximity of the high-symmetry points \mathbf{K} and $-\mathbf{K}$

other van der Waals materials into heterostructures [17] or by changing the dielectric environment [18].

Since TMD monolayers are atomically thin semiconductors, they can be treated as two-dimensional(2D) systems. They exhibit a honeycomb lattice, similar to that of graphene, as illustrated in Fig.2.1. However, in contrast to graphene, TMDs do not feature two identical atoms within the unit cell but rather a transition metal atom M (Mo, W, etc.) on the A site and two out-of-plane separated chalcogenide atoms X (S, Se, or Te) on the B site of the unit cell.

We present the first Brillouin zone of MoSe₂ monolayers in Fig. 2.2, where we emphasize the high-symmetry points \mathbf{K} and $-\mathbf{K}$. To describe (qualitatively) the electron quasiparticles in the vicinity of the $\pm\mathbf{K}$ points we can write down a simple two-band model in terms of the conduction and valence band, by using the $k \cdot p$ expansion:

$$H_{\pm\mathbf{K}} = \begin{bmatrix} \Delta/2 & v_D(\pm k_x + ik_y) \\ v_D(\pm k_x - ik_y) & -\Delta/2 \end{bmatrix} \quad (2.1)$$

where we used \mathbf{k} to denote electrons with momenta $\mathbf{k} \pm \mathbf{K}$. v_D is the Dirac velocity and Δ denotes the semiconductor band gap at $\mathbf{k} = 0$, and it lies in the optical regime. Although this simple model is not quantitatively correct, it does capture the correct qualitative features

To investigate optical transitions we start from Eq. (2.1) and introduce the coupling to a gauge potential by replacing \mathbf{k} with $\mathbf{k} - e\mathbf{A}$. Choosing

$A_x = A_0/\sqrt{2}$ and $A_y = iA_0/\sqrt{2}$ which corresponds to a right-hand circularly polarized light (σ^+) we obtain at $k = 0$:

$$H_{+K} = \begin{bmatrix} \Delta/2 & -\sqrt{2}v_D A_0 \\ -\sqrt{2}v_D A_0 & -\Delta/2 \end{bmatrix} \quad (2.2)$$

$$H_{-K} = \begin{bmatrix} \Delta/2 & 0 \\ 0 & -\Delta/2 \end{bmatrix} \quad (2.3)$$

This shows that σ^+ light can couple the conduction and valence band in the $+K$ valley but not in the other.

It is straightforward to diagonalize the model Hamiltonian in Eq. (2.1). In the close proximity of the $\pm K$ points it becomes:

$$H_{\pm K} \rightarrow \begin{bmatrix} \frac{\Delta}{2} \sqrt{1 + \frac{v_D^2 k^2}{\Delta^2}} & 0 \\ 0 & -\frac{\Delta}{2} \sqrt{1 + \frac{v_D^2 k^2}{\Delta^2}} \end{bmatrix} \quad (2.4)$$

$$= \begin{bmatrix} \frac{\Delta}{2} + \frac{k^2 v_D^2}{4\Delta} & 0 \\ 0 & -\frac{\Delta}{2} - \frac{k^2 v_D^2}{4\Delta} \end{bmatrix} + \mathcal{O}\left(\frac{k^2 v_D^2}{4\Delta}\right)^2 \quad (2.5)$$

Notice that in the proximity of $\pm K$ points, the dispersion is parabolic, and electrons behave like free particles with renormalized masses. More accurate calculations yield the electron and hole effective masses of about $m_e \approx m_h = m \approx 0.5m_0$ where m_0 is the mass of electrons in vacuum.

Our simplistic model completely neglected important effects, such as spin-orbit coupling. It has been shown that this effect is very strong in TMDs and leads to a splitting of the conduction and valence bands, and to valley-spin locking. Indeed, a more rigorous tight-binding analysis for MoSe₂, taking into account the spin-orbit coupling leads to the band-structure and optical selection rules presented in Fig.2.2 [19, 20]. The conduction (valence) band is split due to spin-orbit coupling by an amount of the order of 20(200) meV [21]. In this thesis we will focus only on the lowest energy transition between the highest energy conduction band states and the lowest energy conduction band states, since the other excitations will quickly decay into these states.

Based on the above discussion, and including electron-electron interactions we can write down the following Hamiltonian to describe this system, in second quantized notation:

$$\begin{aligned}
H = & \sum_{\sigma\mathbf{k}} \xi_{\mathbf{k}} e_{\sigma\mathbf{k}}^\dagger e_{\sigma\mathbf{k}} + \sum_{\mathbf{k}} \xi_{\mathbf{k}} h_{\sigma\mathbf{k}}^\dagger h_{\sigma\mathbf{k}} + \sum_{\sigma\mathbf{q}\mathbf{q}_z} \nu_{\mathbf{q}} c_{\sigma\mathbf{q}+\mathbf{q}_z}^\dagger c_{\sigma\mathbf{q}+\mathbf{q}_z} \\
& + \frac{1}{2\mathcal{A}} \sum_{\substack{\sigma\sigma' \\ \mathbf{k}\mathbf{k}'\mathbf{q}}} V_{\mathbf{q}} h_{\sigma\mathbf{k}+\mathbf{q}}^\dagger h_{\sigma'\mathbf{k}'-\mathbf{q}}^\dagger h_{\sigma'\mathbf{k}'} h_{\sigma\mathbf{k}} + \frac{1}{2\mathcal{A}} \sum_{\substack{\sigma\sigma' \\ \mathbf{k}\mathbf{k}'\mathbf{q}}} V_{\mathbf{q}} e_{\sigma\mathbf{k}+\mathbf{q}}^\dagger e_{\sigma'\mathbf{k}'-\mathbf{q}}^\dagger e_{\sigma'\mathbf{k}'} e_{\sigma\mathbf{k}} \\
& - \frac{1}{\mathcal{A}} \sum_{\substack{\sigma\sigma' \\ \mathbf{k}\mathbf{k}'\mathbf{q}}} V_{\mathbf{q}} e_{\sigma\mathbf{k}+\mathbf{q}}^\dagger h_{\sigma'\mathbf{k}'-\mathbf{q}}^\dagger h_{\sigma'\mathbf{k}'} e_{\sigma\mathbf{k}} + \sum_{\sigma\mathbf{k}\mathbf{q}\mathbf{q}_z} g_{\mathbf{k}\mathbf{q}\mathbf{q}_z} (c_{\sigma\mathbf{q}+\mathbf{q}_z}^\dagger e_{\sigma\mathbf{k}+\mathbf{q}}^\dagger h_{\sigma\mathbf{k}}^\dagger + h.c.)
\end{aligned} \tag{2.6}$$

In the above, all momenta are confined to the plane of the monolayer, except for \mathbf{q}_z which lies in the plane perpendicular to the monolayer. The index $\sigma \in \{-, +\}$ labels the valley degree of freedom of electrons/holes and the polarization degree of freedom for photons. $e_{\sigma\mathbf{k}}^\dagger$ creates an electron in the σ valley of the conduction band, of momentum $\sigma\mathbf{K} + \mathbf{k}$. Notice that we directly introduced hole operators, and we will use the convention that $h_{\sigma\mathbf{k}}^\dagger$ destroys an electron of momentum $\sigma\mathbf{K} + \mathbf{k}$ in the σ valley of the valence band. \mathcal{A} denotes the in-plane quantization area. We also introduced the electron and hole dispersions $\xi_{\mathbf{k}} = \mathbf{k}^2/(2m)$. The Coulomb potential $V_{\mathbf{q}} = 1/(2\epsilon_0\epsilon(\mathbf{q})|\mathbf{q}|)$ takes into account the nonlocal dielectric screening specific to monolayers with $\epsilon(\mathbf{q}) = 1 + r_0|\mathbf{q}|$ and $r_0 \approx 5 \text{ nm}$ in MoSe₂ [22]. We also introduced the photon creation operators $c_{\sigma\mathbf{k}'}^\dagger$, the photon dispersion $\nu_{\mathbf{k}} = c|\mathbf{k}|$ and the light matter coupling strength $g_{\mathbf{k}\mathbf{q}\mathbf{q}_z} = \mu \cdot \mathbf{e}_{\mathbf{q}+\mathbf{q}_z, \sigma} \sqrt{\frac{\nu_{\mathbf{q}+\mathbf{q}_z}}{2\epsilon_0 L_z \mathcal{A}}}$, where μ denotes the transition dipole matrix element between the conduction and valence band and L_z denotes the quantization area along the direction perpendicular to the monolayer.

The above Hamiltonian still neglects some processes (such as the electron-hole exchange terms, the non-parabolic nature of the dispersions, etc.), but we will nevertheless use this as a starting point in this thesis for simplicity.

Before moving on, we present a typical experimental setup in Fig.2.3, which can be used for the optical investigations of TMDs.

2.2 EXCITON QUASIPARTICLE

We begin our analysis by considering the exciton problem. As we mentioned in the introduction, electron-hole pair optical excitations attract each

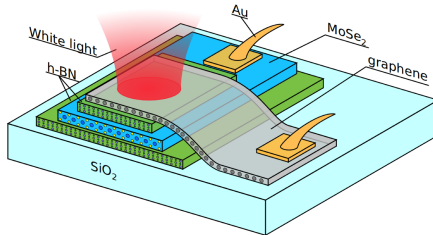


FIGURE 2.3: A sketch of a typical sample structure: A MoSe₂ monolayer is embedded in between h-BN flakes and covered with a graphene flake. The heterostructure is transferred onto a substrate (e.g. SiO₂ on Si, SiO₂ or a DBR). The MoSe₂ monolayer and the graphene are contacted separately with gold in order to apply a voltage in between the graphene top-gate and the TMD monolayer. Figure reprinted with permission from [23].

other due their opposite charges. This attraction leads to the formation of bound states, a process similar to the formation of the hydrogen atoms.

To investigate this problem we first neglect the light matter coupling and focus solely on the problem of a single electron-hole pair excitation. Taking into account the conservation laws of the Hamiltonian in Eq. (2.6) (total momentum is always conserved, while number of electrons and holes is conserved in the absence of the coupling to the light field), we write the most general state of momentum \mathbf{p} with one electron and one hole:

$$|\Psi_{n\mathbf{p}}\rangle = \sum_{\mathbf{k}} \varphi_{n\mathbf{k}} e_{\mathbf{p}/2+\mathbf{k}}^\dagger h_{\mathbf{p}/2-\mathbf{k}}^\dagger |0\rangle \equiv x_{n\mathbf{p}}^\dagger |0\rangle \quad (2.7)$$

where $|0\rangle$ denotes the vacuum state. The label n denotes the internal state of the electron-hole pair and denotes both bound and scattering states. We remark that it is not obvious at this point that the wavefunction φ does not depend on the total momentum but we will see that this will become clear shortly. We mention that from now on we will suppress the valley index σ when no confusion will arise.

We want to solve the Schroedinger equation:

$$H |\Psi_{n\mathbf{k}}\rangle = E_{n\mathbf{p}}^X |\Psi_{n\mathbf{k}}\rangle \quad (2.8)$$

To do this we act on the right with $\langle 0| h_{\mathbf{p}/2-\mathbf{k}} e_{\mathbf{p}/2+\mathbf{k}}$ to obtain the equation:

$$\varphi_{n\mathbf{k}} (\xi_{\mathbf{p}/2+\mathbf{k}} + \xi_{\mathbf{p}/2-\mathbf{k}}) - \sum_{\mathbf{k}'} V_{\mathbf{k}'-\mathbf{k}} \varphi_{n\mathbf{k}'} = E_{n\mathbf{p}}^X \varphi_{n\mathbf{p}} \quad (2.9)$$

Notice that, as mentioned above, the dependence on p is trivial and can be eliminated by redefining the energy $E_{np}^X \rightarrow E_{np}^X + \mathbf{p}^2/(4m)$. This is just a total energy shift due to the center of mass motion of the exciton and does not influence the wavefunction φ .

This is just the hydrogen problem in two dimensions with an interaction potential V_q . The equation has no known analytical solution for the potential V_q introduced above. However, this matrix eigenvalue equation can be easily solved by discretizing the momentum space. Doing this we find that the lowest energy 1s bound state is:

$$E_{1s,p}^X \approx \frac{\mathbf{p}^2}{4m} - 0.5\text{eV} \quad (2.10)$$

The corresponding eigenfunction can be well approximated by the 1s wavefunction:

$$\varphi_{1s,\mathbf{k}} = \frac{2\sqrt{2\pi}a_x}{\sqrt{A}(1 + (|\mathbf{k}|a_x)^2)^{3/2}} \quad (2.11)$$

which is the eigenfunction of the ground state of the 2D Hydrogen problem in the presence of the usual Coulomb interactions. In the above the exciton Bohr radius is $a_x \approx 1\text{nm}$. We mention that the Fourier transform of the above is $\varphi_{1s}(\mathbf{r}) = \frac{1}{\sqrt{A}} \sum_{\mathbf{k}} e^{i\mathbf{k}\mathbf{r}} \varphi_{1s,\mathbf{k}} = \sqrt{\frac{2}{\pi}} \frac{1}{a_x} e^{-ra_x}$.

2.2.1 Bare exciton-exciton interaction

Having found the eigenstates of the system in the single electron-hole pair subspace, does this tell us anything about the more general case of multiple electron-hole pair excitations?

We expect that, as long as the exciton density n_x is small enough, i.e. $n_x a_x^2 \ll 1$, in the ground state, all holes will be paired-up with electrons to form excitons. Therefore, for energies close to the ground state energy, the dynamics of the system should be well approximated by a system of weakly-interacting excitons. Due to the charge neutrality of the exciton, the main contribution to the interaction between two excitons comes from the exchange of electrons or holes between them. We will discuss in the next chapter a simple way to calculate such interactions, when we discuss electron-exciton interactions. For a derivation of this contribution one can check Ref. [24–26]. For simplicity, in this thesis we will approximate this interaction by a contact potential.

In this regime, we will be able to describe a system of excitons with the simplified Hamiltonian:

$$H = \sum_{\mathbf{k}} \omega_{\mathbf{k}} x_{\mathbf{k}}^\dagger x_{\mathbf{k}} + \frac{u}{\mathcal{A}} \sum_{\mathbf{k}\mathbf{k}'\mathbf{q}} x_{\mathbf{k}+\mathbf{q}}^\dagger x_{\mathbf{k}'-\mathbf{q}}^\dagger x_{\mathbf{k}'} x_{\mathbf{k}} \quad (2.12)$$

Notice that in writing down the above Hamiltonian we made the additional simplification of focusing only on the 1s exciton states and therefore the x operators correspond to the 1s exciton operators but we dropped the 1s exciton label. We remark that contact interactions have to be regularized and we do this by introducing a UV cutoff $\Lambda = 1/r_0$ (r_0 can be understood as the range of the interaction in real space, for excitons this should be given by the exciton Bohr radius); therefore we will consider only momenta smaller than this cutoff.

2.3 EXCITON-POLARITONS

In the previous section we have investigated the elementary optical excitations in intrinsic semiconductor materials. We have neglected the light matter coupling, assuming that it will not modify the spectrum of the system significantly. Instead, the role of photons was only to probe the system. We now consider the case when the light matter coupling is so large as to lead to the hybridization of photons and excitons into new quasiparticles called exciton-polaritons.

We begin by considering how the light-matter coupling is modified due to the exciton formation. To do this we can use the completeness relation:

$$e_{\mathbf{k}+\mathbf{p}/2}^\dagger h_{\mathbf{p}/2-\mathbf{k}}^\dagger = \sum_n \varphi_{n\mathbf{k}} x_{n\mathbf{p}}^\dagger \quad (2.13)$$

to write down the light-matter coupling Hamiltonian in the new exciton basis. Neglecting for the moment the momentum dependence of the light matter coupling, i.e. using $g_{\mathbf{k}\mathbf{q}\mathbf{p}_z} \approx g$ we can rewrite the light-matter coupling Hamiltonian as:

$$\begin{aligned} \sum_{\mathbf{k}\mathbf{q}} g c_{\mathbf{q}+\mathbf{q}_z} e_{\mathbf{k}+\mathbf{q}}^\dagger h_{\mathbf{k}}^\dagger &= \sum_{n\mathbf{q}} g c_{\mathbf{q}+\mathbf{q}_z} x_{n\mathbf{q}}^\dagger \sum_{\mathbf{k}} \varphi_{n\mathbf{k}} \\ &= g \sqrt{\mathcal{A}} \sum_{n\mathbf{q}} \varphi_n(0) c_{\mathbf{q}+\mathbf{q}_z} x_{n\mathbf{q}}^\dagger \end{aligned} \quad (2.14)$$

As expected, the light matter coupling is renormalized roughly by a factor of $\sqrt{\mathcal{A}}/a_x$, due to the formation of bound states. Notice that this a massive correction since $\sqrt{\mathcal{A}}/a_x$ diverges as we take the size of the system to

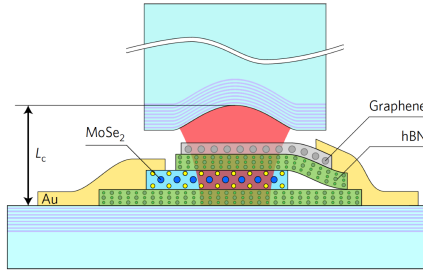


FIGURE 2.4: A sketch of the heterostructure inside a fiber DBR cavity. The thickness of the h-BN layers is chosen such that the TMD layer is in the anti-node and the graphene is in the node of the cavity mode.

infinity (this does not mean that the light-matter coupling diverges since this divergent renormalization factor cancels the factor of $1/\sqrt{A}$ in the definition of g). Notice that the interaction is stronger the smaller the size of the bound state. This is due to the locality of the light matter coupling. For instance when the electron and the hole are bound to each other they will meet each other much more often and emit photons. Diagrammatically, the renormalization of the light matter vertex can be understood as a consequence of vertex corrections (see Fig.1.2). In this context, the diverging correction \sqrt{A}/a_x would appear as a pole in the renormalized light-matter coupling vertex.

Notice that the renormalization factor cancels the corresponding area factor in the definition of $g_{\mathbf{k}\mathbf{q}\mathbf{q}_z}$, effectively replacing it with the exciton area a_x^2 . Another straightforward way to further increase interactions is by confining photons along the z direction, using for instance a distributed Bragg reflector (DBR), as shown in Fig.2.4, and therefore decreasing L_z to a length of the order of the photon wavelength. This will quantize q_z to values of $q_z = n\pi/L_z$ with n a positive integer. One can see that the confinement makes the dispersion of photons quadratic, effectively giving photons a mass [1]:

$$\nu_{\mathbf{q}} = c\sqrt{\mathbf{q}^2 + q_z^2} \approx cq_z + \frac{\hbar^2 \mathbf{q}^2}{2m_c} \quad (2.15)$$

where we assumed that $q \ll q_z$ and introduced the cavity mass $m_c = q_z \hbar/c$. One can check using reasonable values that the resulting mass is orders of magnitude smaller than the corresponding mass of the electrons. The

cavity mass is approximately $m_c \approx 10^{-5} m_0$ [1] and we will use this value in the following.

In such a setup the light matter coupling strength becomes $g_{\mathbf{k}\mathbf{q}\mathbf{q}_z} \approx \mu \cdot \mathbf{e}_{\mathbf{q}_z,\sigma} \sqrt{\frac{\nu_{\mathbf{q}_z}}{2\epsilon_0 L_z \mathcal{A}}} = g$ (where we used the fact that $|\mathbf{q}| \ll q_z$). Using Eq. (2.14) and neglecting the coupling to higher exciton states, we can write down the following quadratic Hamiltonian for the light matter interaction in the exciton basis:

$$H = \sum_{\mathbf{k}} \omega_{\mathbf{k}} x_{\mathbf{k}}^\dagger x_{\mathbf{k}} + \sum_{\mathbf{k}} \nu_{\mathbf{k}} c_{\mathbf{k}}^\dagger c_{\mathbf{k}} + \sum_{\mathbf{k}} \tilde{g} \left(c_{\mathbf{k}}^\dagger x_{\mathbf{k}} + c_{\mathbf{k}} x_{\mathbf{k}}^\dagger \right) \quad (2.16)$$

where we introduced the renormalized light-matter vertex $\tilde{g} = g \sqrt{\frac{2\mathcal{A}}{\pi a_x^2}}$. Notice that we use a tilde to explicitly denote the renormalized vertex here, but we will drop the tilde in following sections where there is no need to distinguish g and \tilde{g} . The above Hamiltonian can be solved with the canonical transformation:

$$a_{l,\mathbf{k}} = \alpha_{\mathbf{k}} x_{\mathbf{k}} + \beta_{\mathbf{k}} c_{\mathbf{k}} \quad (2.17)$$

$$a_{u,\mathbf{k}} = -\beta_{\mathbf{k}}^* x_{\mathbf{k}} + \alpha_{\mathbf{k}}^* c_{\mathbf{k}} \quad (2.18)$$

where $a_{l/u,\mathbf{k}}$ denote the destruction operator of the new degrees of freedom of the system corresponding to upper and lower polaritons. We remark that, by construction the upper and lower polariton operators commute with each other, while the condition $[a_{l/u,\mathbf{k}}, a_{l/u,\mathbf{k}}^\dagger] = 1$ implies that $|\alpha_{\mathbf{k}}|^2 + |\beta_{\mathbf{k}}|^2 = 1$. We can choose these parameters to diagonalize the above Hamiltonian and obtain:

$$H = \sum_{\mathbf{k}} \Omega_{l\mathbf{k}} a_{l\mathbf{k}}^\dagger a_{l\mathbf{k}} + \sum_{\mathbf{k}} \Omega_{u\mathbf{k}} a_{u\mathbf{k}}^\dagger a_{u\mathbf{k}} \quad (2.19)$$

where we introduced the dispersion of the new modes:

$$\Omega_{l/u,\mathbf{k}} = \frac{\omega_{\mathbf{k}} + \nu_{\mathbf{k}}}{2} \pm \sqrt{\frac{(\omega_{\mathbf{k}} - \nu_{\mathbf{k}})^2}{4} + \tilde{g}^2} \quad (2.20)$$

The minus sign is for the lower polariton. The coefficients that diagonalize the Hamiltonian are:

$$\alpha_{\mathbf{k}}^2 = \frac{\nu_{\mathbf{k}} - \Omega_{l\mathbf{k}}}{\Omega_{u\mathbf{k}} - \Omega_{l\mathbf{k}}} \quad (2.21)$$

$$\beta_{\mathbf{k}}^2 = 1 - \alpha_{\mathbf{k}}^2 = \frac{\nu_{\mathbf{k}} - \Omega_{u\mathbf{k}}}{\Omega_{u\mathbf{k}} - \Omega_{l\mathbf{k}}} \quad (2.22)$$

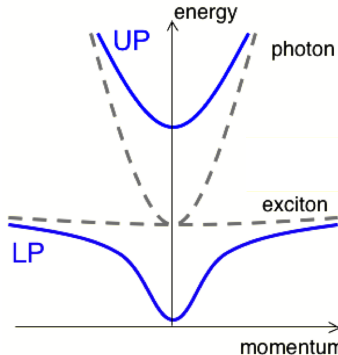


FIGURE 2.5: Polariton dispersion. The dashed lines are the exciton and photon dispersions

We present the dispersion of the new states in Fig.2.5. The dispersion changes shape around a momentum $k_0 \approx \sqrt{2m_c\tilde{g}/\hbar^2}$. Notice that, at momenta much larger than k_0 , the lower(upper) polariton becomes a bare exciton(photon). Only at momenta smaller or equal to k_0 , the two modes hybridize, and both upper and lower polariton inherit an ultra-low mass due to their photonic content β_k .

Most importantly, polaritons interact strongly due to their excitonic content α_k . This can be seen by rewriting the effective Hamiltonian in Eq. (2.12) in the new polariton basis: Using Eq. (2.18) and Eq. (5.10) we obtain:

$$H = \sum_k \Omega_k a_k^\dagger a_k + \frac{u}{\mathcal{A}} \sum_{qkk'} \alpha_{p+q} \alpha_{k'-q} \alpha_{k'} \alpha_k a_{p+q}^\dagger a_{k'-q}^\dagger a_{k'} a_k \quad (2.23)$$

where we neglected the coupling to the higher energy upper-polaritons and also suppress the label l in the lower polariton operators. We mention that the polariton-polariton interaction depends on the polarization of the polaritons and is potentially tunable through the use of Feshbach resonances [27, 28].

2.4 RENORMALIZATION OF INTERACTIONS

In the previous sections we introduced the exciton and exciton-polariton quasiparticles that dominate the optical spectrum of intrinsic transition metal dichalcogenides.

In this section we begin to go beyond previous work in this field and take a closer look the interactions between quasiparticles, focusing on the measureable effects due to interactions. We emphasize that, through our measurements, we do not have direct access to the interaction u , but rather to a smaller renormalized value. We investigate the renormalization of interactions by exactly solving the problem of two excitons. Remarkably, we find that the small mass of the polariton can strongly suppresses this renormalization, making polaritons potentially more strongly interacting than excitons, even though polaritons interact only due to their excitonic component.

To get an intuitive understanding of the renormalization process let's start by considering exciton-exciton interactions system of volume \mathcal{V} with periodic boundary conditions. A common way to measure exciton-exciton interaction is to measure the shift of the exciton resonance when a strong laser is used to pump the exciton branch. It is usually assumed that this shift (i.e. the exciton chemical potential) is well approximated by $n_x u$ where u is the exciton-exciton interaction strength from Eq. (2.12). This approximation is known as the first Born approximation, and actually breaks down when interactions become stronger. Indeed, it is well known that in three dimensional systems, the interaction gets renormalized to the value $\tilde{u} = 4\pi\hbar^2 a/m$ where a is the s-wave scattering length that is related to the initial interaction u . This results in a (lower) chemical potential $n_x \tilde{u}$. However, in two dimensional system the renormalized interaction does not have such a simple form, as we will show below, and the resulting chemical potential does not have a simple linear dependence on n .

The reason for this renormalization of interactions is that excitons can lower their energy by avoiding each other and paying a small kinetic energy price. As mentioned previously, for small u the excitons will prefer to lower their kinetic energy as much as possible, and therefore both will occupy the lowest energy zero-momentum state and pay the repulsion energy u/\mathcal{V} . On the other hand, as the interaction strength u increases, this approximation breaks down and the particles will prefer to lower their interaction energy by avoiding each other and therefore increasing their kinetic energy.

To get an estimate of the scales involved let's calculate the kinetic energy price that the two particles must pay to completely avoid each other. This calculation depends qualitatively on the dimension of the system so we begin the calculation for a 3D system. The probability that the two particles are close enough to interact is given by r_0^3/L^3 , where r_0 is the

effective range of the interaction. When this happens, the two excitons can avoid each other by developing a node in their relative wavefunction. This would require a kinetic energy price given by $\hbar^2/m_x r_0^2$, because the range of the potential determines the curvature the two particle wavefunction would need to develop. Therefore, to completely avoid each other the excitons will have to pay a price of $K_{max} = \frac{\hbar^2 r_0}{m_x L^3}$. Therefore, in general the actual interaction would then be somewhere in between u/L^3 and K_{max} , depending on the range r_0 .

In the 1D case the situation is very different. In this case the particles will prefer to completely localize themselves in different parts of the system and therefore pay a kinetic energy price of $K_{max} = \frac{\hbar^2}{m_x L^2}$ which is much smaller than the interaction strength u/L . This explains the peculiar properties of 1D systems where particles are only free to move between their left and right neighboring particles which implies that the elementary excitations are always collective.

The 2D case is in between, but more closely related to the 3D case. A similar analysis to before shows that $K_{max} = \frac{\hbar^2}{m_x L^2}$ and therefore the range of the interaction plays no role, which provides the first indication of the peculiarities of 2D systems. However, a more careful calculation will reveal logarithmic corrections that reintroduce the dependence on the interaction range.

Let's consider now the renormalization of polariton interactions. Because of their small mass, polaritons have to pay a huge kinetic energy to avoid each other. Essentially, to do this polaritons need to lose their photonic character and pay an energy g . As excitons, they can avoid each other by paying a kinetic energy $\hbar^2/(2mr_0^2)$. However, if $g > \hbar^2/(2mr_0^2)$ then this process is not energetically favourable and therefore they would prefer to minimize their kinetic energy first and pay the potential energy u/\mathcal{V} . When the above condition is satisfied then the polariton-polariton interaction is well described by the first Born approximation.

2.4.1 Exciton-exciton interactions

We now proceed to make the above statements more precise. We consider a system of two excitons described by the Hamiltonian in Eq. (2.12). To solve the two exciton problem we use the approach introduced in Sec.2.2 for the

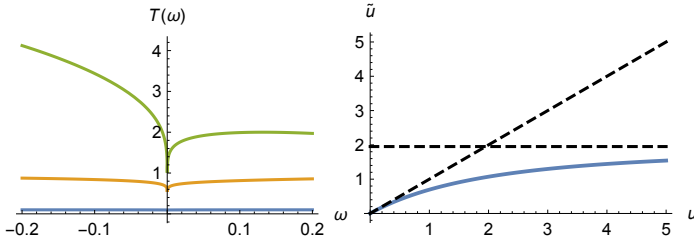


FIGURE 2.6: Left panel: $T_{2D}(\omega)$ for different values of u/r_0^2 . The blue, orange and green lines correspond to $u/r_0^2 = 0.1/(mr_0^2)$, $u/r_0^2 = 1/(mr_0^2)$, and respectively $u/r_0^2 = 10/(mr_0^2)$. Right panel: the solid line denotes renormalized interaction \tilde{u}/r_0^2 as a function of the bare interaction u/r_0^2 . The dashed line is introduced to show the maximum value that the renormalized interaction can reach, in the limit $u \rightarrow \infty$. The energy unit for both panels is $1/(mr_0^2)$.

exciton-problem and write down the most general two-particle wavefunction of total momentum \mathbf{p} :

$$|\Psi_{n\mathbf{p}}\rangle = \sum_{\mathbf{k}} \varphi_{n\mathbf{k}} x_{\mathbf{p}/2+\mathbf{k}}^\dagger x_{\mathbf{p}/2-\mathbf{k}}^\dagger |0\rangle \quad (2.24)$$

Solving the eigenvalue equation $H |\Psi_{n\mathbf{p}}\rangle = E_{n\mathbf{p}} |\Psi_{n\mathbf{p}}\rangle$ we obtain the following set of equations:

$$\varphi_{n\mathbf{k}} (\omega_{\mathbf{p}/2+\mathbf{k}} + \omega_{\mathbf{p}/2-\mathbf{k}} - E) + \frac{u}{\mathcal{V}} \sum_{\mathbf{k}'} \varphi_{n\mathbf{k}'} = 0 \quad (2.25)$$

which represents the momentum space Schrödinger equation for the relative motion of the two excitons.

The use of the simple contact interaction allows us to actually solve the equations. Dividing by the term in parenthesis and then summing over \mathbf{k} the resulting equation we obtain:

$$u^{-1} - \frac{1}{\mathcal{V}} \sum_{\mathbf{k}} \frac{1}{E_{n\mathbf{p}} - \omega_{\mathbf{p}/2+\mathbf{k}} - \omega_{\mathbf{p}/2-\mathbf{k}}} = 0 \quad (2.26)$$

As a sanity check, notice that the solutions of the above equation at $u \rightarrow 0$ appear at the poles of the summation, which correspond to the kinetic energy of two non-interacting excitons.

Although it is tempting to turn the above summation into an integral this will not work, because we are interested in calculating very small

energy changes proportional to $1/\mathcal{V}$ which would be washed out in this process. We are interested in the change in the ground state energy due to interactions. The non-interacting ground state corresponds to two excitons of momentum $\mathbf{p}/2$, and therefore we expect the energy of the interacting ground state to be close to $2\omega_{\mathbf{p}/2}$. We therefore isolate the $\mathbf{k} = 0$ term in the above and obtain the equation:

$$E_{0\mathbf{p}} - 2\omega_{\mathbf{p}/2} = \frac{1}{\mathcal{V}} \left(u^{-1} - \frac{1}{\mathcal{V}} \sum_{\mathbf{k} \neq 0} \frac{1}{E_{0\mathbf{p}} - \omega_{\mathbf{p}/2+\mathbf{k}} - \omega_{\mathbf{p}/2-\mathbf{k}}} \right)^{-1} \quad (2.27)$$

At this point, we are allowed to turn the summation into an integral, because we already isolated the large $\mathbf{k} = 0$ term.

To do this we introduce a quantity that appears often in scattering experiments and will also arise in later chapters known as the T-matrix. We define it in the whole complex plane as:

$$T(\mathbf{p}, \omega)^{-1} = \left(u^{-1} - \frac{1}{\mathcal{V}} \sum_{\mathbf{k} \neq 0} \frac{1}{\omega - \omega_{\mathbf{p}/2+\mathbf{k}} - \omega_{\mathbf{p}/2-\mathbf{k}} + i\eta} \right)^{-1} \quad (2.28)$$

where we introduced the positive infinitesimal η which shifts the poles of the summation to the lower-complex plane and ensures that the summation can be safely turned into an integral as $\mathcal{V} \rightarrow \infty$.

Note that we can express Eq. (2.27) using the T-matrix:

$$E_{0\mathbf{p}} - 2\omega_{\mathbf{p}/2} = \frac{T(\mathbf{p}, E_{0\mathbf{p}})}{\mathcal{V}} \quad (2.29)$$

which shows that the T-matrix also denotes the renormalized interaction between the excitons. It is straightforward to see that the finite momentum T-matrix is related to the zero momentum T-matrix by $T(\mathbf{p}, \omega) = T(\mathbf{p} = 0, \omega - 2\omega_{\mathbf{p}/2})$, so we only need to calculate the zero-momentum one.

In 2D the T-matrix is given by:

$$T_{2D}(\mathbf{p} = 0, \omega) = \left[u^{-1} - \int_0^{1/r_0} \frac{dkk}{2\pi} \frac{1}{\omega - 2\omega_{\mathbf{k}} + i\eta} \right]^{-1} \quad (2.30)$$

$$= \left[u^{-1} - \frac{m}{4\pi} \ln \left(\frac{mr_0^2\omega - 1}{mr_0^2\omega} \right) \right]^{-1} \quad (2.31)$$

Eq. (2.29) can be solved numerically to obtain the renormalized interaction $\tilde{u} = E_{0\mathbf{p}} - 2\omega_0$. We plot the results in Fig.2.6. We see that the interaction

u starts to be renormalized when the interaction energy u/r_0^2 becomes larger than the kinetic energy cost $1/mr_0^2$. It is important to notice that the renormalized interaction cannot exceed maximum value exhibited by the dashed line in Fig.2.6, regardless of the strength of u .

2.4.2 Interaction of two polaritons

We now consider the interaction of polaritons, using a similar approach. As before, we write down the most general two-particle wavefunction (let's focus on the zero total momentum case for simplicity), in the case of a finite g :

$$|\Psi\rangle = \sum_{\mathbf{k}} \left(\varphi_{\mathbf{k}}^{xx} x_{\mathbf{k}}^\dagger x_{-\mathbf{k}}^\dagger + \varphi_{\mathbf{k}}^{xc} x_{\mathbf{k}}^\dagger c_{-\mathbf{k}}^\dagger + \varphi_{\mathbf{k}}^{cc} c_{\mathbf{k}}^\dagger c_{-\mathbf{k}}^\dagger \right) |0\rangle \quad (2.32)$$

Notice that from now on, we will suppress the internal state index n for clarity. Solving the eigenvalue equation $H|\Psi\rangle = E|\Psi\rangle$, where H is the Hamiltonian introduced in Eq. (2.16), we obtain the following set of equations:

$$\varphi_{\mathbf{k}}^{xx}(2\omega_{\mathbf{k}} - E) + \frac{u}{\mathcal{V}} \sum_{\mathbf{k}'} \varphi_{\mathbf{k}'}^{xx} + g\sqrt{2}\varphi_{\mathbf{k}}^{xc} = 0 \quad (2.33)$$

$$\varphi_{\mathbf{k}}^{xc}(\omega_{\mathbf{k}} + \nu_{\mathbf{k}} - E) + g\sqrt{2}\varphi_{\mathbf{k}}^{xx} + g\sqrt{2}\varphi_{\mathbf{k}}^{cc} = 0 \quad (2.34)$$

$$\varphi_{\mathbf{k}}^{cc}(2\nu_{\mathbf{k}} - E) + g\sqrt{2}\varphi_{\mathbf{k}}^{xc} = 0 \quad (2.35)$$

Solving the last two equations and plugging the result into the first one we obtain:

$$\varphi_{\mathbf{k}}^{xx} \left(2\omega_{\mathbf{k}} + \frac{2g^2}{E - \omega_{\mathbf{k}} - \nu_{\mathbf{k}} - 2g^2/(E - 2\nu_{\mathbf{k}})} - E \right) + \frac{u}{\mathcal{V}} \sum_{\mathbf{k}'} u\varphi_{\mathbf{k}'}^{xx} = 0 \quad (2.36)$$

Dividing by the term in parenthesis and then summing over \mathbf{k} the resulting equation we obtain:

$$u^{-1} - \frac{1}{\mathcal{V}} \sum_{\mathbf{k}} \frac{1}{E - 2\omega_{\mathbf{k}} - \frac{2g^2}{E - \omega_{\mathbf{k}} - \nu_{\mathbf{k}} - 2g^2/(E - 2\nu_{\mathbf{k}})}} = 0 \quad (2.37)$$

We rewrite the above equation to make explicit the poles of the summation. To do this we introduce the upper and lower polariton energies and the exciton/photon weights to rewrite Eq. Eq. (2.38) as:

$$u^{-1} - \frac{1}{\mathcal{V}} \sum_k \left(\frac{\alpha_k^4}{E - 2\Omega_{l\mathbf{k}}} + \frac{\beta_k^4}{E - 2\Omega_{u\mathbf{k}}} + \frac{2\alpha_k^2\beta_k^2}{E - \Omega_{l\mathbf{k}} - \Omega_{u\mathbf{k}}} \right) = 0 \quad (2.38)$$

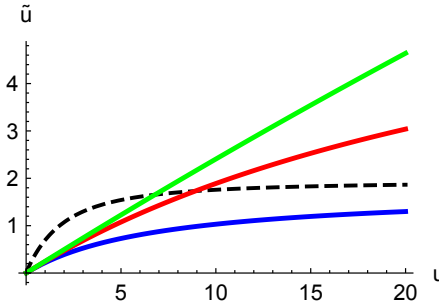


FIGURE 2.7: Renormalized polariton-polariton interaction. The solid lines are for increasing values of gmr_0^2 , ranging between 0.1, 1 and 10. The dashed line represents the renormalized exciton interaction. We worked at resonance where $\nu_0 = \omega_0$ where $\alpha_0 = 1/\sqrt{2}$, where according to the first Born approximation, we would expect that the polariton interaction be 4 times less than the exciton interaction. Instead we see that it can be even larger.

As a sanity check, notice that the solutions of the above equation at $u \rightarrow 0$ appears at the poles of the summation, which correspond to two non-interacting polaritons from either the upper or lower branch.

The above equation can be solved numerically. In the following, we can make some reasonable approximations that allow us to obtain a closed form solution. We are interested in the change in the ground state energy due to interactions. The non-interacting ground state corresponds to two lower polaritons, and therefore we expect the energy to be close to $2\Omega_{l,0}$. Because of this the $\mathbf{k} = 0$ term in the above summation corresponding to 2 lower polaritons has a significant contribution, and therefore we isolate it to obtain:

$$E = 2\Omega_{l,0} + \frac{\alpha_0^4}{\mathcal{V}} \left(u^{-1} - \frac{1}{\mathcal{V}} \sum_{\mathbf{k}} \frac{\alpha_k^4 (1 - \delta_{\mathbf{k},0})}{E - 2\Omega_{l,\mathbf{k}}} \right) \quad (2.39)$$

$$+ \frac{\beta_{\mathbf{k}}^4}{E - 2\Omega_{u\mathbf{k}}} + \frac{2\alpha_k^2 \beta_k^2}{E - \Omega_{l\mathbf{k}} - \Omega_{u\mathbf{k}}} \right)^{-1} \quad (2.40)$$

Notice that the above summation runs up to $k = 1/r_0$. Except for a small region $k < k_\nu$ where $k_\nu \approx 2\pi/\lambda$ (λ is the photon wavelength), $\alpha_k \rightarrow 1$ and $\beta_k \rightarrow 0$ and $\Omega_{l\mathbf{k}} \rightarrow \omega_{\mathbf{k}}$. Therefore we can rewrite the above as:

$$E \approx 2\Omega_{l,0} + \frac{\alpha_0^4}{\mathcal{V}} \left(u^{-1} - \frac{1}{\mathcal{V}} \sum_{\mathbf{k}} \frac{1}{E - 2\omega_{\mathbf{k}}} \right)^{-1} \quad (2.41)$$

We recognize the term in parenthesis as the 2 exciton T-matrix (note that the infinitesimal $i\eta$ does not have any effect here because of E is negative) and therefore we can write more compactly:

$$E \approx 2\Omega_{l,0} + \frac{\alpha_0^4}{\mathcal{V}} T(\mathbf{p} = 0, E) \quad (2.42)$$

where the exciton T-matrix was defined in the previous section. Notice that the interaction term scales as $1/\mathcal{V}$ and therefore the term $|\Omega_{l,0}|$ dominates as we take $\mathcal{V} \rightarrow \infty$ (i.e. when V is the much larger than the other lengthscales in the problem), which implies that:

$$E \approx 2\Omega_{l,0} + \frac{\alpha_0^4}{\mathcal{V}} T(\mathbf{p} = 0, 2\Omega_{l,0}) \quad (2.43)$$

Basically, we see that the renormalization of polariton interactions is still governed by the T-matrix. But crucially the T-matrix has to be evaluated off-shell at twice the energy of the lower polariton. As can be seen from Fig.2.6 the T-matrix increases strongly for negative frequencies and eventually, for frequencies of the order of $-1/mr_0^2$, it is equal to the bare interaction u . This shows that the renormalization is much less effective for polaritons and can in principle make polaritons interact more strongly than excitons.

We plot the renormalized interaction $\tilde{u} = \alpha_0^4 T(\mathbf{p} = 0, 2\Omega_{l,0})$ as a function of u in Fig.2.7, for different values of the light matter coupling g . This figure illustrates what we claimed before and we see that, when g is of the order of $1/mr_0^2$, polaritons interact more strongly than excitons.

These results have important applications to the field of polariton interactions. Our derivation suggests that, in order to increase the measurable effects of polariton interactions, and reach the regime of photon blockade, rather than trying to increase the bare interaction u , one should instead attempt to increase either the range of the interaction r_0 (which can be achieved for instance by using dipolar excitons) or the light-matter coupling g strength.

2.5 CONCLUSION

We have introduced the TMD monolayers, as well as the exciton, and exciton-polariton quasiparticles, concepts which represent the starting point of our work.

Most importantly we focused on the interactions between these quasi-particles and especially on the renormalization of these interactions. We showed that this renormalization process is suppressed for polaritons, when the parameter gmr_0^2 becomes sizeable. Our results suggest that, in order to achieve strong photon nonlinearities, and the photon Blockade regime, one should focus on increasing the light-matter coupling g or the range of interactions r_0 .

3

POLARON PHYSICS WITH LIGHT

We introduce the electron-polariton (and electron-exciton) Bose Fermi mixture, the system that we will investigate for the rest of the thesis. After discussing the origin of the electron-exciton and exciton-polariton interaction, we focus on the density imbalanced regime, where the number of one species of particles is much larger than the number of the other species. We show that the low-energy degrees of freedom are dominated by polaronic quasiparticles, resembling the polaron quasiparticles in solid state systems.

As the title of the thesis suggests, this thesis investigates the many-body physics that can be found in interacting electron-exciton (or polariton) systems. In order to reach the regime where many-body physics starts to become relevant, we need to first have a strong electron-polariton interaction. We begin this chapter by discussing how such an interaction can emerge in doped TMDs. We also discuss the bound electron-exciton state, known as the trion, that can form as a consequence of these interactions.

Then we begin our analysis of the electron-polariton Bose-Fermi mixture, which is a complicated many-body problem. These problems can be extremely complex, and the exact solutions are generally not known. However, many-body problems often simplify considerably if one focuses on the low energy physics. The low energy physics is often dominated by collective degrees of freedom that behave as weakly interacting particles with renormalized properties, i.e. quasiparticles. In this chapter we will analyze the quasiparticles that dominate the low-energy physics in a Bose-Fermi mixture, in the density imbalanced regime.

The problem in this regime connects to the problem of a mobile impurity in a bosonic or fermionic bath. The impurity problem has a rich history, starting with the analysis of the electron motion in solid state systems, first studied by Landau and Peckar [6]. The new quasiparticles in this context, formed by the dressing of the electron by phonon fluctuations in the lattice, are known as polarons. Recently, the subject was revived by numerous experiments in cold atomic systems, due to the possibility of directly observing the dressing of mobile impurities in a fermionic or bosonic bath [3–5, 7, 8, 29–31].

We begin our discussion in the limit $n_x/n_e \ll 1$ (where n_x is the exciton density while n_e represents the electron density), and discuss the emergence of new quasiparticles known as Fermi polarons, which are collective excitations where the polariton is dressed by a polarization cloud in the electron system. Remarkably, this leads to the formation of highly-unusual ultra-low mass polaron quasiparticles [2]. The polaron framework also makes us reevaluate previous assertions in the absence of the cavity, for systems of excitons interacting with electrons. We show that the spectral features of optical absorption or emission experiments in semiconductors can be attributed to exciton-polaron states. This is in contrast to most previous work, which attributed these features to trions.

In the opposite regime $n_x/n_e \gg 1$ we investigate how electrons dress by fluctuations in the polariton system which forms a Bose-Einstein condensate (BEC), to form quasiparticles known as Bose polarons. This opens the possibility for the optical manipulation of electrons, and in later chapters we will investigate how we can use this to induce optically strongly-correlated states of electrons. We find that the peculiar shape of the polariton dispersion acts as a gap for polariton excitations. However, instead of suppressing the dressing, we find that this gap can actually assist the polaron formation.

We perform this analysis using a wavefunction method. Wavefunction methods are especially appealing due to their transparency. There are indeed few cases where many-body problems can be successfully investigated using wavefunction methods. However, this method has its limitations and in the next two chapters we solve the problem through different methods. These complementary methods will allow us to go beyond the calculations in these chapter, and each method serves to better explain the other.

This chapter is organized as follows: after discussing the exciton-electron interaction in Sec.3.1 we discuss the exciton-electron interaction and derive a simplified effective Hamiltonian that describes our Bose-Fermi mixtures. Then, in Sec.3.2 we look at a Bose-Fermi mixture of excitons and electrons in the regime of low exciton density and discuss the exciton-polaron quasiparticles. In Sec.3.3 we generalize these calculations to polaron-polaritons. The calculations in Sec.3.2 and Sec.3.3 are based on Ref. [2] In Sec.3.4 we look at the opposite regime, when we have a low density electron system interacting with a large number of polaritons, which are in a BEC state, and discuss the resulting Bose-polaron quasiparticles. We provide a conclusion in Sec.3.5.

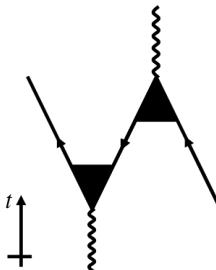


FIGURE 3.1: Electron-photon interaction due to electron exchange

3.1 EXCITON-ELECTRON INTERACTION

In the previous chapter we introduced the concept of excitons and exciton-polaritons and we briefly discussed the interactions between them. For the rest of this thesis we will focus on the interactions between excitons or exciton-polaritons and electrons. Such systems, known as Bose-Fermi mixtures exhibit a wealth of interesting phenomena due to the interplay between interactions and the different statistics of the particles. Additionally, the coupling to photons allows the optical investigation of the correlated states in these systems, and also introduces novel aspects due to the non-equilibrium nature of the optical excitations.

Therefore, before moving on, it is important to better understand the interaction between photons and electrons, as well as the interaction between excitons and electrons. The interaction between photons and electrons comes mainly from the Compton scattering vertex that we already mentioned in the introduction in Fig.1.3. We rewrite it here in Fig.3.1 including the vertex corrections due to exciton formation. The scattering process can be interpreted as follows. At the initial time there is a photon and an electron in the system. The photon creates an exciton and then the initial electron exchanges places with the electron in the exciton. Below we present a very simple way to approximate this process without actually evaluating the Feynman diagram.

Since the interaction of polaritons is through their excitonic component, we only need to know the exciton interactions. So in the following we will assume that our system is described by the Hamiltonian H in Eq. (2.7), but without the coupling to the cavity photons. Our calculation relies on the

two-particle creation operators x_{np}^\dagger defined in Eq. (2.7). We will have four different types of excitons so we introduce the following combinations:

$$x_{\sigma np}^\dagger \equiv \sum_{\mathbf{k}} \varphi_{n\mathbf{k}} e_{\sigma, \mathbf{p}/2+\mathbf{k}}^\dagger h_{\sigma, \mathbf{p}/2-\mathbf{k}}^\dagger \quad (3.1)$$

$$\bar{x}_{\sigma np}^\dagger \equiv \sum_{\mathbf{k}} \varphi_{n\mathbf{k}} e_{-\sigma, \mathbf{p}/2+\mathbf{k}}^\dagger h_{\sigma, \mathbf{p}/2-\mathbf{k}}^\dagger \quad (3.2)$$

where $\sigma \in \{+, -\}$ denotes the $\pm K$ valleys. Notice that \bar{x} denotes excitons, where the electron and the hole are in opposite valleys. We will also use the completeness relation in Eq. (2.13) which allows us to express pairs of electron and hole operators in terms of the exciton operators. Since the 1s exciton state has a much lower energy than all the other states, in the following we will assume that the photon energy is tuned close to the 1s exciton resonance, and therefore to first order we can neglect the coupling to higher lying exciton states.

We introduce a novel method to calculate the exciton-electron interactions that is very simple to use and understand. To calculate the residual interactions between electrons and excitons we calculate the evolution of the exciton operators:

$$-i \frac{dx_{\sigma 1s \mathbf{p}}^\dagger}{dt} = [H, x_{\sigma 1s \mathbf{p}}^\dagger] = E_{1s, \mathbf{p}}^X x_{\sigma 1s \mathbf{p}}^\dagger + \delta H(\sigma, \mathbf{p}) \quad (3.3)$$

$$\begin{aligned} \delta H(\sigma, \mathbf{p}) = & \frac{1}{\mathcal{A}} \sum_{\sigma' \mathbf{k} \mathbf{k}' \mathbf{q}} V_{\mathbf{q}} \varphi_{1s, \mathbf{k}} \left(e_{\sigma \mathbf{p}/2+\mathbf{k}+\mathbf{q}}^\dagger h_{\sigma \mathbf{p}/2-\mathbf{k}}^\dagger - e_{\sigma \mathbf{p}/2+\mathbf{k}}^\dagger h_{\sigma \mathbf{p}/2-\mathbf{k}+\mathbf{q}}^\dagger \right) \\ & \cdot \left(e_{\sigma' \mathbf{k}'-\mathbf{q}}^\dagger e_{\sigma' \mathbf{k}'} - h_{\sigma' \mathbf{k}'-\mathbf{q}}^\dagger h_{\sigma' \mathbf{k}'} \right) \end{aligned} \quad (3.4)$$

where $E_{1s \mathbf{p}}^X$ is the energy of the 1s exciton bound state defined in Eq. (2.10).

Notice that, in addition to the term corresponding to the expected evolution of an eigenmode, there is an additional term containing pairs of terms such as $e^\dagger h^\dagger e^\dagger e$ ($e^\dagger h^\dagger h^\dagger h$). Since we will consider without loss of generality the electron-doped regime, we will neglect the term proportional to $h^\dagger h$, which vanishes when there are no holes in the system. For strong exciton binding energy, these additional terms will oscillate very fast unless one of the electron-hole pairs is an exciton. We want to eliminate the fast-oscillating terms. To do this we use the completeness relation in Eq. (2.13).

We can rewrite $\delta H(\sigma, \mathbf{p})$ in the new basis by replacing the terms in the first parenthesis to obtain:

$$\begin{aligned}\delta H(\sigma, \mathbf{p}) &= \frac{1}{\mathcal{A}} \sum_{n\sigma' \mathbf{k} \mathbf{k}' \mathbf{q}} V_{\mathbf{q}} \varphi_{1s, \mathbf{k}} \left(\varphi_{n, \mathbf{k} + \mathbf{q}/2}^* - \varphi_{n, \mathbf{k} - \mathbf{q}/2}^* \right) x_{\sigma n, \mathbf{p} + \mathbf{q}}^\dagger e_{\sigma' \mathbf{k}' - \mathbf{q}}^\dagger e_{\sigma \mathbf{k}'} \\ &\equiv \frac{1}{\mathcal{A}} \sum_{n\sigma' \mathbf{k}' \mathbf{q}} v_{n\mathbf{q}}^D x_{\sigma n, \mathbf{p} + \mathbf{q}}^\dagger e_{\sigma' \mathbf{k}' - \mathbf{q}}^\dagger e_{\sigma \mathbf{k}}\end{aligned}$$

where we introduced the direct exciton-electron interaction $v_{n\mathbf{q}}$. We can now eliminate the fastly oscillating terms in the above, corresponding to virtual processes, and keep only the term proportional to $x_{1s, \mathbf{p} + \mathbf{q}}^\dagger$. However, since the wavefunction $\varphi_{1s, \mathbf{k}}$ is real, one can see that the direct interaction term vanishes. This can be seen by evaluating the summation:

$$\sum_{\mathbf{k}} \varphi_{1s, \mathbf{k}} \left(\varphi_{1s, \mathbf{k} + \mathbf{q}/2}^* - \varphi_{1s, \mathbf{k} - \mathbf{q}/2}^* \right) \quad (3.5)$$

$$= \sum_{\mathbf{k}} \varphi_{1s, \mathbf{k}} \varphi_{1s, \mathbf{k} + \mathbf{q}/2}^* - \sum_{\mathbf{k}} \varphi_{1s, \mathbf{k} + \mathbf{q}/2} \varphi_{1s, \mathbf{k}}^* = 0 \quad (3.6)$$

where we used the replacement $\mathbf{k} \rightarrow \mathbf{k} + \mathbf{q}/2$ for the dummy variable \mathbf{k} in the second term of the summation and we used $\varphi = \varphi^*$. Intuitively, the direct interaction between excitons and electrons vanishes due to the neutrality of the exciton, coupled with the fact that we chose equal masses for electron and holes. If these masses were different this term wold be nonzero but it would still be very small. Of course, there are higher order processes corresponding to the polarization of the exciton, which would appear if we included excited excitonic states such as $2p$ states. However, since we are only interested in determining the dominant contributions to the electron-exciton interaction we neglect such processes.

We can also rewrite $\delta H(\sigma, \mathbf{p})$ in the exciton basis by replacing the hole creation operator in the first parenthesis and the electron creation operator in the second with exciton operators, to obtain:

$$\delta H(\sigma, \mathbf{p}) = \frac{1}{\mathcal{A}} \sum_{nkk'q} V_q \varphi_{1s,k} \left(\varphi_{n, \frac{k+k'-q-p/2}{2}}^* e_{\sigma, \mathbf{p}/2+k+q}^\dagger x_{\sigma n, \mathbf{p}/2+k'-q-k}^\dagger \right) \quad (3.7)$$

$$- \varphi_{n, \frac{k'-k-2q-p/2}{2}}^* e_{\sigma, \mathbf{p}/2+k}^\dagger x_{n, \sigma, \mathbf{p}/2-k+k'}^\dagger \right) e_{\sigma k'}$$

$$+ \frac{1}{\mathcal{A}} \sum_{nkk'q} V_q \varphi_{1s,k} \left(\varphi_{n, \frac{k+k'-q-p/2}{2}}^* e_{\mathbf{p}/2+k+q}^\dagger \bar{x}_{\sigma n, \mathbf{p}/2+k'-q-k}^\dagger \right)$$

$$- \varphi_{n, \frac{k'-k-2q-p/2}{2}}^* e_{\sigma, \mathbf{p}/2+k}^\dagger \bar{x}_{n, \sigma, \mathbf{p}/2-k+k'}^\dagger \right) e_{-\sigma k'}$$

$$\equiv \frac{1}{\mathcal{A}} \sum_{nkq} v_{nkpq}^X \left(x_{\sigma, n, \mathbf{p}+q}^\dagger e_{\sigma k-q}^\dagger e_{\sigma, k} + \bar{x}_{\sigma, n, \mathbf{p}+q}^\dagger e_{\sigma k-q}^\dagger e_{-\sigma, k} \right) \quad (3.8)$$

where in the last line we rearranged terms to define the exchange interaction v^X . As before, we neglect the fastly oscillating terms in the above and keep only the $n = 1s$ term in the summation, since we are only interested in the dominant contribution. Notice that the last term would be exactly what we would expect if we had a term in the Hamiltonian of the form:

$$H_{xe} = \frac{1}{\mathcal{A}} \sum_{kk'q} v_{1skk'q}^X \left(x_{\sigma, 1s, k'+q}^\dagger x_{\sigma, 1s, k', -q}^\dagger e_{\sigma, k-q}^\dagger e_{\sigma, k} \right. \\ \left. + \bar{x}_{\sigma, 1s, k'+q}^\dagger x_{\sigma, 1s, k', -q}^\dagger e_{\sigma k-q}^\dagger e_{-\sigma, k} \right) \quad (3.9)$$

One can check that similar terms can be obtained by looking at $[H, x_{\mathbf{p}}^\dagger e_k^\dagger]$ which shows that we can indeed represent the interaction between excitons and electrons by the effective Hamiltonian 3.9.

Regarding the form of the exchange interaction, one can easily verify that it is a repulsive short-ranged interaction with a momentum cutoff of about $\Lambda = 1/a_x$ where a_x denotes the exciton Bohr radius. Since it is a short ranged interaction, we approximate it by a contact potential of strength v and range a_x . Furthermore x and \bar{x} have the same dispersion (at least within our approximation which neglects electron-hole exchange terms), so we can simplify the analysis and replace $\bar{x}_\sigma e_\sigma^\dagger$ with $-x_\sigma^\dagger e_{-\sigma}^\dagger$ (notice the minus sign). Although one should remember the origin of the exciton-electron interaction, this replacement does not change the optical spectra, which is what we are actually interested in calculating (one can

explicitly check this for the Fermi-polaron ansatz in Sec.3.2). Doing this we can write down the following effective Hamiltonian to describe the exciton-electron system:

$$H = \sum_{\sigma\mathbf{k}} \omega_{\mathbf{k}} x_{\sigma\mathbf{k}}^\dagger x_{\sigma\mathbf{k}} + \sum_{\sigma\mathbf{k}} \xi_{\mathbf{k}} e_{\sigma\mathbf{k}}^\dagger e_{\sigma\mathbf{k}} - \frac{v}{\mathcal{A}} \sum_{\sigma\mathbf{k}\mathbf{k}'\mathbf{q}} x_{\sigma\mathbf{k}+\mathbf{q}}^\dagger x_{\sigma\mathbf{k}} e_{\sigma\mathbf{k}'-\mathbf{q}}^\dagger e_{\sigma\mathbf{k}'} \\ + \frac{v}{\mathcal{A}} \sum_{\sigma\mathbf{k}\mathbf{k}'\mathbf{q}} x_{\sigma\mathbf{k}+\mathbf{q}}^\dagger x_{\sigma\mathbf{k}} e_{-\sigma\mathbf{k}'-\mathbf{q}}^\dagger e_{-\sigma\mathbf{k}'} \quad (3.10)$$

where we defined v to be negative. We emphasize that in using the above Hamiltonian one should keep in mind that it will yield the correct energy spectra but not the correct wavefunction since we replaced the operators \bar{x} with $-x$.

Notice that excitons interact repulsively(attractively) with electrons in the same (opposite) valley (we remark that the higher order interactions, stemming from the polarization of the exciton, which we neglected, would be attractive in both cases). Since we are in two-dimensions, the attractive interaction leads to the formation of an exciton-electron bound state known as the trion. To get the trion energy we can write down the following trion ansatz:

$$t_{n\sigma\mathbf{p}}^\dagger |0\rangle = \sum_{\mathbf{k}} \varphi_{n\mathbf{k}} x_{\sigma,\beta_x\mathbf{p}-\mathbf{k}}^\dagger e_{-\sigma,\beta_e\mathbf{p}+\mathbf{k}}^\dagger |0\rangle \quad (3.11)$$

where $\beta_x = m_x/(m_e + m_x)$ and $\beta_e = m_e/(m_e + m_x)$ and the internal state n labels both bound and scattering states. We solve $H t_{n\sigma\mathbf{p}}^\dagger |0\rangle = E_{n\mathbf{p}} t_{n\sigma\mathbf{p}}^\dagger |0\rangle$. Acting on the right with $\langle 0| e_{-\sigma,\mathbf{k}+\beta_e\mathbf{p}} x_{\sigma,\beta_x\mathbf{p}+\mathbf{k}}^\dagger$ we obtain:

$$\varphi_{n\mathbf{k}} (\omega_{\beta_x\mathbf{p}-\mathbf{k}} + \xi_{\beta_e\mathbf{p}+\mathbf{k}} - E_{n\mathbf{p}}) + \frac{v}{\mathcal{A}} \sum_{|\mathbf{k}'|<\Lambda} \varphi_{n\mathbf{k}'} = 0 \quad (3.12)$$

Dividing by the term in parenthesis and summing over \mathbf{k} , then dividing by $\sum_{|\mathbf{k}|<\Lambda} \varphi_{n\mathbf{k}}$ we obtain:

$$v^{-1} = \frac{1}{\mathcal{A}} \sum_{|\mathbf{k}|<\Lambda} \frac{1}{\omega_{\beta_x\mathbf{p}-\mathbf{k}} + \xi_{\beta_e\mathbf{p}+\mathbf{k}} - E_{n\mathbf{p}}} \quad (3.13)$$

Notice that the above equation has solutions at the scattering states $E_{n\mathbf{p}} \approx \omega_{\mathbf{p}-\mathbf{k}} + \xi_{\mathbf{k}}$ but it also has a bound state at $E_{n\mathbf{p}} = -\epsilon_T + \mathbf{p}^2/(6m)$. Since the trion binding energy ϵ_T is a readily accessible quantity, we can use express v in terms of this quantity. Therefore from now on, we will use:

$$v^{-1} = \frac{1}{\mathcal{A}} \sum_{|\mathbf{k}|<\Lambda} \frac{1}{\omega_{\beta_x\mathbf{p}-\mathbf{k}} + \xi_{\beta_e\mathbf{p}+\mathbf{k}} + \epsilon_T} \quad (3.14)$$

For the remaining numerical calculations, we use $\epsilon_T = 30 \text{ meV}$ [32] and take the cutoff $\Lambda \rightarrow \infty$ at the end of the calculation.

Before moving on we remark that, because the interaction between excitons and the electrons in the same valley is repulsive, it will not lead to strongly correlated states between excitons and electrons, in contrast to the attractive interaction between excitons and electrons in the opposite valley. Furthermore, as we showed in Sec.2.4, repulsive interactions are strongly renormalized and reduced. For this reason in this chapter, as well as in most of the thesis we will neglect this repulsive interaction. However, this interaction can still have important effects, when electron densities are large. We come back to it in Chapter 2.2, and analyze it in more detail.

To keep things simple, unless otherwise mentioned, we will consider only one species of excitons, interacting with the electrons in the opposite valley. We will consider the interaction between excitons and electrons in the same valley in Chapter 6. Otherwise we will assume that our system is well described by the Hamiltonian:

$$H = \sum_{\mathbf{k}} \omega_{\mathbf{k}} x_{\mathbf{k}}^\dagger x_{\mathbf{k}} + \sum_{\mathbf{k}} \xi_{\mathbf{k}} e_{\sigma\mathbf{k}}^\dagger e_{\mathbf{k}} + \sum_{\mathbf{k}} v_{\mathbf{k}} c_{\sigma\mathbf{k}}^\dagger c_{\mathbf{k}} + \sum_{\mathbf{k}} g(x_{\mathbf{k}}^\dagger c_{\mathbf{k}} + h.c.) \quad (3.15)$$

$$+ \frac{v}{A} \sum_{\mathbf{k}\mathbf{k}'\mathbf{q}} x_{\mathbf{k}+\mathbf{q}}^\dagger x_{\mathbf{k}} e_{\mathbf{k}'-\mathbf{q}}^\dagger e_{\mathbf{k}'} + \frac{u}{2A} \sum_{\mathbf{k}\mathbf{k}'\mathbf{q}} x_{\mathbf{k}+\mathbf{q}}^\dagger x_{\mathbf{k}'-\mathbf{q}}^\dagger x_{\mathbf{k}'} x_{\mathbf{k}}$$

where we reintroduced the exciton-exciton interaction terms and suppressed the valley indices. Notice that we will largely neglect the long-range electron-electron interactions, and discuss them only in Chapter 5.

Before starting our analysis it is useful to sketch the general phase diagram of Bose-Fermi mixtures, so we know what to expect in the following. When the light-matter coupling g is weak, photons merely probe the Bose-Fermi mixture of excitons and electrons. In this regime, our system becomes completely equivalent to the Bose-Fermi mixtures studied in cold atomic gases. Although there has been a lot of recent progress in this field, it is still a largely open problem, and the phase diagram is only partially understood. For this reason we do not attempt to give an accurate description of the different phases in this system, but rather a sketch of what we can reasonably expect. We present a sketch of this phase diagram as a function of n_x and n_e in Fig.3.2.

There are a few points on the phase diagram that are relatively well understood. The point $N_e = N_x = 1$ is a trion state. Since these states are fermionic, it is expected that as we move along the line $n_e = n_x$ the system will be in a Fermi-liquid phase of trions. However, as we increase n_e and

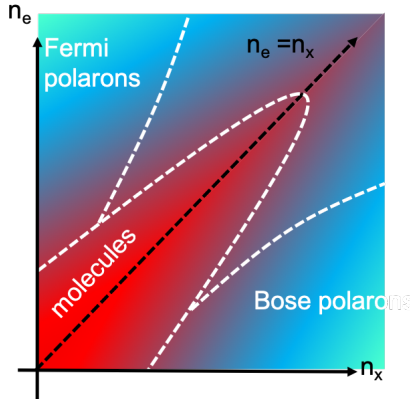


FIGURE 3.2: Rough sketch of the phase diagram of a Bose-Fermi mixture, as a function of the exciton and electron densities

n_x to the point where the inter-trion distance is comparable to the trion Bohr radius, we expect that trions will ionize.

Another regime that is well understood, is the regime of strong density imbalance. In the regime $n_x/n_e \ll 1$ we expect that an exciton, instead of interacting with a single electron to form a trion, would rather prefer to interact with more electrons and form a collective excitation which we call a Fermi polaron. On the other hand, the electron system is barely modified by the presence of excitons, so the electron system forms a normal Fermi sea. Similarly in the opposite limit $n_x/n_e \gg 1$, the low energy physics will be dominated by quasiparticles known as Bose polarons, corresponding to electrons that are dressed by fluctuations in the excitonic system. The exciton system will be only weakly modified by the presence of electrons and will be well approximated by an exciton condensate. We remark that in both of these regimes, there is a competition between trion and polaron formation, and it is generally accepted that the trion state would be lower energy at low densities. However the polaron-trion transition is very sensitive to the dimensionality of the system [33, 34].

3.2 FERMI POLARONS

We restrict our attention now to the case when $n_x \ll n_e$. For clarity we start with the case $g \rightarrow 0$, and then analyze what happens when the light matter coupling is turned on. To understand this regime we start by analyzing the

even more simple problem of a single exciton in the presence of a finite density n_e of electrons.

Our approach is to first find the ground state and low-energy degrees of freedom of a system of N_e electrons (in the absence of the exciton). We will assume that the addition of the exciton can only slightly perturb this ground state, creating few low energy fluctuations. The ground state of a non-interacting electron system is a very simple state called a Fermi sea:

$$|\Theta\rangle = \prod_{|\mathbf{k}| < k_F} e_{\mathbf{k}}^\dagger |0\rangle \quad (3.16)$$

where we introduced the Fermi wavevector $k_F = \sqrt{2\pi n_e}$. The low-energy excitations are electron-hole pair excitations of the form $e_{\mathbf{k}}^\dagger e_{\mathbf{q}} |\Theta\rangle$ where $|\mathbf{q}| \leq k_F$ and $|\mathbf{k}| > k_F$, corresponding to an electron of momentum \mathbf{q} being scattered outside of the Fermi sea to a momentum \mathbf{k} .

The addition of the exciton slightly perturbs the Fermi sea, leading to a new states where the exciton is dressed by low-energy fluctuations. We can write an ansatz for the new eigenstates:

$$|\Psi_{np}\rangle = \varphi_{np} x_{\mathbf{p}}^\dagger |\Theta\rangle + \sum_{\mathbf{kq}} \varphi_{n\mathbf{p}k\mathbf{q}} x_{\mathbf{p}+\mathbf{q}-\mathbf{k}}^\dagger e_{\mathbf{k}}^\dagger e_{\mathbf{q}} |\Theta\rangle \quad (3.17)$$

The first term corresponds to a bare exciton on top of the electron ground state, while the second term corresponds to the exciton creating an electron-hole pair excitation of momentum $\mathbf{k} - \mathbf{q}$ in the ground state. Notice that momentum conservation requires that the exciton feels a recoil of opposite momentum. In principle we could add terms with 2 or more electron-hole pairs. However to be able to solve the problem we truncated the Hilbert space to a single electron-hole pair. This method is aptly called the "truncated-basis method" (it is also called the "Chevy ansatz") and it has been shown to be a particularly useful approximation in cold atom systems [3]. We discuss the extension of the above wavefunction to include higher order terms in Chapter 4. We remark that a very similar approach to describe the exciton spectrum in the presence of an electron gas has been first introduced in [35].

We want to solve $H |\Psi_{np}\rangle = E_{np} |\Psi_{np}\rangle$. Since $|\Psi_{np}\rangle$ is not an eigenstate of the system, acting with H on it takes us outside of the truncated Hilbert

space. We project back into the truncated space, by acting on the left with $\langle \Theta | x_{\mathbf{p}}$ and $\langle \Theta | e_{\mathbf{q}}^{\dagger} e_{\mathbf{k}} x_{\mathbf{p}+\mathbf{q}-\mathbf{k}}$, to obtain the following set of equations:

$$(\omega_{\mathbf{p}} + v n_e) \varphi_{n\mathbf{p}} + \frac{v}{A} \sum_{\mathbf{k}\mathbf{q}} \varphi_{n\mathbf{p}\mathbf{k}\mathbf{q}} = E_{n\mathbf{p}} \varphi_{n\mathbf{p}} \quad (3.18)$$

$$\begin{aligned} & (\omega_{\mathbf{p}+\mathbf{q}-\mathbf{k}} + \xi_{\mathbf{k}} - \xi_{\mathbf{q}} + v n_e) \varphi_{n\mathbf{p}\mathbf{k}\mathbf{q}} \\ & + \frac{v}{A} \varphi_{n\mathbf{p}} + \frac{v}{A} \sum_{\mathbf{k}'} \varphi_{n\mathbf{p}\mathbf{k}'\mathbf{q}} - \frac{v}{A} \sum_{\mathbf{q}'} \varphi_{n\mathbf{p}\mathbf{k}'\mathbf{q}'} = E_{n\mathbf{p}} \varphi_{n\mathbf{p}\mathbf{k}\mathbf{q}} \end{aligned} \quad (3.19)$$

In the above, as well as in the following analysis we will use \mathbf{k}, \mathbf{k}' to denote momenta larger than k_F , and \mathbf{q}, \mathbf{q}' to denote momenta smaller than k_F .

Before we move on, we briefly discuss the origin of the various terms in the above equations. The term in the parenthesis of Eq. (3.18) corresponds to the kinetic energy of a bare exciton $\omega_{\mathbf{p}}$ plus the Hartree interaction between the exciton and the rest of the electrons $v n_e$. The summation in Eq. (3.18) corresponds to processes where the exciton creates an electron-hole pair excitation in the electron system. The terms in the parenthesis of Eq. (3.19) corresponds to the kinetic energy of an exciton of momentum $\mathbf{p} + \mathbf{q} - \mathbf{k}$, an electron of momentum \mathbf{k} and a hole of momentum \mathbf{q} . It also contains the Hartree interaction between the exciton and the Fermi system. The term proportional to $\varphi_{n\mathbf{p}}$ comes due to processes where the electron-hole pair is annihilated. The following two terms correspond to processes where the electron/hole scatters with the exciton due to the exciton-electron interaction.

We remark that the above equations can be solved by discretizing momentum space and turning the resulting equations into a matrix eigenvalue equation. We will discuss this method in more detail in Chapter 6. In this particular case we can simplify the problem further by noticing that the last term on LHS of Eq. (3.19) vanishes as we take the cutoff $\Lambda \rightarrow \infty$ and therefore $v \rightarrow 0$. In contrast, the second to last term survives because (as we will show later) the wavefunction $\varphi_{n\mathbf{p}\mathbf{k}\mathbf{q}}$ scales as $1/|\mathbf{k}|^2$, resulting in a diverging sum which compensates for the decrease in the interaction strength v .

After this simplifications Eq. (3.19) becomes:

$$(\omega_{\mathbf{p}+\mathbf{q}-\mathbf{k}} + \xi_{\mathbf{k}} - \xi_{\mathbf{q}} + v n_e - E_{n\mathbf{p}}) \varphi_{n\mathbf{p}\mathbf{k}\mathbf{q}} + \frac{v}{A} \varphi_{n\mathbf{p}} + \frac{v}{A} \sum_{\mathbf{k}'} \varphi_{n\mathbf{p}\mathbf{k}'\mathbf{q}} = 0 \quad (3.20)$$

The system of equations can be solved by expressing $\sum_{\mathbf{k}} \varphi_{n\mathbf{p}\mathbf{k}\mathbf{q}}$ as a function of $\varphi_{n\mathbf{p}}$ from Eq. (3.20) and plugging this into Eq. (3.18). To do this we

divide Eq. (3.20) by the term in parenthesis and sum the resulting equation over \mathbf{k} . It is straightforward to obtain:

$$\sum_{\mathbf{k}} \varphi_{n\mathbf{p}\mathbf{k}\mathbf{q}} = -\varphi_{n\mathbf{p}} \frac{\frac{v}{\mathcal{A}} \sum_{\mathbf{k}} \frac{1}{\omega_{\mathbf{p}+\mathbf{q}-\mathbf{k}} + \xi_{\mathbf{k}} - \xi_{\mathbf{q}} + v n_e - E_{n\mathbf{p}}}}{1 + \frac{v}{\mathcal{A}} \sum_{\mathbf{k}} \frac{1}{\omega_{\mathbf{p}+\mathbf{q}-\mathbf{k}} + \xi_{\mathbf{k}} - \xi_{\mathbf{q}} + v n_e - E_{n\mathbf{p}}}} \quad (3.21)$$

Plugging this into Eq. (3.18) we obtain:

$$\begin{aligned} & (\omega_{\mathbf{p}} - E_{n\mathbf{p}}) \varphi_{n\mathbf{p}} \\ & + \frac{v}{\mathcal{A}} \sum_{\mathbf{q}} \varphi_{n\mathbf{p}} \left[1 - \frac{\frac{v}{\mathcal{A}} \sum_{\mathbf{k}} \frac{1}{\omega_{\mathbf{p}+\mathbf{q}-\mathbf{k}} + \xi_{\mathbf{k}} - \xi_{\mathbf{q}} + v n_e - E_{n\mathbf{p}}}}{1 + \frac{v}{\mathcal{A}} \sum_{\mathbf{k}} \frac{1}{\omega_{\mathbf{p}+\mathbf{q}-\mathbf{k}} + \xi_{\mathbf{k}} - \xi_{\mathbf{q}} + v n_e - E_{n\mathbf{p}}}} \right] = 0 \end{aligned} \quad (3.22)$$

where we used $n_e = \frac{1}{\mathcal{A}} \sum_{\mathbf{q}}$. Dividing by $\varphi_{n\mathbf{p}}$ and rearranging terms we obtain the following integral equation for the energy:

$$E_{n\mathbf{p}} = \omega_{\mathbf{p}} + \frac{1}{\mathcal{A}} \sum_{\mathbf{q}} \frac{1}{\frac{1}{v} - \frac{1}{\mathcal{A}} \sum_{\mathbf{k}} \frac{1}{E_{n\mathbf{p}} - \omega_{\mathbf{p}+\mathbf{q}-\mathbf{k}} - \xi_{\mathbf{k}} + \xi_{\mathbf{q}} - v n_e}} \quad (3.23)$$

which can be easily solved numerically. It is useful to introduce the exciton-electron T-matrix and the exciton self-energy:

$$T(z, \mathbf{p}) \equiv \left(\frac{1}{v} - \frac{1}{\mathcal{A}} \sum_{|\mathbf{k}| > k_F} \frac{1}{z - \omega_{\mathbf{p}-\mathbf{k}} - \xi_{\mathbf{k}} - v n_e} \right)^{-1} \quad (3.24)$$

$$\Sigma(z, \mathbf{p}) \equiv \frac{1}{\mathcal{A}} \sum_{|\mathbf{q}| < k_F} T(z + \xi_{\mathbf{q}}, \mathbf{p} + \mathbf{q}) \quad (3.25)$$

which allows us to rewrite Eq. (3.23) more compactly as:

$$E_{n\mathbf{p}} = \omega_{\mathbf{p}} + \Sigma(E_{n\mathbf{p}}, \mathbf{p}) \quad (3.26)$$

Notice that we reintroduced the limitations on the \mathbf{q} and \mathbf{k} summations in the above to remind the reader of our convention.

We can also calculate the wavefunction φ . From Eq. (3.20) and Eq. (3.21) we have:

$$\varphi_{n\mathbf{p}\mathbf{k}\mathbf{q}} = \frac{T(E_{n\mathbf{p}} + \xi_{\mathbf{q}}, \mathbf{p} + \mathbf{q})}{E_{n\mathbf{p}} - \omega_{\mathbf{p}+\mathbf{q}-\mathbf{k}} - \xi_{\mathbf{k}} + \xi_{\mathbf{q}} + v n_e} \frac{\varphi_{n\mathbf{p}}}{\mathcal{A}} \quad (3.27)$$

We still need to determine $\varphi_{n\mathbf{p}}$. To do this, we can differentiate the self-energy with respect to the energy:

$$\frac{\partial \Sigma(z, \mathbf{p})}{\partial z} = \frac{1}{\mathcal{A}} \sum_{\mathbf{q}} \frac{\partial T(z + \xi_{\mathbf{q}}, \mathbf{p} + \mathbf{q})}{\partial z} \quad (3.28)$$

$$= -\frac{1}{\mathcal{A}} \sum_{\mathbf{q}} T(z + \xi_{\mathbf{q}}, \mathbf{p} + \mathbf{q})^2 \frac{\partial T^{-1}(z + \xi_{\mathbf{q}}, \mathbf{p} + \mathbf{q})}{\partial z} \quad (3.29)$$

$$= -\frac{1}{\mathcal{A}^2} \sum_{\mathbf{k}\mathbf{q}} \left(\frac{T(z + \xi_{\mathbf{q}}, \mathbf{p} + \mathbf{q})}{z - \omega_{p+q-k} - \xi_k + \xi_q + v n_e} \right)^2 \quad (3.30)$$

$$= -\sum_{\mathbf{k}\mathbf{q}} \left(\frac{\varphi_{n\mathbf{p}\mathbf{k}\mathbf{q}}}{\varphi_{n\mathbf{p}}} \right)^2 \quad (3.31)$$

Using the normalization condition we can solve the above to obtain:

$$\varphi_{n\mathbf{p}}^2 = \left(1 - \frac{\partial \Sigma(\mathbf{p}, z)}{\partial z} \Big|_{z=E_{n\mathbf{p}}} \right)^{-1} \equiv Z(E_{n\mathbf{p}}) \quad (3.32)$$

where we introduced another quantity $Z(\omega)$, which is known as the quasi-particle weight.

At this point we have solved the problem: Eq. (3.26) determines the eigenenergies, while Eq. (3.27) and Eq. (3.32) determine the wavefunctions. Using these equations we can calculate an important observable known as the exciton spectral function, defined as:

$$A_x(\mathbf{p}, \omega) = \sum_n \left| \langle \Psi_{n\mathbf{p}} | x_{\mathbf{p}}^\dagger | 0 \rangle \right|^2 \delta(E_{n\mathbf{p}} - \omega) = \sum_n |\varphi_{n\mathbf{p}}|^2 \delta(E_{n\mathbf{p}} - \omega) \quad (3.33)$$

It can be shown (see Chapter 4) that the spectral function can also be written as:

$$A_x(\mathbf{p}, \omega) = -\pi \text{Im} \left[\frac{1}{\omega + i\eta - \omega_{\mathbf{p}} - \Sigma(\mathbf{p}, \omega + i\eta)} \right] \quad (3.34)$$

where η denotes a positive infinitesimal constant.

We compare the resulting spectral function with experimental absorption data from Ref. [2] in Fig. 3.3. We see that the agreement between the experiment and the theory is remarkable. Looking at the figures, we observe the following features.

When electrons are added to the system, a new resonance appears starting at $-\epsilon_T$. If we did not add the energy shift of $0.8\epsilon_F$ to compensate for

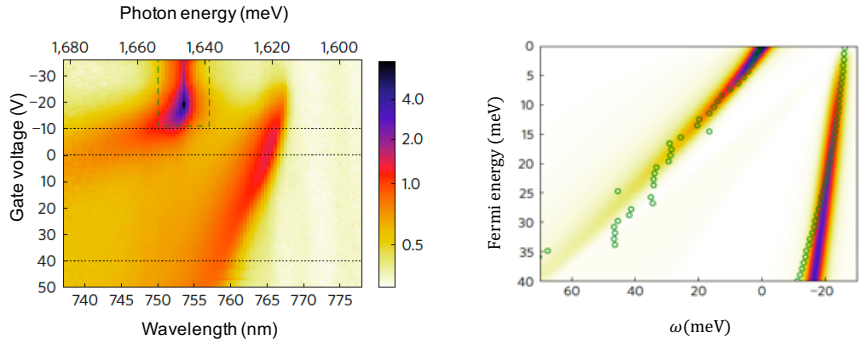


FIGURE 3.3: Left: The MoSe₂ absorption spectrum determined by measuring the enhancement of the cavity linewidth for each cavity frequency and gate voltage (for details see Ref. [2]). Right: Exciton-polaron spectral function $A_x(\mathbf{p} = 0, \omega)$ at different Fermi energies. Since we neglected the repulsive interactions between excitons and electrons in the same valley, in the theory plot, we added by hand a blue shift of all energies by $0.8\epsilon_F$ to compensate. The overlayed green circles denote the position of the attractive/repulsive polaron peaks determined from the experimental data in the left. The agreement is remarkable. We use a broadening of $\eta = 3\text{meV}$.

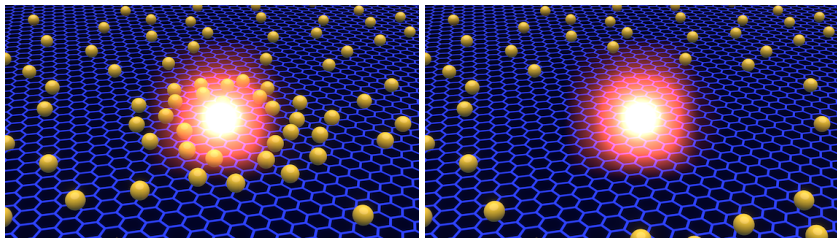


FIGURE 3.4: Schematic representation of attractive-polaron (left) and repulsive polaron (right). The yellow spheres denote the electrons while the shining sphere denotes the exciton

the neglected repulsion between excitons and electrons in the same valley, then this resonance would redshift, signaling attractive interactions with the electrons in the Fermi sea. For this reason we associate this resonance to an *attractive exciton-polaron*. We illustrate this quasiparticle pictorially in Fig. 3.4. Notice that, initially this particle has no oscillator strength but keeps gathering oscillator strength as the Fermi energy increases.

At the same time, the exciton resonance blue-shifts as electrons are added to the system (in addition to the blue-shift term $0.8e_F$ that we added by hand). This shows that this quasiparticle interacts repulsively with the electrons in the Fermi sea, and we call it a *repulsive exciton-polaron*. This is due to the presence of the trion bound state, which acts similar to a Feshbach resonance and induces repulsive interactions for the scattering states. We can represent this quasiparticle pictorially in Fig. 3.4.

Note that our simple model captures remarkably well the energy shift of the two attractive polaron resonances, as well as the oscillator strength transfer between them as the Fermi-energy is increased. It also captures to some extent the broadening of the repulsive polaron. However, as can be seen from the experimental color plot, there is a continuum of states in between the attractive and repulsive polaron which capture a significant portion of the oscillator strength. Although our theoretical model shows that a small portion of this oscillator strength belongs to the trion-hole continuum, the oscillator strength of the trion-hole continuum is barely visible in the theoretical plots. This is due to the limitations of the Chevy ansatz which for instance does not include states corresponding to attractive-polarons accompanied by one or more electron-hole pair. We remedy this to some extent in Chapter 4 when we solve the polaron problem using a

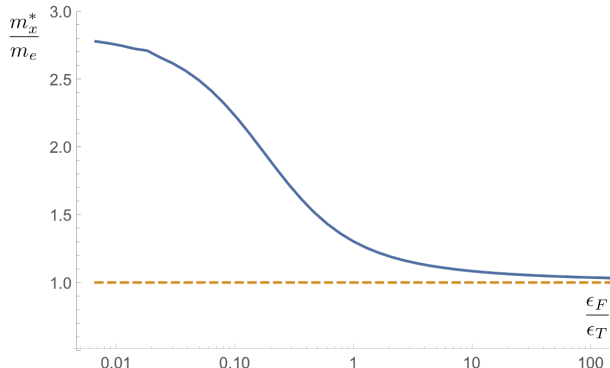


FIGURE 3.5: Polaron mass as a function of Fermi energy, in the Chevy Ansatz.
We took the exciton mass to be twice as large as the electron mass $m_x = 2m_e$.

self-consistent approach that includes an infinite number of electron-hole pair excitations from the Fermi sea.

We emphasize that most previous studies attribute the attractive polaron resonance to the trion, with comparatively few discussions of states similar to the polaron (for a notable exception see Ref. [35]). Our model clearly shows that trions cannot appear in optical excitation spectra because they have vanishing oscillator strength. The proper understanding of the nature of these quasiparticles has important consequences. For instance, while trions are fermionic, polarons are bosonic. As we will show in the later section this ensures that the polaron resonance can couple strongly to photons to form new quasiparticles known as polaron-polaritons.

We also investigate the renormalization of the exciton mass due to the dressing with electrons. Using a Taylor expansion to expand the self-energy around E_{00} and $\mathbf{p} = 0$ we can obtain the dispersion of the attractive polarons. One can check that the polaron mass m_x^* is given by:

$$m_x^* = Z(E_{00}) \left(\frac{1}{m_x} + \left. \frac{\partial^2 \Sigma(E_{00}, \mathbf{p})}{\partial^2 \mathbf{p}} \right|_{\mathbf{p}=0} \right) \quad (3.35)$$

Fig.3.5 shows the dependence of the (normalized) polaron mass m_x^*/m_e on the ratio of the Fermi energy (ϵ_F) to the trion binding energy (ϵ_T). We see that at small Fermi energies the mass of the attractive polaron can be even larger than the trion mass.

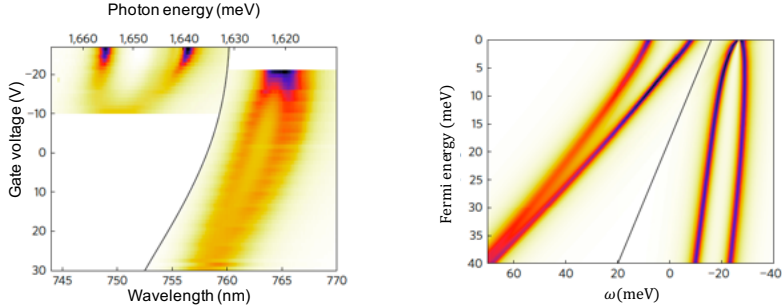


FIGURE 3.6: Left: The white-light transmission spectrum of the fibre cavity incorporating the MoSe₂/hBN/graphene heterostructure, as a function of the gate voltage for two different settings of the cavity length (see Ref. [2]): the left (right) part shows the transmission when the cavity is tuned on resonance with the repulsive (attractive) polaron. For each horizontal line, the cavity frequency is tuned so as to yield two polariton modes with equal peak amplitude. Right: The spectral function calculated using the Chevy ansatz. As before we blue-shift all energies by $0.8\epsilon_F$ to compensate the neglected repulsion with electrons in the same valley.

3.3 FERMI POLARON POLARITONS

Having considered the new quasiparticles that emerge when excitons interacts with electrons, focus now on the case of strong light matter coupling $g \neq 0$ that results in the hybridization of photons with excitons into (exciton) polaritons.

As before we truncate the Hilbert space and make the ansatz:

$$|\Psi_{np}\rangle = \varphi_{np}^c c_p^\dagger |\Theta\rangle + \varphi_{np}^x x_p^\dagger |\Theta\rangle + \sum_k \varphi_{n p k q} x_{p+q-k}^\dagger e_k^\dagger e_q |\Theta\rangle \quad (3.36)$$

Notice that, in the above we neglected the coupling to states such as $e_{p+q-k}^\dagger e_k^\dagger e_q |\Theta\rangle$. This is because such states would be very high energy due to the small photon mass. Therefore, except for a very small phase space (i.e. when $p + q - k$ is smaller than the photon momentum) these states are far detuned and therefore can be neglected.

Performing an analysis similar to the one before we obtain the following equation for the eigenenergies:

$$E_{np} = \omega_p + \frac{g^2}{E_{np} - \nu_p} + \Sigma(p, E_{np}) \quad (3.37)$$

Notice that, in addition to the self-energy due to the interaction with electrons, the exciton acquires a self-energy due to the hybridization with the cavity photons. Once again we can write down the exciton spectral function as:

$$A_x(\mathbf{p}, \omega) = \sum_n |\varphi_{n\mathbf{p}}^x|^2 \delta(\omega - E_{n\mathbf{p}}) \quad (3.38)$$

$$= -\pi \text{Im} \left[\frac{1}{\omega - \omega_{\mathbf{p}} - \frac{g^2}{\omega - \nu_{\mathbf{p}}} - \Sigma(\mathbf{p}, \omega + i\eta) + i\eta} \right] \quad (3.39)$$

We remark that we can rewrite Eq. (3.37) as:

$$E_{n\mathbf{p}} = \nu_{\mathbf{p}} + \frac{g^2}{E_{n\mathbf{p}} - \omega_{\mathbf{p}} - \Sigma(\mathbf{p}, E_{n\mathbf{p}})} \quad (3.40)$$

which shows that we can also interpret the new states as photons being dressed with exciton-polarons. The above equation allows us to write down the photon spectral function as:

$$A_c(\mathbf{p}, \omega) = \sum_n |\varphi_{n\mathbf{p}}^c|^2 \delta(\omega - E_{n\mathbf{p}}) \quad (3.41)$$

$$= -\pi \text{Im} \left[\frac{1}{\omega - \nu_{\mathbf{p}} - \frac{g^2}{\omega - \omega_{\mathbf{p}} - \Sigma(\mathbf{p}, \omega) + i\eta} + i\eta} \right] \quad (3.42)$$

We compare the cavity spectral function with the experimental data in Fig.3.6. Once again, the agreement with the experimental data is quite remarkable. In these figures, the cavity-photon energy is tuned to the repulsive (attractive) polaron energy. We see that the splitting of the repulsive polaron collapses as the electron density is increased. This is due to the loss of oscillator strength compounded by the increase in linewidth of the repulsive polaron. As the electron density is increased, the oscillator strength is not lost but instead it is transferred to the attractive polaron.

Although the experiments show an eventual collapse of the splitting for the attractive polaron resonance, this is not captured by our simple theoretical model. This can be attributed to the limitations of the Chevy ansatz. Extending the ansatz to allow more electron-hole pair excitations should capture the loss of oscillator strength to the continuum of states in between the attractive and repulsive polaron and possibly capture the experimental observation of the collapse of the polariton splitting. However, it is possible that at large electron densities, even the exciton is no longer a rigid object (see Chapter 6), which would also explain the collapse of the splitting.

3.4 BOSE-POLARON POLARITONS

Similar physics can be observed in the opposite regime $n_x \gg n_e$. In this case the problem is directly connected to the problem of a single electron in a bath of polaritons, and therefore we focus on this problem in the following. We remark that closely related Bose-polaron states in TMDs have been investigated in Ref. [36] in the context of Bose-Bose mixtures.

This section is organized as follows. We begin in Sec.3.4.1 by analyzing the excitations of a driven-dissipative polariton condensate. Then in Sec.3.4.2 we introduce a simple ansatz for the Bose-polaron quasiparticles resulting from the dressing of electrons by fluctuations in the polariton condensate. After this, in Sec.3.4.3 we show how similar results can be obtained from a much simpler effective model, that better illustrates the nature of the quasiparticles and will be useful later on.

3.4.1 Weakly interacting polariton gas

By pumping the lower polariton branch with a resonant laser field we can sustain a polariton BEC at $k = 0$. In contrast to the classic BEC, the polariton condensate is a driven-dissipative condensate, in which the pump must compensate the polariton losses. In our system the losses are mainly due to the leakage of photons through the cavity mirrors. However, the effects due to the driven-dissipative nature of the condensate are limited to small momenta around $k = 0$ and for the purpose of our paper we can just assume that the pump compensates losses to sustain a finite polariton number in the $k = 0$ state [1]. We do not discuss polarization effects although this extra degree of freedom might be used for our advantage. For example the polariton-polariton interaction is polarization dependent [28].

In order to discuss this problem we have to first solve the problem of the (weakly) interacting Bose gas. Fortunately (in contrast to the interacting electron system), this is one of the few many-body problems that is comparatively well understood. It is well established that the ground state of a Bose gas at zero temperature is a Bose-Einstein condensate (BEC) and the low energy excitations are so-called bogolon excitations.

Compared to the Fermi polaron analysis we consider directly the strong-coupling regime, i.e. $g \neq 0$. This is because in realistic systems, disorder would destroy the exciton coherence and prohibit the formation of condensates, making the a discussion of the $g \rightarrow 0$ regime largely academic.

In contrast, polaritons are not very susceptible to disorder, due to their ultra-low mass and they can routinely form condensates.

Since we want to focus on the low-energy physics, we neglect the coupling to the higher energy upper-polaritons in the following. We can write down the following Hamiltonian for the interacting polariton system:

$$H_{aa} = \sum_{\mathbf{k}} \Omega_{\mathbf{k}} a_{l\mathbf{k}}^\dagger a_{l\mathbf{k}} + \frac{u}{2\mathcal{A}} \sum_{\mathbf{k}\mathbf{k}'\mathbf{q}} \alpha_{\mathbf{k}+\mathbf{q}} \alpha_{\mathbf{k}} \alpha_{\mathbf{k}'-\mathbf{q}} \alpha_{\mathbf{k}'} a_{l,\mathbf{k}+\mathbf{q}}^\dagger a_{l,\mathbf{k}'-\mathbf{q}}^\dagger a_{l\mathbf{k}'} a_{l\mathbf{k}}$$
(3.43)

In the absence of interactions all polaritons would occupy the $\mathbf{k} = 0$ state. It seems reasonable that, if interactions are weak enough, the ground state in the presence of interactions will not be very different from the non-interacting ground state. Because of this we expect that the most important terms in the interaction term (the one proportional to u) are the ones proportional to a_0^\dagger or a_0 . We therefore make the approximation of keeping only terms that contain four or two such operators (there are no terms with three such operators due to momentum conservation), to obtain the Hamiltonian:

$$H_{aa} \approx \sum_{\mathbf{k}} \omega_{\mathbf{k}} a_{\mathbf{k}}^\dagger a_{\mathbf{k}} + \frac{u}{2\mathcal{A}} \left[\alpha_0^4 x_0^\dagger a_0^\dagger a_0 a_0 + 4\alpha_0^2 a_0^\dagger a_0 \sum_{\mathbf{k} \neq 0} a_{\mathbf{k}}^\dagger a_{\mathbf{k}} \right. \\ \left. + \sum_{\mathbf{k} \neq 0} \left(\alpha_0^2 a_0^\dagger a_0^\dagger a_{\mathbf{k}} a_{-\mathbf{k}} + h.c. \right) \right]$$
(3.44)

Introducing the particle number $N_a = a_0^\dagger a_0 + \sum_{\mathbf{k} \neq 0} a_{\mathbf{k}}^\dagger a_{\mathbf{k}}$ we can rewrite the Hamiltonian as:

$$H_{aa} \approx \frac{N_a(N_a - 1)u\alpha_0^4}{2\mathcal{A}} + \Omega_0 x_0^\dagger a_0 + \sum_{\mathbf{k} \neq 0} (\Omega_{\mathbf{k}} + n_a \alpha_0^2 u) a_{\mathbf{k}}^\dagger a_{\mathbf{k}} \\ + \frac{u\alpha_0^2}{2\mathcal{A}} \sum_{\mathbf{k} \neq 0} \left(a_0^\dagger a_0^\dagger a_{\mathbf{k}} a_{-\mathbf{k}} + h.c. \right)$$
(3.45)

where we neglected terms of the order of $\sum_{\mathbf{k} \neq 0} a_{\mathbf{k}}^\dagger a_{\mathbf{k}}$ assuming that most polaritons remain in the condensate once interactions are turned on.

We now make the crucial approximation of replacing $a_0^\dagger \approx a_0 \approx \sqrt{N_0}$ to obtain a quadratic Hamiltonian:

$$H_{aa} = E_0 + \sum_{\mathbf{k} \neq 0} \left[\left(\Omega_{\mathbf{k}} + n_a u \alpha_0^2 \right) a_{\mathbf{k}}^\dagger a_{\mathbf{k}} + \frac{u\alpha_0^2 n_a}{2} (a_{\mathbf{k}} a_{-\mathbf{k}} + h.c.) \right]$$
(3.46)

where $E_0 = N_a\Omega_0 + n_a(N_a - 1)u\alpha_0^4$ is a constant energy shift.

The Hamiltonian above can be diagonalized by performing a symplectic transformation known as the Bogolyubov transformation:

$$b_{\mathbf{k}} = u_k a_{\mathbf{k}} + v_k a_{-\mathbf{k}}^\dagger \quad (3.47)$$

For this to be a canonical transformation we have to impose $[b_{\mathbf{k}}, b_{\mathbf{k}}^\dagger] = 1$ which implies that $|u_k|^2 - |v_k|^2 = 1$. Notice that the phases are irrelevant and therefore we choose $u_k, v_k \in \text{Re}$ (also, notice that u_k, v_k depend only on the magnitude of \mathbf{k}). The above can be inverted to obtain:

$$a_{\mathbf{k}} = u_k b_{\mathbf{k}} - v_k b_{-\mathbf{k}}^\dagger \quad (3.48)$$

To diagonalize the Hamiltonian we must choose:

$$u_k = \sqrt{\frac{\Omega_{\mathbf{k}} + n_a u \alpha_0^2 + E_{\mathbf{k}}}{2E_{\mathbf{k}}}} \quad (3.49)$$

$$v_k = -\sqrt{\frac{\Omega_{\mathbf{k}} + n_a u \alpha_0^2 - E_{\mathbf{k}}}{2E_{\mathbf{k}}}} \quad (3.50)$$

where we introduced the excitation spectrum of the new quasiparticles:

$$E_{\mathbf{k}} \equiv \sqrt{\Omega_{\mathbf{k}}(\Omega_{\mathbf{k}} + 2n_a u \alpha_0^2)} \quad (3.51)$$

We can rewrite the Hamiltonian in the new basis as:

$$H_{xx} = E_0 + \sum_{\mathbf{k} \neq 0} E_{\mathbf{k}} b_{\mathbf{k}}^\dagger b_{\mathbf{k}} \quad (3.52)$$

The new collective degrees of freedom are called bogolons, and are the (gapless) Goldstone modes that appear due to the breaking of gauge symmetry.

Given the form of the mean-field Hamiltonian Eq. (3.46) we can immediately guess that the ground state should contain coherent superpositions of \mathbf{k} and $-\mathbf{k}$ pairs, and we can write it as:

$$|\Theta\rangle = C e^{\sqrt{N_0} a_0^\dagger + \beta_{\mathbf{k}} a_{\mathbf{k}}^\dagger a_{-\mathbf{k}}^\dagger} |0\rangle \quad (3.53)$$

where C is a normalization constant, and N_0 denotes the number of excitons in the condensate. The coefficients β can be obtained by imposing the condition $b_{\mathbf{k}} |\Theta\rangle = 0$ which implies that $\beta_{\mathbf{k}} = -v_k/u_k$.

It is important to investigate these modes in more detail. Notice that, at small momenta $\mathbf{k} \rightarrow 0$, the bogolon dispersion is linear $E_{\mathbf{k}} \propto \mathbf{k}$ and the bogolon modes represent collective sound modes of the condensate. On the other hand, at large momenta the bogolon dispersion returns to the free exciton dispersion and the bogolon modes turn into free excitons. The point in momentum space where this transition happens is given by the inverse of the healing length defined as $\xi = (n_a u \alpha_0^2 m_a)^{-1/2}$. Notice that we also implicitly assumed that $g \gg \hbar^2 / (2m_a \xi^2)$ which means that $g \gg u \alpha_0^2 n_a$, otherwise we would have to take into account the non-parabolic nature of the polariton dispersion when defining the scattering length. We remark that the healing length is very large for polariton systems due to the ultra-low polariton mass.

In the following we will focus on the regime $g \gg u \alpha_0^2 n_a$ and investigate the dressing of electrons by bogolon excitations from the condensate. The size of the dressing cloud is going to be orders of magnitude smaller than the healing length (as well as the photon wavelength), meaning that the long-wavelength collective excitations will play virtually no role in the dressing. Therefore, for our purposes, we can approximate the many-body ground state and excitations by:

$$|\Theta\rangle \approx C e^{\sqrt{N_0} a_0^\dagger} |0\rangle, \quad b_{\mathbf{k}} \approx a_{\mathbf{k}}, \quad u_k \approx 1, \quad v_k \approx 0. \quad (3.54)$$

At this point, the reader might wonder why we kept the previous discussion so general, when it could have been simplified by focusing on the regime $g \gg u \alpha_0^2 n_a$ from the beginning. The reason is twofold. First, the previous discussion allowed us to better justify Eq. (3.54). Furthermore, in Chapter 8 we will consider a parameter regime where this condition is no longer satisfied, and we will require the results of the previous discussion.

3.4.2 Bose-polaron formation

Having discussed the ground state and low energy fluctuations of a weakly interacting polariton gas, we investigate now what happens when we add an electron in this Bose gas.

Before proceeding we rewrite the Hamiltonian in the new basis. Using Eq. (3.54):

$$\begin{aligned} H = & \sum_{\mathbf{k}} \xi_{\mathbf{k}} e_{\mathbf{k}}^{\dagger} e_{\mathbf{k}} + \sum_{\mathbf{k}} (\omega_{\mathbf{k}} + \Delta) x_{\mathbf{k}}^{\dagger} x_{\mathbf{k}} + \frac{u}{\mathcal{A}} \sum_{\mathbf{kq}} x_{\mathbf{k}+\mathbf{q}}^{\dagger} x_{\mathbf{k}'-\mathbf{q}}^{\dagger} x_{\mathbf{k}'} x_{\mathbf{k}} \quad (3.55) \\ & + \frac{v\sqrt{N_0}\alpha_0}{\mathcal{A}} \sum_{\mathbf{kq}} e_{\mathbf{k}+\mathbf{q}}^{\dagger} e_{\mathbf{k}} \left(x_{\mathbf{q}} - x_{-\mathbf{q}}^{\dagger} \right) + \frac{v}{\mathcal{A}} \sum_{\mathbf{k}\mathbf{k}'\mathbf{q}} e_{\mathbf{k}+\mathbf{q}}^{\dagger} e_{\mathbf{k}} x_{\mathbf{k}'-\mathbf{q}}^{\dagger} x_{\mathbf{k}'} \end{aligned}$$

where $\Delta \equiv \omega_0 - \Omega_0$ and we replaced the polariton operators by exciton operators since we will be looking at short-wavelength excitations.

Notice that, after our simplifying assumptions, the excitations out of the condensate have a gap Δ . While this is an artefact of our approximation, it nevertheless captures the correct physics. Furthermore, this ideal regime could in principle be reached by making the size of the cavity in the 2D plane so small to be essentially zero-dimensional cavities. This allows us to study the physics of mobile impurities in incompressible states, and could provide valuable insights into the physics of impurities in more complicated incompressible states such as the states in the integer and fractional quantum Hall states.

At this point we can write down an ansatz for the Bose polaron, similar to our Fermi polaron ansatz:

$$|\Psi_{n\mathbf{p}}\rangle = \varphi_{n\mathbf{p}} e_{\mathbf{p}}^{\dagger} |\Theta\rangle + \sum_{\mathbf{k}} \varphi_{n\mathbf{p}\mathbf{k}} e_{\mathbf{p}-\mathbf{k}}^{\dagger} x_{\mathbf{k}}^{\dagger} |\Theta\rangle \quad (3.56)$$

where we truncated the Hilbert space to a single excitation from the condensate. While this proved to be a good approximation for the Fermi polaron, this was closely related to the statistics of the bath particles, since Pauli blocking would forbid the accumulation of many fermions close to the exciton. If excitons were true bosons then it is not clear how good such an approximation is. But in fact excitons are composite bosons and behave like bosons as long as they live in extended states. Indeed, it is well known that, when the exciton densities reach values of $n_x a_x^2 \approx 0.1$ the excitons tend to dissociate due to their composite nature, implying that repulsive interactions are crucial when the distance between excitons is comparable to their Bohr radius.

However, these assumptions should be evaluated more carefully. We remark that it would be straightforward to extend the above ansatz to include terms with two bogolons (excitons), to double check the effect of exciton-exciton interactions, and whether our truncated ansatz is a good approximation.

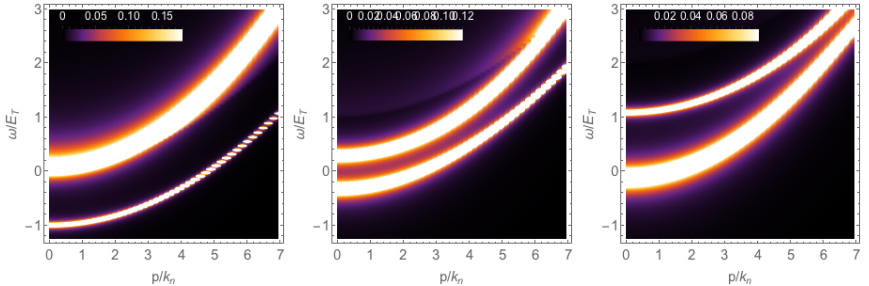


FIGURE 3.7: Bose-polaron spectral function $A_e(\mathbf{p}, \omega)$ as a function of momentum \mathbf{p} (in units of the inter-exciton distance $k_n \equiv \sqrt{4\pi n_0}$) and energy ω in units of the trion binding ϵ_T . On the left $\Delta = 0.1\epsilon_T$, in the middle $\Delta = \epsilon_T$ and on the right $\Delta = 2\epsilon_T$. We used an artificial broadening $\eta = \epsilon_T/100$, an exciton density $k_n/a_{2D} = 0.5$ where $a_{2D} \equiv \sqrt{m_e\epsilon_T}/\hbar$, and $\alpha_0 = 1/\sqrt{2}$.

A similar analysis to the one in the previous section yields the following equation for the polaron energy:

$$E_{n\mathbf{p}} = \xi_{\mathbf{p}} + \Sigma(\mathbf{p}, E_{n\mathbf{p}} + i\eta) \quad (3.57)$$

where we introduced the self-energy and the same exciton-electron T-matrix that we encountered in the Fermi-polaron problem:

$$\Sigma(\mathbf{p}, z) = n_0\alpha_0^2 T(\mathbf{p}, z - \Delta) \quad (3.58)$$

$$T(\mathbf{p}, z)^{-1} = u^{-1} - \frac{1}{A} \sum_{\mathbf{k}} \frac{1}{z - \xi_{\mathbf{k}} - \omega_{\mathbf{k}}} = \frac{2\pi}{\mu} \frac{1}{\log(\epsilon_T/z) + i\pi} \quad (3.59)$$

The electron spectral function is simply:

$$A_e(\mathbf{p}, \omega) = -\pi \text{Im} \left[\frac{1}{\omega + i\eta - \xi_{\mathbf{p}} - \Sigma(\mathbf{p}, \omega + i\eta)} \right] \quad (3.60)$$

We plot the Bose-polaron spectral function in Fig. 3.7 for different values of Δ/ϵ_T . We see that the spectral function exhibit very similar features to the Fermi-polaron spectral function. Remarkably, we see that transfer of oscillator strength is strongest when $\Delta/\epsilon_T = 1$. At this point the electron quasiparticle will be formed by equal superpositions of an electron and a trion.

Compared to the Fermi-polaron problem, we do not have direct access experimentally to the electron spectral function, we cannot verify the accuracy of our results.

3.4.3 Effective Bose-polaron model

Notice that, in the vicinity of the trion energy $-\epsilon_T$ we can approximate as a simple pole:

$$T \approx \frac{2\pi}{\mu} \frac{\epsilon_T}{z + \epsilon_T} + \mathcal{O}\left(\frac{z + \epsilon_T}{\epsilon_T}\right)^2 \quad (3.61)$$

Therefore as long as $|z + \epsilon_T| \ll \epsilon_T$ we write down an effective theory that takes into account only the coupling to the trion:

$$\begin{aligned} H_{eff} = & \sum_{\mathbf{k}} \xi_{\mathbf{k}} e_{\mathbf{k}}^\dagger e_{\mathbf{k}} + \sum_{\mathbf{k}} \Omega_{\mathbf{k}} a_{\mathbf{k}}^\dagger a_{\mathbf{k}} + \sum_{\mathbf{k}} (\omega_{\mathbf{k}}^T - \epsilon_T + \Delta) t_{\mathbf{k}}^\dagger t_{\mathbf{k}} \quad (3.62) \\ & + \sum_{\mathbf{kq}} \frac{g}{\sqrt{A}} t_{\mathbf{q}}^\dagger (\alpha_{\mathbf{k}} a_{\mathbf{k}} e_{\mathbf{q}-\mathbf{k}} + h.c.) \end{aligned}$$

where $g = \sqrt{\frac{2\pi}{\mu} \epsilon_T}$ and $\omega_{\mathbf{k}}^T = \mathbf{k}^2 / (2(m_x + m_e))$, and we should remember that the interaction g should have a UV cutoff of the order of the inverse trion Bohr radius. Notice that we switched back to the polariton operators a .

We caution that the trion is formed from the exciton-electron interaction and therefore in writing down the above we have already taken this interaction into account. To avoid double counting the trion mode should not be dressed again by the interaction with electrons and excitons.

Making the Bogolyubov approximation $a_0 = a_0^\dagger = \sqrt{n_0}$ and keeping only the terms proportional to $\sqrt{n_0}$ we obtain the Hamiltonian:

$$\begin{aligned} H_{eff} = & \sum_{\mathbf{k}} \xi_{\mathbf{k}} e_{\mathbf{k}}^\dagger e_{\mathbf{k}} + \sum_{\mathbf{k}} \left(\Delta + \omega_{\mathbf{k}} x_{\mathbf{k}}^\dagger x_{\mathbf{k}} \right) + \sum_{\mathbf{k}} (\omega_{\mathbf{k}}^T - \epsilon_T + \Delta) t_{\mathbf{k}}^\dagger t_{\mathbf{k}} \\ & + \sum_{\mathbf{k}} g \alpha_{\mathbf{k}} \sqrt{n_0} t_{\mathbf{k}}^\dagger e_{\mathbf{k}} + \sum_{\mathbf{kq}} \frac{g}{\sqrt{A}} t_{\mathbf{q}}^\dagger (x_{\mathbf{k}} e_{\mathbf{q}-\mathbf{k}} + h.c.) \end{aligned}$$

where we used once again the fact that $a_{\mathbf{k}} \rightarrow x_{\mathbf{k}}$ for $\mathbf{k} \neq 0$ as we justified in Eq. (3.54).

Focusing only on the coupling proportional to $\sqrt{n_0}$ we remark that the problem is reduced to a simple problem of the hybridization of two modes. This can be solved through the same type of canonical transformation as introduced for the trion. Doing this it is easy to check that we obtain the new modes:

$$e_{l\mathbf{k}}^\dagger = \gamma_{\mathbf{k}} e_{\mathbf{k}}^\dagger + \theta_{\mathbf{k}} t_{\mathbf{k}}^\dagger \quad (3.63)$$

$$e_{u\mathbf{k}}^\dagger = -\theta_{\mathbf{k}} e_{\mathbf{k}}^\dagger + \gamma_{\mathbf{k}} t_{\mathbf{k}}^\dagger \quad (3.64)$$

(for the precise values of these terms check Eq. (2.21) and Eq. (2.22)). The new energies can also be obtained easily:

$$E_{l/u,\mathbf{k}} = \frac{\xi_{\mathbf{k}} + \omega_{\mathbf{k}}^T + \Delta - \epsilon_T}{2} \mp \sqrt{\frac{(\xi_{\mathbf{k}} - \omega_{\mathbf{k}}^T - \Delta + \epsilon_T)^2}{4} + n_0 \alpha_0^2 g^2} \quad (3.65)$$

which are precisely the same energies as in our more rigorous derivation.

To conclude this Section we remark that the gap Δ that appears due to the light matter coupling allows us to tune the amount of dressing. Indeed if we choose $\Delta \approx \epsilon_T$ then we bring the trion state into resonance, and we strongly increase the interactions between electrons and the polariton condensate. Remarkably, in this regime the electrons and trions will hybridize, and the electron quasiparticle weight would be $Z = 0.5$, regardless of the strength of the coupling $g\sqrt{n_0}$. This can be used in essence as a Feshbach resonance, in the sense that it allows us to tune the position of the trion resonance at will.

3.5 CONCLUSION

In this chapter we first introduced the electron-polariton interaction that is at the basis of the Bose-Fermi mixtures that we will investigate for the rest of the thesis. We then analyzed this system in two different regimes.

We considered first the regime of small exciton/polariton densities when the excitons/polaritons form new Fermi-polaron quasiparticles. The results in this chapter establish electron-polariton Bose-Fermi mixtures in TMD monolayers, as a new paradigm for quantum impurity and polaron physics. In stark contrast to prior work, we identify the optical excitations that are accessible in resonant spectroscopy as repulsive and attractive exciton polarons and polaron-polaritons, which are simultaneously present for Fermi energies that are smaller than the molecular (trion) binding energy.

We also investigated the opposite regime $n_x/n_e \gg 1$. In this case we showed the emergence of new Bose-polaron quasiparticles and we discussed the effect of the polariton dispersion on the polaron dressing. This is a first step towards controlling the electron properties using light fields. We will discuss a similar scenario in Ch.8 where we show that in a repulsively interacting electron-polariton Bose-Fermi mixture, polaritons can induce strong attractive interactions between electrons, that can lead to superconductivity. It would be interesting to investigate the superconducting transition starting from the Bose-polaron framework.

4

POLARON INTERACTIONS

We solve the polaron problem using a self-consistent ladder approximation, going beyond the Chevy ansatz approach in the previous chapter. We introduce the Baym-Kadanoff conserving approximation and show how to use it to derive all diagrams corresponding to the interaction between quasiparticles. We estimate these diagrams using some reasonable approximations and show that interactions are strongly enhanced due to the polaron dressing.

In the previous chapter we mentioned Landau's quasiparticle framework, which allows one to build a hierarchical understanding of interactions by treating collective excitations of particles as if they were particles themselves with renormalized properties. We looked at a Bose-Fermi mixture formed by polaritons and electrons in the density imbalanced regime, and obtained the polaron quasiparticles that dominate the low energy physics. In this chapter we complete the quasiparticle description by investigating the interactions between the polaron quasiparticles.

In order to treat interactions and go beyond the Chevy ansatz approach introduced in the previous chapter, we introduce the many-body Green's function technique. To present this method in the simplest way possible we show how one can solve the Fermi polaron-problem using a diagrammatic technique. The specific characteristics of the impurity problem allows the Green's function approach to be greatly simplified and we do not need to introduce the concept of time ordered Green's functions, Wick's theorem or other concepts that are usually used to justify this method. Still, this simplified problem exhibits similar features to the more general Green's function theory, such as the diagrammatic representation of equations and Dyson's equation for the self-energy. We remark that the reason why the treatment of the impurity problem using many-body techniques is greatly simplified is also the reason why we were able to solve the polaron problem using the simple wavefunction approach presented in Chapter 3.

Then, we discuss the importance of choosing the right diagrams and we introduce the ideas behind the conserving approximation which provides a prescription for generating approximations that conserve energy, momentum and particle number. This conserving approximation will be

our guiding principle in choosing diagrams, which we will often use in this thesis.

We also derive the diagrams corresponding to the interaction between two polarons, in a conserving approximation. We identify three types of interactions between polarons. The first type of interaction relies on exchange of excitations between the polarons, and corresponds to the usual mechanism describing particle interactions. The second type of interaction, comes from the dressing of the bath particles due to the interaction with the mobile impurities, a contribution which is generally neglected when discussing polaron physics. The third type of interaction arises from a change in chemical potential of the bath due to the addition of impurities, an effect which is present only in experiments where the number of impurities is conserved. The latter terms are usually neglected when discussing polaron interactions, under the assumption that the mobile impurities have a negligible effect on the bath particles. However, this effect cannot be neglected when discussing polaron interactions, because it is of the same order as the usual mechanism relying on exchange of quasiparticles.

We argued that the latter process should dominate the interactions of polaron-polaritons. Remarkably, an estimate of this contribution yielded an interaction between polaron-polaritons that is 20 times larger than the interaction between bare polaritons, showing how the dressing with polarization waves in the electron system can strongly enhance photon nonlinearities, by more than an order of magnitude.

We also investigated the interaction between Bose-polarons. In this case we concentrated on the interaction between polarons mediated by the exchange of bogolons from the condensate. We find that the strength of electron-electron interactions can be tuned by the cavity detuning, and the laser intensity, opening up the possibility to tune electron-electron interactions using light. We leave a discussion of the consequences of polariton-mediated electron-electron attraction to Ch.8.

The chapter is organized as follows. We begin by introducing the concept of Feynman diagrams through solving the Fermi-polaron problem using a diagrammatic method based on retarded many-body Green's functions in Sec.4.1. After this we present the conserving approximation in Sec.4.2. We then solve the Fermi-polaron problem using a self-consistent ladder approximation in Sec.4.3. This approximation allows us to go well beyond the Chevy ansatz and actually include an infinite number of excitations in the polaron dressing cloud. We extend this analysis to polaron-polaritons

in Sec.4.4 . We end this chapter with a discussion of polaron interactions in Sec.4.5 followed by a conclusion.

4.1 MANY-BODY GREEN'S FUNCTIONS

Before beginning our analysis of polaron interactions we discuss the theoretical tools that we will employ. Although the wavefunction technique that we used in the previous chapter was very useful and allowed us to gain a very good understanding of the polaron quasiparticles, this technique has its drawbacks. In particular, it is difficult to extend the ansatz that we used to capture the residual interactions between quasiparticles. Diagrammatic techniques are better suited for such tasks, but they can often seem unnecessarily complicated. For this reason, we briefly discuss these techniques before moving on.

In the previous chapter we introduced a method that allowed us to obtain all the eigenstates of the system in a truncated Hilbert space. Clearly, this method would quickly become impracticable if we enlarged the Hilbert space. Indeed, even for the problem of two polarons, the Hilbert space would be too large. Furthermore, most of the information contained in the eigenstates was not interesting, and we were interested only in a combination of eigenstates corresponding to the impurity spectral function. For the Fermi polaron this physical observable was the Fourier transform of:

$$A(\mathbf{p}, \tau) = -\frac{1}{\pi} \text{Im} \left[-i\theta(\tau) \langle \Theta | [x_{\mathbf{p}}(t + \tau), x_{\mathbf{p}}^\dagger(t)] | \Theta \rangle \right] \quad (4.1)$$

where $\theta(\tau)$ denotes the Heaviside step function, while $|\Theta\rangle$ denotes the many-body ground state, and we introduced the time dependent operators $x_{\mathbf{p}}(t) \equiv e^{iHt} x_{\mathbf{p}} e^{-iHt}$. The quantity inside the square brackets is aptly called a propagator (more specifically, it is the retarded propagator). It corresponds to a thought experiment where one subtracts the amplitudes of two related processes. In the first process an additional exciton is introduced at time t in the system. The interactions with other particles result in a complicated evolution of the many-body state of the system. One then calculates the amplitude of the overlap of this many-body state at time $t + \tau$ with the initial state at t . To obtain the propagator, one subtracts from this the amplitude for a very similar process where one removes an exciton from the system at time t , let's the system evolve for a time τ and then looks at the overlap with the initial ground-state.

The Green's function method is based on the fact that most observables depend only on few particle correlations, such as the single particle propa-

gator that we introduced above. This reduces the complexity of determining the eigenstates of the many-body system to determining such correlations. However, except for a few special cases these Green's functions can be calculated only perturbatively, starting from the Green's functions in the absence of interactions.

4.1.1 Green's function approach to the Fermi polaron problem

Introductions to the theory of many-body Green's functions can be found in many good references [10, 37], so we will not attempt to rederive it here. However, it is probably useful to sketch the main ideas behind it. Therefore, we illustrate in this subsection how to solve the many-body Fermi-polaron problem (that we already solved in Sec.3.2) using diagrammatic techniques. Then, in the next subsection we present the general (Feynman) rules governing the calculation of diagrams, without attempting to justify them.

Before moving on, we remark that the problem of a single polaron does not require the development of all the machinery of Feynman diagrams. This is because (in Eq. (4.1)) the many-body ground state $|\Theta\rangle$ is already known before the addition of the exciton. Indeed, the usefulness of the many-body Green's functions is precisely for cases when the state $|\Theta\rangle$ is unknown. However, even in this simple case, we will encounter most of the general ideas behind this method. Furthermore, this simple derivation will also clarify which class of many-body problems can be solved using the simple wavefunction method introduced in the previous chapter.

We want to calculate the exciton Green's function, defined as (the $-i$ phase is convention):

$$G_x(\mathbf{p}, \tau) = -i\theta(\tau) \langle \Theta | x_{\mathbf{p}}(t + \tau) x_{\mathbf{p}}^\dagger(t) | \Theta \rangle = -i\theta(\tau) \langle \Theta | x_{\mathbf{p}} e^{-iH\tau} x_{\mathbf{p}}^\dagger | \Theta \rangle \quad (4.2)$$

where we defined the energy of the electrons ground state in the absence of the exciton to be zero, to neglect a trivial phase. Taking the Fourier transform of the above we obtain:

$$G_x(\mathbf{p}, \omega) = \int d\tau e^{i\omega\tau} G_x(\mathbf{p}, \tau) = \langle \Theta | x_{\mathbf{p}} \frac{1}{\omega - H + i\eta} x_{\mathbf{p}}^\dagger | \Theta \rangle \quad (4.3)$$

where η is a small positive constant coming from the step function. Notice that, if we found the eigenstates of H then we could introduce the identity $1 = \sum |\Psi_{n\mathbf{p}}\rangle \langle \Psi_{n\mathbf{p}}|$ in the above to obtain:

$$G_x(\mathbf{p}, \omega) = \sum_n \frac{\langle \Theta | x_{\mathbf{p}} | \Psi_{n\mathbf{p}} \rangle \langle \Psi_{n\mathbf{p}} | x_{\mathbf{p}}^\dagger | \Theta \rangle}{\omega - E_n + i\eta} \quad (4.4)$$

In the previous chapter we determined these eigenstates approximately in a truncated Hilbert space to calculate G_x .

Another perturbative way to calculate the propagator G is to divide the Hamiltonian H into a diagonalizable part H_0 and an interaction part H_I , and then expand $1/(\omega - H_0 - H_I + i\eta)$ into a series to obtain:

$$\begin{aligned} G_x(\mathbf{p}, \omega) &= \langle \Theta | x_{\mathbf{p}} \frac{1}{\omega - H_0 + i\eta} x_{\mathbf{p}}^\dagger | \Theta \rangle \\ &+ \langle \Theta | x_{\mathbf{p}} \frac{1}{\omega - H_0 + i\eta} H_I \frac{1}{\omega - H_0 + i\eta} x_{\mathbf{p}}^\dagger | \Theta \rangle \\ &+ \langle \Theta | x_{\mathbf{p}} \frac{1}{\omega - H_0 + i\eta} H_I \frac{1}{\omega - H_0 + i\eta} H_I \frac{1}{\omega - H_0 + i\eta} x_{\mathbf{p}}^\dagger | \Theta \rangle + \dots \end{aligned} \quad (4.5)$$

For the Fermi-polaron problem we have:

$$H_0 = \sum_{\mathbf{k}} \xi_{\mathbf{k}} e_{\mathbf{k}}^\dagger e_{\mathbf{k}} + \sum_{\mathbf{k}} \omega_{\mathbf{k}} x_{\mathbf{k}}^\dagger x_{\mathbf{k}} \quad (4.6)$$

$$H_I = \frac{v}{A} \sum_{\mathbf{k}\mathbf{k}'\mathbf{q}} e_{\mathbf{k}+\mathbf{q}}^\dagger e_{\mathbf{k}} x_{\mathbf{k}'-\mathbf{q}}^\dagger x_{\mathbf{k}'} \quad (4.7)$$

At this point we can use the fact that we know the spectrum of H_0 and introduce in between all operators the identity $1 = \sum_n |n\rangle \langle n|$ where $|n\rangle$ denote the eigenstates in the absence of H_I . We already know them from Sec.3.2:

$$|\mathbf{p}\rangle \equiv x_{\mathbf{p}}^\dagger |\Theta\rangle, \quad (4.8)$$

$$|\mathbf{p}; \mathbf{k}; \mathbf{q}\rangle \equiv x_{\mathbf{p}+\mathbf{q}-\mathbf{k}}^\dagger e_{\mathbf{k}}^\dagger e_{\mathbf{q}} |\Theta\rangle, \quad (4.9)$$

$$|\mathbf{p}; \mathbf{k}\mathbf{k}'; \mathbf{q}\mathbf{q}'\rangle \equiv x_{\mathbf{p}+\mathbf{q}+\mathbf{q}'-\mathbf{k}-\mathbf{k}'}^\dagger e_{\mathbf{k}}^\dagger e_{\mathbf{k}'}^\dagger e_{\mathbf{q}} e_{\mathbf{q}'} |\Theta\rangle, \quad (4.10)$$

and so on, where $|\Theta\rangle = \prod_{|\mathbf{k}| < k_F} e_{\mathbf{k}}^\dagger |0\rangle$. We will later make the same approximation as before and truncate the Hilbert space to a single electron-hole pair.

Introducing these identities we see that G_x is a sum of the amplitudes of all the different paths that start in the state $x_{\mathbf{p}}^\dagger |\Theta\rangle$, interact for a time τ and

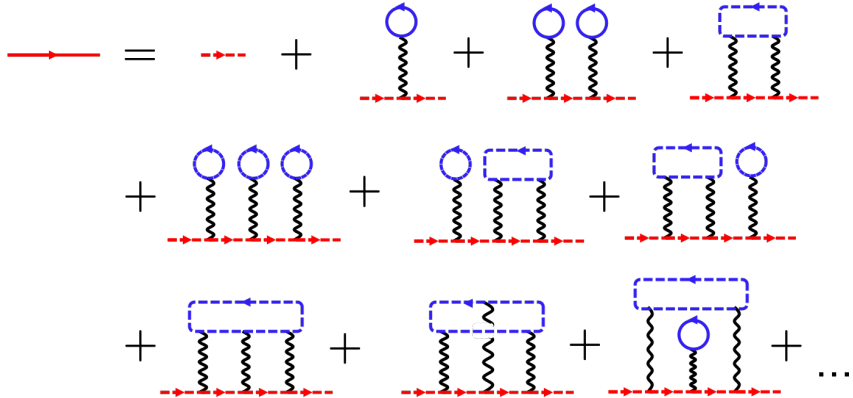


FIGURE 4.1: First few diagrams. The dressed exciton propagator is the thick red arrow, while the bare exciton propagator is the dashed red arrow. The dashed blue arrows correspond to the bare electron propagators, while the squiggly lines denote the electron-exciton interaction (through electron-exchange)

then go back into the same state. One advantage of this method, is that all the different paths have a clear physical meaning and can be represented pictorially, as we illustrate in Fig.4.1.

We proceed to evaluate G_x (solid line in Fig.4.1) starting from Eq. (4.5). There is one contribution where the exciton evolves without interacting at all with the electrons, and it is just the bare Green's function of the exciton (dashed lines in Fig.4.1):

$$I_0 = \langle \mathbf{p} | \frac{1}{\omega - H_0 + i\eta} | \mathbf{p} \rangle = \frac{1}{\omega - \omega_{\mathbf{p}} + i\eta} \equiv G_x^{(0)}(\mathbf{p}, \omega) \quad (4.11)$$

The contribution to first order in H_I contains only one contribution called the Hartree term (second term in 4.1):

$$I_1 = \langle \mathbf{p} | \frac{1}{\omega - H_0 + i\eta} | \mathbf{p} \rangle \langle \mathbf{p} | H_I | \mathbf{p} \rangle \langle \mathbf{p} | \frac{1}{\omega - H_0 + i\eta} | \mathbf{p} \rangle \quad (4.12)$$

$$= G_x^{(0)}(\mathbf{p}, \omega)^2 \frac{v}{\mathcal{A}} \sum_{\mathbf{q} < k_F} \quad (4.13)$$

The Hartree term corresponds to a mean-field interaction between the exciton and electrons, where the Fermi sea (and the exciton) remain in the same state.

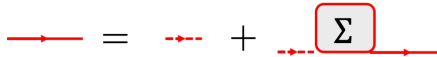


FIGURE 4.2: Dyson's equation

The second order term has two contributions (second and third diagrams in Fig.4.1):

$$I_2 = G_x^{(0)}(\mathbf{p}, \omega) \langle \mathbf{p} | H_I | \mathbf{p} \rangle G_x^{(0)}(\mathbf{p}, \omega) \langle \mathbf{p} | H_I | \mathbf{p} \rangle G_x^{(0)}(\mathbf{p}, \omega) \quad (4.14)$$

$$\begin{aligned} & + G_x^{(0)}(\mathbf{p}, \omega) \langle \mathbf{p} | H_I | \mathbf{p}; \mathbf{k}; \mathbf{q} \rangle \frac{1}{\omega - \omega_{\mathbf{p}+\mathbf{q}-\mathbf{k}} - \xi_{\mathbf{k}} + \xi_{\mathbf{q}} + i\eta} \\ & \cdot \langle \mathbf{p}; \mathbf{k}; \mathbf{q} | H_I | \mathbf{p} \rangle G_x^{(0)}(\mathbf{p}, \omega) \\ & = \frac{I_1^2}{G_x^{(0)}(\mathbf{p}, \omega)} + \frac{v^2}{\mathcal{A}^2} \sum_{|\mathbf{k}| > k_F, |\mathbf{q}| < k_F} \frac{G_x^{(0)}(\mathbf{p}, \omega)^2}{\omega - \omega_{\mathbf{p}+\mathbf{q}-\mathbf{k}} - \xi_{\mathbf{k}} + \xi_{\mathbf{q}} + i\eta} \end{aligned} \quad (4.15)$$

Notice that the first of the above is just two Hartree contributions. The second term corresponds to the exciton creating an electron-hole pair in the Fermi sea, then evolving for some time, and then annihilating this electron-hole pair to go back to the non-interacting state.

We could go on, but things can be greatly simplified by properly grouping terms. One can check that the terms in Fig.4.1 can be ordered to obtain the following equation, known as the *Dyson's equation* (see Fig.4.2):

$$G_x(\mathbf{p}, \omega) = G_x^{(0)}(\mathbf{p}, \omega) + G_x^{(0)}(\mathbf{p}, \omega) \Sigma(\mathbf{p}, \omega) G_x(\mathbf{p}, \omega) \quad (4.16)$$

In the above we introduced the self-energy which is formed by all the diagrams that are "one-particle irreducible" (or 1PI), i.e. diagrams which do not fall into two pieces if you cut one internal line. Notice that, from the diagrams illustrated on the LHS of Fig.4.1, the 2nd, the 4th, the 8th 9th and 10th are 1PI. Notice that Eq. (4.16) can easily be inverted to obtain $G_x(\mathbf{p}, \omega) = G_x^{(0)}(\mathbf{p}, \omega)^{-1} - \Sigma(\mathbf{p}, \omega)$.

We cannot evaluate Σ exactly, so we make some approximations. We make the same (two) approximations that we made in Sec.3.2. First, we neglect all diagrams corresponding to more than one excited electron-hole pair (for example the 10th diagram). From the remaining diagrams we eliminate all diagrams such as the 9th. One can check, using the procedure outlined above, the 9th diagram corresponds to the process where the exciton creates an electron-hole pair, then, after evolving for some time, scatters with the created hole, and then annihilates the electron-hole pair to go

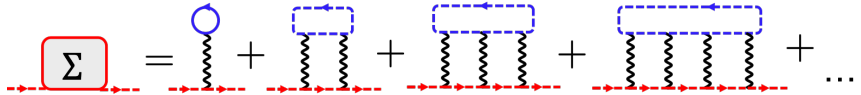


FIGURE 4.3: ladder approximation for the self-energy

back to the initial state. But, as we argued in Sec.3.2 the scattering between the exciton and the hole can be safely neglected. We present all the remaining terms in Fig.4.3. Based on how these terms look this approximation is sometimes called a *ladder approximation*.

It is straightforward to evaluate the self-energy in this approximation:

$$\begin{aligned} \Sigma(\mathbf{p}, \omega) = & \frac{u}{\mathcal{A}} \sum_{\mathbf{q} < k_F} (1 + v\chi(\mathbf{p} + \mathbf{q}, \omega + \xi_{\mathbf{q}})) \\ & + (v\chi(\mathbf{p} + \mathbf{q}, \omega + \xi_{\mathbf{q}}))^2 + \dots \end{aligned} \quad (4.17)$$

where we introduced:

$$\chi(\mathbf{p}, \omega) \equiv \frac{1}{\mathcal{A}} \sum_{|\mathbf{k}| > k_F} \frac{1}{\omega - \omega_{\mathbf{p}-\mathbf{k}} - \xi_{\mathbf{k}} + i\eta} \quad (4.18)$$

The term inside the parenthesis in Eq. (7.12) is just a geometric series that can be evaluated easily (assuming that the summation is convergent) to obtain:

$$\Sigma(\mathbf{p}, \omega) = \frac{1}{\mathcal{A}} \sum_{\mathbf{q} < k_F} T(\mathbf{p} + \mathbf{q}, \omega + \xi_{\mathbf{q}}) \quad (4.19)$$

where we introduced the T-matrix:

$$T(\mathbf{p}, \omega) = \frac{v}{1 - v\chi(\mathbf{p}, \omega)} \quad (4.20)$$

which is precisely the result that we obtained in Sec.3.2.

We remark that our derivation so far was simple enough so we did not spend much time discussing how to evaluate these diagrams. However, if the diagrams would have been more complicated we could have written some rules (known as *Feynman rules*) to guide us on how to evaluate the various diagrams.

4.1.2 Feynman diagrams

In the previous derivation we used the fact that we knew the many-body state $|\Theta\rangle$ and its excitations in evaluating Eq. (4.2), which is not usually the case.

In the general case, we still want to calculate the retarded Green's function that we introduced previously. However, the calculations simplify if one works with another propagator, known as the time ordered propagator and defined as:

$$G_x(\mathbf{p}, \omega) = -i \int d\tau e^{i\omega\tau} \langle \Theta | \mathcal{T} x_{\mathbf{p}}(t + \tau) x_{\mathbf{p}}^{\dagger}(t) | \Theta \rangle \quad (4.21)$$

where \mathcal{T} denotes the time-ordering operator. The time-ordered Green's function is related to the retarded and advanced Green's function through:

$$G_x(\mathbf{p}, \omega) = G_x^R(\mathbf{p}, \omega)\theta(\omega) + G_x^A(\mathbf{p}, \omega)\theta(-\omega) \quad (4.22)$$

where we introduced the retarded Green's function:

$$G_x^R(\mathbf{p}, \omega) = -i \int d\tau e^{i\omega\tau} \theta(\tau) \langle \Theta | [x_{\mathbf{p}}(t + \tau) x_{\mathbf{p}}^{\dagger}(t)] | \Theta \rangle \quad (4.23)$$

and the advanced one, which is the conjugate of the retarded $G_x^A(\mathbf{p}, \omega) = G_x^R(\mathbf{p}, \omega)^*$. Notice that from now on we will denote retarded(advanced) quantities with the explicit superscript $R(A)$ to distinguish them from their time-ordered counterparts.

As we saw in the previous section, the Green's function can be calculated perturbatively starting from the non-interacting or bare Green's function. The two are connected through the Dyson equation:

$$G_x(\mathbf{p}, \omega) = G_x^{(0)}(\mathbf{p}, \omega) + G_x^{(0)}(\mathbf{p}, \omega) \Sigma_x(\mathbf{p}, \omega) G_x(\mathbf{p}, \omega) \quad (4.24)$$

where $\Sigma(\mathbf{p}, \omega)$ contains all the 1PI diagrams.

Although we introduced the above relations for the exciton Green's functions, similar relations can be obtained for the electrons. However, because we are dealing with fermions, the commutator in the definition of the retarded Green's function should be replaced by the anticommutator.

The starting point of the calculations of the full Green's functions are the bare exciton/electron Green's functions (as mentioned before, these are the propagators in the absence of any interactions):

$$G_{x/e}^{(0)}(\mathbf{p}, \omega) = \frac{1}{\omega - \omega_{\mathbf{p}} + \mu_{x/e} + i\eta \operatorname{sgn}\omega} \quad (4.25)$$

where we introduced the exciton/electron chemical potentials $\mu_{x/e}$, while the advanced/retarded bare propagators are given by:

$$G_{x/e}^{(0,R/A)}(\mathbf{p}, \omega) = \frac{1}{\omega - \omega_{\mathbf{p}} + \mu_{x/e} \pm i\eta} \quad (4.26)$$

If we want to investigate polaron physics, we can assume that there are no excitons (or polarons) in the many-body ground state $|\Theta\rangle$. To capture this regime, the exciton chemical potential must be set below the attractive-polaron dispersion. In this scenario, one can check that:

$$\begin{aligned} G_x(\mathbf{p}, \omega) &= G_x^R(\mathbf{p}, \omega) - 2i\text{Im}G_x^R(\mathbf{p}, \omega)\theta(-\omega) \\ &\approx G_x^R(\mathbf{p}, \omega) + \frac{2}{\pi}\delta(\omega - \omega_{\mathbf{p}} - \Sigma_x(\mathbf{p}, \omega) + \mu_x) = G_x^R(\mathbf{p}, \omega) \end{aligned} \quad (4.27)$$

where, in going to the second line we used the relation $\text{Im}[1/(x + i\eta)] \rightarrow \delta(x)$. The above relation greatly simplifies the calculations of Green's functions for Fermi polarons.

Before concluding this section we remark that there are prescriptions on how to write down equations in terms of $G_{x/e}$ and $G_{x/e}^{(0)}$ for corresponding diagrams, which are known as Feynman rules. In the following we will assume that these rules are known (if not one can check [10, 37]) and we will use them to evaluate diagrams.

4.2 CONSERVING APPROXIMATION

The main difficulty in using the Green's function method in practice lies in deciding what diagrams to include in the self-energy Σ . It is often very difficult to know which diagrams are important without first actually solving the problem at hand (or a very similar problem).

One might argue that the least we can do, is to use approximations for the Green's functions that satisfy the conservation laws of the system. For example, we would like to have approximate Green's functions yielding a particle density $\rho(\mathbf{x}, t)$ and a current density $\mathbf{j}(\mathbf{x}, t)$ that obey the continuity equation, or a total momentum $\mathbf{P}(t)$ and an applied force $\mathbf{F}(t)$ that obey Newton's equation $\mathbf{F}(t) = \dot{\mathbf{P}}(t)$ and so on. The correct treatment of the above issues is crucial in obtaining sensible results in non-equilibrium scenarios (see the polaron transport problem in Chapter 7).

In contrast, the above relations are trivially obeyed in equilibrium. For instance, in equilibrium, observables do not have a time dependence and

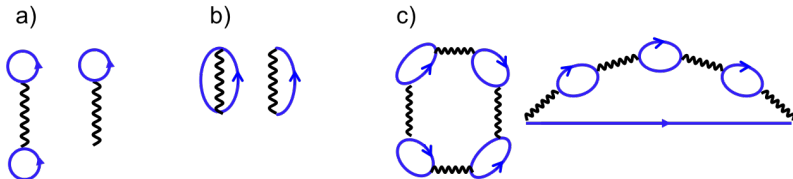


FIGURE 4.4: Free energy functional and corresponding self energy for the Hartree approximation, the Fock term from the Hartree-Fock approximation and respectively the RPA approximation. The blue arrows correspond to full electron propagators while a squiggly line denotes the Coulomb interaction.

the current is zero, leading to a trivial fulfillment of the continuity equation. However, even if the conservation laws are not explicitly broken it is still desirable to work with Green's functions that would obey these conservation laws if the system were slightly perturbed.

Such approximations are aptly known as *conserving* approximations. Baym and Kadanoff [38, 39] found that a sufficient condition for an approximation to be conserving was to be *Φ -derivable*, which means that there should exist a function of the Green function $\Phi[G]$ whose functional derivative yields the self-energy:

$$\Sigma(\mathbf{p}, \omega) = \frac{\delta\Phi[G]}{\delta G(\mathbf{p}, \omega)} \quad (4.28)$$

In a diagrammatic language, this procedure amounts to simply cutting a Green's function line in Φ , leading to the desired self energy.

We remark that, crucially, the Φ is a functional of the full (or dressed/bold) Green's function G . We remark that the functional Φ is also known as the *Luttinger-Ward* functional. Since the self-energy is a sum of all 1PI diagrams, the exact Luttinger-Ward functional is the sum of all closed, 2PI diagrams, i.e. all diagrams without particles going in or out that do not fall apart if one removes two propagator lines. To make sure that approximations are conserving one should find reasonable approximations for Φ and then obtain Σ from Φ through Eq. (4.28).

We present a few examples of useful approximations to Φ in Fig.4.4.

4.2.1 Two-particle correlation functions

So far, we have discussed only single-particle correlation functions. However, in order to investigate particle interactions we have to calculate two particle correlation functions. More generally, such correlations determine the linear response of the system to external perturbations, according to Kubo's formula [10]. As we will show below, the two particle Green's functions are not independent of the single-particle Green's functions but can be expressed as functional derivatives of the latter.

To find the relationship between two particle correlation functions and the single particle Green's function let's calculate the response of the system to a small perturbation. A general perturbation breaks the translational invariance of the system, so we temporarily go back to real space in this subsection. We start from the equation of motion

$$\int d2G^{-1}(1,2)G(2,3) = \delta(1,3) \quad (4.29)$$

where we have used the Keldysh notation $(1) \equiv (\mathbf{r}_1, t_1)$ and defined the operator

$$G^{-1}(1,2) = [i\partial_\tau - h(1)]\delta(1,2) - \Sigma(1,2) \quad (4.30)$$

where h is the single-particle Hamiltonian and τ a time on the Keldysh contour. We now consider the variation δG of the Green's function with respect to some perturbation of the single-particle Hamiltonian δh .

From Eq. (4.29) we obtain

$$\int d2[\delta G^{-1}(1,2)G(2,3) + G^{-1}(1,2)\delta G(2,3)] = 0 \quad (4.31)$$

and thus

$$\delta G(1,3) = \int d2d4G(1,2)\delta G^{-1}(2,4)G(4,3) \quad (4.32)$$

$$= - \int d2d4G(1,2)[\delta(2,4)\delta h(4) + \delta\Sigma(2,4)] \\ \times G(4,3). \quad (4.33)$$

with $\delta\Sigma = \Sigma[G + \delta G] - \Sigma[G]$.

Equation (4.33) defines a recursive relation for δG as we can write $\delta\Sigma(1,2) = \int d3d4K(1,3;2,4)\delta G(3,4)$, where $K = \delta^2\Phi/\delta G^2$ is the irreducible two par-



FIGURE 4.5: Left: Bethe-Salpeter equation for the reducible vertex L . Right: response function χ contracted from L

ticle vertex, which is obtained from Φ by cutting two lines. We can reorganize Eq. (4.33) to find

$$\delta G(1,3) = - \int d2d4\delta(2,4)\delta h(4)L(1,2;3,4), \quad (4.34)$$

where $L(1,2;3,4)$ is a reducible vertex functions, which is related to the irreducible vertex K via the Bethe–Salpeter equation

$$\begin{aligned} L(1,2;3,4) &= G(1,4)G(2,3) \\ &+ \int d5d6d7d8G(1,5)G(6,3)K(5,8;6,7)L(7,2;8,4) \end{aligned} \quad (4.35)$$

shown in Fig. 4.5.

The two-particle function L relates the change of the Green's function to a perturbation in the single-particle Hamiltonian and can be used to calculate arbitrary response functions. For instance, the current response to a vector potential reads

$$\delta J_\mu(1) = \int d2\chi_{\mu\rho}(1,2)\delta A^\rho(2), \quad (4.36)$$

where Einstein sum convention is implied and

$$\begin{aligned} \chi_{\mu\rho}(1,2) &= \\ &- i\left(\frac{p_{1,\mu} - p_{1',\mu}}{2m_1}\right)\left(\frac{p_{2,\rho} - p_{2',\rho}}{2m_2}\right)L(1,2;1',2')|_{\substack{1' \rightarrow 1 \\ 2' \rightarrow 2}} \end{aligned} \quad (4.37)$$

Diagrammatically this amounts to connecting pairs of outer legs of the two-point function L to current vertices as shown in right panel of Fig 4.5.

In addition to determining the response, the two particle function L also gives the two-particle Green's function:

$$\begin{aligned} G_2(1,2;1',2') &\equiv -\langle \Theta | \mathcal{T}\psi(1)\psi(2)\psi^\dagger(2')\psi^\dagger(1') | \Theta \rangle \\ &= G(1,1')G(2,2') - L(1,2;1',2') \end{aligned} \quad (4.38)$$

4.3 EXCITON-POLARONS

We will use the two point function L to calculate polaron interactions in Sec.4.5 and to calculate the response to external electric fields in Ch.7. Before moving on to these issues, in this section we first rederive the polaron quasiparticles from Chapter 3 using the diagrammatic techniques introduced above. The Chevy ansatz approximation that we used in 3 has an equivalent diagrammatic approximation known as the (non-self-consistent) ladder approximation. However, this is not a conserving approximation. In this chapter we will go beyond the approximation in Chapter 3 and employ the self-consistent ladder approximation, which is actually conserving.

We begin our discussion by analyzing the regime $n_x/n_e \ll 1$, for weak light matter coupling $g \rightarrow 0$. This system is described by the Hamiltonian

$$H = \sum_{\mathbf{k}} \xi_{\mathbf{k}} e_{\mathbf{k}}^\dagger e_{\mathbf{k}} + \sum_{\mathbf{k}} \omega_{\mathbf{k}} x_{\mathbf{k}}^\dagger x_{\mathbf{k}} + \frac{v}{\mathcal{A}} \sum_{\mathbf{k}\mathbf{k}'\mathbf{q}} e_{\mathbf{k}+\mathbf{q}}^\dagger e_{\mathbf{k}} x_{\mathbf{k}'-\mathbf{q}}^\dagger x'_{\mathbf{k}} \\ + \sum_{\mathbf{k}\mathbf{q}j} u_{dis,e} e^{i\mathbf{r}_{e,j}\cdot\mathbf{q}} e_{\mathbf{k}+\mathbf{q}}^\dagger e_{\mathbf{k}} + \sum_{\mathbf{k}\mathbf{q}j} u_{dis,x} e^{i\mathbf{r}_{x,j}\cdot\mathbf{q}} x_{\mathbf{k}+\mathbf{q}}^\dagger x_{\mathbf{k}} \quad (4.39)$$

In the above we also introduced for completeness the coupling of excitons and electrons to disorder, who are assumed to be infinitely massive particles at positions $\mathbf{r}_{e/x,j}$. While it is not crucial to introduce disorder properly in order to treat polaron interactions, we will also use the discussion here to investigate transport phenomena in Chapter 7 where disorder plays a crucial, non-perturbative role.

Although disorder breaks the translational invariance of the system, it can be shown that most observables remain the same if, instead of considering a single sample with a particular disorder configuration, one averages all the possible configurations. This technique, known as disorder self-averaging restores the translational invariance of the system. Since it is not straightforward to prove the above assertions, in the following we will simply perform disorder averaging and point the reader to other references for more details on why this is justified [10].

The restoration of translational invariance allows us to work in Fourier space. We want to evaluate the time-ordered electron and exciton Green's functions in Fourier space:

$$G_x(p) = -i \int d\tau e^{i\omega\tau} \langle \Theta | T x_{\mathbf{p}}(t + \tau) x_{\mathbf{p}}^\dagger(t) | \Theta \rangle \quad (4.40)$$

$$G_e(p) = -i \int d\tau e^{i\omega\tau} \langle \Theta | T e_{\mathbf{p}}(t + \tau) e_{\mathbf{p}}^\dagger(t) | \Theta \rangle \quad (4.41)$$

$$\Phi = \frac{1}{2} \text{(red circle)} + \frac{1}{2} \text{(blue circle)} + \text{(red circle with blue arrow)} + \frac{1}{2} \text{(blue circle with red arrow)} + \frac{1}{3} \text{(blue circle with two red arrows)} + \dots$$

FIGURE 4.6: Free energy functional Φ that can be used to derive the self-energy in Fig.4.7. The solid blue(red) arrows represent full (or bold/dressed) electron(exciton) propgators. The black squiggly line denotes the interaction between exciton and electron. The dahsed black line denotes disorder scattering, after self-averaging.

where $|\Theta\rangle$ denotes the many-body ground state and we introduced $p \equiv (\mathbf{p}, \omega)$ for notational simplicity (we will later also use $k \equiv (\mathbf{k}, \epsilon)$). Moreover, we will incorporate factors of $1/2\pi$ into the definition of integral measure such that $dp = d\mathbf{p} d\omega / (2\pi)^3$.

The effect of disorder and interactions is taken into account by introducing self energy corrections to the Green's functions shown in Fig. 4.7.

$$G_e^{-1}(p) = \omega - \xi_{\mathbf{p}} - \Sigma_{\text{dis},e}(p) \quad (4.42)$$

$$G_x^{-1}(p) = \omega - \omega_{\mathbf{p}} - \Sigma_{\text{int}}(p) - \Sigma_{\text{dis},x}(p) \quad (4.43)$$

where we introduced the exciton self energy from interactions with electrons Σ_{int} as well as the disorder self energies $\Sigma_{e,\text{dis}}$ and $\Sigma_{x,\text{dis}}$. Note that, since we assumed a small density of excitons in the system, we neglected the effect of excitons on the electron system.

The calculation of the self energies requires some approximations. To make sure that the approximations are conserving we start from (an approximation of) the Luttinger-Ward functional Φ , as presented in Fig.4.6 . Notice that we treat the effect of disorder in an approximation known as the self-consistent Born approximation, which ignores any quantum interference effects such as weak-localization. We treat the electron-exciton interaction in the (self-consistent) ladder approximation.

The self-energies are functional derivatives of Φ , i.e. $\Sigma_{e,x} = \frac{\delta\Phi[G_e, G_x]}{\delta G_{e,x}}$ which corresponds to removing either one of the electron or exciton Green's functions from the functional. The disorder self energies can be evaluated as

$$\Sigma_{\text{dis},e/x}(p) = \int \frac{d\mathbf{k}}{(2\pi)^2} \gamma_{e/x} G_{e/x}(k)|_{\epsilon=\omega} = \frac{-i}{2\tau_{e/x}} \text{sgn}(\omega). \quad (4.44)$$

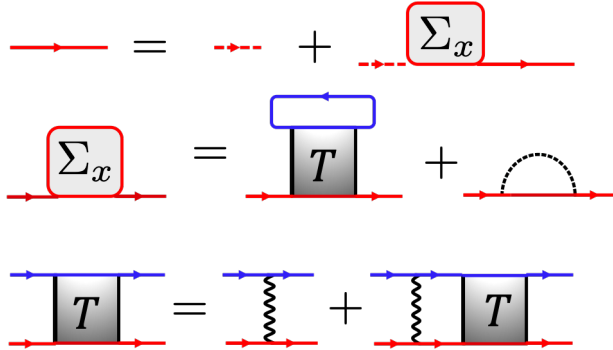


FIGURE 4.7: Exciton self-energy. The thick(dashed) red lines correspond to the dressed(bare) exciton propagator, while the blue lines correspond to the electron-propagator. The squiggly line denotes electron-exciton interaction, while the dashed black line denotes the disorder interaction, after self-averaging. Similar equations hold for the electron propagator, except that the colors are switched

where the lifetimes are defined as

$$\tau_{e,x} = \frac{1}{2\pi\rho_{e,x}\gamma_{e,x}} \quad (4.45)$$

with $\rho_{e,x}$ the densities of states per unit volume at the Fermi surface. Importantly, in the self-consistent theory the exciton Green's functions in Eq. (4.44) is dressed by disorder and interactions and hence ρ_x refers to the renormalized exciton dispersion to be determined below.

The exciton self energy due to interactions can be evaluated in the self-consistent T-matrix approximation

$$\Sigma_{int}(p) = -i \int dk G_e(k) T(k+p) \quad (4.46)$$

where we introduced the self-consistent T-matrix shown in Fig. 4.7

$$T(p) = v + iv \int dk G_e(k) G_x(p-k) T(p). \quad (4.47)$$

The contact interaction allows for a simple solution

$$T^{-1}(p) = v^{-1} - i \int dk G_e(k) G_x(p-k). \quad (4.48)$$

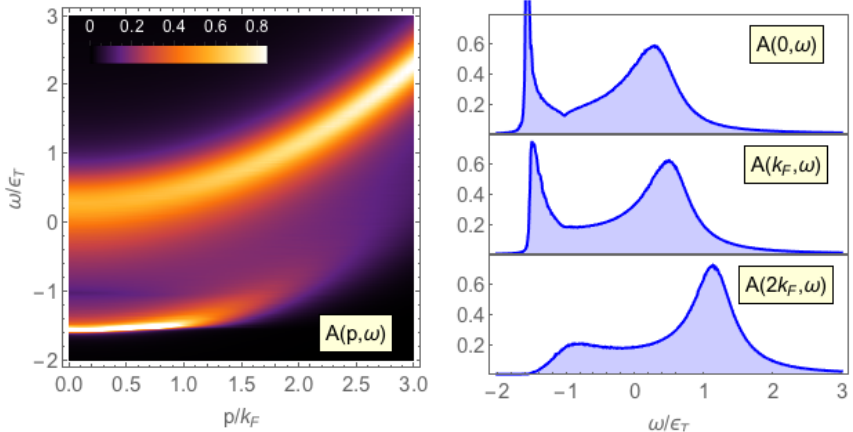


FIGURE 4.8: Self-consistent spectral function of excitons at zero exciton density, $\mu_e = \epsilon_T/2$, $m_x = 2m_e$, and disorder broadening $1/2\tau_x = \epsilon_T/100$.

At vanishing exciton density (i.e. $n_x \rightarrow 0$) we can evaluate the self energy by replacing $G_x \rightarrow G_x^R$ in the above equations (see Eq. (4.27)). We can evaluate all frequency integrals by closing the contour in the upper half-plane, where the retarded exciton Green's function is analytical, and obtain

$$\Sigma_{int}^{(0)}(p) = \int \frac{d\mathbf{k}}{(2\pi)^2} n_F(\xi_{\mathbf{k}}) T^{(0)}(\omega + \xi_{\mathbf{k}}, \mathbf{k} + \mathbf{p}), \quad (4.49)$$

$$\begin{aligned} T^{(0)}(p)^{-1} &= v^{-1} + \int \frac{d\mathbf{k}}{(2\pi)^2} [1 - n_F(\xi_{\mathbf{k}})] \\ &\quad \times G_x^R(\omega - \xi_{\mathbf{k}}, \mathbf{p} - \mathbf{k}), \end{aligned} \quad (4.50)$$

where the superscript ⁽⁰⁾ denotes quantities at $n_x = 0$ and $n_F(x)$ is the Fermi-Dirac distribution function.

We remark that, if we replace the exciton propagator G_x^R in Eq. (4.49) with its bare counterpart, i.e. $G_x^R(p) \rightarrow (\omega - \xi_{\mathbf{p}} + i\eta)^{-1}$ Eq. (4.49) we precisely recover the results in Chapter 3, which establishes the equivalence between the non-self-consistent ladder approximation and the Chevy-ansatz.

However, to go beyond the approximation in the previous chapter and to have a conserving approximation we solve Eq. (4.49) self-consistently, by discretizing momentum and energy and using an iterative method. The self-consistent exciton spectral function $A_x(p) = -\pi^{-1} \text{Im} G_x^R(p)$ for $n_x = 0$ and $\mu_e = \epsilon_T/2$ is plotted in Fig. (4.8). We see that we recover the same

spectral features as in the previous chapter: at negative frequencies the *attractive polaron* is a well-defined quasiparticle excitation at sufficiently low momenta, while a second well-defined, metastable *repulsive polaron* quasiparticle exists at positive energies. In comparison to the previous derivation, we see that with the self-consistent approach, we are able to capture continuum of excitations between the repulsive and attractive polarons, because the self-consistent approach captures the residual interactions between the polaron and the electrons.

4.4 POLARON POLARITONS

The above calculation can be readily generalized to the case of exciton polaron polaritons. The coupling to the cavity photons implies an additional term in the Hamiltonian:

$$H' = \sum_{\mathbf{k}} \nu_{\mathbf{k}} c_{\mathbf{k}}^\dagger c_{\mathbf{k}} + g \sum_{\mathbf{k}} (x_{\mathbf{k}}^\dagger c_{\mathbf{k}} + h.c.) \quad (4.51)$$

where $c_{\mathbf{k}}^\dagger$ are the photon creation operators. Since the coupling to the cavity photon is easily diagonalizable, the simplest way to treat the exciton-photon coupling in a perturbative calculation is to include it in the known Hamiltonian H_0 instead of including it in the interaction Hamiltonian H .

This would redefine the bare exciton propagator:

$$G_x^{(0)}(p) = \frac{1}{\omega - \omega_{\mathbf{p}} - \frac{g^2}{\omega - \nu_{\mathbf{p}} + i\eta} + i\eta + \mu_x} \quad (4.52)$$

and we introduced the dispersion of cavity photons, $\nu_{\mathbf{k}} = \mathbf{k}^2/2m_c + \Delta$, where $m_c \simeq 10^{-5} m_e$ and we assume for simplicity that photons have an infinite lifetime. Notice that nothing else changes. The functional Φ remains the same, as well as the exciton self-energies. This is because all other vertices depend on the exciton operators.

Performing a similar analysis to before we can determine the new exciton propagator :

$$G_x(p) = \frac{1}{\omega - \omega_{\mathbf{p}} - \frac{g^2}{\omega - \nu_{\mathbf{p}} + i\eta} - \Sigma_{int}(p) - \Sigma_{dis,x}(p) + i\eta + \mu_x}. \quad (4.53)$$

We remark that $\Sigma_{int}(p)$ and $\Sigma_{dis,x}(p)$ have to be calculated self-consistently as a function of the new G_x . This will make virtually no difference in the real parts of the self-energies, because they involve summations over large

momenta, where the coupling to the cavity can be neglected. In contrast the imaginary parts of the self-energies will be strongly suppressed due to the small polariton density of states $\sim m_\nu \ll m_x^*$.

It is straightforward to see that the photon propagator can be written in terms of the exciton propagator as:

$$G_c(p) = \frac{1}{\omega - \nu_{\mathbf{k}} + i\eta} + \frac{1}{\omega - \nu_{\mathbf{k}} + i\eta} g^2 G_x(p) \frac{1}{\omega - \nu_{\mathbf{k}} + i\eta} \quad (4.54)$$

$$= \frac{1}{\omega - \nu_{\mathbf{p}} + \frac{g^2}{\omega - \omega_{\mathbf{p}} - \Sigma_{int}(p) - \Sigma_{dis,x}(p) + i\eta + \mu_x} + i\eta} \quad (4.55)$$

4.5 POLARON INTERACTIONS

The powerful many-body Green's function techniques introduced previously allowed us to go beyond Chevy ansatz and capture the residual scattering between polarons and the Fermi sea. We also discussed how these techniques can be used to calculate polaron response functions or interactions. Indeed, there has been a lot recent work concerning the interaction of polarons [40–44]. As we will see below, there are different mechanisms that can mediate interactions between polarons, which has led to sometimes contradictory claims regarding the nature and strength of these interactions [40–44]. This is where the Baym-Kadanoff conserving approximation is particularly useful, because it allows us to derive all the interaction terms that conserve energy, momentum and particle number.

We begin the discussion of these interactions by deriving all the interactions terms. This allows one to connect the various calculations about polaron interactions that exist in the literature. Then, we will evaluate only the dominant contributions when we discuss polaron polariton and Bose polaron interactions.

We derive the terms corresponding to Fermi-polaron interactions. However, similar terms can be obtained for Bose-polarons (by exchanging the exciton with the electron Green's functions). One can check that, to zeroth order in the exciton-density, the irreducible vertex $K = \frac{\delta^2 \Phi}{\delta^2 G}$ is the one given in Fig.4.9. Any other diagrams would contain at least one exciton loop which is of order n_x and therefore would go to zero as $n_x \rightarrow 0$ (see Sec.7.3.2 for a proof).

From the irreducible vertex K , we can calculate the reducible vertex L corresponding to exciton-exciton interactions using the Bethe-Salpeter

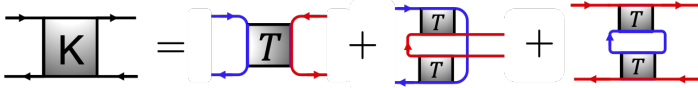


FIGURE 4.9: The reducible vertex K for the ladder approximation. Notice that we neglect the vertex corrections due to disorder since we assume gaussian disorder. The black arrows stand for either electron or exciton propagators.

equation in Eq. (4.35) and Fig.4.5. one can check that the exciton-exciton interaction term is given by the terms presented in Fig.4.10.

We remark that the first term in Fig.4.10, which we denote by \mathcal{L} , corresponds to interactions between excitons that are mediated by exchange of excitations from the Fermi sea. This terms agrees with our usual intuition that interactions between particles are mediated by exchange of virtual particles, which are excitations in some medium (in our case, the Fermi sea).

In contrast, the other terms come from the modification of the medium itself due to the presence of other particles. We completely neglected such effects in the preceding derivations (see Eq. (6.9)), assuming that we are in the Fermi-polaron limit, where excitons cannot have a sizable effect on the Fermi sea. However, when dealing with interactions we have to consider corrections to exciton self-energy which are of order n_x , which means that we can no longer neglect the dressing of electrons by excitons, which is of this order. This fact is sometimes lost in recent publications on the subject of polaron interactions (see for instance Ref. [42]).

In the above we derived the terms corresponding to the interaction between two polarons, which we obtained using the Baym-Kadanoff conserving approximation. This was an equilibrium calculation, which assumed that the electron/exciton chemical potentials $\mu_{e/x}$ remain fixed. However, this is not the case in most experimental situations. In fact, the idea of a grand canonical ensemble is often a concept that is introduced to simplify calculations, assuming that the underlying physics remains the same, which turns out not to be the case when considering polaron interactions. In particular, in optical experiments with TMD materials, one uses top/botom electrical gates which act as capacitors and fix the number of itinerant electrons in the semiconductor. This means that, in these experiments, the electron chemical potential is not fixed but rather the electron-number. We can consider the modification of the electron chemi-

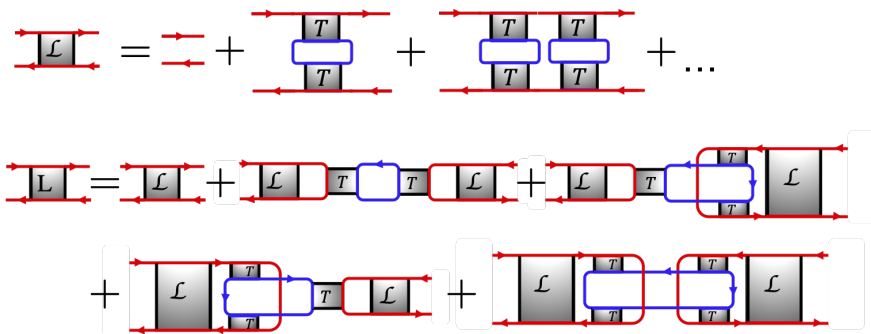


FIGURE 4.10: Exciton-exciton interaction vertex L in the conserving approximation. The diagram \mathcal{L} , is the term associated to exchange of excitations between quasiparticles. The rest of the diagrams correspond to the effect of Pauli blocking, and appear due to the fact that the electron self-energy can no longer be neglected. The black arrows stand for either electron or exciton propagators.

cal potential due to the presence of excitons as an additional interaction mechanism, which is not captured by our diagrams in Fig.4.10.

Having discussed all the mechanisms that can mediate interactions between polarons we now evaluate the dominant contributions to polaron-polariton and Bose-polaron interactions.

4.5.1 Interaction between Fermi-polaron polaritons

In the limit of very large light matter coupling, where polaron-polaritons are formed, we expect that the latter interaction will dominate. We can justify this with a simple estimate. Let's assume that the attractive polaron splitting is $g_{pol} \propto gZ_x$ (where g is the exciton-photon coupling and Z_x is the exciton polaron quasiparticle weight). If we add $N_x = N_e$ excitons to the system, there is just one electron per exciton, and the system would prefer to form a trion Fermi liquid. Since trions do not couple efficiently to the cavity photons, due to their vanishing oscillator strength, the splitting g_{pol} will effectively collapse. This simple argument shows that the interaction between polaron-polaritons must be of the order of g_{pol}/N_e . Interestingly, this interaction scales proportionally with the light matter coupling g , which shows that this Pauli blocking effect is enhanced by a strong cou-

pling between excitons and photons. For this reason, in the following we will focus on this contribution and neglect the other interactions.

According to the Chevy ansatz, adding an exciton will create a polarization wave in the Fermi sea and scatter $1 - Z_x$ electrons above the Fermi sea. Notice that, if we go beyond Chevy ansatz, then the addition of the exciton can scatter more than $1 - Z_x$ electrons out of the Fermi sea. Therefore, we expect that our estimate will underestimate the strength of this interaction.

For simplicity, let's focus on the regime of very low electron densities, where the quasiparticle weight of the attractive exciton-polaron $Z_x \rightarrow 0$. According to the above argument each exciton will scatter an electron from within the Fermi sea to a state above. When the next exciton is added, it will feel the missing electron and its self-energy will decrease slightly, because it will not be able to dress as effectively. Since the Fermi-polaron interacts roughly equally with all electrons on the Fermi sea, we can assume that this electron is taken from the surface of the Fermi sea, to keep calculations simple. Notice that we are not concerned with the effect of the electrons on top of the Fermi sea, since they have a much larger phase-space available, and therefore they will not prohibit as much the formation of additional polarons.

Let's assume that the energy of an attractive polaron as a function of electron density is given by $\omega(n_e)$. Then, if we put N_x excitons in the system, the energy of the next exciton is going to be $\omega(n_e - n_x)$. This means that the exciton is experiencing an interaction $\frac{u}{A} N_x = \omega(n_e - n_x) - \omega(n_e)$ which implies that

$$u = \frac{\partial \omega(n_e)}{\partial n_e} \quad (4.56)$$

The same reasoning applies to the polaron-polariton quasiparticles, with the only difference being that, due to the hybridization between the Fermi polaron and the photon, when we add a polaron-polariton to the system we only remove $1/2(1 - Z_x)$ electrons from the Fermi sea (we assume for simplicity that the cavity photons are resonant with the attractive polaron quasiparticles). Therefore, defining the polaron polariton energy as a function of electron density as $\Omega(n_e)$ we obtain the following formula for the polaron-polariton interactions:

$$u = \frac{1}{2} \frac{\partial \Omega(n_e)}{\partial n_e} \quad (4.57)$$

While analytical expression could be obtained for the above interactions we instead evaluate the above interactions numerically. For a light matter

coupling $g = \epsilon_T/2 = 12\text{meV}$ we obtain an interaction strength between polaritons $u \approx 0.2\mu\text{eV}\mu\text{m}^2$ (using the Chevy ansatz approach from the previous chapter, and choosing for simplicity $m_x = m_e$). This is 20 times larger than the polariton-polariton interaction in the absence of electron dressing, which is about $0.01\mu\text{eV}\mu\text{m}^2$ [12] and is in good agreement with recent experimental results [12] which claim repulsive interactions that are about twice as large as the value we obtained. However, as we mentioned in the beginning, our simple approximation is likely to underestimate this effect.

Our results show that the dressing of polaritons with polarization waves in the electron system lead to increases in the interaction between polaritons of at least an order of magnitude. This shows that the polaron formation could be leveraged to strongly modify the photon properties and study novel phenomena of strongly interacting photons.

4.5.2 Interaction between Bose-polarons

In the Fermi-polaron polariton regime that we just investigated we saw that the special nature of the Fermi-polaron polaritons strongly increased the interaction effects due to the change of μ_e . Since we do not expect a similar effect in the case of Bose-polarons, we evaluate instead the diagrams due to exchange of bogolons from the exciton condensate, which is the mechanism believed to dominate in this limit [42, 45, 46].

Although a diagrammatic approach would yield similar results, to keep the derivation simple we evaluate this interaction starting from the simplified model introduced in Sec.??:

$$\begin{aligned} H_{eff} &= \sum_{\mathbf{k}} \xi_{\mathbf{k}} e_{\mathbf{k}}^\dagger e_{\mathbf{k}} + \sum_{\mathbf{k}} \Omega_{\mathbf{k}} a_{\mathbf{k}}^\dagger a_{\mathbf{k}} + \sum_{\mathbf{k}} (\omega_{\mathbf{k}}^T - \epsilon_T) t_{\mathbf{k}}^\dagger t_{\mathbf{k}} \\ &+ \sum_{\mathbf{kq}} \frac{g}{\sqrt{A}} t_{\mathbf{q}}^\dagger (\alpha_{\mathbf{k}} a_{\mathbf{k}} e_{\mathbf{q}-\mathbf{k}} + h.c.) \end{aligned} \quad (4.58)$$

As before we introduce the mean-field approximation $a_0 = a_0^\dagger = \sqrt{N_0}$ and diagonalize the term proportional to $\sqrt{N_0}$ in terms of the new modes:

$$e_{l\mathbf{k}}^\dagger = \gamma_{\mathbf{k}} e_{\mathbf{k}}^\dagger + \theta_{\mathbf{k}} t_{\mathbf{k}}^\dagger \quad (4.59)$$

$$e_{u\mathbf{k}}^\dagger = -\theta_{\mathbf{k}} e_{\mathbf{k}}^\dagger + \gamma_{\mathbf{k}} t_{\mathbf{k}}^\dagger \quad (4.60)$$

Using the above relations we can rewrite the part of the interaction that was not diagonalized, in terms of the modes $e_{l\mathbf{k}}^\dagger$ (neglecting the coupling to the higher energy modes $e_{u\mathbf{k}}^\dagger$). This yields the following effective Hamiltonian:

$$\begin{aligned} H_{eff} &= \sum_{\mathbf{k}} \xi_{\mathbf{k}} e_{l\mathbf{k}}^\dagger e_{l\mathbf{k}} + \sum_{\mathbf{k}} (\omega_{\mathbf{k}} + \Delta) x_{\mathbf{k}}^\dagger x_{\mathbf{k}} \\ &+ \sum_{\mathbf{kq}} \frac{g}{\sqrt{A}} \theta_{\mathbf{k}+\mathbf{q}} \gamma_{\mathbf{k}} e_{l\mathbf{k}+\mathbf{q}}^\dagger e_{l\mathbf{k}} (x_{\mathbf{q}}^\dagger + h.c.) \end{aligned} \quad (4.61)$$

From the above we can trace out the excitons (see for example the derivations in Ch.8 and App.A.8.2) to obtain effective interactions between electrons. Assuming that the electrons are close to the Fermi surface we obtain the effective interaction:

$$u_{eff}(\mathbf{q}) = -2 \frac{(\theta_{k_F} \gamma_{k_F} g)^2}{\Delta + \omega_{\mathbf{q}}} \quad (4.62)$$

where g was defined previously to be $g = \sqrt{\frac{2\pi}{\mu} \epsilon_T}$.

We will discuss in Ch.8 how this attractive interaction can lead to a superconducting transition in the electron system. For now we discuss how the above interaction can be increased. First, notice that it is proportional to the trion binding, which means that strongly bound trion states are lead to stronger interactions. Second, notice the dependence on the quasiparticle weights $\theta_{k_F}, \gamma_{k_F}$. These are determined by the ratio of gn_0 and $\Delta - \epsilon_T$. Therefore, there are two ways to increase interactions. Either increasing gn_0 (by increasing ϵ_T or n_0) or by bringing the trion into resonance to the bare electron so that $\Delta - \epsilon_T \ll gn_0$ (by tuning Δ for instance).

4.6 CONCLUSION

In this chapter we solved the polaron problem using a many-body Green's function approach. This allowed us to go beyond the Chevy ansatz approximation and include multiple electron-hole excitations in the polaron dressing cloud. In addition, we also introduced the powerful concept of conserving approximations, and showed how to calculate two-particle correlation functions starting from the single-particle Green's functions.

This allowed us to derive all the contributions to polaron interactions in a conserving approximation. This should clarify the connection between different works on polaron interactions that often focus only a particular mechanism. Furthermore, we evaluated the dominant contributions to the

interaction between the polaron-polariton and the Bose-polaron quasiparticles that we introduced in Chapter 3.

5

FERMI-POLARONS IN INTERACTING FERMIONIC SYSTEMS

We use a wavefunction approach to discuss the excitations of an interacting electron system going beyond the often used Hartree-Fock and random-phase approximation. We show that the same technique can be used to analyze the dynamics of a mobile impurity in an interacting fermionic bath, and could in principle be generalized to tackle other many-body problems.

In the previous chapters we have investigated Bose-Fermi mixtures, but we have completely neglected the long range electron-electron interactions, leaving the justification of this approximation to this chapter. This is an important issue, since it represents one of the distinguishing features of our solid state implementation of a Bose-Fermi mixture.

In this chapter we provide a wavefunction based approach that allows the controlled study of the modification of the elementary excitations of Fermi liquid due to the long-ranged electron interactions, going beyond the often used Hartree-Fock or random phase approximation (RPA). We also discuss how these long-ranged electron interactions can be included in the study of the mobile impurities in electron systems.

We remark that, the analysis of the interacting electron gas cannot be done with the simple wavefunction approach introduced in Chapter 3. This is unfortunate, since the transparency afforded by simple wavefunction approaches can often lead to new insights, as has been the case with the Chevy ansatz in the context of Fermi polarons [3]. In contrast, diagrammatic techniques can often be confusing for the uninitiated. We show that this problem can also be solved using a wavefunction based approach if, instead of attempting to find an approximate wavefunction for the low-energy degrees of freedom, we determine an approximate creation operator for these excitations.

We emphasize that this chapter focuses on introducing and justifying a wavefunction method that could be used to solve the problem of an impurity in an interacting electron-system. Although time constraints prohibited us from actually solving the impurity problem, meaning that this chapter does not contain any new physics, it is nevertheless important to

include this work in the thesis, because it nicely illustrates the similarities and differences between the different methods that can be used to tackle many-body problems: the wavefunction method from Chapter 2 and the many-body Green's function method from Chapter 4.

This chapter is organized as follows. We begin in Sec.5.1 by briefly introducing the main difficulties for treating the long-ranged electron-electron interactions. We then present a wavefunction based perturbative approach which allows us to obtain the excitations of an interacting electron system beyond RPA. In Sec.5.2 we discuss how the method introduced above could be used to investigate the effect of electron-electron interactions on the dynamics of Fermi polarons. We present a brief conclusion and outlook in Sec.5.3.

5.1 LOW-ENERGY DEGREES OF FREEDOM OF A SYSTEM OF INTERACTING ELECTRONS

Our goal in this Section is to find a simple wavefunction approach that would allow the analysis of the mobile impurity problem in an interacting fermionic bath.

To set the stage for the discussion of the dressing of a mobile impurity in an interacting Fermi sea, we first discuss the excitation spectrum of an electron system interacting through long-ranged Coulomb interactions.

This problem has a long history, and there are still many open problems [10]. However, the limits of very high or very low electron densities are relatively well understood. The parameter that characterizes these two density regimes is conventionally denoted as $r_s = a/a_0$ where a is the mean interparticle distance $a = 1/\sqrt{\pi n}$, and a_0 the Bohr radius of the electrons. Since the average kinetic energy per particle scales as $1/r_s^2$ while the average Coulomb energy scales as $1/r_s$ the parameter r_s provides a good indication of which of the two dominates. Therefore in the high density regime $r_s \ll 1$, the kinetic energy dominates, and the system forms a Fermi sea, while the Coulomb interaction can be treated as a perturbation. In the opposite regime $r_s \gg 1$, the Coulomb interaction dominates, leading to the formation of a Wigner crystal, while the kinetic energy leads to weak perturbations around this state.

However, most systems of interest are in the intermediate regime. In our case for instance the parameter $r_s \approx 30$ when the Fermi energy is 20 meV. This would suggest that any interacting Fermi liquid at this small density should be far from a degenerate Fermi sea. However, one might

argue that we should not use the electron Bohr radius a_0 as the scale for distances in our system, because of the short-range screening characteristic of monolayers. If, instead of using this, we use the exciton Bohr radius $a_x \approx 1\text{nm}$ we get an $r_s \approx 3$, and we are still not in a regime where $r_s \ll 1$.

A useful approximation that is justified only in the regime $r_s \ll 1$ is the RPA, which greatly simplifies the type of correlations that are considered in an interacting electron system. Although this approximation is often used even in the intermediate regime $r_s \approx 1$, this is mostly for convenience.

In this section we present a very simple wavefunction based approach which allows us to treat the low-energy degrees of freedom of an interacting electron system beyond RPA, effectively including all vertex corrections to the RPA bubble diagram. Although in the following we will consider only single electron-hole pair excitations from the many-body ground state, (in diagrammatic language, we will sum only single polarization bubbles), it could be possible to use a similar approach to include more excitations. Although our approach is still perturbative, it should provide useful insights as we approach the intermediate regime $r_s \approx 1$ coming from $r_s \ll 1$, and should capture to some extent the failure of the RPA.

To begin our analysis we write down the electron Hamiltonian:

$$H = H_0 + H_I = \sum_{\mathbf{k}} \xi_{\mathbf{k}} e_{\mathbf{k}}^\dagger e_{\mathbf{k}} + \frac{1}{2A} \sum_{\mathbf{kk}'\mathbf{q}} V_{\mathbf{q}} e_{\mathbf{k}+\mathbf{q}}^\dagger e_{\mathbf{k}'-\mathbf{q}}^\dagger e_{\mathbf{k}'} e_{\mathbf{k}} \quad (5.1)$$

In the absence of interactions $r_s \rightarrow 0$ the ground state of the system is a simple Fermi sea:

$$|\Theta_0\rangle = \Pi_{|\mathbf{k}| < k_F} e_{\mathbf{k}}^\dagger |0\rangle \quad (5.2)$$

We want to find the single electron-hole pair excitation spectrum:

$$|\Psi_{n\mathbf{q}}\rangle = b_{n\mathbf{q}}^\dagger |\Theta\rangle = \sum_{\mathbf{k}} \varphi_{n\mathbf{q}\mathbf{k}} e_{\mathbf{k}+\mathbf{q}}^\dagger e_{\mathbf{k}} |\Theta\rangle \quad (5.3)$$

where $|\Theta\rangle$ denotes the interacting ground state.

Notice the main difference between this problem and the polaron problem. Although both are many-body problems, the polaron problem was greatly simplified by the fact that we already knew the ground state $|\Theta\rangle$ before analyzing the excitations on top of $|\Theta\rangle$. Now, we don't even have this starting point. This is precisely where many-body Green's function techniques are most useful, because they provide a perturbative way to calculate the excitations of an interacting many-body system, without first calculating the ground state of this system.

In the above we introduced the bosonic operators b which obey the commutation relations:

$$\langle \Theta | [b_{n\mathbf{q}}, b_{n\mathbf{q}}^\dagger] | \Theta \rangle = \sum_{\mathbf{k}} |\varphi_{n\mathbf{q}}|^2 (f_{\mathbf{k}+\mathbf{q}} - f_{\mathbf{k}}) \quad (5.4)$$

where we introduced the occupation factors:

$$f_{\mathbf{k}} = \langle \Theta | e_{\mathbf{k}}^\dagger e_{\mathbf{k}} | \Theta \rangle \approx \langle \Theta_0 | e_{\mathbf{k}}^\dagger e_{\mathbf{k}} | \Theta_0 \rangle = \begin{cases} 1 & \text{if } |\mathbf{k}| < k_F \\ 0 & \text{otherwise} \end{cases} \quad (5.5)$$

Notice that the states where $|\mathbf{k}| > k_F$ and $|\mathbf{k} + \mathbf{q}| < k_F$ contribute with a negative sign to the above normalization condition. This is similar to the interacting Bose gas where we found that the excitations are bogolons with $b^\dagger = ux^\dagger + vx$ and we had the condition $u^2 - v^2 = 1$.

We wish to determine the energy spectrum of these excitations. If these operators would have been the creation operators for the actual excitations in the system they would behave like ladder operators:

$$[H, b_{n\mathbf{q}}^\dagger] = E_{n\mathbf{q}} b_{n\mathbf{q}}^\dagger \quad (5.6)$$

and we could use them to create states with many excitations. However, because of our approximations they will obey the above condition only approximately.

Our approach is to satisfy the condition in Eq.5.6 by neglecting all operators that take us outside the Hilbert space defined by $b_{n\mathbf{q}}^\dagger | \Theta \rangle$. To do this we need to evaluate the commutators:

$$[H_0, e_{\mathbf{k}+\mathbf{q}}^\dagger e_{\mathbf{k}}] = \xi_{\mathbf{k}+\mathbf{q}} - \xi_{\mathbf{k}} \quad (5.7)$$

$$[H_I, e_{\mathbf{k}+\mathbf{q}}^\dagger e_{\mathbf{k}}] = \sum_{\mathbf{q}'\mathbf{k}'} V_{\mathbf{q}'} \left(e_{\mathbf{k}+\mathbf{q}+\mathbf{q}'}^\dagger e_{\mathbf{k}'-\mathbf{q}'}^\dagger e_{\mathbf{k}'} e_{\mathbf{k}} - e_{\mathbf{k}+\mathbf{q}}^\dagger e_{\mathbf{k}'-\mathbf{q}'}^\dagger e_{\mathbf{k}'} e_{\mathbf{k}-\mathbf{q}'} \right) \quad (5.8)$$

We now expand the number operators around their mean-field values $c_{\mathbf{k}}^\dagger c_{\mathbf{k}} = f_{\mathbf{k}} + \delta n_{\mathbf{k}}$, where $\delta n_{\mathbf{k}}$ is an operator. Introducing this in the above we can rewrite:

$$[H_I, e_{\mathbf{k}+\mathbf{q}}^\dagger e_{\mathbf{k}}] = \frac{1}{A} \sum_{\mathbf{k}'} (f_{\mathbf{k}+\mathbf{q}} - f_{\mathbf{k}}) (V_{\mathbf{k}'-\mathbf{k}} - V_{\mathbf{q}}) e_{\mathbf{k}'+\mathbf{q}}^\dagger e_{\mathbf{k}'} \quad (5.9)$$

$$\begin{aligned} & - \frac{1}{A} \sum_{\mathbf{k}'} f_{\mathbf{k}'} \left(V_{\mathbf{k}'-\mathbf{k}-\mathbf{q}} - V_{\mathbf{k}'-\mathbf{k}} \right) e_{\mathbf{k}+\mathbf{q}}^\dagger e_{\mathbf{k}'} \\ & \equiv \frac{1}{A} \sum_{\mathbf{k}'} u_{\mathbf{k}\mathbf{k}'\mathbf{q}} e_{\mathbf{k}'+\mathbf{q}}^\dagger e_{\mathbf{k}'} \end{aligned} \quad (5.10)$$

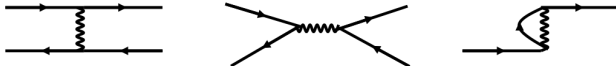


FIGURE 5.1: Left: direct electron-electron interaction. Middle: exchange interaction. Right: Fock exchange term

where we neglected the terms proportional to $\delta n_{\mathbf{k}}$ that take us outside of our Hilbert space.

The nice feature of the above equation is that all the terms have particular meanings. We illustrate them in Fig.5.1. The term proportional to $V_{\mathbf{k}'-\mathbf{k}}$ in the first summation corresponds to the direct scattering of the electron and the hole (the first term in Fig.5.1). This is the term that was responsible for the vertex corrections that led to the formation of excitons. The term proportional to $V_{\mathbf{q}}$ in the first summation corresponds to processes where the electron and the hole annihilate each other, by giving their momentum to the photon and then reappear as an electron-hole pair at a later time (second term in Fig.5.1). This is the only term that is kept in the RPA approximation. Finally the second summation in the above corresponds to the Fock exchange interaction between the electron(hole) and the other fermions. The first term in the summation, proportional to $V_{\mathbf{k}'-\mathbf{k}-\mathbf{q}}$ corresponds to the Fock term for the electron and is represented in the third diagram in Fig.5.1, with a corresponding contribution for the hole. The nice thing about this approach is that it allows us to treat all these terms at once and then decide which is the dominant one.

Plugging the above result into Eq. (5.6) we obtain:

$$\sum_{\mathbf{k}} e_{\mathbf{k}+\mathbf{q}}^\dagger e_{\mathbf{k}} \left[(\xi_{\mathbf{k}+\mathbf{q}} - \xi_{\mathbf{k}} - E_{n\mathbf{q}}) \varphi_{n\mathbf{q}\mathbf{k}} + \frac{1}{A} \sum_{\mathbf{k}'} u_{\mathbf{k}\mathbf{k}'\mathbf{q}} \varphi_{n\mathbf{q}\mathbf{k}'} \right] = 0 \quad (5.11)$$

which can be solved by setting the term in the square brackets to zero leading to the matrix eigenvalue equation:

$$(\xi_{\mathbf{k}+\mathbf{q}} - \xi_{\mathbf{k}}) \varphi_{n\mathbf{q}\mathbf{k}} + \frac{1}{A} \sum_{\mathbf{k}'} u_{\mathbf{k}\mathbf{k}'\mathbf{q}} \varphi_{n\mathbf{q}\mathbf{k}'} = E_{n\mathbf{q}} \varphi_{n\mathbf{q}\mathbf{k}} \quad (5.12)$$

It is straightforward to discretize the above equation and solve it. Notice that the above approach can easily be extended to other many-body problems, where we want to (approximately) determine the low-energy degrees of freedom of an interacting system, without first determining its ground

state. We remark that the Hilbert space is quite small since we have to take into account only one momentum. Therefore, it should be possible to extend this approach to include excitations of two electron-hole pairs.

5.1.1 Plasmons in the RPA limit

We remark that in the RPA limit, we can directly solve the above matrix equation. This RPA consists of keeping only the middle term in Fig.5.1, which corresponds to choosing $u_{\mathbf{k}\mathbf{k}'\mathbf{q}} = -(f_{\mathbf{k}+\mathbf{q}} - f_{\mathbf{k}})V_{\mathbf{q}}$ which simplifies the above eigenvalue equation to:

$$(\xi_{\mathbf{k}+\mathbf{q}} - \xi_{\mathbf{k}}) \varphi_{n\mathbf{q}\mathbf{k}} - \frac{(f_{\mathbf{k}+\mathbf{q}} - f_{\mathbf{k}})V_{\mathbf{q}}}{\mathcal{A}} \sum_{\mathbf{k}'} \varphi_{n\mathbf{q}\mathbf{k}'} = E_{n\mathbf{q}} \varphi_{n\mathbf{q}\mathbf{k}} \quad (5.13)$$

which can be rewritten as:

$$\varphi_{n\mathbf{q}\mathbf{k}} - \frac{(f_{\mathbf{k}+\mathbf{q}} - f_{\mathbf{k}})}{\xi_{\mathbf{k}+\mathbf{q}} - \xi_{\mathbf{k}} - E_{n\mathbf{q}}} \frac{V_{\mathbf{q}}}{\mathcal{A}} \sum_{\mathbf{k}'} \varphi_{n\mathbf{q}\mathbf{k}'} = 0 \quad (5.14)$$

Summing over \mathbf{k} and dividing by $\sum_{\mathbf{k}} \varphi_{n\mathbf{q}\mathbf{k}}$ we obtain:

$$V_{\mathbf{q}}^{-1} + \frac{1}{\mathcal{A}} \sum_{\mathbf{k}} \frac{f_{\mathbf{k}+\mathbf{q}} - f_{\mathbf{k}}}{E_{n\mathbf{q}} - \xi_{\mathbf{k}+\mathbf{q}} + \xi_{\mathbf{k}}} = 0 \quad (5.15)$$

One can check that the above equation has solutions when the energy is close to the single electron-hole pair excitation energy $E_{n\mathbf{q}} \approx \xi_{\mathbf{k}+\mathbf{q}} - \xi_{\mathbf{k}}$. These correspond to either adding an electron-hole pair to the wavefunction $|\Theta\rangle$ (when the energy is positive) or removing an electron-hole pair from $|\Theta\rangle$ (negative energy). This will form a continuum of excitations.

We remark that, due to these excitations, we cannot turn the above summation into an integral. If we wanted to do this, we could slightly shift the poles in the upper or lower complex plane by adding an infinitesimal imaginary part $i\eta$ to the energy $E_{n\mathbf{q}}$ and then the continuum of excitations will appear as a branch cut as we take $\eta = 0$.

Separated from the continuum there is also a collective excitation known as the plasmon, corresponding to the whole Fermi sea oscillating back and forth. This is the only solution in the above equation which survives when we turn the summation into an integral. One can check that the energy of the plasmon is given by $\omega_{pl}(\mathbf{q}) = \sqrt{n_e |\mathbf{q}|^2 V_{\mathbf{q}} / m_e}$.

Using the more general approach suggested above we could check how the plasmon energy is changed when the RPA is no longer valid.

5.2 FERMI POLARONS IN INTERACTING FERMI LIQUID

Having discussed how to determine the excitations of an interacting Fermi system, we show how the same approach can be used to discuss the dynamics of mobile impurities in interacting fermionic systems, and possibly investigate the effects of plasmon dressing.

In this section we will consider the following Hamiltonian:

$$\begin{aligned} H = & H_0 + H_{ex} + H_{ee} = \sum_{\mathbf{k}} \xi_{\mathbf{k}} e_{\mathbf{k}}^\dagger e_{\mathbf{k}} + \sum_{\mathbf{k}} \omega_{\mathbf{k}} x_{\mathbf{k}}^\dagger x_{\mathbf{k}} \\ & + \frac{1}{2A} \sum_{\mathbf{k}\mathbf{k}'\mathbf{q}} V_{\mathbf{q}} e_{\mathbf{k}+\mathbf{q}}^\dagger e_{\mathbf{k}'-\mathbf{q}}^\dagger e_{\mathbf{k}'} e_{\mathbf{k}} + \frac{v}{A} \sum_{\mathbf{k}\mathbf{k}'\mathbf{q}} e_{\mathbf{k}+\mathbf{q}}^\dagger x_{\mathbf{k}'-\mathbf{q}}^\dagger x_{\mathbf{k}'} e_{\mathbf{k}} \end{aligned} \quad (5.16)$$

and assume there is only one exciton in the system.

Similar to before, we start from the ground state of the interacting Fermi liquid $|\Theta\rangle$ and want to find a Fermi-polaron operator a^\dagger , such that $a^\dagger |\Theta\rangle$ is an approximate eigenstate of the system. The exciton will be dressed by excitations in the Fermi sea. We truncate the excitation Hilbert space to a single electron-hole pair and introduce the (zero-momentum) polaron creation operator:

$$a^\dagger = \varphi x_0^\dagger + \sum_{\mathbf{k},\mathbf{q}} \varphi_{\mathbf{k}\mathbf{q}} x_{\mathbf{q}-\mathbf{k}}^\dagger e_{\mathbf{k}}^\dagger e_{\mathbf{q}} \quad (5.17)$$

We would like to impose the condition that the polaron excitations are (approximately) bosonic, i.e. $[a, a^\dagger] \approx 1$. The polaron commutator is an operator valued quantity:

$$\begin{aligned} [a, a^\dagger] = & |\varphi|^2 + \sum_{\mathbf{k}\mathbf{q}\mathbf{k}'} \varphi_{\mathbf{k}\mathbf{q}}^* \varphi_{\mathbf{k}'\mathbf{q}'} e_{\mathbf{q}}^\dagger e_{\mathbf{k}} e_{\mathbf{k}'}^\dagger e_{\mathbf{q}-\mathbf{k}+\mathbf{k}'} \\ & + \sum_{\mathbf{k}\mathbf{q}\mathbf{k}'\mathbf{q}'} \varphi_{\mathbf{k}\mathbf{q}}^* \varphi_{\mathbf{k}'\mathbf{q}'} x_{\mathbf{q}'-\mathbf{k}'}^\dagger x_{\mathbf{q}-\mathbf{k}} \left(e_{\mathbf{q}}^\dagger e_{\mathbf{q}'} \delta_{\mathbf{k}\mathbf{k}'} - e_{\mathbf{k}'}^\dagger e_{\mathbf{k}} \delta_{\mathbf{q}\mathbf{q}'} \right) \end{aligned} \quad (5.18)$$

However, all we want to require is that $\langle \Theta | [a, a^\dagger] | \Theta \rangle = 1$. Notice that this immediately destroys the last term in the above, because there are no excitons in the state $|\Theta\rangle$. In addition, since we have truncated the Hilbert space to a single electron-hole pair excitation, we factorize all higher order correlations since this does not represent an additional approximation.

Doing this we obtain:

$$\langle \Theta | [a, a^\dagger] | \Theta \rangle \approx |\varphi|^2 + \sum_{\mathbf{k}\mathbf{q}} |\varphi_{\mathbf{k}\mathbf{q}}|^2 (1 - f_{\mathbf{k}}) f_{\mathbf{q}} = 1 \quad (5.19)$$

Notice that the only nonzero contributions to the summation come from excitations where $|\mathbf{k} + \mathbf{q}| > k_F$ and $|\mathbf{q}| < k_F$ or vice-versa. This should be contrasted with the Fermi polaron ansatz in Chapter 3, where the excitations $|\mathbf{k} + \mathbf{q}| < k_F$ and $|\mathbf{q}| > k_F$ were not considered, since these would not be allowed in the noninteracting ground state $|\Theta_0\rangle$.

We want now to find the wavefunction φ to satisfy the condition $[H, a^\dagger] \approx E a^\dagger$. The commutators with the kinetic energy term H_0 are again straightforward:

$$[H_0, x_0^\dagger] = \omega_0 x_0^\dagger \quad (5.20)$$

$$[H_0, x_{\mathbf{q}-\mathbf{k}}^\dagger e_{\mathbf{k}}^\dagger e_{\mathbf{q}}] = (\omega_{\mathbf{q}-\mathbf{k}} + \xi_{\mathbf{k}} - \xi_{\mathbf{q}}) x_{\mathbf{q}-\mathbf{k}}^\dagger e_{\mathbf{k}}^\dagger e_{\mathbf{q}} \quad (5.21)$$

The commutators with the exciton-electron interaction term can also be calculated easily:

$$[H_{xe}, x_0^\dagger] = x_0^\dagger \frac{v}{A} \sum_{\mathbf{q}} f_{\mathbf{q}} + \frac{v}{A} x_{\mathbf{q}-\mathbf{k}}^\dagger e_{\mathbf{k}}^\dagger e_{\mathbf{q}} \quad (5.22)$$

$$\begin{aligned} [H_{xe}, x_{\mathbf{q}-\mathbf{k}}^\dagger e_{\mathbf{k}}^\dagger e_{\mathbf{q}}] &= \frac{v}{A} \sum_{\mathbf{q}'\mathbf{k}'} x_{\mathbf{q}-\mathbf{k}+\mathbf{q}'}^\dagger e_{\mathbf{k}}^\dagger e_{\mathbf{q}} e_{\mathbf{k}'-\mathbf{q}'}^\dagger e_{\mathbf{k}'} \\ &\quad + \frac{v}{A} \sum_{\mathbf{q}'\mathbf{k}'} x_{\mathbf{k}'+\mathbf{q}'}^\dagger x_{\mathbf{k}'} x_{\mathbf{q}-\mathbf{k}}^\dagger (e_{\mathbf{k}-\mathbf{q}'}^\dagger e_{\mathbf{q}} - e_{\mathbf{k}}^\dagger e_{\mathbf{q}+\mathbf{q}'}) \\ &\approx \frac{v}{A} x_0^\dagger f_{\mathbf{q}} + x_{\mathbf{q}-\mathbf{k}}^\dagger e_{\mathbf{k}}^\dagger e_{\mathbf{q}} \frac{v}{A} \sum_{\mathbf{q}'} f'_{\mathbf{q}} \\ &\quad + \frac{v}{A} \sum_{\mathbf{k}' \neq \mathbf{q}} x_{\mathbf{q}-\mathbf{k}'}^\dagger e_{\mathbf{k}'}^\dagger e_{\mathbf{q}} (1 - f_{\mathbf{k}}) - \frac{v}{A} \sum_{\mathbf{q}' \neq \mathbf{k}} x_{\mathbf{q}'-\mathbf{k}}^\dagger e_{\mathbf{k}}^\dagger e_{\mathbf{q}'} f_{\mathbf{q}} \end{aligned} \quad (5.23)$$

where, we used the same approximation technique introduced in the previous section, to remain in the same Hilbert space.

The commutator with the electron-electron interaction part can be also calculated using Eq. (5.10):

$$\begin{aligned} [H_{ee}, x_{\mathbf{q}-\mathbf{k}}^\dagger e_{\mathbf{k}}^\dagger e_{\mathbf{q}}] &= \frac{1}{A} \sum_{\mathbf{k}'} (f_{\mathbf{k}} - f_{\mathbf{q}}) (V_{\mathbf{q}'-\mathbf{q}} - V_{\mathbf{k}-\mathbf{q}}) x_{\mathbf{q}-\mathbf{k}}^\dagger e_{\mathbf{k}+\mathbf{q}-\mathbf{q}'}^\dagger e_{\mathbf{q}'} \\ &\quad - \frac{1}{A} \sum_{\mathbf{q}'} f_{\mathbf{q}'} (V_{\mathbf{q}'-\mathbf{k}} - V_{\mathbf{q}'-\mathbf{q}}) x_{\mathbf{q}-\mathbf{k}}^\dagger e_{\mathbf{k}}^\dagger e_{\mathbf{q}} \\ &= \frac{1}{A} \sum_{\mathbf{q}'} u_{\mathbf{q}, \mathbf{q}', \mathbf{k}-\mathbf{q}} x_{\mathbf{q}-\mathbf{k}}^\dagger e_{\mathbf{k}+\mathbf{q}-\mathbf{q}'}^\dagger e_{\mathbf{q}'}^\dagger \end{aligned} \quad (5.24)$$

Gathering all commutators we arrive at the equations:

$$x_0^\dagger \left[\varphi \left(\omega_0 + \frac{v}{\mathcal{A}} \sum_{\mathbf{q}} f_{\mathbf{q}} - E \right) + \frac{v}{\mathcal{A}} \sum_{\mathbf{kq}} \varphi_{\mathbf{kq}} f_{\mathbf{q}} \right] = 0 \quad (5.25)$$

$$x_{\mathbf{q}-\mathbf{k}}^\dagger e_{\mathbf{k}}^\dagger e_{\mathbf{q}} \left[\varphi_{\mathbf{kq}} \left(\omega_{\mathbf{q}-\mathbf{k}} + \xi_{\mathbf{k}} - \xi_{\mathbf{q}} + \frac{v}{\mathcal{A}} \sum_{\mathbf{q}'} f_{\mathbf{q}'} \right) + \varphi \frac{v}{\mathcal{A}} \right. \\ \left. + \frac{v}{\mathcal{A}} \sum_{\mathbf{k}' \neq \mathbf{q}} \varphi_{\mathbf{k}'\mathbf{q}} (1 - f_{\mathbf{k}'}) - \frac{v}{\mathcal{A}} \sum_{\mathbf{q}' \neq \mathbf{k}} \varphi_{\mathbf{kq}'} f_{\mathbf{q}'} + \frac{1}{\mathcal{A}} \sum_{\mathbf{q}'} u_{\mathbf{q}'\mathbf{q}\mathbf{k}'-\mathbf{q}'} \varphi_{\mathbf{k}+\mathbf{q}'-\mathbf{q},\mathbf{q}'} \right] = 0 \quad (5.26)$$

The above equations can be solved by setting the terms in the square brackets to zero, which results in a matrix eigenvalue equation. Notice that the size of the above Hilbert space is only twice as large as the Hilbert space spanned by the Chevy ansatz that we used when solving the Fermi polaron problem in non-interacting fermionic systems. Therefore, the above equations can be solved numerically by discretizing momentum space, a technique that we discuss in more detail in Chapter 6.

This could allow us to investigate new polaron states, where the mobile impurity in addition to being dressed by the electron-hole pair excitations (which we investigated in previous chapters) is also dressed by the plasmonic collective excitations of the Fermi sea.

5.3 CONCLUSION AND OUTLOOK

We have proposed a perturbative wavefunction based approach to finding the excitations of many-body systems, without knowing the interacting ground state of the system.

We showed how this method could be used to treat electron interactions beyond RPA and actually include all vertex corrections to the polarization bubble. This simple and transparent method could be used to investigate the failure of the RPA, coming from the $r_s \ll 1$ limit and approaching the experimentally relevant regime $r_s \approx 1$, using the screened Coulomb interactions specific for TMDs.

We also showed how this method could be used to investigate the mobile impurity problem. In addition to providing a way to analyze the importance of long-range electron interactions on the dressing cloud, this method could be used to determine the quasiparticles in the system, away from the polaron limit $n_x \ll n_e$, which is still quite poorly understood.

Still another important contribution of this approach is to better clarify the connection between the wavefunction approach and the many-body Green's function approach and emphasize the limitations of the wavefunction approach used in Chapter 3.

6

ROTON STATES IN OPTICAL SPECTRA

We investigate the effects of the interaction between excitons and electrons in the same valley. We show that the exciton develops a roton-like dispersion due to these interactions, a feature that is particularly robust in monolayers due to the non-local dielectric screening characteristic of monolayers. We find indirect evidence for these roton-states in photoluminescence spectra.

In previous chapters we focused on the effects of the attractive interaction between excitons and electrons in the opposite valley. However, we largely neglected the repulsive interaction between excitons and the electrons in the same valley. Crucially, we did not neglect this interaction because it was weak. In fact, the diagram in Fig.3.1 yielded an interaction with the same magnitude as that between excitons and electrons in the opposite valley. However, we neglected this interaction because we believed it will not lead to strongly correlated states between excitons and electrons, due to its repulsive nature.

In this chapter we revisit this issue and investigate in detail the interaction between excitons and electrons in the same valley. We show that it has a nontrivial momentum dependence. Because of this, upon increasing the electron density, the optical excitation spectrum changes qualitatively and the elementary optical excitations develop a roton-like dispersion. This is evidenced by a shift of the lowest energy state to a finite momentum on the order of the Fermi momentum. We show that this roton state is particularly robust in our system due to the long-range nature of the Coulomb interaction and the non-local dielectric screening characteristic of monolayers

We also show that the emergence of rottons could be related to the hitherto unexplained aspects of photoluminescence spectra in doped transition metal dichalcogenides, providing indirect evidence for such roton states.

We investigate this problem using a variational approach. We first consider the interaction between excitons and electrons in the same valley. We then extend the Hilbert space to consider the interaction with electrons in the opposite valley, treating this interaction in a similar way as we did in

previous chapters. We use this to calculate experimental observables such as absorption and emission spectra.

This chapter is structured as follows. After a general introduction to the concept of rotons in Sec.6.1 we focus on the interaction between excitons and electrons in the same valley and show that excitons in the system develop a roton-like dispersion. In Sec.6.3 we discuss the limitations of our approach and argue why we believe that a proper treatment that obeys the conservation laws in the system (i.e. a conserving approximation) should make the roton states more robust. In Sec. 6.4 we extend the approach in the previous sections to include the interaction between excitons and electrons in the opposite valley. This calculation allows us to investigate the optical signatures of the roton states in Sec.6.5, where we show that rotors could explain the stark differences between optical photoluminescence and absorption in TMDs.

This chapter is based on Ref. [13].

6.1 ROTONS

Before starting our analysis we place our work in context. After introducing the concept of rotons, we discuss the mechanism leading to the roton-formation in our system. Then we compare this mechanism to the mechanisms of roton formation in other systems.

Rotons are quasiparticles whose dispersion exhibits a minimum at finite momentum. The concept was first proposed by Landau as an explanation for the properties of superfluid ^4He [14, 47]. More recently, rotons have been predicted and observed in ultracold Bose gases with long-range interactions [48, 49], engineered spin-orbit coupling [50, 51], and shaken optical lattices [52]. However, the study of rotons and other many-body effects in ultracold gases is impeded by the weak interactions between neutral atoms. It is therefore desirable to explore platforms with strong interparticle interactions that simultaneously retain a greater degree of tunability than conventional condensed matter systems such as ^4He .

Let us investigate the mechanism that can lead to the emergence of rotons in our system. Consider an exciton of zero momentum, as defined through Eq. (6.2). It is a superposition of electron and hole states with momenta of the order of $1/a_x$ (a_x denotes the exciton Bohr radius). The electron states with momenta smaller than k_F are occupied by the Fermi sea electrons, a Pauli blocking effect that will manifest itself as a repulsive interaction which will blue-shift the exciton energy. Let us consider

now an exciton with momentum $p > k_F + 1/a_x$. The electron forming this exciton is already orthogonal to the Fermi sea electrons, and therefore will not experience any Pauli blocking. This simple argument shows how Pauli-blocking results in a repulsive interaction between excitons and the electrons in the Fermi sea that is largest for zero momentum excitons and decreases as the exciton momentum increases. The exciton dispersion can be significantly altered by this momentum dependent repulsion. We will show that, as the Fermi energy is increased from zero, the exciton mass (at zero momentum) increases. At a critical Fermi energy, the mass (at zero momentum) diverges and the energy minimum is shifted to a finite momentum p_{rot} , which we refer to as a roton minimum.

An equivalent way to view the emergence of this roton minimum is to look directly at the exciton formation in the presence of electrons, as illustrated in Fig. 6.1(b). Let us consider the lowest energy configuration for an optically excited interband electron-hole pair in the presence of a Fermi sea of electrons. Clearly, if we neglect the Coulomb attraction between the electron and the hole, clearly the lowest energy configuration would be of finite center-of-mass momentum k_F , with the hole at zero momentum and an electron of momentum k_F . As we will show, this tendency also survives when we include the Coulomb attraction leading to the binding of the electron-hole pair in the exciton, for large enough k_F .

A closely related effect has been predicted for the molecular state of an impurity in an ultracold Fermi gas, where the roton minimum is associated with the formation of FFLO states [53]. These states have however never been observed as they are expected to be unstable over a wide range of parameters [54]. Similar states have been predicted for the indirect exciton states in electron-hole bilayers in GaAs heterostructures [55–57]. In these systems, as well as in TMDs considered here, the roton states are more robust owing to the long-ranged nature of the Coulomb interaction compared to short-range interatomic interactions in ultracold gases.

6.2 ROTON STATES IN DOPED SEMICONDUCTOR

We start our analysis by considering the simplified case of an interacting electron-hole system with only one type of electrons/holes (i.e. we assume we can focus on a single valley in TMDs). Such systems can be realized in practice by breaking time reversal symmetry, with moderate magnetic fields [58, 59] or by bringing the TMD in contact with a ferromagnetic material such as CrI₃ [60]. The treatment of this regime is also useful for

pedagogical reasons, since it allows us to isolate the reasons for the emergence of the roton quasiparticles. Furthermore, it is also a useful starting point for the experimentally more common case where time reversal is satisfied, which we will analyze in the next section.

The Hamiltonian describing such a system was already given in Chapter 3:

$$\begin{aligned} H = & \sum_{\mathbf{k}} \xi_{\mathbf{k}} e_{\mathbf{k}}^{\dagger} e_{\mathbf{k}} + \sum_{\mathbf{k}} \xi_{\mathbf{k}} h_{\mathbf{k}}^{\dagger} h_{\mathbf{k}} + \frac{1}{2A} \sum_{\mathbf{kk}'\mathbf{q}} V_{\mathbf{q}} e_{\mathbf{k}+\mathbf{q}}^{\dagger} e_{\mathbf{k}'-\mathbf{q}}^{\dagger} e_{\mathbf{k}'} e_{\mathbf{k}} \\ & + \frac{1}{2A} \sum_{\mathbf{kk}'\mathbf{q}} V_{\mathbf{q}} h_{\mathbf{k}+\mathbf{q}}^{\dagger} h_{\mathbf{k}'-\mathbf{q}}^{\dagger} h_{\mathbf{k}'} h_{\mathbf{k}} - \frac{1}{A} \sum_{\mathbf{kk}'\mathbf{q}} V_{\mathbf{q}} e_{\mathbf{k}+\mathbf{q}}^{\dagger} h_{\mathbf{k}'-\mathbf{q}}^{\dagger} h_{\mathbf{k}'} e_{\mathbf{k}} \end{aligned} \quad (6.1)$$

e^{\dagger} (h^{\dagger}) creates an electron in the conduction band (hole in the valence band) with the respective dispersion $\xi_{\mathbf{k}} = |\mathbf{k}|^2 / (2m)$, A denotes the quantization area and $V_{\mathbf{q}} = 1/(2\epsilon_0|\mathbf{q}|(1+r_0|\mathbf{q}|))$ where $r_0 \approx 5 \text{ nm}$ in MoSe₂ [22].

6.2.1 Exciton Schroedinger equation

To investigate the exciton bound states we make a molecular ansatz of the form:

$$|\Psi_{n\mathbf{p}}\rangle = \sum_{\mathbf{k}} \phi_{n\mathbf{p}\mathbf{k}} e_{\mathbf{k}}^{\dagger} h_{\mathbf{p}-\mathbf{k}}^{\dagger} |\Theta\rangle \quad (6.2)$$

where $|\Theta\rangle$ denotes the ground state of the system in the absence of the excitonic excitation. This is a complicated many-body ground state, but for simplicity we use the so-called Hartree-Fock approximation to approximate this state by the ground state of a non-interacting Fermi gas:

$$|\Theta\rangle = \Pi_{|\mathbf{k}| < k_F} e_{\mathbf{k}}^{\dagger} |0\rangle. \quad (6.3)$$

where $k_F = \sqrt{2\pi n_e}$. Notice that the energy of the ground state in the Hartree-Fock approximation can be calculated to obtain:

$$E_0 = \langle \Theta | H | \Theta \rangle = \frac{1}{2A} \sum_{|\mathbf{k}|, |\mathbf{k}'| < k_F} (V_0 - V_{k'-k}) \quad (6.4)$$

Since we assumed that the system is charge-neutral we have $V_0 = 0$ and therefore the first contribution (also known as the Hartree contribution) and the energy is determined only by the Fock or exchange contribution.

Basically the energy of the ground state is lowered because the electrons have to avoid each other due to Pauli exclusion.

With the above definition of the ground state we remark that the summation in Eq. (6.2) is restricted to $|\mathbf{k}| < k_F$. We solve $H |\Psi_{n\mathbf{p}}\rangle = (\omega_{n\mathbf{p}} + E_0) |\Psi_{n\mathbf{p}}\rangle$, in the truncated Hilbert space spanned by $|\Psi_{n\mathbf{p}}\rangle$. Acting with $\langle \Theta | h_{\mathbf{k}} e_{\mathbf{p}-\mathbf{k}}$ on the left in the above equation we obtain:

$$\phi_{n\mathbf{p}\mathbf{k}} (\xi_{\mathbf{k}} + \xi_{\mathbf{p}-\mathbf{k}} + \beta(\mathbf{k})) + \sum_{|\mathbf{k}'| > k_F} V_{\mathbf{k}'-\mathbf{k}} \phi_{n\mathbf{p}\mathbf{k}'} = E_{n\mathbf{p}} \phi_{n\mathbf{p}\mathbf{k}} \quad (6.5)$$

where $\beta(\mathbf{k})$ denotes Fock term corresponding to the exchange interaction between the electron forming the exciton and the rest of the electrons, and is given by:

$$\beta(\mathbf{k}) = -\frac{1}{A} \sum_{|\mathbf{k}'| < k_F} V_{\mathbf{k}'-\mathbf{k}} \approx \beta(0) \quad (6.6)$$

where in the last step we assumed that $\beta(\mathbf{k})$ leads only to a band gap renormalization, i.e. its momentum dependence is negligible. From now on, we will disregard the contribution from $\beta(\mathbf{k})$ since it will lead to a trivial shift of all states by a constant amount and will not influence our conclusions about the emergence of the roton state.

We solve Eq. (6.5) numerically using angular momentum eigenstates on a nonuniform radial grid. We include angular momentum quantum numbers up to $m = 5$ and employ a nonuniform grid (quadratically increasing spacing) of 1000 radial momenta from 0 to 0.5 \AA^{-1} . The electron and hole masses used for the calculation are $m_e = 0.56m_0$, $m_h = 0.59m_0$, where m_0 [61] denotes the mass of a free electron. We perform all numerical integrations using a trapezoidal rule, adjusting the grid size to reach convergence.

6.2.2 Results

The dispersion thus obtained is shown in Fig. 6.1(a) for Fermi energies between $\epsilon_F = 0 \text{ meV}$ and $\epsilon_F = 50 \text{ meV}$. At large doping, the dispersion minimum shifts to finite momentum. The schematic illustration in Fig. 6.1(b) provides a qualitative explanation for the emergence of such a roton state. With the electron constrained to states above the Fermi sea, an electron-hole pair with zero total momentum carries a larger kinetic energy than an electron-hole pair in which the hole occupies a state closer to the valence band maximum. At small Fermi energies, the Coulomb attraction

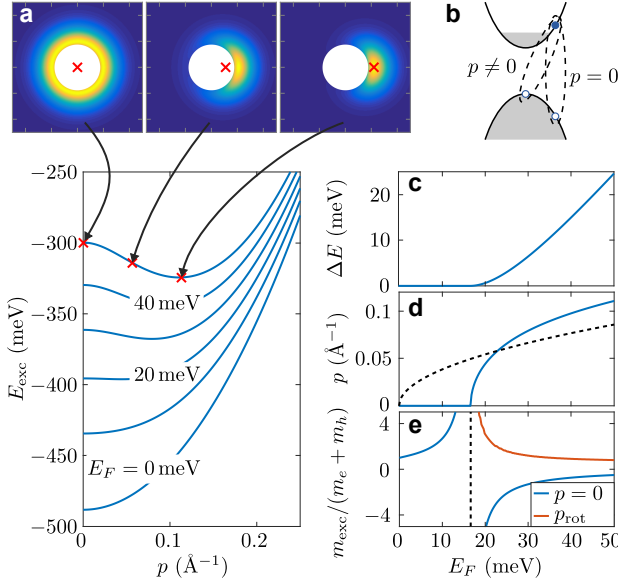


FIGURE 6.1: (a) Lower panel: Exciton dispersion at different Fermi energies, ϵ_F . Upper panels: Electron wavefunction $|\varphi_p(\mathbf{k})|^2$ as a function of (k_x, k_y) at three different center of mass momenta \mathbf{p} indicated by the red crosses. The blocked out circle is Fermi sea. The axis limits are $\pm 0.25 \text{\AA}^{-1}$. (b) Schematic drawing illustrating the origin of the roton-like dispersion. As a function of Fermi energy: (c) Energy difference $\Delta E = E_{\text{exc}}(0) - \min E_{\text{exc}}(\mathbf{p})$ between the zero momentum exciton and the lowest energy state. (d) Momentum of the lowest energy exciton state (solid) and Fermi momentum (dashed). (e) Exciton mass at zero momentum (blue) and at the roton minimum (red).

more than compensates for the cost in kinetic energy, allowing the lowest energy exciton to remain at zero momentum. The energy cost increases with increasing Fermi energy such that the excitonic ground state eventually shifts to finite momentum. While the roton minimum originates from Pauli blocking, the exact form of the electron-hole interaction plays a crucial role in determining the Fermi energy at which the roton minimum appears. In our case, using the dielectrically screened Coulomb potential, the roton minimum develops at $\epsilon_F \approx 20 \text{ meV} \approx E_0/25$, where E_0 denotes the exciton binding energy at zero Fermi energy. By contrast, a much greater Fermi energy of $\epsilon_F = E_0/2$ would be required if the electron and hole interacted via contact interaction (assuming equal carrier masses) [54]. The

Pauli blocking effect is more pronounced for long-range interactions because scattering with large momenta to accessible states across the Fermi sea is suppressed. It is especially efficient in monolayer materials due to the short-range dielectric screening which further suppresses contributions from momenta on the order of $1/r_0$.

The properties of the dispersion are explored more quantitatively in Fig. 6.1(c)–(e). Fig. 6.1(c) shows the energy separation between the exciton at zero momentum and the lowest energy state, indicating that the ground state is no longer at zero momentum when the Fermi energy exceeds $\epsilon_F \approx 20$ meV. In Fig. 6.1(d), we plot the momentum at which the dispersion minimum occurs. As expected from the qualitative argument given in the context of Fig. 6.1(b), the momentum of the roton is on the order of the Fermi momentum (dashed line). Finally, the effective mass both at zero momentum and at the roton minimum, p_{rot} , is plotted Fig. 6.1(e). The effective mass at the roton minimum corresponds to the curvature of the dispersion along the radial direction, while the mass in the tangential direction diverges as a consequence of rotational symmetry.

6.2.3 Bethe-Salpeter equation

We remark that our calculation is completely equivalent to a diagrammatic calculation based on the (non-self-consistent) ladder approximation, which results in an equation known as the Bethe-Salpeter equation. We briefly discuss this equivalence since it provides additional insight into our results and can be used to further refine calculations.

Let us introduce the time-ordered electron and hole Green's functions in Fourier space:

$$G_e(p) = -i \int d\tau e^{i\omega\tau} \langle \Theta | \mathcal{T} e_p(t+\tau) e_p^\dagger(\tau) | \Theta \rangle \quad (6.7)$$

$$G_h(p) = -i \int d\tau e^{i\omega\tau} \langle \Theta | \mathcal{T} h_p(t+\tau) h_p^\dagger(\tau) | \Theta \rangle \quad (6.8)$$

where $|\Theta\rangle$ denotes the many-body ground state of N interacting electrons and we will use again the 4 vector notation $p \equiv (\mathbf{p}, \omega)$ for notational simplicity (we will later also use $k \equiv (\mathbf{k}, \epsilon)$) and we will incorporate factors of $1/(2\pi)$ into the definition of integral measure such that $dp = d\mathbf{p} d\omega / (2\pi)^3$.

The Green's functions are related to their self-energies through Dyson's equation:

$$G_{e,h}(p)^{-1} = G_{e,h}^{(0)}(p)^{-1} - \Sigma_{e,h}(p) \quad (6.9)$$

$$G_{e,h}^{(0)}(p)^{-1} = \omega - \xi_{\mathbf{k}} + \mu_{e,h} + i0^+ \operatorname{sgn}(\omega) \quad (6.10)$$

where $G_{e,h}^{(0)}$ denotes the bare propagators in the absence of interactions, $\xi_{\mathbf{p}}$ denotes the bare electron(hole) dispersion and $\mu_{e,h}$ the electron and hole chemical potentials.

Notice that, since we are in the regime $n_h \ll n_e$ we can neglect the self-energy acquired by electrons through their interaction with the holes. As we did in the variational calculation we treat the electron-electron interaction within Hartree-Fock approximation, which yields an electron self-energy $\Sigma_e(p) = \beta(0)$ where $\beta(0)$ was defined in Eq. (6.6). Diagrammatically, the exciton pairing instability emerges as a pole in the two particle Green's function of a conduction band electron and valence band hole, or in the T-matrix for the electron and hole scattering (and therefore also in the light-matter coupling vertex). Within the ladder approximation the T-matrix is defined recursively as:

$$T(\mathbf{k}, \mathbf{k}', p) = V_{\mathbf{k}'-\mathbf{k}} + i \int dk'' V_{\mathbf{k}''-\mathbf{k}} G_e(k'') G_h(p - k'') T(\mathbf{k}'', \mathbf{k}', p) \quad (6.11)$$

In the regime $n_h \ll n_e$ we can set the hole chemical potential below the (dressed) hole dispersion, which implies that we can replace the time-ordered hole propagator by its retarded counterpart $G_h(p) = G_h^R(p)$. The energy integral over ϵ can be easily performed now (see Ch.3) to obtain:

$$T(\mathbf{k}, \mathbf{k}', p) = V_{\mathbf{k}'-\mathbf{k}} + \int \frac{d\mathbf{k}}{(2\pi)^2} V_{\mathbf{k}''-\mathbf{k}} G_h^R(\mathbf{p} - \mathbf{k}'', \omega - \xi_{\mathbf{k}''} + \mu_e) T(\mathbf{k}'', \mathbf{k}', p) \quad (6.12)$$

We still need to discuss G_h . In the non-self-consistent ladder approximation we replace G_h by its bare value $G_h^{(0)}$. It is straightforward to check that with this we recover the Schrödinger equation in the previous calculation Eq. (6.5). Indeed, performing this substitution we obtain:

$$T(\mathbf{k}, \mathbf{k}', p) = V_{\mathbf{k}'-\mathbf{k}} + \int \frac{d\mathbf{k}}{(2\pi)^2} V_{\mathbf{k}''-\mathbf{k}} \frac{1}{\omega - \xi_{\mathbf{k}''} - \xi_{\mathbf{p}-\mathbf{k}''} + \mu_e + i0^+} T(\mathbf{k}'', \mathbf{k}', p) \quad (6.13)$$

We remark that, as ω approaches the exciton energy the T-matrix blows up which means that we can neglect the small term $V_{\mathbf{k}'-\mathbf{k}}$ in the above equation, to obtain:

$$T(\mathbf{k}, \mathbf{k}', p) = \int \frac{d\mathbf{k}}{(2\pi)^2} V_{\mathbf{k}''-\mathbf{k}} \frac{1}{\omega - \xi_{\mathbf{k}} - \xi_{\mathbf{p}-\mathbf{k}} + \mu_e + i0^+} T(\mathbf{k}'', \mathbf{k}', p) \quad (6.14)$$

Summing over \mathbf{k}' and introducing the wavefunction:

$$\varphi_{\mathbf{k}} = \frac{1}{\omega - \xi_{\mathbf{k}} - \xi_{\mathbf{p}-\mathbf{k}} + \mu_e + i0^+} \sum_{\mathbf{k}'} T(\mathbf{k}, \mathbf{k}', p) \quad (6.15)$$

we can rewrite the above as a Schrödinger equation:

$$(\omega - \xi_{\mathbf{k}} - \xi_{\mathbf{p}-\mathbf{k}} + \mu_e + i0^+) \varphi_{\mathbf{k}} = \sum_{\mathbf{k}'} V_{\mathbf{k}'-\mathbf{k}} \varphi_{\mathbf{k}'} \quad (6.16)$$

which is precisely the same as Eq. (6.5).

6.3 BACKFLOW CORRECTIONS

With the above approach we have seen that a roton-minimum develops at Fermi energies of about 20 meV. However, because of the limitations of the simple approach that we have used, we have reason to believe that it would develop much sooner.

Indeed, one of the main limitations of our approach is that the quasiparticles that we obtained do not obey the continuity equation. Because of this we remark that the roton wavepacket does not satisfy the continuity equation in our approximation. Indeed, one can see that a roton wavepacket would carry a large electron current of order $p_{\text{rot}}/(2m)$. However, according to our calculation such a state should have a zero group velocity which implies that the local density will remain constant in time. This proves that our ansatz is far from an energy eigenstate. Notice that this breakdown is most pronounced at the roton minimum, which implies that a modified ansatz that obeys the continuity equation could improve the robustness of the roton. This argument was used by Feynman to motivate the introduction of backflow corrections in superfluid helium [62], which significantly lower the variational energy of the roton. A quantitative treatment of these effects is however beyond the scope of this work, and therefore we only suggest ways to improve this.

Before moving on, let us clarify what are the so-called backflow corrections. This important concept was first introduced by Landau in the context

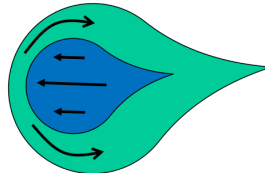


FIGURE 6.2: Schematic representation of the backflow current.

of Fermi-Liquid theory. Let us consider a normal Fermi liquid with a single quasiparticle excitation at momentum \mathbf{p} . Let us assume that in the absence of interactions the mass of the particle is m , and that interactions lead to a mass renormalization of the quasiparticle excitation to m^* . Notice that, in the absence of interactions the current in the system is \mathbf{p}/m . As we turn on interactions the current cannot change its value since interactions conserve momentum, meaning that $\mathbf{p}/m = \mathbf{p}/m^* + \mathbf{J}_b$, where \mathbf{J}_b is an additional current, due to the particles that the quasiparticle drags with it when it moves. We can rewrite the above as:

$$\frac{\mathbf{p}}{m^*} = \frac{\mathbf{p}}{m} - \mathbf{J}_b \quad (6.17)$$

which illustrates that the quasiparticle current is composed from the bare particle current \mathbf{p}/m minus a backflow current \mathbf{J}_b of the electrons in the Fermi sea, as we illustrate in Fig.6.2. Notice that in our approach we are unable to capture the backflow current, because our wavefunction does not allow for the modification of the Fermi sea, due to exciton-electron scattering.

To allow such processes, we can extend our ansatz to include the dressing of the excitons obtained in Eq. (6.5) by additional density fluctuations in the Fermi sea. Defining an exciton creation operator for the lowest energy eigenstate obtained from solving Eq. (6.5):

$$x_{\mathbf{p}}^\dagger = \sum_{\mathbf{k}} \phi_{0\mathbf{p}\mathbf{k}} e_{\mathbf{k}}^\dagger h_{\mathbf{p}-\mathbf{k}}^\dagger \quad (6.18)$$

we can write down a similar ansatz to Feynman's extended ansatz for rotons in superfluid helium with backflow corrections (this ansatz goes slightly beyond Feynman's approach):

$$|\tilde{\Psi}_{\mathbf{p}}\rangle = \xi_{n\mathbf{p}} x_{\mathbf{p}}^\dagger |\Theta\rangle + \sum_{\mathbf{q}} \xi_{n\mathbf{q}} x_{\mathbf{p}-\mathbf{q}}^\dagger e_{\mathbf{k}+\mathbf{q}}^\dagger e_{\mathbf{k}} |\Theta\rangle \quad (6.19)$$

Notice that, in the above ansatz the exciton obtained in Eq. (6.5) is treated as a rigid particle whose internal structure cannot be modified by the in-

teractions with the electrons. A further improvement to the above ansatz would be to allow ξ_{nq} in the last summation to also depend on \mathbf{k} . An even better ansatz, although computationally more challenging to handle, would be to allow the modification of the exciton internal structure. This would correspond to an ansatz of the form:

$$|\Psi_{np}\rangle = \sum_{\mathbf{k}} \phi_{npk} e_{\mathbf{k}}^{\dagger} h_{\mathbf{p}-\mathbf{k}}^{\dagger} |\Theta\rangle + \sum_{\mathbf{kk}'\mathbf{q}} \phi_{npkk'\mathbf{q}} e_{\mathbf{k}}^{\dagger} h_{\mathbf{p}-\mathbf{q}-\mathbf{k}}^{\dagger} e_{\mathbf{k}'+\mathbf{q}}^{\dagger} |\Theta\rangle \quad (6.20)$$

Such an ansatz has been shown to increase the robustness of the roton-like dispersion in ultracold Fermi gases [54, 63], where the simpler contact interaction potential between particles allows for an exact solution. Indeed, in that case, it was shown that in two dimensions, the Fermi-energy where the roton-minimum develops is 4 times lower when the extended ansatz is used.

Notice that, the extended ansatzes presented above allow for dynamical screening due to the Fermi sea. This should be contrasted with the common approach to include screening for the exciton problem, based on the GW approximation and the corresponding screened ladder approximation [64, 65]. Although this approach is widely used in the literature, we expect that, since the plasma frequency ($\omega_{pl}(\mathbf{q}) = \sqrt{n_e |\mathbf{q}|^2 V(|\mathbf{q}|) / m_e} \approx 90 \text{ meV}$ at $|\mathbf{q}| = k_F$ for a Fermi energy of $\epsilon_F = 20 \text{ meV}$) is much smaller than the exciton binding energy, the electron gas is unable to respond on the time scales characteristic for the electron-hole interaction. More specifically, the time scale for the bound electron-hole pair to scatter off each other via Coulomb interaction is set by $1/E_{exc} \ll 1/\omega_{pl}$, implying that many scattering events may occur during the lifetime of a virtual plasmon. This is in stark contrast to the physical picture of the noncrossing, screened ladder approximation, in which virtual excitations of the Fermi sea are created and annihilated sequentially before the bound electron-hole pair scatters again. Therefore, the aforementioned treatment of screening is likely be valid only in the limit $1/E_{exc} \gg 1/\omega_{pl}$, while in the opposite limit, the electrons might prefer to screen the exciton as a whole [66]. The above discussion highlights that an accurate treatment of screening is challenging and offers an explanation for the observed stability of excitons at high carrier densities [67], which is unexpected from the screened ladder calculations [65].

Before concluding this section we remark that the non-self-consistent T-matrix approach introduced previously is not conserving because the hole self-energy from Eq. (6.13) cannot be derived from a Luttinger-Ward functional Φ . We see that here we have a prime example of the importance of

conserving approximations, even in an equilibrium context. Therefore, another way to improve our simple ansatz, is to use a conserving approximation. This can be done by evaluating the hole self-energy self-consistently as $\Sigma(p) = \int dq G_e(q) T(p+q)$, with the T-matrix in Eq. (6.11) defined in terms of the full hole Green's function $G_h(p)^{-1} = G_h^{(0)}(p)^{-1} + \Sigma(p)$. This would essentially correspond to treating the hole using the Fermi-polaron theoretical framework developed in Chapter 4, except that this time the hole would represent the mobile impurity.

6.4 FERMI POLARON QUASIPARTICLES

In the previous section we have looked at the effects of the interaction between excitons and electrons in the same valley, and completely neglected the interactions with electrons in the same valley. We now include this interaction similar to the way that we included it in Ch.3, by treating the exciton as a rigid object, with a fixed internal structure. As we have shown in Ch.3, excitons will form new quasi-particles, and we show that the new quasiparticles also exhibit the roton minimum.

Similarly to Ch.3, we use the fact that the exciton binding is very large to trace out higher energy degrees of freedom and obtain an effective low-energy Hamiltonian for the excitons:

$$H_{\text{eff}} = \sum_{\mathbf{k}} \omega_{\mathbf{k}} x_{\mathbf{k}}^\dagger x_{\mathbf{k}} + \sum_{\mathbf{k}} \xi_{\mathbf{k}} e_{\mathbf{k}}'^\dagger e_{\mathbf{k}}' + \frac{u}{\mathcal{A}} \sum_{|\mathbf{k}| < \Lambda, |\mathbf{k}'| < \Lambda, \mathbf{q}} x_{\mathbf{k}+\mathbf{q}}^\dagger e_{\mathbf{k}'-\mathbf{q}}'^\dagger e_{\mathbf{k}'}' x_{\mathbf{k}}, \quad (6.21)$$

where $x_{\mathbf{k}}^\dagger$ creates an exciton at momentum \mathbf{k} in the K valley and was defined in Eq. (6.2), while $e_{\mathbf{k}}'^\dagger$ creates an electron at in the K' valley, of momentum $\mathbf{K}' + \mathbf{k}$.

Notice that for simplicity we treat the exciton-electron interaction as a contact interaction, regularized by the UV cutoff Λ . The strength of the interaction is given by:

$$u^{-1} = \frac{1}{\mathcal{A}} \sum_{|\mathbf{k}| < \Lambda} \frac{1}{\omega_{\mathbf{p}-\mathbf{k}} + \xi_{\mathbf{k}} + \epsilon_T} \quad (6.22)$$

where ϵ_T denotes the trion binding energy at vanishing electron density. For the remaining numerical calculations, we use $\epsilon_T = 30 \text{ meV}$ [32] and employ a finite cutoff, $\Lambda = 1 \text{ nm}^{-1}$.

We emphasize that, due to the important role of Pauli blocking, we do not take the exciton mass to be independent of the Fermi energy but we

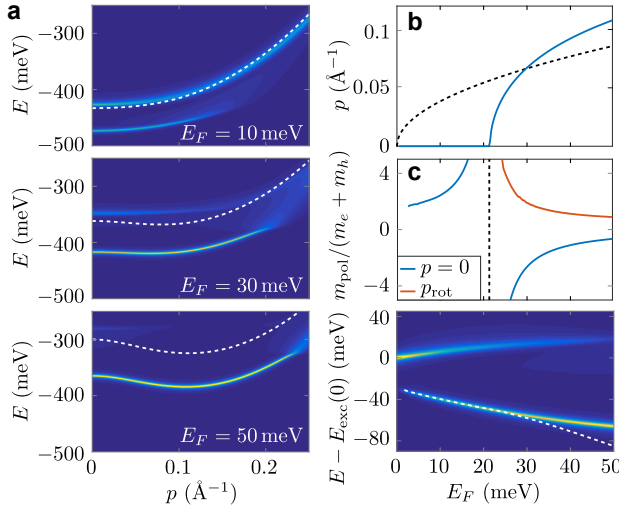


FIGURE 6.3: (a) Spectral function $S(E, \mathbf{p})$ for three different Fermi energies, ϵ_F . The dashed line indicates the exciton dispersion $E_{\text{exc}}(\mathbf{p})$. As a function of Fermi energy: (b) Momentum of the lowest energy attractive polaron state (solid) and Fermi momentum (dashed). (c) Mass of the attractive polaron at zero momentum (blue) and at the roton minimum (red). (d) Optical conductivity $\sigma(E)$ according to Eq. (6.25). The lowest energy of the attractive polaron is shown by the dashed line. A linewidth of $\gamma = 3$ meV was used.

instead use the detailed exciton dispersion $\omega_{\mathbf{k}}$ computed in the previous Section.

We make an ansatz for an exciton dressed by electron-hole pair excitations:

$$|\tilde{\Psi}_{n\mathbf{p}}\rangle = \left(\psi_{\mathbf{p}} x_{\mathbf{p}}^\dagger + \sum_{\mathbf{kq}} \psi_{n\mathbf{p}\mathbf{k}\mathbf{q}} x_{\mathbf{p}+\mathbf{q}-\mathbf{k}}^\dagger e_{\mathbf{k}}^\dagger e_{\mathbf{q}} \right) |\Theta\rangle \quad (6.23)$$

Similar to before we solve $H |\tilde{\Psi}_{n\mathbf{p}}\rangle = (E + E_0) |\tilde{\Psi}_{n\mathbf{p}}\rangle$ in the Hilbert space spanned by $|\tilde{\Psi}_{n\mathbf{p}}\rangle$, where E_0 is the ground state energy in the absence of the exciton.

The result is shown in Fig. 6.3(a) at three different Fermi energies, where we plot the exciton spectral function:

$$S(E, \mathbf{p}) = -2 \text{Im} [E - E_{\text{exc}}(\mathbf{p}) - \Sigma(E, \mathbf{p}) + i\gamma/2]^{-1} \quad (6.24)$$

as a function of energy E and momentum \mathbf{p} , having introduced a momentum independent broadening γ . The polaron states appear as peaks in the exciton spectral function, with the lower and higher energy peak corresponding to the attractive and repulsive polaron, respectively. The attractive polaron is bound to a dressing cloud of electrons, which lowers the energy below that of the bare exciton (dashed line). It also inherits the roton minimum from the exciton as shown in Fig. 6.3(b), (c). We emphasize that the roton minimum in the exciton spectral function is distinct from the minimum in the trion spectral function, which occurs even if the exciton mass is assumed to be independent of Fermi energy [5, 68]. While the range of validity of the approximations employed here might not extend to the highest electron densities considered, we expect the roton minimum to be a robust feature of the polaron dispersion.

6.5 EXPERIMENTAL SIGNATURES OF THE ROTON MINIMUM

The reflection, transmission, and absorption by the monolayer is determined in linear response by the optical conductivity [68]

$$\sigma(E) \propto \left| \sum_{\mathbf{k}} \varphi_0(\mathbf{k}) \right|^2 S(E, 0). \quad (6.25)$$

The in-plane momentum is zero since the momentum transferred by a photon is negligible for all incident angles. The optical conductivity is therefore insensitive to the presence or absence of the roton state. This is illustrated in Fig. 6.3(d), where we plot the optical conductivity as a function of Fermi energy. At high doping, the spectral weight is transferred from the repulsive polaron to the attractive polaron at zero momentum rather than the lowest energy state corresponding to the roton minimum (dashed line).

In contrast to the optical conductivity, the roton state drastically modifies the photoluminescence properties of MoSe₂. To compute the emission spectrum and radiative decay rates, we apply Fermi's Golden Rule to the fully quantized light-matter interaction Hamiltonian using the polaronic wavefunction obtained from the Chevy ansatz as the initial state. This yields the spectral emission rate $\Gamma_{\text{tot}}(\nu)$ of a photon with frequency ν , which may be split into four separate terms, $\Gamma_{\text{tot}}(\nu) = \sum_{i=1}^4 \Gamma_i(\nu)$, according to four different physical processes (see [69]). The first rate, Γ_1 , corresponds to decay of the pure excitonic component of the polaron (amplitude $\alpha_{\mathbf{p}}$ in $b_{\mathbf{p}}^{\dagger}$). For a zero momentum state, it is sharply peaked at $\nu = E_{\text{pol}}(0)$ with a magnitude comparable to the decay rate Γ_0 of an exciton at zero

momentum in undoped MoSe₂. The rate vanishes if $|\mathbf{p}| > v/c$ and the decay is instead determined by the remaining three rates, whose underlying process is represented schematically in Fig. 6.4(a). The process associated with Γ_2 is similar to Γ_1 as it involves the recombination of the correlated electron-hole pair forming the exciton but it does so while leaving behind an electron-hole pair in the opposite Fermi sea. The rates Γ_3 and Γ_4 result from radiative recombination of the valence band hole with an electron from the Fermi sea.

In Fig. 6.4(b), we plot the emission spectrum $\Gamma_{\text{tot}}(\nu)$ of the roton-like polaronic ground state at different Fermi energies. The zero of the frequency axis is chosen to coincide with the energy of the attractive polaron at zero momentum, where maximum absorption is expected. The emission is clearly redshifted relative to absorption. In fact, the emission peak occurs an energy of roughly ϵ_F below the roton state (dashed line) as a result of the electron-hole pair excitations left behind in the Fermi sea. The spectrally integrated decay rates, defined by $\Gamma_i = \int d\nu \Gamma_i(\nu)$, are shown in Fig. 6.4(c).

Phonons may significantly contribute to the decay rate since they offer an additional pathway for the roton-like state to deposit its excess momentum. However, we expect that phonon-assisted decay gives rise to a qualitatively similar redshift and broadening as the decay channels discussed above. A complete calculation of the photoluminescence (PL) spectrum must further take into account the distribution of occupied states, which depends on pumping and relaxation mechanisms [70]. A detailed understanding of the relevant processes in TMDs is currently missing.

Our results offer a potential explanation for experimental observations in absorption and PL spectra [71]. In particular, at high electron densities, the emission spectrum begins to redshift relative to the absorption peak and concurrently broadens and decreases in intensity. Both the energy shift and the broadening scale linearly with the Fermi energy ϵ_F , with a proportionality constant of order unity. This doping dependent splitting between absorption and PL with an onset at a finite electron density is consistent with our model, where absorption probes zero momentum states, while PL can originate from states close to the lowest energy polaron. Additional experiments may provide further verification of the proposed mechanism. A measurement of the sign change of the polaron mass at zero momentum would provide direct evidence for the emergence of a roton state. Due to the small photon momentum, such measurements are challenging although near-field techniques [72] or acoustic waves [73] could allow

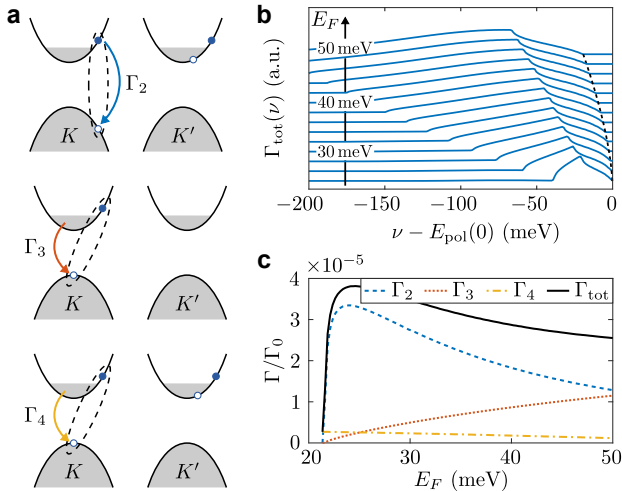


FIGURE 6.4: (a) Illustration of different polaron decay channels. (b) Emission spectra computed for the polaronic roton state at different Fermi energies. The dashed line indicates the energy of the roton state, where zero energy is defined by the attractive polaron at zero momentum. (c) Radiative recombination rates Γ_i of the polaronic roton state as a function of Fermi energy. Here, Γ_0 is the decay rate of an exciton at zero momentum and zero Fermi energy.

one to couple to polaron states with momenta exceeding ν/c . PL lifetime measurements offer a simpler but more indirect probe of the polaron dispersion. Our above treatment suggests that the PL lifetime is drastically increased when the roton minimum is fully developed.

6.6 CONCLUSION

In summary, in this Chapter we proposed a mechanism for the formation of roton states of optical excitations in TMD monolayers. Besides playing an important role in determining optical properties, the roton states open up exciting avenues for creating exotic phases of optical excitations such as supersolids [74] or chiral spin liquids [75]. In particular, if the optical excitations condense into the roton-like minimum, the exact form of interactions between excitations determines whether it is energetically favorable for the condensate to occupy a single momentum state or to fragment [74]. The latter scenario gives rise to a superfluid state with periodic density

modulation, corresponding to a supersolid. Future work may extend the quantitative validity of our approach by including backflow corrections.

POLARON TRANSPORT

We consider imbalanced Bose-Fermi mixtures, and discuss the effect of the motion of one species of particles on the other. We show that the motion of one type of particles creates an effective gauge field on the other particles. On the one hand, this effect can make photons respond to electric and magnetic fields as if they were charged objects. On the other hand, it can facilitate optical control of electron transport.

In the previous chapter we investigated a system of polaritons interacting with an electron gas, in the limit of low polariton density. We showed how the non-perturbative interactions with the electron gas lead to the emergence of new quasiparticles that we named polaron-polaritons, and showed that photon interactions can be significantly increased through this dressing. In the current chapter we investigate the response of these new quasiparticles to a low-frequency electric or magnetic field applied to the electron system.

Remarkably, we find that the polaron-polariton quasiparticles, despite being charge neutral, respond in certain regimes to the applied fields as if they were charged. In essence, we prove that it is possible to use the interaction of photons with charge carriers to induce effective photonic gauge fields that are linearly proportional to the external fields. Moreover, we show that a reciprocal effect may facilitate optical manipulation of electron transport. Our findings establish transport measurements as a novel, powerful tool for probing the many-body physics of mobile quantum impurities.

The backbone of this chapter is a diagrammatic linear response calculation of the photon current induced by the electric field applied to the electron system. To obtain sensible results in this non-equilibrium context, it is crucial to only make approximations that satisfy conservation laws such as the continuity equation or Newton's second law of motion. To ensure this we use the Baym-Kadanoff conserving approximation that we introduced previously (see Ch.4) to calculate the fully self-consistent, frequency-dependent transconductivity at zero temperature.

The chapter is organized as follows. We start our analysis by first putting our work into context in Sec. 7.1. Then, we present a heuristic derivation

of the polaron drag force based on intuitive arguments in Sec. 7.2. Moreover, we solve the semiclassical equations of motion of a polaron in an electric field. In Sec. 7.3 we corroborate these results by a microscopic calculation of the polaron drag conductivity in an electric field using diagrammatic perturbation theory within the Kadanoff-Baym conserving approximation. In Sec. 7.4 we extend our results to polaritons and comment on non-equilibrium effects in Sec. 7.5. After discussing extension of our analysis to the case of magnetic field response in Sec. 7.6, we conclude by presenting an outlook on possible extensions of our work. We remark that the theoretical calculations in Sec. 7.2, 7.3, 7.4 and 7.6 assume an equilibrium scenario where the impurity does not decay radiatively, and therefore these results do not apply directly to the experimental scenario that we proposed. Our purpose for this was twofold. First, this keeps the discussion completely general, and allows our results to be directly applied to the usual bilayer systems or to cold-atom experiments. Second, it allows us to identify the physical process responsible for Coulomb drag, and then analyze the polaron-polariton drag using a Boltzmann equation in Sec. 7.5, without performing an even more cumbersome non-equilibrium diagrammatic calculation.

The derivations in this chapter will parallel closely the derivations in Ref. [15].

7.1 INTRODUCTION

The relevance of the present work can be seen from two different perspectives. On the one hand, our work demonstrates an efficient novel implementation of effective gauge fields in photonic systems. On the other hand, our work addresses the more general question of the effect of the motion of one species of particles on another species of particles, due to non-perturbative interactions between the two species and is part of the larger field of Coulomb drag.

There has been a significant interest in recent years in the realization of topological states of polaritons [76–78] which demonstrates the importance of implementing effective gauge fields in photonic systems. The main difficulty is due to the fact that exciton polaritons are charge-neutral particles, and hence their center-of-mass motion does not couple directly to dc electric or magnetic fields. Prior work has exploited a combination of spin-orbit-coupling of light and magnetic field response of polariton polarization degree of freedom in lattice structures. Alternatively, we show that

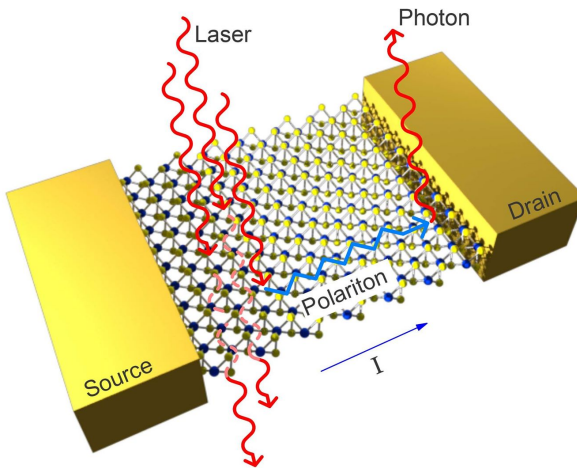


FIGURE 7.1: Schematic of the experimental setup: a photon is absorbed by the TMD-monolayer, forming a polariton which is then dragged by the drifting electrons and subsequently emitted at a different position.

it is possible to exploit the interaction of polaritons with charge carriers to induce effective photonic gauge fields that are linearly proportional to the external fields. Due to the strong exciton bindings in monolayers we envision an experimental setup as described in Fig.7.1

As we showed in the previous chapter, the non-perturbative dressing of polaritons with polarization waves in the electron system leads to the emergence of polaron polariton quasiparticles. Initially, one might expect that, since these quasiparticles are charge neutral they will not respond to applied electric fields. However, we show that polaron-polaritons prefer to minimize their energy by following the dressing cloud surrounding them. Although the idea of moving photons by leveraging their interactions with an electron system has been introduced before [16, 79–81], a key difference to previous investigations originates from the non-perturbative nature of the polaronic coupling, which gives rise to a remarkably efficient drag mechanism. Indeed, we find that the zero-temperature drag conductivity of polaritons can ideally be of the same order as the electron conductivity, implying the realization of sizable photonic gauge fields. In stark contrast, the polariton drag conductivity calculated in previous work is proportional

to the square of the temperature, and therefore vanishes at zero temperature.

From a more general perspective, our work addresses the problem of non-perturbative Coulomb drag, and is unique in that it analyses the drag effect in the regime of strong interactions that can lead to the formation of inter-species molecular bound states (trions in our setup) as well as many-body excitations (exciton-polarons). Although in this work we consider the regime of large density imbalance between the different species of particle, which allows us to model the problem using the quantum impurity framework, our results will likely be relevant even in the balanced density regime [82]. As we discussed in the previous chapter, there are two types of emerging quasiparticles in our system, which have very different drag properties.

The drag of the molecular states is closely related to previous work on indirect excitons in bilayer systems in the quantum Hall regime, where the phenomenon of perfect Coulomb drag has been observed [16, 83]. In these systems, one of the layers hosts holes while the other contains electrons. The strong interlayer attractive interaction leads to the formation of bound molecular states known as indirect excitons. Because of the pairing process, any force applied on one of the particles is felt by the molecule as a whole, leading to the emergence of phenomena such as perfect Coulomb drag. The direct analog in our system is provided by trions which are bound molecular states of an exciton and a single electron; we expect the trion to respond as a charged particle to any applied electric field and exhibit perfect Coulomb drag, as long as it remains bound.

The drag of polarons on the other hand, which is the focus of the present work, is more subtle and was not analyzed previously. We find that the response of polarons, which are many-body optical excitations, is very different from the response of trions, which are two-body bound molecular excitations. Indeed, in equilibrium setups with disorder and static electric fields, polarons do not respond at all to a force on the bath particles (at zero temperature). Remarkably however, in the case of dynamical fields (more specifically, when the frequency of the field is much larger than the inverse disorder lifetime of the bath particles) or in non-equilibrium scenarios where the impurities have a finite lifetime, the response of the polarons can be as large as the response of the molecules. The (zero-temperature) polaron drag effect that we investigate can be understood as arising from a shift in the polaron dispersion proportional to the velocity of the majority

particles, and therefore can be understood as an effective gauge potential for the impurity particles.

Furthermore, our work establishes transport measurements as powerful tools to probe the nature of the many body ground state in mobile impurity experiments, and should be of central interest to a large subset of low energy physics, ranging from ultra-cold atoms through semiconductor quantum optics to strongly correlated materials. Indeed, the fundamentally different transport response of polarons compared to molecules provides a way of identifying experimentally the polaron to molecule transition in two dimensions, as well as also providing a way to measure the mass of the polaron or molecule quasi-particles.

7.2 HEURISTIC DERIVATION OF POLARON DRAG

We begin our analysis with a heuristic derivation that illustrates our results in a very intuitive manner. The results in this section are very general and apply to any system with two species of particles with strong inter-species interaction. The inter-species interaction will lead to the mass renormalization of the two types of particles. Using semiclassical arguments, we show that, the movement of one type of particles generates an effective gauge field proportional to its current, not unlike a charged current generates magnetic fields. We find a very general relationship between the mass renormalization of the stationary particles and this effective gauge field.

7.2.1 Polaron drag in clean systems

Although it is straightforward to check that the following arguments in this section apply more generally, for clarity we only consider the more particular case of a mobile exciton with mass m_x interacting with a Fermi sea of electrons with mass m_e . For simplicity, we neglect the finite radiative lifetime of the exciton in this section. Applying a force on the electrons, causes an acceleration \mathbf{a}_e of the Fermi sea. We now go to the rest frame of the electrons. Because this is a non-inertial reference frame, a fictitious force acts on the exciton $\mathbf{F} = -m_x \mathbf{a}_e$ accelerating it. Crucially the force is proportional to the bare mass of the exciton. The interaction with the electrons, however, impairs the motion of the exciton and, hence, the dressed exciton quasiparticle is heavier than the bare exciton with an effective mass m_x^* . The acceleration of this quasiparticle in the electron rest frame is thus

$F/m_x^* = -\mathbf{a}_e m_x / m_x^*$. Going back to the lab frame, we have to add the acceleration of the reference frame and we thus arrive at an exciton acceleration

$$\mathbf{a}_x = \left(1 - \frac{m_x}{m_x^*}\right) \mathbf{a}_e \quad (7.1)$$

This equation relates any force acting on the electron system to a somewhat smaller force on the dressed exciton. This force can be qualitatively understood as friction between electrons and excitons, which originates from the ability of the excitons to minimize their energy by following the dressing cloud surrounding them.

7.2.2 Polaron drag in dirty systems

The above discussion is completely general and does not make any assumptions regarding the nature of the quasiparticles, and therefore it is equally valid for both molecules and polarons. This is because we assumed that all electrons accelerate with \mathbf{a}_e . However, in the presence of disorder, this is no longer the case, leading to the emergence of a distinction between the trion and polaron response. For trions, the situation is relatively simple: because the trion is a two-particle bound state, formed by an exciton which binds to a single electron from the Fermi sea, it follows the motion of this particular electron. Therefore the trion motion is still described by Eq. 7.1 as long as we let \mathbf{a}_e denote the instantaneous acceleration of one electron. This means that trions will respond to applied fields like charged particles, and will exhibit drag properties similar to the ones investigated in the work of Ref. [83]. In contrast, we recall that exciton-polarons are many-body excitations where an exciton is dressed with a polarization wave of the electron system. Since all electrons in the Fermi sea contribute to this polarization wave, we can describe the polaron motion using Eq. 7.1 if and only if we let \mathbf{a}_e denote the average acceleration of the electron system. This interpretation is justified a posteriori by the rigorous diagrammatic calculation in the following section. In the following we will focus only on the response of polarons.

7.2.3 Semiclassical drag transconductivity

We can write down general semiclassical equations of motion for the coupled electron and polaron motion:

$$m_e \frac{d}{dt} \mathbf{v}_e(t) = \mathbf{F}_e(t) + \frac{n_x}{n_e} (m_x^* - m_x) \frac{\mathbf{F}_x(t)}{m_x^*} \quad (7.2)$$

$$m_x^* \frac{d}{dt} \mathbf{v}_x(t) = \mathbf{F}_x(t) + (m_x^* - m_x) \frac{\mathbf{F}_e(t)}{m_e} \quad (7.3)$$

We can evaluate the polaron drag conductivity in an ac electric field $\mathbf{E}(t)$ in the presence of disorder for both electrons and excitons by choosing

$$\mathbf{F}_e(t) = -e\mathbf{E}(t) - \frac{m_e \mathbf{v}_e(t)}{\tau_e}, \quad \mathbf{F}_x(t) = -\frac{m_x^* \mathbf{v}_x(t)}{\tau_x^*}, \quad (7.4)$$

where $\tau_e(\tau_x^*)$ is the transport lifetime of electrons (exciton-polarons).

To leading order in the polaron density, we can ignore the drag force on electrons. The solution in Fourier space reads

$$\mathbf{v}_e(\Omega) = \frac{-e\mathbf{E}(\Omega)}{m_e} \frac{\tau_e}{1 - i\Omega\tau_e} \quad (7.5)$$

$$\mathbf{v}_x(\Omega) = \left(1 - \frac{m_x}{m_x^*}\right) \left(\frac{-i\Omega\tau_x^*}{1 - i\Omega\tau_x^*}\right) \mathbf{v}_e(\Omega). \quad (7.6)$$

Notice that in the absence of excitonic disorder, $\tau_x^* \rightarrow \infty$, the drag is the only force acting on the excitons and their drift velocity is simply $v_x = (1 - m_x/m_x^*)v_e$. This case is particularly relevant for exciton polaritons, which are expected to be largely immune to exciton disorder (see Sec.7.4). We emphasize that this results only holds at small polaron densities as we neglect electron drag forces generated by polarons. From the exciton drift velocity, we obtain the transconductivity to first order in the polaron density n_x :

$$\sigma_{xe}(\Omega) = \frac{en_x}{m_e} \left(1 - \frac{m_x}{m_x^*}\right) \frac{i\Omega\tau_e\tau_x^*}{(1 - i\Omega\tau_e)(1 - i\Omega\tau_x^*)}. \quad (7.7)$$

7.2.4 Reverse effect

We remark that the electrons should also experience a drag force, when the excitons are accelerated by an external force. Such a force can be effected by applying an ac field perpendicular to the 2D plane that modifies

the exciton energy through a quantum-confined Stark effect with a spatial and/or time dependence determined through the applied laser field [84].

Equation (7.1) corresponds to the combined force all electrons exert on a single polaron. Hence, the average inverse drag force on an electron in the Fermi sea in the presence of an exciton force \mathbf{F}_x should be $(n_x/n_e)(1 - m_x/m_x^*)\mathbf{F}_x$, where $n_{e,x}$ is the density of electrons (excitons). We can find the drag conductivity of electrons from Eqs. (7.2) and (7.3) with

$$\mathbf{F}_e(t) = -\frac{m_e \mathbf{v}_e(t)}{\tau_e}, \quad \mathbf{F}_x(t) = \mathbf{f}_x(t) - \frac{m_x^* \mathbf{v}_x(t)}{\tau_x^*}. \quad (7.8)$$

In this case, we need to include the drag force on electrons in Eq. (7.2). We can, however, neglect the drag term in the polaron equation of motion (7.3), since $F_e \propto v_e \propto n_x/n_e$ only contributes at higher order in polaron density. With this we again arrive at a transconductivity given by Eq. (7.7), as guaranteed by Onsager's reciprocity principle. An experimentally more relevant quantity is the electric voltage which builds up as a response to an exciton force when no current can flow. The electric field can be found by setting $\mathbf{v}_e = 0$ in the equations of motion which yields

$$e\mathbf{E}(\Omega) = \frac{n_x}{n_e} \left(1 - \frac{m_x}{m_x^*}\right) \left(\frac{-i\Omega\tau_x^*}{1 - i\Omega\tau_x^*}\right) \mathbf{f}_x(\Omega) \quad (7.9)$$

7.2.5 Effective gauge field

The polaron drag force in Eq. 7.1 is fully determined by the force acting on the electrons and the mass renormalization, and specifically does not depend on the exciton velocity. This enables us to reinterpret the polaron drag effect as a consequence of an effective gauge field. This interpretation is further supported by a microscopic investigation of the drag mechanism. As we show in App.A.3, the exciton-polaron dispersion $\zeta_{\mathbf{k}}$ shifts by an amount proportional to the electron drift velocity (implying that $k = 0$ excitons experience a finite group velocity). We can introduce a gauge potential $\mathbf{A}_x(t)$ to write the new dispersion as $\tilde{\zeta}_{\mathbf{k}} = \zeta_{\mathbf{k}-e\mathbf{A}_x}$. In the case of a time-dependent drive, this gauge potential is given by:

$$e\mathbf{A}_x(t) = (m_x^* - m_x) \mathbf{v}_e(t) = \frac{m_x^* - m_x}{m_e} \frac{-e\tau_e \mathbf{E} e^{-i\Omega t}}{1 - i\Omega\tau_e} \quad (7.10)$$

which corresponds to an effective electric field E_x given by:

$$eE_x(t) = -e\dot{A}(t) = \frac{m_x^* - m_x}{m_e} \frac{i\Omega\tau_e E e^{-i\Omega t}}{1 - i\Omega\tau_e} \quad (7.11)$$

Although the field strength vanishes in the dirty regime $\Omega\tau_e \ll 1$, the finite (constant) gauge potential can still have measurable effects. Indeed, in Sec. 7.5 we discuss at length the role of this gauge potential on photon transport.

We now investigate the magnitude of the polaron drag effect and the role played by the trion binding energy, which determines the energy scale of the exciton-electron interaction in the limit of vanishing electron density. Figure 3.5 shows the dependence of the (normalized) polaron mass m_x^*/m_e on the ratio of the Fermi energy (ϵ_F) to the trion binding energy (ϵ_T): since the magnitude of the effective electric field seen by the polaron is proportional to $\frac{m_x^* - m_x}{m_e}$, we conclude that for a given electron density, a stronger trion binding leads to a larger mass renormalization for the polaron, and consequently to a more efficient drag. Remarkably, the polaron drag can ideally be even more efficient than the drag of trions.

7.2.6 Conclusion

It is important to note that our analysis so far has neglected incoherent scattering of electrons and polarons. In addition to coherent scattering of electrons and excitons that lead to polaron formation there may also be incoherent scattering events that lead to a finite lifetime of polarons in an excited state. We investigate this effect in more detail in Sec. 7.3.4 and 7.5.2, and discuss in what parameter regimes it can be neglected.

To conclude this section, we emphasize that in the exciton-polaron transconductivity problem we are analyzing the drag process takes place in an interacting system consisting of a fixed number of excitons and electrons. Even in the case of finite exciton or polariton lifetime, an underlying assumption is that laser excitation leads to creation of real particles with a lifetime much longer than the characteristic timescales associated with their interactions with electrons. This is in stark contrast to polarons in interacting electron-phonon system where dynamic screening of the electron by the lattice can be described in terms of virtual phonon emission and absorption processes. Consequently, in the limit of linear response at vanishing temperature, there is no natural setting to talk about drag conductivity of phonons. The opposite limit of large applied electric fields on

the other hand, constitute a very interesting problem where electron transport can be associated with multiple real phonon emission and absorption processes and the associated phonon drag could have signatures in current noise [85, 86].

7.2.7 Summary of results

Before proceeding, we summarize the consequences of our results:

- (i) The polaron drag can be extremely efficient, promising a drag mobility of the same order as the electron mobility. This is a consequence of the nonperturbative interaction that is responsible for the polaron formation, which leads to a drag transconductivity proportional to the mass renormalization of the polaron.
- (ii) When the inter-species interaction is weak, the mass renormalization of the polaron is proportional to V^2 (where V denotes the inter-species interaction strength; the contribution linear in V can only lead to a shift of the polaron energy and will not affect the polaron mass). According to Eq.7.7 this will result in a zero-temperature drag transconductivity proportional to V^2 . While in the (dirty) limit ($\Omega\tau_e, \Omega\tau_x^* \ll 1$) the transconductivity is proportional to Ω , in the opposite (clean) limit ($\Omega\tau_e, \Omega\tau_x^* \gg 1$) the transconductivity is proportional to $1/\Omega$. This clean limit result shows that second order processes do not vanish as $\Omega \rightarrow 0$ at $T = 0$, in contrast to previous claims that in these limits the only non-zero contributions to drag (in both the clean and dirty regime) must be higher order in the inter-species interaction [16, 81]. It would be interesting to check whether our result holds also in the regime of balanced interspecies densities analyzed in Ref. [81].
- (iii) The electrons should also experience a drag force, when the excitons are accelerated by an external force, in accordance with Onsager's reciprocity principle.
- (iv) The drag effect that we investigate emerges from an effective gauge potential that the exciton-polaron experiences due to the motion of the electrons. Even in the $\Omega\tau_e \ll 1$ limit, when the effective electric field vanishes, the finite gauge potential still has important consequences for the exciton-polaron transport (Sec. 7.5).
- (v) The semiclassical analysis presented here can be extended to include an external magnetic field (see also [87, 88]). The drag force could then give rise to a Hall effect and a cyclotron resonance of exciton polarons, a phenomenon which we discuss at length in Sec. 7.6.

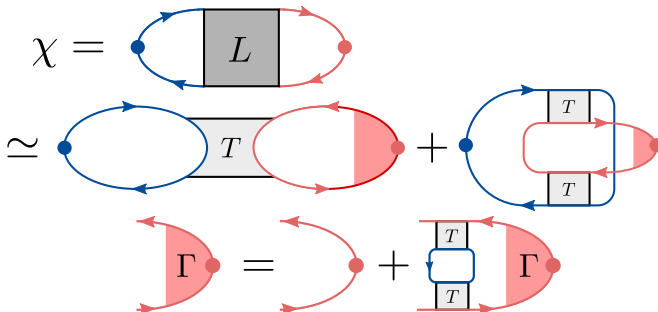


FIGURE 7.2: Linear response theory for polaron drag within the conserving approximation to lowest order in polaron density. Dashed (wavy) lines represent disorder (interactions). Blue lines indicate dressed electron propagators and red lines indicate dressed exciton propagators as defined in Fig. ???. The transconductivity diagram obtained from Eq. (4.37)

7.3 DIAGRAMMATIC CALCULATION OF TRANSCONDUCTIVITY USING THE CONSERVING APPROXIMATION

We now evaluate the polaron drag within a microscopic theory in order to verify the heuristic results discussed in the previous section. To this end, we use diagrammatic perturbation theory taking into account the effect of electron-exciton interactions as well as disorder for electrons and excitons, that we introduced in 4.

We are interested in a nonperturbative effect of the interaction and must therefore proceed with care. We already mentioned in Sec.4.2 that simply evaluating a certain class of diagrams might lead to erroneous results as an incomplete set of diagrams does not necessarily satisfy the conservation laws of the physical systems, a crucial condition in non-equilibrium problems. We mentioned that a powerful technique to generate diagrams obeying conservation laws is the *conserving approximation*. We used this approximation in Chapter 4 to solve the Fermi and Bose polaron problems in a conserving approximation and to obtain the diagrams corresponding to polaron interactions.

To briefly recap the procedure for generating conserving approximations, we remind the reader that a sufficient condition to have a conserving approximation is that the self-energy be a derivative of the Luttinger-Ward functional such that $\Sigma = \delta\Phi/\delta G$. The functional Φ and the resulting the

self energy Σ for the polaron problem were presented in Fig.4.6 and 4.6 respectively. The irreducible two particle vertex is the second derivative of the functional $K = \delta^2\Phi/\delta^2G$, which was then derived Fig.4.9. This can be used to construct the reducible two-particle vertex L through the recursive relation presented in Fig.4.5. The vertex L is directly related to the response function of the system as shown in Fig.4.5. Using this procedure we can write down the response function to leading order in exciton density in Fig.7.2. As we will show below in Sec.7.3.2, any exciton loop introduces a factor of exciton density n_x , therefore to leading order in n_x we only keep diagrams that have a single exciton loop.

Working in Fourier space, the transconductivity σ is related to the response function χ through:

$$\sigma_{\alpha\beta}(\Omega) = \frac{e}{i\Omega} \chi_{\alpha\beta}(\Omega) \quad (7.12)$$

and the response function reads, according to Fig.7.2:

$$\chi_{\alpha\beta}(\Omega) = -i \int dp \pi_\alpha(p; \Omega) G_x(p) G_x(p + \Omega) \Gamma_\beta(p; \Omega), \quad (7.13)$$

where $p + \Omega \equiv (\mathbf{p}, \omega + \Omega)$. Here, we have defined the exciton current vertex

$$\begin{aligned} \Gamma(p; \Omega) &= \frac{\mathbf{p}}{m_x} + \int dk dk' G_e(q) G_e(p + k' - k + \Omega) \\ &\times T(p + k') T(p + k' + \Omega) G_x(k) G_x(k + \Omega) \Gamma(k; \Omega). \end{aligned} \quad (7.14)$$

The vertex Γ describes the renormalization of the exciton velocity due to many-body interactions (see Fig. 7.2). The vertex function π describes the coupling of excitons to an electric current and is given by

$$\begin{aligned} \pi(p; \Omega) &= -i \int dk \frac{\mathbf{k}}{m_e} G_e(k) G_e(k + \Omega) \left[T(p + k + \Omega) \right. \\ &+ i \int dk' G_e(k') T(p + k') T(p + k' + \Omega) \\ &\times G_x(p + k' - k) \left. \right]. \end{aligned} \quad (7.15)$$

7.3.1 Attractive polaron quasiparticles

We focus on the limit of very small exciton density where the statistics of excitons becomes irrelevant. We exploit this fact by treating the low-density

excitons as an effective Fermi gas which allows to simplify calculations. Since we are moreover interested in the regime where no exciton condensation takes place, treating excitons effectively as fermions allows to take the corresponding limit of $T \rightarrow 0$ without technical complications from Bose condensation. We emphasize that all results are independent of the statistics.

The ground state of a single exciton in a Fermi sea, described by the model in Eq. (4.39), depends on the dimensionless interaction strength given by the ratio ϵ_F/ϵ_T of Fermi energy of electrons and trion energy. While the attractive polaron is stable at higher electron densities, diagrammatic Monte Carlo simulations predict a trion ground state for Fermi energies below $0.1\epsilon_T$ for contact interaction models [89, 90]. We henceforth assume a sufficiently large electron density so that the physics at low exciton densities is dominated by the formation of attractive polarons. In this regime, it is instructive to introduce an effective (or projected) Green's function \tilde{G}_x , describing the propagation of attractive polaron quasiparticles (see App. A.1):

$$\tilde{G}_x(p) = \frac{1}{\omega - \zeta_{\mathbf{p}} + i/2\tau_x^*(\mathbf{p}) \operatorname{sgn}(\omega)}. \quad (7.16)$$

Here we have introduced the polaron dispersion

$$\zeta_{\mathbf{p}} = \frac{\mathbf{p}^2}{2m_x^*} - \mu_x^* \quad (7.17)$$

with the polaron chemical potential μ_x^* measured from the bottom of the polaron band. Moreover, we have defined the effective polaron mass m_x^* , the polaron lifetime $\tau_x^*(\mathbf{p})$, and the quasiparticle weight Z as

$$(m_x^*)^{-1} = Zm_x^{-1} + Z\partial_{\mathbf{p}}^2 \operatorname{Re}\Sigma_{\text{int}}(\mathbf{p}, 0) \Big|_{\mathbf{p}=\mathbf{p}_F} \quad (7.18)$$

$$1/2\tau_x^*(\mathbf{p}) = Z/2\tau_x - Z\operatorname{Im}\Sigma_{\text{int}}(\mathbf{p}, \zeta_{\mathbf{p}}) \quad (7.19)$$

$$Z^{-1} = 1 - \partial_{\omega}\Sigma_{\text{int}}(\mathbf{p}_F, \omega) \Big|_{\omega=0}. \quad (7.20)$$

where we introduced the exciton Fermi momentum p_F . The polaron density of states in Eq. (4.45) is hence $\rho_x = m_x^*/2\pi$. The polaron lifetime has a constant part from disorder scattering as well as a momentum dependent part due to incoherent electron-polaron scattering (see App. A.4 for an estimate of $\operatorname{Im}\Sigma_{\text{int}}(p)$ as well as the discussion in Ref. [91]). We emphasize that

it is crucial to evaluate the polaron self energy self-consistently to obtain the momentum-dependent lifetime.

In Sec. 7.3.4, we shall make use of the fact that the full exciton Green's function can be approximated by the effective expression, $G_x(p) \simeq Z\bar{G}_x(p)$ near the resonance $\omega \simeq \zeta_p$ and $|\mathbf{p}| \ll k_F$. The interaction vertex between electrons and polarons, however, is determined by virtual transitions to excited states and knowledge of the full exciton Green's function is required to accurately determine the vertex functions.

7.3.2 Low exciton density expansion

Before embarking on the evaluation of the response function, we clarify the regime of validity of our calculation. As mentioned above we are interested in the result to linear order in the exciton density $n_x \propto \mu_x^*$. Nevertheless, we assume both electron and exciton Fermi levels to exceed the frequency and disorder scattering rate, which allows us to linearize the dispersions around the Fermi levels, and neglect localization effects. To be precise we consider the limiting case $\Omega, 1/\tau_x \ll \mu_x^*$ and $\Omega, 1/\tau_e \ll \mu_e$. At the same time we assume $\mu_x^* \ll \mu_e$, which ensures that the Fermi-polaron picture remains valid.

Within this approximation we can simply set $T(p + \Omega) \simeq T(p)$ to lowest order in Ω . The external frequency thus only enters in products of Green's functions, $G_x(p)G_x(p + \Omega)$ and $G_e(k)G_e(k + \Omega)$, where Ω separates the branch cuts of the two Green's functions. We can now write the exciton current vertex as

$$\Gamma(p; \Omega) = \frac{\mathbf{p}}{m_x} + \int dk w(p, k) G_x(k) G_x(k + \Omega) \Gamma(k; \Omega), \quad (7.21)$$

where we introduced the kernel

$$w(p, k) = \frac{\delta \Sigma_{\text{int}}(p)}{\delta G_x(k)} = \int dq G_e(q) G_e(p + q - k) T^2(p + q), \quad (7.22)$$

which corresponds to the last term in Fig. 7.2(b). The vertex function π reads

$$\pi(p; \Omega) = -i \int dk \frac{\mathbf{k}}{m_e} G_e(k) G_e(k + \Omega) \frac{\delta \Sigma_{\text{int}}(p)}{\delta G_e(k)} \quad (7.23)$$

$$\begin{aligned} &= -i \int dk \frac{\mathbf{k}}{m_e} G_e(k) G_e(k + \Omega) \left[T(p + k) \right. \\ &\quad \left. + i \int dk' G_e(k') T(p + k')^2 G_x(p + k' - k) \right] \end{aligned} \quad (7.24)$$

We can alternatively apply the vertex corrections to the vertex π and rewrite Eq. (7.13) as

$$\chi_{\alpha\beta}(\Omega) = -i \int dp \Pi_\alpha(p; \Omega) G_x(p) G_x(p + \Omega) \frac{p_\beta}{m_x} \quad (7.25)$$

where we introduced the dressed vertex Π defined by

$$\begin{aligned} \Pi(p; \Omega) &= \pi(p; \Omega) \\ &+ \int dk \Pi(k; \Omega) G_x(k) G_x(k + \Omega) w(k, p). \end{aligned} \quad (7.26)$$

We now outline our strategy for expanding Eqs. (7.13) and (7.21) to linear order in n_x . While we have restricted the calculation to diagrams with only a single exciton loop, thereby neglecting certain higher order contributions, single-loop diagrams may still contain terms nonlinear in n_x that should be eliminated. Our starting point is the following decomposition of the exciton Green's function

$$G_x(p) = G_x^R(p) + 2i\text{Im}G_x^A(p)\theta(-\omega). \quad (7.27)$$

In the diagrams, each Green's function G_x appears inside a frequency integration and we can write

$$\begin{aligned} \int dp f(p) G_x(p) &= \int dp f(p) G_x^R(p) \\ &+ \int dp f(p) 2i\text{Im}G_x^A(p)\theta(-\omega), \end{aligned} \quad (7.28)$$

where the second term is proportional to n_x for any function $f(p)$ that does not have poles in the lower half-plane $\omega < 0$. Hence, we can use Eq. (7.28) to expand a loop diagram in powers of n_x . The zeroth order is given by replacing all exciton Green's functions in a loop by retarded functions. This contribution to the transconductivity trivially vanishes. The decomposition (7.28) thus suggests a simple recipe to generate the diagrams at first order in n_x : consider all diagrams, where a single line exciton line is replaced by $\text{Im}G_x^A(p)\theta(-\omega)$ and all others are assumed to be retarded functions.

Indeed, this recipe works for the functions $w(p, k)$ and $\pi(p, \Omega)$ in Eqs. (7.22) and (7.24) as all exciton Green's functions in these expressions, including the internal Green's functions in the definition of the T matrix, are of the form of Eq. (7.28). The only exception to this simple expansion rule are the expressions in Eqs. (7.13) and (7.21), where products of two

exciton Green's functions within the same frequency integral appear. The expansion of such terms will be derived in Sec. 7.3.4 below.

To simplify bookkeeping, we consider π and w to be functionals of G_x . The expansion $\pi \simeq \pi^{(0)} + \pi^{(1)}$ can then be expressed to first order in n_x as

$$\pi^{(0)} = \pi[G_x^R] \quad (7.29)$$

$$\pi^{(1)} = \int dp \frac{\delta \pi[G_x^R]}{\delta G_x^R(p)} 2i\text{Im}G_x^A(p)\theta(-\omega) \quad (7.30)$$

where $\pi[G_x^R]$ means that all exciton Green's functions inside the vertex have been replaced by retarded functions. Similarly, the function w can be expressed as $w \simeq w^{(0)} + w^{(1)}$ with

$$w^{(0)} = w[G_x^R] \quad (7.31)$$

$$w^{(1)} = \int dp \frac{\delta w[G_x^R]}{\delta G_x^R(p)} 2i\text{Im}G_x^A(p)\theta(-\omega). \quad (7.32)$$

Naively, it may seem cumbersome to expand all exciton Green's functions as described above for both diagrams shown in Fig. 7.2(d), however, we can considerably simplify the solution by symmetry arguments. Importantly, both diagrams have been derived by functional derivatives of the Φ functional and, therefore, the representation of the expansion in n_x in terms of functional derivatives is particularly suitable for our problem. Most terms in the expansion simply correspond to some higher order derivatives of the Φ functional or the self energy. The fact that the order of differentiation does not matter leads to important symmetry properties, for instance, $w(p, p') = \delta\Sigma(p)/\delta G_x(p') = w(p', p)$, which can be readily verified from Eq. (7.22). Moreover, this relation is immediately obvious from the diagrammatic representation of w , shown as the last term in Fig. 7.2(b).

We make use of symmetry properties as well as the Ward identity in the evaluation of the transconductivity below. Indeed, we find at the end of Sec. 7.3.4 that the various contributions from the expansion of the self energy and vertex corrections eventually combine into a simple final expression that can be readily computed. As mentioned above, however, the product $G_x(p)G_x(p + \Omega)$ cannot be simply expanded using functional derivatives. This term accounts for the mobility of excitons and depends sensitively on the parameter $\Omega\tau_x$. A similar expression $\sim G_e(k)G_e(k + \Omega)$ occurs in the definition of $\pi(p; \Omega)$ in Eq. (7.23) and contains information about the electron mobility. The latter expression can be simplified by ex-

panding the Green's functions in terms of delta functions around the quasi-particle resonance $\epsilon = \xi_{\mathbf{k}}$. In App. A.6 we show that the approximation

$$\frac{\mathbf{k}}{m_e} G_e(k) G_e(k + \Omega) \simeq \frac{\left(i\tau_e \Omega \frac{\mathbf{k}}{m_e} \partial_{\epsilon} + \partial_{\mathbf{k}} \right) G_e(k)}{1 - i\tau_e \Omega}, \quad (7.33)$$

is valid to leading order in $\Omega, 1/\tau_e \ll \mu_e$. We cannot immediately use this relation for the exciton Green's function because its nonperturbative interaction self-energy correction precludes a description in terms of on-shell properties only. We will discuss this issue in more detail in Sec. 7.3.4 below.

7.3.3 Evaluation of the vertex functions to zeroth order in n_x

We begin with the evaluation of the vertex functions $\Gamma(p, \Omega)$, $\pi(p, \Omega)$ and $\Pi(p, \Omega)$ to zeroth order in the polaron density by simply replacing all exciton Green's functions by retarded functions. Equation (7.21) reads at zeroth order in n_x

$$\Gamma^{(0)}(p) \simeq \frac{\mathbf{p}}{m_x} + \int dk w^{(0)}(p, k) \Gamma^{(0)}(k) G_x^R(k)^2, \quad (7.34)$$

where we have approximated $G_x^R(k) G_x^R(k + \Omega) \rightarrow G_x^R(k)^2$ to lowest order in Ω . Using the chain rule

$$\partial_{\mathbf{p}} \Sigma_{\text{int}}^{(0)}(p) = \int dq \frac{\delta \Sigma_{\text{int}}^{(0)}(p)}{\delta G_x^R(q)} \partial_{\mathbf{q}} G_x^R(q), \quad (7.35)$$

which immediately follows from the definition of Σ_{int} and T in Eqs. (4.46) and (4.48), as well as $\delta \Sigma_{\text{int}}^{(0)}(p)/\delta G_x^R(q) = w^{(0)}(p, q)$, we can readily verify that the solution of equation (7.34) is given by the Ward identity

$$\Gamma^{(0)}(p) = \frac{\mathbf{p}}{m_x} + \partial_{\mathbf{p}} \Sigma_{\text{int}}^{(0)}(p) \quad (7.36)$$

$$= [G_x^R(p)]^{-2} \partial_{\mathbf{p}} G_x^R(p). \quad (7.37)$$

In order to evaluate $\pi^{(0)}(p, \Omega)$, defined by Eq. (7.24), we employ Eq. (7.33) and write

$$\begin{aligned} \pi^{(0)}(p; \Omega) &= i \int dk G_e(k) \frac{i\tau_e \Omega \frac{\mathbf{k}}{m_e} \partial_{\epsilon} + \partial_{\mathbf{k}}}{1 - i\tau_e \Omega} \left[T^{(0)}(p + k) \right. \\ &\quad \left. + i \int dk' G_e(k') T^{(0)}(p + k')^2 G_x^R(p + k' - k) \right] \end{aligned} \quad (7.38)$$

where we have performed a partial integration. Using

$$\partial_p T(p) = i \int dk T^2(p) G_e(k) \partial_p G_x(p - k), \quad (7.39)$$

which follows directly from the definition of the T matrix in Eq. (4.48), we find that the momentum derivative in Eq. (7.38) drops out and we obtain

$$\boldsymbol{\pi}^{(0)}(p; \Omega) = \frac{-i\tau_e \Omega}{1 - i\tau_e \Omega} \int dk \frac{\mathbf{k} - \mathbf{p}}{m_e} w(k, p) \partial_\epsilon G_x^R(k). \quad (7.40)$$

The dressed vertex $\boldsymbol{\Pi}^{(0)}(p, \Omega)$ at zero polaron density can be determined by plugging this expression into Eq. (7.26) and approximating $G_x^R(k)G_x^R(k + \Omega) \simeq [G_x^R(k)]^2$. Using the chain rule

$$\partial_\omega \Sigma_{\text{int}}^{(0)}(p) = \int dk w^{(0)}(p, k) [G_x^R(k)]^2 \partial_\epsilon [G_x^R(k)]^{-1} \quad (7.41)$$

and an analogous identity for $\partial_p \Sigma_{\text{int}}^{(0)}(p)$ as well as $[G_x^R]^{-1} = \omega - \omega_{\mathbf{p}} + (i/2\tau_x) - \Sigma_{\text{int}}^{(0)}(p)$ one can readily verify that Eq. (7.26) is satisfied by the expression

$$\boldsymbol{\Pi}^{(0)}(p; \Omega) = \frac{i\tau_e \Omega}{1 - i\tau_e \Omega} \left(\frac{m_x}{m_e} \partial_{\mathbf{p}} + \frac{\mathbf{p}}{m_e} \partial_\omega \right) \Sigma_{\text{int}}^{(0)}(p). \quad (7.42)$$

7.3.4 Evaluation of transconductivity to first order in n_x

With the results above we are prepared to evaluate the response function $\chi_{\alpha\beta}$ in Eq. (7.13) to linear order in n_x . As outlined previously, we can use the representation of the exciton Green's function in Eq. (7.28). By expanding the different terms of Eq. (7.13) separately, we obtain three contributions

$$\chi_{\alpha,\beta}(\Omega) = \chi_{\alpha,\beta}^i(\Omega) + \chi_{\alpha,\beta}^{ii}(\Omega) + \chi_{\alpha,\beta}^{iii}(\Omega) + \mathcal{O}(n_x^2) \quad (7.43)$$

$$\chi_{\alpha,\beta}^i(\Omega) = -i \int dp \pi_\alpha^{(1)}(p; \Omega) G_x^R(p)^2 \Gamma_\beta^{(0)}(p) \quad (7.44)$$

$$\begin{aligned} \chi_{\alpha,\beta}^{ii}(\Omega) &= -i \int dp \int dk \Pi_\alpha^{(0)}(p; \Omega) G_x^R(p)^2 W^{(1)}(p, k) \\ &\quad \times G_x^R(k)^2 \Gamma_\beta^{(0)}(k) \end{aligned} \quad (7.45)$$

$$\chi_{\alpha,\beta}^{iii}(\Omega) = -i \int dp \Pi_\alpha^{(0)}(p; \Omega) \Gamma_\beta^{(0)}(p) G_x(p) G_x(p + \Omega) \quad (7.46)$$

To evaluate the first contribution, we use Eq. (7.30) as well as the Ward identity for $\Gamma^{(0)}$ in Eq. (7.37) and obtain

$$\begin{aligned}\chi_{\alpha,\beta}^i(\Omega) = & 2 \int dp dp' \frac{\delta\pi_\alpha^{(0)}(p; \Omega)}{\delta G_x^R(p')} \text{Im}G_x^A(p')\theta(-\omega') \\ & \times \partial_{p_\beta} G_x^R(p).\end{aligned}\quad (7.47)$$

Writing the first order term in n_x as a functional derivatives turns out to be very useful. We first use Eq. (7.23) to express the vertex $\pi_\alpha(p)$ in terms of the self energy Σ_{int} and we subsequently have to evaluate $\delta\Sigma_{\text{int}}(p)/\delta G_x(p') = W(p, p')$. From its definition in Eq. (7.22), however, we immediately observe that the function $W(p, p')$ is symmetric under exchange of momentum arguments, which implies the simple relation

$$\frac{\delta\pi_\alpha(p; \Omega)}{\delta G_x(p')} = \frac{\delta\pi_\alpha(p'; \Omega)}{\delta G_x(p)}.\quad (7.48)$$

Making use of this expression together with the chain rule

$$\int dp' \frac{\delta\pi_\alpha(p; \Omega)}{\delta G_x(p')} \partial_{p'} G_x(p') = \partial_p \pi_\alpha(p; \Omega),\quad (7.49)$$

we find

$$\chi_{\alpha,\beta}^i(\Omega) = 2 \int dp \text{Im}G_x^A(p)\theta(-\omega) \partial_{p_\beta} \pi_\alpha^{(0)}(p, \Omega).\quad (7.50)$$

The structure of the second term given by Eq. (7.45) is similar to the first contribution. Using the Ward identity as well as the expansion of w in Eq. (7.32) we obtain

$$\begin{aligned}\chi_{\alpha,\beta}^{ii}(\Omega) = & 2 \int dp dk dk' \Pi_\alpha^{(0)}(p; \Omega) G_x^R(p)^2 \theta(-\epsilon') \\ & \times \text{Im}G_x^A(k') \frac{\delta w^{(0)}(p, k)}{\delta G_x^R(k')} \partial_{k_\beta} G_x^R(k).\end{aligned}\quad (7.51)$$

We now use the identities

$$\frac{\delta w(p, k)}{\delta G_x(k')} = \frac{\delta^2 \Sigma_{\text{int}}(p)}{\delta G_x(k) \delta G_x(k')} = \frac{\delta w(p, k')}{\delta G_x(k)},\quad (7.52)$$

$$(\partial_p + \partial_k)w(p, k) = \int dk' \frac{\delta w(p, k)}{\delta G_x(k')} \partial_{k'} G_x(k'),\quad (7.53)$$

where the second line immediately follows from the definition of T and w in Eqs. (4.48) and (7.22). We arrive at

$$\begin{aligned}\chi_{\alpha,\beta}^{ii}(\Omega) = & 2 \int dp dk \Pi_\alpha^{(0)}(p; \Omega) G_x^R(p)^2 \theta(-\epsilon) \\ & \times \text{Im}G_x^A(k)(\partial_{p_\beta} + \partial_{k_\beta})w^{(0)}(p, k).\end{aligned}\quad (7.54)$$

The third contribution χ^{iii} in Eq. (7.43) contains a term $G_x(p)G_x(p + \Omega)$ which cannot be expanded by the simple recipe in Eq. (7.28) because two exciton Green's functions are evaluated at nearby frequencies. A similar expression for the electronic Green's function has been evaluated in Eq. (7.33), however, we cannot use the same formula for excitons because their self energy has an energy dependent imaginary part. In particular, when evaluated away from the polaron resonance at $\omega = \zeta_p$, $\text{Im}\Sigma_{\text{int}}(p)$ is not necessarily small. Hence, the imaginary part of the exciton Green's function cannot be simply replaced by a delta function at the polaron resonance and the energy integral has both on-shell and off-shell contributions.

The evaluation of the on-shell contribution, where $G_x \simeq \bar{G}_x$ given by Eq. (7.16), is further complicated by the momentum dependent lifetime broadening $1/2\tau_x + \text{Im}\Sigma_{\text{int}}(p)$ of the polarons. For simplicity, we neglect this momentum dependence in the following, writing

$$\bar{G}_x(p) \simeq \frac{1}{\omega - \zeta_p + i/2\tau_x^* \text{sgn}(\omega)} \quad (7.55)$$

with $1/\tau_x^* = Z/\tau_x$, which is formally justified in the limit $\text{Im}\Sigma_{\text{int}}(0, -\mu_x^*) \ll 1/2\tau_x$. This approximation ignores the effect of electron-polaron scattering on transport, which is expected to be suppressed at small external frequencies due to the small available phase space. We discuss this issue in more detail in Sec. 7.3.5 below.

The distinction between on- and off-shell contributions can now be made explicit by writing

$$\text{Im}G_x(p) = Z\text{Im}\bar{G}_x + |G^R(p)|^2\text{Im}\Sigma_{\text{int}}(p, \omega). \quad (7.56)$$

For the relevant energies $\omega < 0$, the first term is entirely determined by on-shell contributions, whereas the second term vanishes near the polaron resonance. With the help of Eq. (7.27), we find

$$\begin{aligned}G_x(p)G_x(p + \Omega) \simeq & [G_x^R(p) + 2iZ\text{Im}\bar{G}_x(p)\theta(-\omega)] \\ & \times [G_x^R(p + \Omega) + 2iZ\text{Im}\bar{G}_x(p + \Omega)\theta(-\omega)] \\ & + 4iG_x^R(p)|G^R(p)|^2\text{Im}\Sigma_{\text{int}}(p, \omega)\theta(-\omega),\end{aligned}\quad (7.57)$$

where we have approximated $\omega + \Omega \rightarrow \omega$ in the second term and we have neglected terms of order $\text{Im}\Sigma_{\text{int}}(p)^2 \propto n_x^2$. Using this expression, we can rewrite Eq. (7.46) as

$$\begin{aligned} \chi_{\alpha,\beta}^{iii}(\Omega) = & -i \int dp \Pi_{\alpha}^{(0)}(p; \Omega) \Gamma_{\beta}^{(0)}(p) [Z^2 \bar{G}_x(p) \bar{G}_x(p + \Omega) \\ & + 4i \text{Re}G_x(p) |G_x^R(p)|^2 \text{Im}\Sigma_{\text{int}}(p) \theta(-\omega)], \end{aligned} \quad (7.58)$$

where we have replaced $G_x \rightarrow Z \bar{G}_x$ in the first term as this integral is dominated by on-shell contributions. The second term has only off-shell contributions and we can therefore write to leading order $\text{Re}G_x(p) |G_x^R(p)|^2 \simeq G_x^R(p)^3$. We obtain

$$\begin{aligned} \chi_{\alpha,\beta}^{iii}(\Omega) = & -i \int dp \Pi_{\alpha}^{(0)}(p; \Omega) \Gamma_{\beta}^{(0)}(p) [Z^2 \bar{G}_x(p) \bar{G}_x(p + \Omega) \\ & + 4i [G_x^R(p)]^3 \text{Im}\Sigma_{\text{int}}(p) \theta(-\omega)]. \end{aligned} \quad (7.59)$$

To make a connection with Eq. (7.54), we express $\text{Im}\Sigma(p)$ in terms of $\text{Im}G_x(p)$ using straightforward manipulations (see App. A.5), and employing the Ward identity we arrive at

$$\begin{aligned} \chi_{\alpha,\beta}^{iii}(\Omega) = & \int dp \Pi_{\alpha}^{(0)}(p; \Omega) \{-i \Gamma_{\beta}^{(0)}(p) Z^2 \bar{G}_x(p) \bar{G}_x(p + \Omega) \\ & + 2 \text{Im}G_x(k) \theta(-\epsilon) w^{(0)}(p, k) \partial_{\mathbf{p}} [G_x^R(p)]^2\}, \end{aligned} \quad (7.60)$$

Adding all three contributions, we obtain

$$\begin{aligned} \chi_{\alpha,\beta}(\Omega) = & -iZ^2 \int dp \Pi_{\alpha}^{(0)}(p; \Omega) \Gamma_{\beta}^{(0)}(p) \bar{G}_x(p) \bar{G}_x(p + \Omega) \\ & + 2Z \int dp \text{Im} \bar{G}_x(p) \theta(-\omega) \partial_{\mathbf{p}} \Pi_{\beta}^{(0)}(p; \Omega) \\ & + 2 \int dp dk \Pi_{\alpha}^{(0)}(k; \Omega) \theta(-\omega) \\ & \times \text{Im}G_x^A(p) \partial_{k\beta} [w^{(0)}(p, k) G_x^R(k)^2]. \end{aligned} \quad (7.61)$$

We can perform a partial integration in the last term and using:

$$\int dk w^{(0)}(p, k) G_x^R(k)^2 \simeq -Z \partial_{\omega} \Sigma(\omega) \simeq 1 - Z \quad (7.62)$$

we can write the response function in the form

$$\begin{aligned} \chi_{\alpha,\beta}(\Omega) = & -iZ^2 \int dp \Pi_{\alpha}^{(0)}(p; \Omega) \Gamma_{\beta}^{(0)}(p) \bar{G}_x(p) \bar{G}_x(p + \Omega) \\ & + Z \int dp \bar{G}_x(p) \partial_{\mathbf{p}} \Pi_{\beta}^{(0)}(p; \Omega), \end{aligned} \quad (7.63)$$

where we have used Eq. (7.28) and $\int dp G_x(p) = \int dp \bar{G}_x(p)$.

We have arrived at an expression that depends exclusively on the on-shell Green's function $\bar{G}_x(p)$. Using the explicit expression in Eq. (7.55), we can rewrite Eq. (7.63) using Eq. (7.33) as

$$\begin{aligned} \chi_{\alpha\beta}(\Omega) &= -iZ \int dp \bar{G}_x(p) \partial_{\mathbf{p}_\beta} \Pi_\alpha^{(0)}(p; \Omega) \\ &\quad - iZ^2 \int dp \Pi_\alpha^{(0)}(p; \Omega) \Gamma_\beta^{(0)}(p) \\ &\quad \times \frac{\left(\Omega \frac{\mathbf{p}_\beta}{m_x^*} \partial_\omega + \partial_{\mathbf{p}_\beta} i/\tau_x^* \right) \bar{G}_x(p)}{\Omega + i/\tau_x^*}. \end{aligned} \quad (7.64)$$

Moreover, the vertex functions in Eqs. (7.37) and (7.42) can be evaluated explicitly

$$\Gamma^{(0)}(\mathbf{p}, \zeta_{\mathbf{p}}) = \frac{\mathbf{p}}{Zm_x^*}, \quad (7.65)$$

$$\Pi^{(0)}(\mathbf{p}, \zeta_{\mathbf{p}}; \Omega) = \frac{-i\tau_e \Omega}{1 - i\tau_e \Omega} \frac{\mathbf{p}}{Zm_e} \left(1 - \frac{m_x}{m_x^*} \right). \quad (7.66)$$

Using these expressions and the identities $-i \int dp \bar{G}_x(p) = n_x$ and $\int d\omega \partial_\omega \bar{G}_x(\omega) = 0$ as well as integration by parts, we readily obtain

$$\chi_{\alpha\beta} = -\frac{\delta_{\alpha\beta} n_x}{m_e} \left(1 - \frac{m_x}{m_x^*} \right) \frac{\tau_e \tau_x^* \Omega^2}{(1 - i\tau_e \Omega)(1 - i\tau_x^* \Omega)}. \quad (7.67)$$

The longitudinal transconductivity $\sigma_{xe} = e\chi_{\alpha\alpha}/i\Omega$ thus reads

$$\sigma_{xe}(\Omega) = \frac{en_x}{m_e} \left(1 - \frac{m_x}{m_x^*} \right) \frac{i\Omega \tau_e \tau_x^*}{(1 - i\Omega \tau_e)(1 - i\Omega \tau_x^*)}, \quad (7.68)$$

which is identical to the expression in Eq. (7.7).

7.3.5 Transconductivity in terms of low-energy excitations

We can rederive the result in Eq. (7.63) starting from an effective theory based on attractive polarons as the only low-energy excitations of the system. The effective low-energy Hamiltonian in terms the attractive polaron operators $a_{\mathbf{p}}$ in the absence of electric fields reads

$$H_0 = \sum_{\mathbf{p}} \zeta_{\mathbf{p}} a_{\mathbf{p}}^\dagger a_{\mathbf{p}} + \sum_{\mathbf{p}, \mathbf{q}, j} U e^{i\mathbf{q}\mathbf{r}_j} a_{\mathbf{p}+\mathbf{q}}^\dagger a_{\mathbf{p}}, \quad (7.69)$$

where the first term denotes the dispersion of polarons, while the second term corresponds to disorder scattering of polarons. The effective polaron Green's function can be written as $\tilde{G}_x(p) = \int d\omega e^{-i\omega t} \langle 0 | T a_p(t) a_p^\dagger(0) | 0 \rangle$.

In the presence of an electric field $\mathbf{E}(t) = \mathbf{E}e^{-i\Omega t}$, the polaron quasiparticles are no longer eigenstates of the system as the field induces a drift in the Fermi sea. Solving the polaron problem with average electron velocity \mathbf{v}_e , we find that the polaron dispersion is shifted in momentum space $\mathbf{p} \rightarrow \mathbf{p} + \mathbf{v}_e(m_x^* - m_x)$ (see App. A.3 App. A.2 for a detailed calculation). This shift can be interpreted as an effective vector potential for polarons induced by the electric field. Assuming an electronic drift velocity $\mathbf{v}_e = -e\tau_e \mathbf{E}e^{-i\Omega t}/m_e(1 - i\Omega\tau_e)$, we can account for the shifted dispersion by introducing an additional term in the effective polaron Hamiltonian

$$H' = -\sum_{\mathbf{p}} a_{\mathbf{p}}^\dagger a_{\mathbf{p}} Z\Pi^{(0)}(\mathbf{p}, \zeta_{\mathbf{p}}; \Omega) \cdot \mathbf{A}(t), \quad (7.70)$$

where $\Pi^{(0)}$ is the vertex evaluated at vanishing exciton density given by Eq. (7.66) and $\mathbf{A}(t) = \mathbf{E}e^{-i\Omega t}/i\Omega$ is the electric vector potential.

Alternatively, Eq. (7.70) can be derived by evaluating the effective electron current vertex of polarons. Following the same arguments as in Sec. 4.2, one can readily convince oneself that this vertex is given by

$Z\Pi = \frac{\partial}{\partial \mathbf{A}} \Sigma_{\text{int}}[G_e(\mathbf{A})] \Big|_{\mathbf{A}=0}$. The evaluation of the vertex $\Pi^{(0)}$ is straightforward and has been performed in Sec. 7.3.3.

The attractive polaron current resulting from the Hamiltonian H' is

$$\begin{aligned} \hat{\mathbf{j}}_x &= \sum_{\mathbf{p}} \left[\frac{\mathbf{p}}{m_x^*} + \frac{e\mathbf{E}e^{-i\Omega t}}{i\Omega} Z\partial_{\mathbf{p}}\Pi^{(0)}(\mathbf{p}, \zeta_{\mathbf{p}}; \Omega) \right] a_{\mathbf{p}}^\dagger a_{\mathbf{p}} \\ &= \hat{\mathbf{j}}_x + \frac{e\mathbf{E}e^{i\Omega t}}{i\Omega} Z\partial_{\mathbf{p}}\Pi^{(0)}(\mathbf{p}, \zeta_{\mathbf{p}}; \Omega) \hat{n}_x \end{aligned} \quad (7.71)$$

where we introduced $\hat{\mathbf{j}}_x \equiv \sum_{\mathbf{p}} (\mathbf{p}/m_x^*) a_{\mathbf{p}}^\dagger a_{\mathbf{p}}$ and we used the fact that $\partial_{\mathbf{p}}\Pi^{(0)}(\mathbf{p}, \zeta_{\mathbf{p}}; \Omega)$ does not depend on momentum. The first term corresponds to the paramagnetic contribution that can be evaluated using Kubo's formula. The second term is the diamagnetic contribution that originates from the change in polaron velocity due to the shift of the dispersion implied by Eq. (7.70). These two terms precisely recover Eq. (7.63).

We can hence interpret Eq. (7.63) as the para- and diamagnetic contributions to the conductivity in terms of effective polaron quasiparticles with propagator \tilde{G}_x . In the derivation of this equation in Sec. 7.3.4, we have neglected the momentum dependence of the lifetime thereby ignoring in-

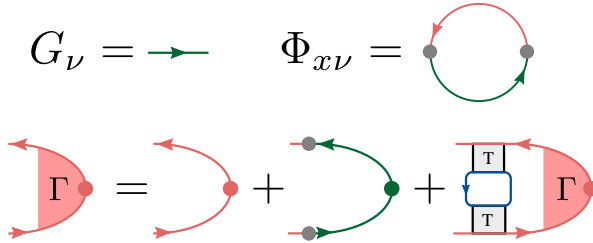


FIGURE 7.3: Functional describing exciton-photon interaction $\Phi_{x\nu}[G_x, G_\nu]$ and vertex correction Γ for polaritons with photon propagators represented by green (dark gray) lines.

coherent electron-polaron scattering. Here, we have not made such an assumption, which suggests that Eq. (7.63) holds even for a more general momentum-dependent lifetime.

Nevertheless the result for the transconductivity remains unchanged. Obviously, only quasiparticles within a thin shell of width $\sim \Omega$ around the Fermi energy contribute to the conductivity. In close analogy to Landau Fermi liquid theory, we find that the electron scattering rate of an attractive polaron of energy Ω is proportional to Ω^2 (see App. A.4). In accordance with our expansion to lowest order in Ω , the electron-scattering lifetime $\text{Im}\Sigma_{\text{int}}(p)$ of the quasiparticles relevant for transport can therefore be neglected.

7.4 TRANSCONDUCTIVITY OF POLARON POLARITONS

The above calculation can be readily generalized to the case of exciton polaron polaritons. We simply add a term $\Phi_{x\nu}$ describing the coupling of excitons to the cavity mode to the functional Φ discussed in Sec. 4.2. The term is depicted in Fig. 7.3 and reads explicitly

$$\Phi_{x\nu} = g^2 \int d1d2 G_x(1,2) G_\nu(2,1), \quad (7.72)$$

where the photon propagator is defined as:

$$G_\nu(k)^{-1} = \omega - \nu_k + i0 \operatorname{sgn}(\omega) \quad (7.73)$$

and we introduced the dispersion of cavity photons, $\nu_k = \mathbf{k}^2/2m_c + \Delta$, where $m_c \simeq 10^{-5}m_e$ and we assume for simplicity that photons have an

infinite lifetime. The functional $\Phi_{x\nu}$ leads to an additional self energy for the exciton

$$\Sigma_{x\nu}(k) = g^2 G_\nu(k) = \frac{g^2}{\omega - \nu_{\mathbf{k}} + i0 \operatorname{sgn}(\omega)}, \quad (7.74)$$

and the exciton propagator is changed accordingly

$$G_x(p) = \frac{1}{\omega - \omega_{\mathbf{p}} - \Sigma_{\text{int}}(p) - \Sigma_{\text{dis},x}(p) - \Sigma_{x\nu}(p)}. \quad (7.75)$$

To make connection with our previous result, we assume that we can describe the exciton as an attractive polaron neglecting other excitations such as the trion. In our approach this is formally justified if g is much smaller than the energy difference between attractive polaron and trion. Nevertheless, we expect our results to be valid also at somewhat stronger couplings because, in reality, the coupling strength between cavity photons and trions is vanishingly small, even though this fact is not captured by our simple model.

Hence, approximating the bare exciton Green's function by the attractive polaron Green's function in Eq. (7.16), we find

$$G_x(p) \simeq \frac{Z}{\omega - \zeta_{\mathbf{p}} - iZ \operatorname{Im}[\Sigma_{\text{int}}(p) + \Sigma_{\text{dis},x}(p)] - Z\Sigma_{x\nu}(p)}. \quad (7.76)$$

The resonances of G_x are determined by the equation

$$(\omega - \zeta_{\mathbf{p}})(\omega - \nu_{\mathbf{k}}) = Zg^2. \quad (7.77)$$

Near zero momentum the lower-energy branch can be approximated by a quadratic dispersion

$$\gamma_{\mathbf{p}} = \gamma_0 + \frac{\mathbf{p}^2}{2m_\gamma}. \quad (7.78)$$

Hence, near the lower polariton resonance, G_x takes the approximate form

$$G_\gamma(p) = \frac{Z_\gamma}{\omega - \gamma_{\mathbf{p}} - iZ_\gamma \operatorname{Im}[\Sigma_{\text{int}}(p) + \Sigma_{\text{dis},x}(p)]}. \quad (7.79)$$

When the cavity photon is tuned into resonance with the attractive polaron, $\Delta = \zeta_0$, we find

$$\gamma_0 = \Delta - g\sqrt{Z} \quad (7.80)$$

$$\frac{1}{m_\gamma} = \frac{1}{2} \left(\frac{1}{m_x^*} + \frac{1}{m_c} \right) \quad (7.81)$$

$$Z_\gamma = \frac{Z}{2} \quad (7.82)$$

We have arrived at an effective polariton Green's function that is formally identical to the attractive polaron Green's function in Eq. (7.16), albeit with renormalized parameters. We emphasize, that the broadening $\text{Im}[\Sigma_{\text{int}}(p) + \Sigma_{\text{dis},x}(p)]$ has to be calculated self-consistently and thus disorder scattering as well as electron scattering will be strongly suppressed due to the small polariton density of states $\sim m_c \ll m_x^*$.

The calculation of the transconductivity between electrons and polaron polaritons is closely related to the one for polarons. The relation for the exciton current vertex in Eq. (7.21) acquires an additional term and reads

$$\begin{aligned} \Gamma(p; \Omega) = & \frac{\mathbf{p}}{m_x} + g^2 G_v(p) G_v(p + \Omega) \frac{\mathbf{p}}{m_c} \\ & + \int dk W(p, k) G_x(k) G_x(k + \Omega) \Gamma(k; \Omega). \end{aligned} \quad (7.83)$$

This equation is also displayed in Fig. 7.3. Following the same steps as in Sec. 7.3.3, we can verify that the vertex at zeroth order in the polariton density satisfies the Ward identity

$$\Gamma^{(0)}(p) = [G_\gamma^R(p)]^{-2} \partial_{\mathbf{p}} G_\gamma^R(p). \quad (7.84)$$

For small wavevectors $|\mathbf{p}| \ll \sqrt{m_\gamma g}$, where $G_x(p) \simeq G_\gamma(p)$ we have

$$\Gamma^{(0)}(p) = \frac{\mathbf{p}}{Z_\gamma m_\gamma}. \quad (7.85)$$

In contrast, the derivation of the vertex function $\Pi^{(0)}(p; \Omega)$ in Eq. (7.42) remains unchanged. Moreover, the real part of the self energy $\text{Re}\Sigma_{\text{int}}(p)$ is largely independent of the cavity coupling and hence the on-shell expression for $\Pi^{(0)}(p; \Omega)$ Eq. (7.66) is retained.

In Sec. 7.3.4, most expressions involving G_x remain unchanged as they involve an integral over a large area in momentum space. The only exceptions occur after Eq. (7.56) where the on-shell Green's function \bar{G} of

occupied states is used. In these expressions we can thus simply substitute $Z\bar{G}_x$ with $Z_\gamma\bar{G}_\gamma$. These changes result in an additional factor Z_γ/Z in the final result Eq. (7.68). In addition, the lifetime τ_x is replaced by the polariton lifetime $\tau_\gamma = \tau_x m_x^*/m_\gamma \gg \tau_x$. Based on these considerations, we finally arrive at the transconductivity between electrons and polaritons

$$\sigma_{\gamma e}(\Omega) = \frac{Z_\gamma}{Z} \frac{en_x}{m_e} \left(1 - \frac{m_x}{m_x^*}\right) \frac{i\Omega\tau_e\tau_\gamma}{(1 - i\Omega\tau_e)(1 - i\Omega\tau_\gamma)}. \quad (7.86)$$

The additional factor Z_γ/Z takes into account the fact that the drag requires a finite excitonic quasiparticle weight. At resonance this factor reduces the polaron velocity to half its value. Moreover, we emphasize that polariton drag is much less affected by excitonic disorder because the small density of states of polaritons suppresses disorder scattering.

7.5 NONEQUILIBRIUM EFFECTS

We have seen that our intuitive picture of polaron drag developed in Sec. 7.2 correctly reproduces the results of the fully microscopic model presented in Sec. 7.3. This is encouraging as the semiclassical theory can be extended to include other effects that could not be captured within the linear-response calculation, but that are potentially relevant for experiments. Most notably, optically excited excitons have a finite lifetime due to recombination processes, which requires a nonequilibrium calculation.

For exciton polarons in monolayer TMDs, an ultrashort radiative lifetime of ~ 1 ps for low momentum excitons implies that the assumption of an equilibrium exciton gas is not justified. Moreover, disorder scattering in state-of-the-art samples is comparable to the radiative decay rate, rendering it unlikely that a spatial displacement in exciton photoluminescence induced by an applied low-frequency electric field can be observed.

In general, we envision three different experimental scenarios, where our findings are potentially observable:

(i) In the case of interlayer excitons in TMD heterobilayers, where electrons and holes occupy conduction and valence band states in different monolayers, the exciton lifetime can be tuned electrically and can well exceed 100 ns. Since timescales for disorder scattering are considerably shorter, we expect the interlayer excitons to be in equilibrium. Provided that the spatially indirect trion state remains bound, our results could also be used to describe drag of indirect exciton polarons, where disorder or electron scattering times can be shorter than the radiative lifetime. In this

case, the resonantly generated polarons will be scattered to momentum states outside the light cone, where they can decay nonradiatively or by phonon-assisted radiative decay. The nonzero drag velocity may be detected in photoluminescence.

(ii) Alternatively, our results may be relevant to heterobilayers at very large electron density. In this limit, screening of the interaction between valence band holes and conduction band electrons has to be taken into account, which invalidates our assumption that excitons can be regarded as rigid quasiparticles. Instead, we may consider the valence band hole as a quantum impurity interacting with a Fermi sea of conduction band electrons. For sufficiently high electron densities, it may become favorable for the hole to form a polaron rather than an exciton. This approach bears some similarity with Ref. [92] and it can be used to analyze the Fermi-edge singularity problem within the framework of Fermi polarons. Our analysis of the transport problem carries over to the case of hole polarons with the trion binding energy replaced by the screened exciton binding energy. To ensure that $\Omega\tau > 1$ is satisfied, it may be possible to use microwave or Terahertz irradiation and monitor the polaron response as sidebands in optical response.

(iii) Arguably the most promising platform for observation of electric-field induced displacement of neutral optical excitations is provided by exciton polaron polaritons observed when a monolayer with a 2DES is embedded inside a 2D microcavity [2, 93, 94], or when a monolayer is embedded in a dielectric structure that supports in-plane propagating photonic modes [95]. Small-momentum excitations in the lower-energy polaron polariton branch have two striking features: first, due to their extremely small effective mass, polaritons are to a large extent protected from disorder scattering. This effect has been observed in exciton polaritons in 1990s in GaAs heterostructures [96, 97]. Second, low-momentum polaritons can only decay radiatively through cavity mirror loss: it is therefore possible to ensure that the polariton lifetime is much longer than that of excitons by using high quality-factor cavities. Nevertheless, interactions between polaritons are also weak and we cannot expect a low density of polaritons to thermalize, rendering it essential to develop a nonequilibrium description of transport.

7.5.1 Boltzmann equation

Our aim is to develop a kinetic theory for the distribution function $g_{\mathbf{k}}(\mathbf{r}, t)$ of exciton polarons, including the effects of pumping, recombination, disorder as well as a nonzero electron drift velocity $\mathbf{v}_e(t)$ due to an electric field $\mathbf{E}(t)$. In the most general case, we can write the Boltzmann equation as

$$\frac{dg_{\mathbf{k}}(\mathbf{r}, t)}{dt} = \frac{\partial g_{\mathbf{k}}(\mathbf{r}, t)}{\partial t} + \dot{\mathbf{k}} \frac{\partial g_{\mathbf{k}}(\mathbf{r}, t)}{\partial \mathbf{k}} + \dot{\mathbf{r}}_{\mathbf{k}} \frac{\partial g_{\mathbf{k}}(\mathbf{r}, t)}{\partial \mathbf{r}} \quad (7.87)$$

Importantly, the electric field does not exert a direct force on polarons, whose canonical momentum \mathbf{k} is conserved. Instead, it shifts the polaron dispersion by changing the electron velocity. A straightforward solution of the polaron problem in the presence of an electron drift (see App. A.2 and App. A.3) yields the dispersion

$$\tilde{\zeta}_{\mathbf{k}}(t) = \zeta_{\mathbf{k} + (m_x^* - m_x)\mathbf{v}_e(t)}, \quad (7.88)$$

which is shifted from the equilibrium dispersion $\zeta_{\mathbf{k}} = \mathbf{k}^2/2m_x^*$ such that the polaron state at $\mathbf{k} = 0$ has a velocity $(1 - m_x/m_x^*)\mathbf{v}_e(t)$. Even though an electric field does not affect the conjugate momentum of the polaron, $\dot{\mathbf{k}} = 0$, it changes its kinetic momentum $m_x^*\mathbf{v}_x(\mathbf{k}, t)$ with the polaron velocity

$$\mathbf{v}_x(\mathbf{k}, t) = \frac{\partial \tilde{\zeta}_{\mathbf{k}}(t)}{\partial \mathbf{k}} = \frac{\mathbf{k}}{m_x^*} + \left(1 - \frac{m_x}{m_x^*}\right) \mathbf{v}_e(t). \quad (7.89)$$

For simplicity, we assume a spatially homogeneous distribution, $\partial_{\mathbf{r}}g_{\mathbf{k}}(\mathbf{r}, t) = 0$ and we suppress the spatial dependence in the following. Hence, the distribution function does not have an implicit time-dependence and Eq. (7.87) can be written as

$$\frac{dg_{\mathbf{k}}(t)}{dt} = R\delta(\mathbf{k}) - \frac{g_{\mathbf{k}}(t)}{\tau_r} + \left(\frac{\partial g_{\mathbf{k}}(t)}{\partial t}\right)_{\text{dis}} + \left(\frac{\partial g_{\mathbf{k}}(t)}{\partial t}\right)_{\text{int}}. \quad (7.90)$$

The first term is due to pumping of polarons at a rate R in the polaron state at $\mathbf{k} = 0$ by resonant laser absorption. The incidence angle of a collimated laser field determines the in-plane momentum of the exciton polarons, which is in turn much smaller than the other characteristic momentum scales in the problem such as k_F and $m_e\mathbf{v}_e$. By tuning the frequency of a normal-incidence single-mode laser field, it is possible to ensure that only $\mathbf{k} = 0$ attractive polarons can be created. The second term in Eq. (7.90)

corresponds to the loss of attractive polarons due to the recombination processes at a rate $1/\tau_r$. In general τ_r is expected to depend on momentum, since the recombination rate should be strongest for small momenta \mathbf{k} that lie inside the light-cone, whereas the decay from states outside the light cone requires the generation of additional excitations such as phonons. Here we neglect the momentum dependence of τ_r , for simplicity, although the generalization of our results to include this effect is straightforward. The last two terms in Eq. (7.90) conserve the number of polarons and correspond to collision processes, either due to exciton disorder or incoherent scattering off electrons. These terms will be discussed in more detail below.

Integrating Eq. (7.90) over momentum space, we obtain the time evolution of the exciton density $n(t) \equiv n_x(t) = \int (d\mathbf{k}/4\pi^2) g_{\mathbf{k}}(t)$ as

$$\dot{n}(t) = R - \frac{n(t)}{\tau_r}, \quad (7.91)$$

where we have used that the collision integrals conserve the number of polarons. We are moreover interested in evaluating the exciton current density defined as

$$n(t)\bar{\mathbf{v}}_x(t) = \int \frac{d\mathbf{k}}{(2\pi)^2} g_{\mathbf{k}}(t) \mathbf{v}_x(\mathbf{k}, t). \quad (7.92)$$

Differentiating with respect to time, we obtain

$$\begin{aligned} n(t) \frac{d\bar{\mathbf{v}}_x(t)}{dt} + \dot{n}(t)\bar{\mathbf{v}}_x(t) &= \int \frac{d\mathbf{k}}{(2\pi)^2} \left[g_{\mathbf{k}}(t) \frac{d\mathbf{v}_x(\mathbf{k}, t)}{dt} \right. \\ &\quad \left. + \frac{dg_{\mathbf{k}}(t)}{dt} \mathbf{v}_x(\mathbf{k}, t) \right] \end{aligned} \quad (7.93)$$

The first term on the right-hand side can be readily evaluated using Eq. (7.89) and $\dot{\mathbf{k}} = 0$ as

$$\int \frac{d\mathbf{k}}{(2\pi)^2} g_{\mathbf{k}}(t) \frac{d\mathbf{v}_x(\mathbf{k}, t)}{dt} = n(t) \frac{m_x^* - m_x}{m_x^* m_e} \mathbf{F}_e(t) \quad (7.94)$$

with $\mathbf{F}_e = m_e \dot{\mathbf{v}}_e(t)$. The second integral in Eq. (7.93) can be evaluated using the Boltzmann equation (7.90) and, with the help of Eq. (7.91), we obtain

$$\begin{aligned} m_x^* \frac{d\bar{\mathbf{v}}_x(t)}{dt} &= \frac{R}{n(t)} [(m_x^* - m_x) \mathbf{v}_e(t) - m_x^* \bar{\mathbf{v}}_x(t)] \\ &\quad + \frac{m_x^* - m_x}{m_e} \mathbf{F}_e(t) + \mathbf{F}_{\text{dis}}(t) + \mathbf{F}_{\text{int}}(t), \end{aligned} \quad (7.95)$$

In this expression, the first and second term account for polarons in the $\mathbf{k} = 0$ state with velocity $\mathbf{v}_x(0, t) = (1 - m_x/m_x^*)\mathbf{v}_e(t)$ that are generated by the laser or lost by the recombination of excitons, respectively. The third term corresponds to the drag force acting on the exciton system due to the polaronic coupling to electrons, which was the main focus of the equilibrium calculation in Sec. (7.3). The last two terms correspond to the friction due to exciton disorder and incoherent scattering with electrons

$$\mathbf{F}_{\text{dis}}(t) = \frac{m_x^*}{n(t)} \int \frac{d\mathbf{k}}{(2\pi)^2} \left(\frac{\partial g_{\mathbf{k}}}{\partial t} \right)_{\text{dis}} \mathbf{v}_x(\mathbf{k}, t), \quad (7.96)$$

$$\mathbf{F}_{\text{int}}(t) = \frac{m_x^*}{n(t)} \int \frac{d\mathbf{k}}{(2\pi)^2} \left(\frac{\partial g_{\mathbf{k}}}{\partial t} \right)_{\text{int}} \mathbf{v}_x(\mathbf{k}, t). \quad (7.97)$$

These forces depend sensitively on the polaron distribution and can lead to nonlinear effects in the time evolution. We discuss them in more detail in the next section.

7.5.2 Estimation of the friction forces from disorder and incoherent scattering with electrons

Friction from excitonic disorder can be described by the collision integral

$$\left(\frac{\partial g_{\mathbf{k}}}{\partial t} \right)_{\text{dis}} = \int \frac{d\mathbf{k}'}{(2\pi)^2} [g_{\mathbf{k}'}(t) - g_{\mathbf{k}}(t)] \tilde{M}_{\mathbf{k}\mathbf{k}'} \quad (7.98)$$

where $\tilde{M}_{\mathbf{k}\mathbf{k}'}$ denotes the matrix element corresponding to the scattering of a polaron from state \mathbf{k} to state \mathbf{k}' . In the simplest case, we can assume Gaussian white noise as in Sec. 7.3.1 and we obtain

$$\tilde{M}_{\mathbf{k}\mathbf{k}'} = \frac{1}{v_x^* \tau_x^*} \delta[\tilde{\zeta}_{\mathbf{k}}(t) - \tilde{\zeta}_{\mathbf{k}'}(t)] \quad (7.99)$$

Note that the matrix elements depend on the shifted dispersion in the presence of the electric field. With this approximation, the collision integral simplifies to

$$\left(\frac{\partial g_{\mathbf{k}}}{\partial t} \right)_{\text{dis}} = \frac{1}{v_x^* \tau_x^*} \int \frac{d\mathbf{k}'}{(2\pi)^2} g_{\mathbf{k}'}(t) \delta[\tilde{\zeta}_{\mathbf{k}}(t) - \tilde{\zeta}_{\mathbf{k}'}(t)] - \frac{g_{\mathbf{k}}(t)}{\tau_x^*} \quad (7.100)$$

and the friction force reads

$$\mathbf{F}_{\text{dis}}(t) = - \frac{m_x^* \bar{\mathbf{v}}_x(t)}{\tau_x^*}. \quad (7.101)$$

Hence, for Gaussian white noise correlated disorder, the polaron disorder scattering time is also the relaxation time for the drift velocity of the exciton system. We emphasize that this result holds, even though we cannot treat the collision integral in Eq. (7.98) in the relaxation time approximation.

The force introduced in Eq. (7.97) corresponds to an additional drag force originating from the residual interaction between electrons and polarons. While coherent scattering events of electrons and excitons result in polaron formation and the polaron drag phenomenon described in Sec. 7.2 and 7.3, incoherent collisions lead to a lifetime broadening of the polarons. This broadening appears as a term $\text{Im}\Sigma_{\text{int}}(p)$ in the Green's function description of polarons discussed in Sec. 7.3.1.

The qualitative effect of incoherent broadening can be estimated from a simple argument by temporarily disregarding polaronic disorder. For concreteness, we imagine a narrow distribution of polarons around zero momentum, which corresponds to the distribution shortly after the laser has been switched on. In the comoving frame of the electrons, the zero momentum polarons have a velocity $-\mathbf{v}_e m_x / m_x^*$ and thus are in an excited state. Excited polaron states, however, have a finite lifetime due to the interaction with electrons and will decay into lower-energy states, which also have a smaller absolute velocity. Hence, incoherent electron-polaron scattering will lead to a relaxation of the polaron velocity to zero *in the comoving frame*. In the lab frame, this corresponds to an acceleration of polarons until they reach a velocity \mathbf{v}_e . This justifies the following ansatz for the electron friction force on the polarons

$$\mathbf{F}_{\text{int}} = -m_x^* \frac{\bar{\mathbf{v}}_x(t) - \mathbf{v}_e}{\tau_{\text{int}}(t)} \quad (7.102)$$

with an effective time scale τ_{int} that depends on details of the polaron distribution at time t . A rough estimate for τ_{int} is given by the interaction lifetime of an excited polaron state with velocity $-m_x \mathbf{v}_e / m_x^*$. After this time, all the polarons at zero momentum have scattered at least once. In the comoving frame of electrons, the scattering probability does not have a very strong dependence on the direction of the final polaron momentum. Hence the polarons reach an average velocity $\simeq \mathbf{v}_e$ already after a few scattering events, even though the time for each individual polaron to reach that velocity is expected to be much longer.

The expression for the friction force in Eq. (7.102) captures the conventional Coulomb drag effect, e.g., in electron bilayer systems [16, 79–81]. Indeed, for perturbative interactions, \mathbf{F}_{int} is the only contribution to drag. As we have shown in Sec. 7.3, nonperturbative interactions result in an

additional polaron drag effect that dominates at low temperatures and frequencies, whereas the drag force in Eq. (7.102) is a subleading correction that we have neglected in the linear response calculation in Sec. 7.3. We emphasize that in nonequilibrium systems or at finite temperatures, F_{int} cannot necessarily be ignored.

An explicit expression for the collision integral reads

$$\left(\frac{\partial g_{\mathbf{k}}}{\partial t} \right)_{\text{int}} = \int \frac{d\mathbf{k}'}{(2\pi)^2} \left[g_{\mathbf{k}'}(1 - g_{\mathbf{k}})\tilde{Q}_{\mathbf{k}\mathbf{k}'} - g_{\mathbf{k}}(1 - g_{\mathbf{k}'})\tilde{Q}_{\mathbf{k}\mathbf{k}'} \right] \quad (7.103)$$

where the transition probability $\tilde{Q}_{\mathbf{k}\mathbf{k}'}$ denotes the scattering rate of an attractive polaron of momentum \mathbf{k} to a momentum \mathbf{k}' due to interactions with an electron Fermi sea drifting at velocity \mathbf{v}_e . In order to derive an expression for $\tilde{Q}_{\mathbf{p}\mathbf{p}'}$, we first consider the polaron scattering rate $Q_{\mathbf{p}\mathbf{p}'}$ when the electron drift velocity is zero. The electron-polaron scattering amplitude is simply given by the T matrix, and, hence, Fermi's Golden rule yields

$$Q_{\mathbf{p}\mathbf{p}'} = Z^2 \pi \int \frac{d\mathbf{k}}{(2\pi)^2} |T(\mathbf{p} + \mathbf{k}, \zeta_{\mathbf{p}} + \xi_{\mathbf{k}})|^2 f_{\mathbf{k}} \left[1 - f_{\mathbf{k}+\mathbf{p}-\mathbf{p}'} \right] \times \delta(\zeta_{\mathbf{p}} - \zeta_{\mathbf{p}'} - \xi_{\mathbf{k}+\mathbf{p}-\mathbf{p}'} + \xi_{\mathbf{k}}) \quad (7.104)$$

where f denotes the equilibrium electron distribution. One can readily verify that this scattering rate reproduces the lifetime broadening of the on-shell polaron Green's function (see App. A.4.3 for the case of an empty polaron band)

$$\text{Im}\Sigma_{\text{int}}(\mathbf{p}, \zeta_{\mathbf{p}}) = \int \frac{d\mathbf{k}'}{(2\pi)^2} (1 - g_{\mathbf{k}'})\tilde{Q}_{\mathbf{k}\mathbf{k}'} \quad (7.105)$$

In the presence of a nonzero electron drift velocity, Eq. (7.104) has to be modified, by shifting both the polaron dispersion $\zeta_{\mathbf{p}} \rightarrow \tilde{\zeta}_{\mathbf{p}}$ and the electron distribution $f_{\mathbf{k}} \rightarrow f_{\mathbf{k}-m_e \mathbf{v}_e(t)}$. A straightforward calculation along the lines of App. A.2 establishes a relation between the scattering amplitude with and without an electric field

$$\tilde{Q}_{\mathbf{p}\mathbf{p}'} = Q_{\mathbf{p}-m_e \mathbf{v}_e(t), \mathbf{p}'-m_e \mathbf{v}_e(t)}. \quad (7.106)$$

Indeed, this result confirms the intuition that the friction between polarons and electrons results in the relaxation of the polaron velocity in the comoving frame of electrons. To see this, we observe that the lowest energy state

has an infinite lifetime, i.e., $Q_{0,\mathbf{k}} = 0$. In the presence of an electric field, this means a polaron state with momentum $\mathbf{p} = m_x \mathbf{v}_e$ is stable with respect to scattering off electrons. According to Eq. (7.89) this state has a velocity \mathbf{v}_e , i.e., it is moving at the same speed as the electron Fermi sea.

In order to obtain an estimate for the friction force F_{int} in Eq. (7.97) on a narrow distribution centered at zero momentum, $g_{\mathbf{k}} \simeq n\delta(k)$, we can make the same approximation as above that the average velocity after a single scattering event is \mathbf{v}_e . We can hence write the force from first term in Eq. (7.103) as

$$\frac{m_x^*}{n(t)} \int \frac{d\mathbf{k}}{(2\pi)^2} \frac{d\mathbf{k}'}{(2\pi)^2} \mathbf{v}_x(\mathbf{k}, t) g_{\mathbf{k}'}(1 - g_{\mathbf{k}}) \tilde{Q}_{\mathbf{k}'\mathbf{k}} \simeq \frac{m_x^* \mathbf{v}_e}{\tau_{\text{int}}(t)}. \quad (7.107)$$

and for the second term we obtain

$$\frac{m_x^*}{n(t)} \int \frac{d\mathbf{k}}{(2\pi)^2} \frac{d\mathbf{k}'}{(2\pi)^2} \mathbf{v}_x(\mathbf{k}, t) g_{\mathbf{k}}(1 - g'_{\mathbf{k}}) \tilde{Q}_{\mathbf{k}\mathbf{k}'} \simeq \frac{m_x^* \bar{\mathbf{v}}_x}{\tau_{\text{int}}(t)}. \quad (7.108)$$

Here we have defined the scattering time

$$\frac{1}{\tau_{\text{int}}(t)} = \sum_{\mathbf{k}'} \tilde{Q}_{0\mathbf{k}'}, \quad (7.109)$$

which is identical to the interaction lifetime of a polaron at momentum $-m_x \mathbf{v}_e$. With these results we indeed recover Eq. (7.102).

To obtain a rough estimate of τ_{int} , we can approximate the T matrix by a constant $ZT(\mathbf{p} + \mathbf{k}, \zeta_{\mathbf{p}} + \xi_{\mathbf{k}}) \simeq U \equiv ZT(k_F, 0)$ which is valid in the relevant limit $|\mathbf{p}| \ll k_F$ and $|\mathbf{k}| \simeq k_F$. The scattering time at zero temperature can then be obtained from a straightforward calculation (assuming $m \equiv m_x \simeq m_e$, see App. A.4) as

$$\frac{1}{\tau_{\text{int}}(t)} \sim \rho_e U^2 \frac{(mv_e)^3}{k_F}. \quad (7.110)$$

At frequencies close to the trion energy the T-matrix is dominated by the trion pole. The interaction between attractive polarons and electrons originates from virtual scattering events into a higher energy state comprising a trion and a hole which results in an effective attractive interaction. This yields the estimate

$$U \simeq -\frac{Z\epsilon_T}{\rho_e \Delta}, \quad (7.111)$$

where Δ is the energy separation between the trion-hole continuum and the attractive polaron. Assuming a quasiparticle weight $Z \simeq \sqrt{\mu_e/\epsilon_T}$, the friction force on polarons at zero momentum is of the order of

$$\mathbf{F}_{\text{int}} \simeq \frac{m^2 k_F \epsilon_T}{\Delta^2} v_e^3 \mathbf{v}_e. \quad (7.112)$$

The friction force therefore scales with the electric field as $F_{\text{int}} \propto E^4$, which illustrates why this effect has not been captured in the linear response calculation in Sec. 7.3.

We emphasize that this result is valid at zero temperature. At finite temperatures, the friction force is still expected to have the form in Eq. (7.102), but the scattering rate acquires an additional temperature-dependent contribution due to the enhanced phase space available for electron-polaron scattering.

7.5.3 Equations of motion for polarons and polaritons

After the pump has been switched on for a time $\sim \tau_r$, the polaron density saturates to the value $n = R\tau_r$. Even though the density has reached a steady-state value, the solution of the nonlinear Boltzmann equation (7.90) depends sensitively on the ratio of the various time scales and in general requires numerical calculations. To ensure a strong hybridization of polarons and photons, it is desirable to work in a limit where the radiative lifetime is the shortest time scale, $\tau_r \ll \tau_x^*, \tau_{\text{int}}$. In this case, the polarons remain mostly near $\mathbf{k} = 0$, and therefore within the light cone, as disorder and electron scattering, which change the polaron momentum, are suppressed.

This limit guarantees that the friction caused by electrons can be described by Eq. (7.102) and we can make the connection to the semiclassical equations in Sec. 7.2 more explicit. Assuming a density $n(t) = R\tau_r$, Eq. (7.95) can be written as

$$\begin{aligned} m_x^* \frac{d\bar{\mathbf{v}}_x(t)}{dt} &= \frac{(m_x^* - m_x) \mathbf{v}_e(t)}{\tau_r} - \frac{m_x^* \bar{\mathbf{v}}_x(t)}{\tau_r} - \frac{m_x^* \bar{\mathbf{v}}_x(t)}{\tau_x^*} \\ &\quad + \frac{m_x^* - m_x}{m_e} \mathbf{F}_e(t) - \frac{m_x^* (\bar{\mathbf{v}}_x(t) - \mathbf{v}_e)}{\tau_{\text{int}}(t)}. \end{aligned} \quad (7.113)$$

A comparison with the corresponding Eq. (7.3) in Sec. 7.2 reveals three extra contributions in the non-equilibrium case. The first term originates from pumping polarons into the state $\mathbf{k} = 0$ with velocity $\mathbf{v}_x(\mathbf{k} = 0, t) = (1 - m_x/m_x^*) \mathbf{v}_e(t)$. The second term describes recombination of polarons.

Finally, the last term originates from incoherent scattering of electrons, which has been neglected in Sec. 7.2. This assumption is justified in the limit of weak electric fields.

Eq. (7.113) can be readily generalized to polaritons. As has been argued in Sec. 7.4, polaritons are much less affected by scattering processes because of their ultra-low mass and the correspondingly small scattering phase space. Resonant coupling between polarons and the cavity mode creates a local minimum near zero momentum in the polariton dispersion. For a sufficiently strong coupling, ($g > (m_x v_e)^2 / 2m_x^*$ in the notation of Sec. 7.4), disorder or interaction scattering of low-energy polaritons to large momenta $\sim m_x |\mathbf{v}_e|$ are energetically forbidden. In this case the polariton scattering rates $1/\tau_x^*$ and $1/\tau_{\text{int}}$ are reduced by a factor (m_γ/m_x^*) compared to exciton polarons. As typical values are $(m_\gamma/m_x^*) \sim 10^{-5}$, we conclude that such scattering processes can be neglected. Following similar steps as above, we arrive at the equation of motion for polaritons

$$\frac{d\bar{\mathbf{v}}_x(t)}{dt} = \left(1 - \frac{m_x}{m_x^*}\right) \frac{\mathbf{v}_e(t)}{2\tau_r} - \frac{\bar{\mathbf{v}}_x(t)}{\tau_r} + \left(1 - \frac{m_x}{m_x^*}\right) \frac{\mathbf{F}_e(t)}{2m_e} \quad (7.114)$$

The additional factor of $1/2$ in the first and third term reflects the ratio of the polariton and polaron quasiparticle weights. This equation can be readily solved. Assuming a static electric field, such that $\mathbf{F}_e(t) = 0$, the polaritons move at a velocity $\bar{v}_x = (1 - m_x/m_x^*)\mathbf{v}_e(t)/2$ during their entire lifetime, which corresponds to an approximate distance $\Delta = (1 - m_x/m_x^*)\mathbf{v}_e(t)\tau_r/2$.

We also perform a quick estimate of the magnitude of Δ . The ratio m_x/m_x^* depends on the Fermi energy but is of the order 1 , and therefore we can conservatively take $m_x/m_x^* = 1/2$. The electron drift velocity can be calculated from $v_e = E\mu$. In TMDs the applied source-drain electric field E can be of the order of $1000V/cm$, while the electron mobilities can reach $\mu = 10^4 cm^2/(Vs)$ [98, 99], which results in drift velocities of the order of $v_e = 10^5 m/s$. Assuming polariton lifetimes of $\tau_r \approx 10ps$, we obtain a drag induced polariton displacement of roughly $\Delta \approx 250nm$. We envision an experiment where polaritons are injected with a finite group velocity using a resonant laser field, upon which they travel distances exceeding $3\mu m$ while decaying due to cavity losses: by interfering the polariton emission with the same laser field, drag induced polariton displacement of the order of $30nm$ can be easily measured [100]. The displacement can easily be further improved by using higher quality cavities leading to larger polariton lifetimes [101].

7.6 MAGNETIC FIELD RESPONSE OF EXCITON POLARONS

We can include the effect of a dc magnetic field by adding a Lorentz force to Eq. (7.2).

$$\frac{d}{dt} \mathbf{v}_e(t) = \mathbf{a}_e(t) = -\frac{e\mathbf{E}(t)}{m_e} - \mathbf{v}_e(t) \times \frac{e\mathbf{B}}{m_e} - \frac{\mathbf{v}_e(t)}{\tau_e} \quad (7.115)$$

We can readily solve this and find

$$\mathbf{v}_e(\Omega) = \frac{e}{m_e} \frac{\mathbf{E}(\Omega) \times e\mathbf{B}/m_e - \mathbf{E}(\Omega)(\tau_e^{-1} - i\Omega)}{(\tau_e^{-1} - i\Omega)^2 + \omega_c^2} \quad (7.116)$$

where $\omega_c = eB/m_e$ is the cyclotron frequency. As the magnetic field does not directly couple to excitons, Eq. (7.6) remains valid. Hence, when $\omega_c \gg \Omega, 1/\tau_e$ and $\Omega\tau_x \gg 1$, the electrons and polarons drift in the direction perpendicular to the electric and magnetic field realizing a Hall effect of neutral excitons!

More generally, Eq. (7.6) predicts that excitons will follow the trajectory of electrons (scaled by a factor) on time scales shorter than the exciton impurity scattering time. In the absence of an electric field, excitons should therefore move in cyclotron orbits, which suggests that polarons could experience a phenomenon similar to Landau quantization. Equivalently, one can argue that excitons should be affected by the quantizing magnetic field as they are dressed by particle-hole excitations with a discrete energy spectrum due to electronic Landau levels. A signature of this would be a polaron spectral function with a series of peaks on top of an incoherent background present at higher energies roughly spaced by the cyclotron frequency. A related phenomenon has been discussed in the context of Bose polarons, in particular, for electrons strongly coupled to dispersionless phonons. In this case, phonon shake-off processes lead to a series of broad peaks in the polaron spectral function separated in energy by multiples of the phonon frequency [102].

Observation of Landau levels in the absorption spectrum where the energy separation is given by the electron cyclotron frequency would represent yet another manifestation the central role played by polaron physics in optical excitations out of a 2DES. If bound trions were observable in absorption, the observed Landau level spacing would be determined by the trion mass, which is a factor of 3 larger than that of the electron in TMD monolayers. In the opposite limit of very high electron densities, we expect screening to lead to ionization of excitons: in this regime, the level separation will be determined by the reduced mass of electron-hole pairs.

Conversely, the motion of electrons in a magnetic field can be influenced by the presence of excitons. Excitons at an appreciable density can lead to a polaronic dressing of electrons thereby increasing their effective mass, which could be detected in Shubnikov–de Haas oscillations or cyclotron resonance measurements. With increasing density of excitons, the electronic resonance frequency is expected to shift as a result of a polaronic dressing. In contrast, bound trions would appear as a new resonance in addition to the bare electron resonance and no shift is expected as a function of trion density.

7.7 CONCLUSION AND OUTLOOK

Our work opens up new frontiers in nonequilibrium many-body physics by showing that external electric and magnetic fields could be used to control and manipulate elementary optical excitations such as excitons or polaritons.

In addition to the potential applications in realizing effective gauge fields for photonic excitations that we already highlighted, we envision several extensions of our work that by themselves constitute open theory problems. It would be interesting to analyze the same problem in the case when the polariton density is much larger than the electron density. If similar results hold this would allow the manipulation of electron transport properties using light. Another interesting extension would be to consider a similar setup in magnetic field. While our semiclassical analysis suggests that polaritons should follow the electron motion in magnetic fields, a more rigorous calculation is required to verify this prediction.

8

SUPERCONDUCTIVITY

We investigate the collective phenomena that emerge in a repulsively interacting Bose-Fermi mixture of polaritons and electrons. On the one hand, we show that polaritons can mediate strong attractive interactions between electrons, that could lead to the pairing of electrons in a long-range ordered superconducting state. At the same time, excitations in the electronic system can mediate strong attractive interactions between polaritons, that could lead to the emergence of roton states and eventually to a phase transition towards a supersolid phase. Treating both phenomena simultaneously, we show that the superconducting critical temperature increases in proximity to the supersolid transition.

In previous chapters we investigated how interactions between polaritons and electrons can lead to significant renormalization of the properties of these particles. We focused primarily on the density imbalanced regime that allowed us to simplify the problem by making an analogy to mobile impurity problems.

In this chapter we consider a similar polariton-electron Bose-Fermi mixture, but in contrast to the previous investigations the interspecies interactions are repulsive and we treat the polariton and the electron dressing on similar footing. We show that the interspecies interactions can lead to phase transitions in the electron system (to either superconducting or charge density wave) or in the polariton system (to a supersolid phase). We show that these transitions are intertwined and should be treated simultaneously. Remarkably, the robustness of the superconducting phase is increased in the proximity of the supersolid transition. Because of this we predict that critical temperatures on the order of a few Kelvins can be achieved in heterostructures consisting of transition metal dichalcogenide monolayers that are embedded in an open cavity structure.

The derivations in this chapter are based on the Migdal-Eliashberg theory, that was initially developed in the context of electron-phonon superconductivity, and allows a solution to the superconducting problem that treats retardation effects more properly than the often used BCS theory. It starts from the Migdal theorem which argues that dressing of electrons with more than one phonon is highly unlikely. This allows a truncation of

the Hilbert space to manageable dimension. To connect it to the theoretical methods developed so far, we remark that this is a conserving approximation, and can be considered as the equivalent of the GW approximation in superconductivity.

The chapter is structured as follows. After introducing the system composed of a bosonic polariton condensate interacting with a 2DES in Section 8.1, we use simple canonical transformations to calculate the attractive interaction between electrons that can be mediated by polaritons in 8.2. We then proceed with a rigorous calculation based on Migdal Eliashberg theory in Sec.8.3. In Section 8.4 we use the theoretical framework developed earlier and analyze the interactions between a polariton condensate and a 2DES self-consistently. We notice that the strong interactions can lead to instabilities both in the condensate and in the 2DES. We investigate quantitatively the instability of the 2DES towards superconductivity [46, 103, 104] while also taking into account the effect of the 2DES on the BEC. We also comment briefly on the instability of the 2DES towards the formation of an unconventional CDW ordered state as a consequence of the renormalized electron-polariton interaction becoming strongly peaked at wavevector q_r . In Section 8.5 we investigate how to reach the strong coupling regime experimentally in order to observe these phase transitions. We find that superconductors with temperatures of a few Kelvins can be obtained in transition metal dichalcogenide (TMD) monolayers. We briefly summarize our results and provide a short description of new physics and applications enabled by our analysis in Section 8.6.

The work presented in this chapter will be closely related to the work in Ref. [45].

8.1 INTRODUCTION

The system that we investigate can be considered an implementation of Ginzburg's proposal for high temperature exciton-mediated superconductors [105]. Although similar physics can be investigated in the monolayer systems introduced in Chapter 2, in this chapter we consider a different system, because this is the system that we initially analyzed in Ref. [45]. It consists of semiconductor heterostructure hosting a 2DES in close proximity to a quantum well (QW) in which excitons can be created by shining a laser resonantly without influencing the 2DES. The whole system is embedded in a cavity formed by a pair of distributed Bragg reflectors (DBRs),

which confine light, leading to the formation of exciton polaritons, as illustrated in Fig.8.1.

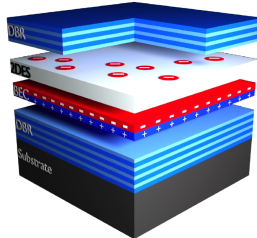


FIGURE 8.1: The schematic of the semiconductor heterostructure that is analyzed.

The pumping laser that induces and sustains the BEC in the lower QW is not shown in the schematic in order not to complicate the figure

Compared to the systems we investigated previously, the excitons and the electrons are separated specially, and some method (DC electric fields, for instance) is used to induce a permanent dipole in the excitons. We choose the direction of the dipole to make the electron-exciton interaction repulsive and therefore avoiding the theoretical complications that arise due to the formation of bound trion states. Furthermore, enhancing the size of the dipole can enhance the strength of electron-exciton interactions.

Before proceeding, we remark that the interactions between a 2DES and an indirect-exciton BEC has been theoretically shown to lead to the formation of an excitonic supersolid [106, 107]. This prior work however, did not take into account the effect of the exciton BEC on the 2DES. Concurrently, the effect of a polariton condensate on a 2DES has been investigated without considering the back-action of electrons on the polaritons and it has been predicted that the 2DES can undergo a superconducting phase transition [46, 103, 104]. The work in this chapter unifies and extends the above mentioned prior work showing that the predicted phase transitions are closely intertwined.

The central finding of our work is that when screening effects are taken into account, the long-range polariton-electron interaction is peaked at a wavevector q_0 that is determined by the distance between the 2DES and the quantum well (QW) hosting the polaritons. Remarkably, increasing the polariton condensate occupancy by increasing the resonant laser intensity leads to a substantial softening of the polariton dispersion at q_r (near q_0). We find that the electron-polariton interaction and conse-

quently the effective electron-electron attractive interaction mediated by polaritons increases significantly due the softening of the polaritons and is strongly peaked at the wavevector q_r . In the strong-coupling regime, characterised by a significant polariton softening, both the polariton BEC and the 2DES are susceptible to phase transitions. As far as we know, this strongly peaked interaction in momentum space at a tunable wavevector is unique to our system and stands in stark contrast to the contact interaction in neutral Bose-Fermi mixtures formed with cold-atoms or the Kohn anomaly in solid-state systems that can result in large interactions at twice the Fermi wavevector.

Leaving a detailed analysis of competition between superconductivity and potential charge density wave (CDW) state associated with polariton mode softening as an open problem, we focus primarily on the superconducting phase transition.

The system that we investigate can be described by the Hamiltonian:

$$\begin{aligned} H = & \sum_{\mathbf{k}} \xi_{\mathbf{k}} e_{\mathbf{k}}^{\dagger} e_{\mathbf{k}} + \sum_{\mathbf{k}} \Omega_{\mathbf{k}} a_{\mathbf{k}}^{\dagger} a_{\mathbf{k}} + \frac{1}{2\mathcal{A}} \sum_{\mathbf{kk}'\mathbf{q}} V_{\mathbf{q}} e_{\mathbf{k}+\mathbf{q}}^{\dagger} e_{\mathbf{k}'-\mathbf{q}}^{\dagger} e_{\mathbf{k}} e_{\mathbf{k}} \\ & + \frac{1}{2\mathcal{A}} \sum_{\mathbf{kk}'\mathbf{q}} u_{\mathbf{kk}'\mathbf{q}} a_{\mathbf{k}+\mathbf{q}}^{\dagger} a_{\mathbf{k}'-\mathbf{q}}^{\dagger} a_{\mathbf{k}} a_{\mathbf{k}} + \frac{1}{2\mathcal{A}} \sum_{\mathbf{kk}'\mathbf{q}} v_{\mathbf{kq}} a_{\mathbf{k}+\mathbf{q}}^{\dagger} e_{\mathbf{k}'-\mathbf{q}}^{\dagger} e_{\mathbf{k}'} a_{\mathbf{k}} \end{aligned} \quad (8.1)$$

where we used the creation operators a to denote lower polaritons and suppressed the subscript l for clarity, whose dispersion we discussed in Sec.2.3. For the electron/polariton dispersions we use parameters characteristic to GaAs heterostructures with $m_e = 0.063m_0$, $m_h = 0.046m_0$ and the light matter coupling $g = 2\text{meV}$.

Notice that we focus exclusively on excitations within the lower polariton branch (which we will pump resonantly), since the upper polaritons can be unstable against relaxation into lower energy polariton states. For clarity we will also drop the l index, i.e. we will use the notation $\Omega_{\mathbf{k}} \equiv \Omega_{lk}$. Unless otherwise stated, for the rest of the paper we will assume that the exciton transition is resonant to cavity photon energy (*i.e.* $\omega_0 = \nu_0$, where $\omega_{\mathbf{k}}$ and $\nu_{\mathbf{k}}$ are the underlying exciton and cavity photon dispersions).

The electron-electron interaction in these heterostructures is a (statically) screened Coulomb interaction $V_{\mathbf{q}} = \frac{2\pi}{4\pi\epsilon|\mathbf{q}|}$. Assuming contact interactions of strength u between excitons the polariton-polariton interaction is given by:

$$u_{\mathbf{kk}'\mathbf{q}} = \alpha_{\mathbf{k}} \alpha_{\mathbf{k}'} \alpha_{\mathbf{k}+\mathbf{q}} \alpha_{\mathbf{k}'-\mathbf{q}} u \quad (8.2)$$

As expected, this interaction is proportional to the exciton fraction $\alpha_{\mathbf{k}}$ of the polaritons involved. Since it is potentially tunable through the use of Feshbach resonances [27, 28], we will treat u as a freely tunable parameter.

The exciton-electron interaction, whose form is at the basis of the following discussion requires slightly more justification. This interaction is increased through inducing a permanent dipole in the neutral excitons. This can be achieved in various ways depending on the choice of the material. For example, one can use an electric field perpendicular to the exciton plane to polarise the excitons, however, this will result in small dipoles. A better approach is to use two tunnel-coupled QWs and bias the energy bands in such a way that holes can live only in the first QW, while electrons can freely tunnel between the QWs. This leads to a new type of polariton which has both a large dipole (from the indirect exciton part) and a large light matter coupling (from the direct exciton part). In this way polaritons with dipoles of lengths comparable to the exciton Bohr radius, known as dipolaritons, can be produced [108].

Regardless of the mechanism, in the approximation of infinitely thin QWs, one can obtain an analytical expression for the electron-polariton interaction v as shown in Ref. [46]. We will use this analytical expression in numerical simulations but below we show how to obtain an approximate but simpler expression. First, v is electrostatic in origin and it will be proportional to $V_{\mathbf{q}}$. Since the interaction is due to the partially excitonic nature of polaritons it will be proportional to the exciton fraction of the polaritons involved. Finally, v should be proportional to the exciton dipole length d . We expect that polaritons will not be able to respond to momentum transfers larger than $1/a_B$ (a_B denotes the exciton Bohr radius), $1/d$ and $1/L$, where L denotes the distance between the 2DES and the position of the centre of mass of the polaritons in the direction orthogonal to the 2D planes. In the limit of $d, a_B \leq L$ the $1/L$ cutoff dominates and v takes the following approximate form: ¹:

$$v_{\mathbf{k}\mathbf{q}} \approx \alpha_{\mathbf{k}} \alpha_{\mathbf{k}+\mathbf{q}} V_{\mathbf{q}} |\mathbf{q}| d e^{-|\mathbf{q}|L} \quad (8.3)$$

8.2 ELECTRON-ELECTRON INTERACTIONS MEDIATED BY POLARITONS

Before discussing the rigorous Migdal Eliashberg theory, we first show how polaritons can mediate electron-electron attractive interactions. We do

¹ We mention that this expression has been obtained by assuming that the in-plane exciton wavefunction is not modified by the induced dipole. A better exciton wavefunction is the one used in Ref. [109], unfortunately, this expression is no longer analytical.

this using much simpler canonical transformations that are only justified a posteriori by the calculation in Sec.8.3.

8.2.1 Bogolyubov transformation

By pumping the lower polariton branch with a resonant laser field we can sustain a polariton BEC at $k = 0$. Neglecting the driven-dissipative nature of the condensate (which only affects small momenta around $\mathbf{k} = 0$) we follow the Bogolyubov prescription and set $a_0 = a_0^\dagger = \sqrt{N_0}$. We denote by N_0 (n_0) the number (density) of polaritons in the BEC. We then make the Bogolyubov approximation and ignoring terms of lower order in N_0 .

Following the procedure in Sec.3.4.1 we obtain the Hamiltonian:

$$\begin{aligned} H = & \sum_{\mathbf{k}} \xi_{\mathbf{k}} e_{\mathbf{k}}^\dagger e_{\mathbf{k}} + \sum_{\mathbf{k} \neq 0} \Omega_{\mathbf{k}} a_{\mathbf{k}}^\dagger a_{\mathbf{k}} + \frac{1}{2\mathcal{A}} \sum_{\mathbf{k}\mathbf{k}'\mathbf{q}} V_{\mathbf{q}} e_{\mathbf{k}+\mathbf{q}}^\dagger e_{\mathbf{k}'-\mathbf{q}}^\dagger e_{\mathbf{k}} e_{\mathbf{k}'} \\ & + \sum_{\mathbf{k} \neq 0} \frac{n_0 u_{\mathbf{k}}}{2} \left(a_{\mathbf{k}}^\dagger a_{-\mathbf{k}}^\dagger + a_{\mathbf{k}} a_{-\mathbf{k}} + 2a_{\mathbf{k}}^\dagger a_{\mathbf{k}} \right) + n_0 u_0 \sum_{\mathbf{k} \neq 0} b_{\mathbf{k}}^\dagger b_{\mathbf{k}} \\ & + \sum_{\mathbf{k}\mathbf{k}'\mathbf{q}} \sqrt{\frac{n_0}{\mathcal{A}}} v_{\mathbf{q}} e_{\mathbf{k}'+\mathbf{q}}^\dagger e_{\mathbf{k}'} \left(a_{\mathbf{q}}^\dagger - a_{\mathbf{q}} \right) \end{aligned} \quad (8.4)$$

where we also neglected a constant energy shift, and introduced $u_{\mathbf{k}} = u_{0,0,\mathbf{k}}$ and $v_{\mathbf{k}} = v_{0,\mathbf{q}}$.

Given the formal correspondence between the electron-phonon and electron-polariton interaction Hamiltonians, we apply the well-known Migdal-Eliashberg theory [110, 111] developed for the electron-phonon Hamiltonian to analyze the electron-polariton interaction. This theory was developed by Eliashberg starting from Migdal's theorem, which is the equivalent of the Born-Oppenheimer approximation in Green's function language. We find that our system also satisfies Migdal's theorem, which justifies the use of Migdal-Eliashberg theory.

8.2.2 Polariton softening

One of the important results of our theoretical analysis revolve around the substantial softening of the polariton dispersion at a wavevector q_r and the appearance of a roton-like minimum at this wavevector (see upper panel of Figure 8.2). The softening of the phonon modes is accompanied by the squeezing of polaritons from the condensate, leading to Bose-enhancement effects when new excitations are created. The electron-electron attractive

interaction mediated by polaritons increases significantly due to this softening which can lead to phase transitions in either systems.

To facilitate the understanding of this effect, we present a more simple derivation of polariton mediated electron interactions based on canonical transformations, before embarking in rigorous diagrammatic calculations. To get sensible results it is also important to include screening effects due to electron-electron interactions, which reduce the exciton-electron interaction. We will treat electron screening within RPA, which should be valid at large electron densities.

We first wish to investigate the effect of electrons on the polaritons. The effect of electrons on polaritons is to induce an effective attraction between polaritons. Assuming that the interaction is weak enough we can treat it to second order. Intuitively, a polariton of momentum \mathbf{k} creates a potential $v_{\mathbf{k}}$ in the 2DES, and the 2DES responds (to linear order) by creating a charge density $\delta n(\mathbf{k}) = \chi(\mathbf{k})v(\mathbf{k})$ where the proportionality factor $\chi(\mathbf{q})$ is known as the response function of the interacting electron system. This charge density will in turn create a potential $v_{\mathbf{k}}$ at the polariton condensate, thus resulting in an attraction $\chi(\mathbf{k})v_{\mathbf{k}}$ between a polariton of momentum \mathbf{k} and a polariton in the condensate at $\mathbf{k} = 0$.

We treat the response of the electron system within RPA, where the response function χ is related to the polarization bubble χ_0 (i.e. the Lindhard function; we will calculate it below) through the relation $\chi(\mathbf{k}) = \chi_0(\mathbf{k})/\epsilon(\mathbf{k})$ where $\epsilon(\mathbf{q}) = 1 - V_{\mathbf{q}}\chi_0(\mathbf{q}) = 1 + k_{TF}/|\mathbf{q}|$ is the static dielectric function of the electron system. The Thomas Fermi wavevector is $k_{TF} = m_e e^2 / 2\pi\epsilon\hbar^2 = 2/a_B$.

This effect leads to a renormalization of exciton-exciton interactions in Eq. (8.4), such that:

$$\tilde{u}_{\mathbf{k}} = u_{\mathbf{k}} + \chi(\mathbf{k})v_{\mathbf{k}}^2 \quad (8.5)$$

Having taken into account the effect of exciton-electron interactions we can diagonalize the (quadratic) exciton Hamiltonian. Following the derivation in Sec.3.4.1, we can perform the Bogolyubov canonical transformation by introducing the bogolon operators:

$$b_{\mathbf{k}}^\dagger = \chi_{\mathbf{k}} a_{\mathbf{k}}^\dagger + \theta_{\mathbf{k}} a_{-\mathbf{k}} \quad (8.6)$$

Changing the basis to the new bogolon modes (see Sec.3.4.1) the Hamiltonian becomes:

$$\begin{aligned} H = & \sum_{\mathbf{k}} \xi_{\mathbf{k}} e_{\mathbf{k}}^{\dagger} e_{\mathbf{k}} + \sum_{\mathbf{k} \neq 0} \tilde{\Omega}_{\mathbf{k}} b_{\mathbf{k}}^{\dagger} b_{\mathbf{k}} + \frac{1}{2\mathcal{A}} \sum_{\mathbf{k}\mathbf{k}'\mathbf{q}} V_{\mathbf{q}} e_{\mathbf{k}+\mathbf{q}}^{\dagger} e_{\mathbf{k}'-\mathbf{q}}^{\dagger} e_{\mathbf{k}} e_{\mathbf{k}} \\ & + \sum_{\mathbf{k}\mathbf{k}'\mathbf{q}} \sqrt{\frac{n_0}{\mathcal{A}}} \tilde{v}_{\mathbf{q}} e_{\mathbf{k}'+\mathbf{q}}^{\dagger} e_{\mathbf{k}'} \left(b_{\mathbf{q}}^{\dagger} - b_{\mathbf{q}} \right) \end{aligned} \quad (8.7)$$

where we introduced the renormalized bogolon dispersion and the renormalized interaction with the electron system:

$$\tilde{\Omega}_{\mathbf{k}} = \sqrt{\Omega_{\mathbf{k}} (\Omega_{\mathbf{k}} + 2n_0 \tilde{u}_{\mathbf{k}})} \quad (8.8)$$

$$\tilde{v}_{\mathbf{q}} = v_{\mathbf{q}} \sqrt{\frac{\Omega_{\mathbf{q}}}{\tilde{\Omega}_{\mathbf{q}}}} \quad (8.9)$$

We remark that the form of the renormalized electron-polariton interaction is valid only for attractive exciton-exciton interactions $\tilde{u}_{\mathbf{q}} < 0$. We also caution that in writing down the above effective Hamiltonian, the effect of electrons on excitons has already been taken into account, so one should exercise caution to neglect this effect from now on, in order to avoid double counting.

To keep the derivation self-contained we remark that the Hamiltonian above was obtained by choosing the parameters:

$$\chi_{\mathbf{k}}, \theta_{\mathbf{k}} = \pm \sqrt{\frac{1}{2} \sqrt{\frac{\Omega_{\mathbf{k}} + n_0 \tilde{u}_{\mathbf{k}}}{E_{\mathbf{k}}} \pm 1}}, \quad (8.10)$$

We will find it useful to introduce the quantity:

$$M_{\mathbf{q}} = \sqrt{n_0 / A} \frac{u_{\mathbf{q}}}{\epsilon(\mathbf{k})} \quad (8.11)$$

with a similar relationship for the renormalized quantity \tilde{M} .

We present the renormalized dispersion in Fig.8.2. Remarkably, as the electron-polariton interaction increases the polaritons tend to soften due to interactions with the electrons.

The underlying reason for the softening can be traced to the screening by the mobile carriers of the electron system. This screening ensures that the screened exciton-electron interaction peaks (weakly) at some wavevector q_0 . The bare electron-polariton interaction has an exponential cutoff in

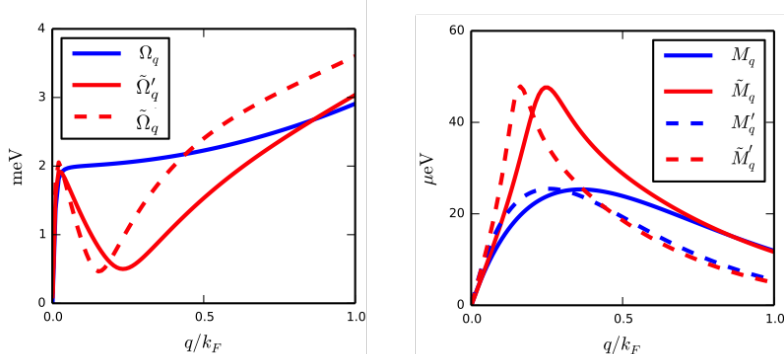


FIGURE 8.2: Left panel: bare polariton dispersion (blue) versus renormalised polariton dispersion (red). Right panel: screened electron-polariton matrix element $M_{\mathbf{q}} = \sqrt{N_0 u_{\mathbf{q}} / \epsilon(\mathbf{q})}$ (blue) versus screened and renormalised electron-polariton matrix element $\tilde{M}_{\mathbf{q}}$ (red). The parameters used for the solid lines are typical GaAs parameters: $d = a_B = 10\text{nm}$, $L = 20\text{nm}$, $g_0 = 2\text{meV}$, $\epsilon = 13\epsilon_0$, $m_e = 0.063m_0$, $m_h = 0.046m_0$, $n_e = 2 \times 10^{11}\text{cm}^{-2}$, $u = 0.209\mu\text{eV}\mu\text{m}^2$, $n_0 = 4 \times 10^{11}\text{cm}^{-2}$. The parameters used for the dashed lines are the same as for the solid lines except for $L' = 1.5L$ and $n'_0 = 2n_0$.

momentum space due to the distance L between the polariton and electron planes. At the same time, $v_{q \rightarrow 0} \rightarrow \text{constant}$. When screening is taken into account (the right panel of Figure 8.2) we have to renormalize v as $\tilde{v}_{\mathbf{q}} \rightarrow \tilde{v}_{\mathbf{q}}/\epsilon(\mathbf{q})$ where $\epsilon(\mathbf{q}) = 1 + 2/a_B|\mathbf{q}|$. As one can easily observe, the effect of screening is to cut off the contribution of small wavevectors such that $\tilde{v}_{\mathbf{q} \rightarrow 0} \rightarrow 0$. This small momentum cutoff together with the large momentum cutoff mentioned above leads to a maximum in the interaction in momentum space at the wavevector

$$q_0 = \frac{1}{a_B} \left[\sqrt{1 + \frac{2a_B}{L}} - 1 \right], \quad (8.12)$$

as shown in the right panel of Figure 8.2 in blue solid line. The broad maximum in the interaction becomes very strongly peaked as the polaritons soften and the electron-polariton interaction approaches the strong coupling regime.

The position of q_0 depends only on the electron Bohr radius a_B and the distance between the BEC and the 2DES. As a consequence, q_0 can be tuned by changing the distance L between the BEC and the 2DES. We show the

tunability of this interaction by changing the distance L in the right panel of Figure 8.2 in dashed blue line. Alternatively, one can tune the relative position of q_0 with respect to the Fermi wavevector k_F by changing the 2DES Fermi energy. This latter method can provide real-time control of q_0/k_F .

Coming back to the renormalized polariton dispersion presented in the left panel of Figure 8.2 we want to determine the position of the roton minimum q_r . This can be obtained by maximizing the induced attraction (since the momentum dependence of the bare interaction u is negligible by comparison). Doing this we determine the roton minimum:

$$q_r \approx \frac{1}{a_B} \left[\sqrt{1 + \frac{a_B}{L}} - 1 \right] \quad (8.13)$$

Note the slight difference between q_r and q_0 which stems from the fact that the exponential cutoff is twice as effective for a second order interaction. This softening has been investigated theoretically for excitons in the context of supersolidity [106, 107].

Notice that, whenever the modes soften, the resulting exciton-electron interaction \tilde{v}_q increases by a factor of $\sqrt{\Omega_q/E_q} = \chi_q - \theta_q$, as we show Fig.6.3. This is due to the squeezing of polaritons from the condensate into pairs \mathbf{k} and $-\mathbf{k}$. Indeed we showed in Sec.3.4.1 that the ground state of the polariton system is $|\Theta\rangle = e^{\sqrt{N_0}a_{\mathbf{k}}^\dagger - \theta_{\mathbf{k}}/\chi_{\mathbf{k}}} |0\rangle$. Therefore, the amplitude for creating an excitation of momentum \mathbf{k} is increased due to Bose-enhancement factor $\langle \Theta | b_{\mathbf{k}} a_{\mathbf{k}}^\dagger | \Theta \rangle$. Therefore, we can increase interactions by increasing the condensate depletion. However, one must always make sure that the condensate depletion remains small compared to the number of polaritons in the condensate to ensure that Bogolyubov's approximation remain valid. The peak of the renormalized matrix element will be between q_0 and q_r depending on the strength of this renormalisation factor.

We remark that it is not necessary to rely on interactions with electrons to squeeze polaritons out of the condensate. Instead, similar enhancement could in principle be obtained by directly pumping pairs of excitons of momenta \mathbf{k} and $-\mathbf{k}$ using squeezed light [112], which could lead to even stronger enhancement of interactions.

8.2.3 Electron-electron interaction

To calculate the electron-electron interaction mediated by polaritons, we want to trace out the bogolon excitations from the above Hamiltonian. We

can achieve this by performing a Schrieffer-Wolff transformation and keeping only second order terms. There are different Schrieffer-Wolff transformations that can be done as we explain in Appendix A.8. However, the situation is simplified if we consider scattering only on the Fermi surface. Because this is an energy conserving process it could be measured experimentally and therefore in this case all the different transformations must yield the same second order result. Performing this transformation (see App A.8 for details) the electron-electron Coulomb interactions are renormalized to:

$$V_{\mathbf{q}}^{\text{eff}} = V_{\mathbf{q}} - N_0 \frac{2(\tilde{v}_{\mathbf{q}})^2}{\tilde{\Omega}_{\mathbf{q}}} \quad (8.14)$$

We want to determine whether the induced attraction can win over Coulomb repulsion and lead to pairing of electrons in Cooper pairs. To understand the pairing mechanism we want to roughly reduce the problem to the problem of two interacting electrons, i.e. find the residual interactions between the low-energy degrees of freedom or quasiparticles. This is of course very difficult to do, but we assume that the effect of the other electrons is simply to screen (and strongly reduce) the interaction of two electrons, and we treat this screening process within RPA. The dynamically screened interaction renormalizes the electron-electron interaction to:

$$V_{\mathbf{q}}^{\text{eff}} \rightarrow \frac{V_{\mathbf{q}}^{\text{eff}}}{1 - V_{\mathbf{q}}\chi(\mathbf{q})} = \frac{V_{\mathbf{q}}}{\epsilon(\mathbf{q})} - \left(\frac{\tilde{v}_{\mathbf{q}}}{\epsilon(\mathbf{q})} \right)^2 \frac{2N_0}{\tilde{\Omega}_{\mathbf{q}}} \quad (8.15)$$

where we introduced the (RPA) response function and dielectric function that we introduced before.

The first term in the LHS of the above is the screened Coulomb repulsion while the second term is the effective attraction mediated by exchanging polaritons.

Since it might be useful to have an idea of the shape of the interaction in real space, we look at the Fourier transform of the total interaction compared to the screened Coulomb interaction for some typical TMD monolayer parameters in Figure 8.3. Notice the oscillatory behaviour of the interaction at the wavelength $2\pi/q_r$ that appears due to the softening of the polaritons. In comparison to the long range attractive interaction, the screened Coulomb interaction looks like a contact interaction. This means that the attractive interaction would favour the pairing of electrons in higher angular momentum states such as p-states, where the electrons can avoid the strong Coulomb repulsion.

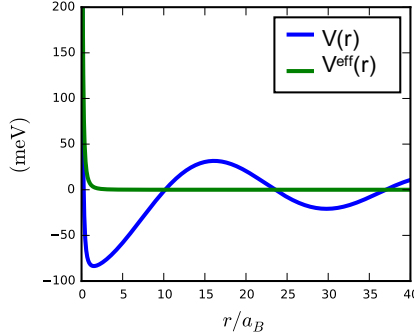


FIGURE 8.3: The total interaction (blue) compared to the screened Coulomb repulsion (green) for the parameters used in Figure 8.4 with $n_0 = n_e$.

8.3 RENORMALIZED HAMILTONIAN

We can gather all the results from the previous analysis and write down a renormalised Hamiltonian for the new quasi-particles:

$$H = \sum_{\mathbf{k}} \tilde{\xi}_{\mathbf{k}} \tilde{e}_{\mathbf{k}}^\dagger \tilde{e}_{\mathbf{k}} + \sum_{\mathbf{k}} \omega_{\mathbf{k}} \tilde{b}_{\mathbf{k}}^\dagger \tilde{b}_{\mathbf{k}} \quad (8.16)$$

$$+ \frac{1}{2} \sum_{\mathbf{k} \mathbf{k}' \mathbf{q}} \frac{V_{\mathbf{q}}}{\epsilon(\mathbf{q})} \tilde{e}_{\mathbf{k}}^\dagger \tilde{e}_{\mathbf{k}'}^\dagger \tilde{e}_{\mathbf{k}+\mathbf{q}} \tilde{e}_{\mathbf{k}'-\mathbf{q}}, + \sum_{\mathbf{k} \mathbf{q}} \tilde{M}_{\mathbf{q}} \tilde{e}_{\mathbf{k}}^\dagger \tilde{e}_{\mathbf{k}-\mathbf{q}} (\tilde{b}_{\mathbf{q}}^\dagger + \tilde{b}_{-\mathbf{q}}),$$

where we denoted the new quasi-particles and quasi-particle interactions with a tilde. In the above $\tilde{\xi}_{\mathbf{k}} = \hbar^2 \mathbf{k}^2 / (2m_e^*)$. We remark that the effect of polaritons on the electron dispersion is to increase the electron mass from m_e to m_e^* as shown in Eq. (A.120). We caution that in using the above Hamiltonian in perturbative calculations one should be careful to avoid double counting since electron-hole bubble diagrams have already been taken into account.

When using the diagrammatic techniques, we make two important approximations. The first approximation is to ignore the finite linewidth of the polariton and electron spectral functions, due to many-body interactions. We investigate the validity of this approximation below. The second and arguably the most important approximation that we make is to choose which diagrams to discard and which diagrams to sum over. Our choice was motivated by the Migdal-Eliashberg theory.

In order to investigate the validity of these approximations, we first introduce the Eliashberg function and the electron-polariton coupling (EPC) constant. In analogy to the Migdal-Eliashberg theory for phonons the electron-polariton interaction can be characterised by the EPC constant λ :

$$\lambda = 2 \int_0^\infty \frac{d\omega}{\omega} \alpha^2 F(\omega), \quad (8.17)$$

where we introduced the commonly used Eliashberg function $\alpha^2 F(\omega)$, the only quantity we need to know in order to assess the effect of the polaritons on the electrons [110]. The Eliashberg function is related to the scattering probability of an electron on the Fermi surface through a virtual polariton of frequency ω :

$$\alpha^2 F(\omega) = \sum_{\mathbf{k}, \mathbf{k}'} |\tilde{M}_{\mathbf{k}-\mathbf{k}'}|^2 \delta(\omega - \tilde{\Omega}_{\mathbf{k}-\mathbf{k}'}) \delta(\xi_{\mathbf{k}}) \delta(\xi_{\mathbf{k}'}) / N(0), \quad (8.18)$$

where $N(0)$ is the electron density of states at the Fermi surface.

The EPC constant quantifies the strength of the electron-polariton coupling and the strong coupling regime is characterised by large values of this parameter. Many properties of the interacting electron-polariton system depend on this constant (for example the electron mass gets renormalised such that $m_e^* = m_e(1 + \lambda)$).

8.3.1 Quasi particle approximation

In the strong coupling regime one has to check whether the quasi-particle description remains valid for electrons, i.e. whether the quasi-particle linewidth is much smaller than the quasi-particle energy.

At zero temperature, according to Eq. (A.121), the electron quasi particle linewidth Γ at energy ω above the Fermi surface is given by:

$$\Gamma(\omega) = \pi \int_0^\omega d\omega' \alpha^2 F(\omega'). \quad (8.19)$$

Generically, as long as the polariton energy scale is much larger than the superconducting gap, the electrons forming the Cooper pairs will be good quasi-particles since they will interact only virtually with polaritons. While this is guaranteed to the extent that polaritons themselves are good quasi-particles, in the limit of substantial polariton softening we need to

ensure that $\Gamma(k_B T_c) \ll k_B T_c$, where T_c is the critical temperature of the superconductor.

If we neglect cavity losses, the polariton excitations can decay only by creating electron-hole pairs. Even if the polariton excitations in the strong-coupling regime are not well-defined excitations, our investigation of the transitions of the 2DES are not affected as long as the electrons close to the Fermi surface remain good quasiparticles. The finite polariton excitations' linewidth can be incorporated in our calculations by changing the Eliashberg function. We comment on this in Appendix A.7 and show that this in fact does not influence our results and that the electron quasi-particle picture remains valid since $\Gamma(\omega) \propto \omega^2$ for small frequencies.

In addition to the above there are, of course, intrinsic decoherence mechanisms that appear due to interactions that are neglected when writing down the initial Hamiltonian in Eq. (8.4). The most important decoherence mechanism is the scattering by impurities in the system. Impurities will lead to a broadening of the polariton dispersion due to localisation effects. This will limit how much the polaritons can soften. Since impurity induced broadening is typically Gaussian, it can be neglected provided that the polariton energy exceeds the corresponding linewidth. Since the electrons are in a high mobility 2DES we do not expect any disorder/localization effects to significantly affect them.

8.3.2 *A Debye energy for polaritons?*

In normal metals there is a frequency cutoff for phonons which is much lower than the Fermi energy. This energy scale separation is crucial for theoretical investigations, because it allows one to make an adiabatic approximation in which electrons instantaneously follow the lattice motion. In our system there is no energy cutoff; however, not all polaritons interact as strongly with electrons. The polaritons that couple most strongly to electrons have energies bounded roughly by ω_D , in analogy to the Debye frequency in the case of phonons. We consider this to be the relevant energy scale of the polaritons.

As mentioned above, the separation of electron and polariton energy scales allows one to make a Born-Oppenheimer approximation (known as Migdal's theorem in diagrammatic language) and obtain a perturbative expansion in the small parameter $\hbar\omega_D/\epsilon_F$. In some materials (as in GaAs) this condition is already satisfied, without including renormalisation effects, due to the different electron/exciton masses. However, in other mate-

rials, the electron/exciton masses are comparable (as in TMD monolayers). In these materials renormalization effects are crucial in creating a small Debye frequency and allowing the use of Migdal's theorem for a theoretical investigation of the system.

We notice that the polaritons at the roton minimum will interact most strongly with the electrons, as shown in Figure 8.2. Furthermore, as we will see in the next section, the effective electron-electron attraction between the electrons on the Fermi surface is inversely proportional to the frequency of the polaritons mediating the interaction, which is what one would also expect from a second order perturbation theory. Therefore, we expect the typical energy scale of the polaritons that dominate the contributions to attractive electron-electron interactions, to be of the order of the polariton energy at the roton minimum. Quantitatively, we define the following Debye frequency:

$$\omega_D = 2 \int_0^\infty d\omega \alpha^2 F(\omega) / \lambda. \quad (8.20)$$

Notice that for weak coupling the Debye frequency ω_D will be of the order of the light matter coupling g_0/\hbar .

8.4 SUPERCONDUCTIVITY AND CHARGE DENSITY WAVES

In the previous section we developed the theoretical framework needed to understand a system of fermions interacting with a bosonic condensate. The theory is general within the framework of the Migdal's theorem and up to the assumption that density-density interactions depend only on the momentum transfer.

In this section, we restrict our analysis to the system introduced in Section 8.1: a 2DES interacting with a polariton BEC. We are interested in the phase transitions that are possible in this system. We find that the polariton BEC can undergo a phase transition into a supersolid, a superfluid with a spatially ordered structure similar to a crystal. At the same time, there are two closely intertwined instabilities in the 2DES: one towards a CDW phase and the other towards a superconducting phase. All of these transitions are possible due to the softening of the polaritons. We notice the similarity to strongly correlated electron systems such as high temperature superconductors which exhibit a quantum critical point.

In Section 8.4.1 we investigate quantitatively the superconducting transition in the 2DES. This transition has been previously investigated [46, 103,

[104] without taking into account either the screening effects due to the 2DES or the polariton softening, which we find to be crucial for reaching the strong coupling regime. Moreover, we show in Appendix A.8 that the Fröhlich [113] type potential is not suitable for a reliable calculation of the critical temperature.

In the next subsection we investigate qualitatively the possibility of an unconventional CDW in the 2DES due to the proximity of the BEC to a supersolid phase transition.

8.4.1 *Superconductivity*

As mentioned above, as we reach the strong coupling regime the 2DES can become superconducting. Contrary to previous assertions [46, 103, 104] we find that polariton mediated superconductivity is not possible in the presence of electronic screening without taking into account the softening of the polaritons. As the polaritons soften and the polariton BEC approaches the supersolid transition, the electron-polariton interaction greatly increases and the system enters the strong coupling regime. Since materials with lower dielectric constants are more suitable for reaching the strong coupling regime (as we will show in Section 8.5), in this section we choose to look at TMD monolayers.

In the 2D polariton-electron system that we consider, the biggest uncertainty originates from the polariton-polariton repulsion. We note however that the strength of this interaction can be tuned so as to reach a parameter range where our analysis is justified. The other unknown is the broadening of the polariton dispersion around q_r due to the impurities in the system, which in turn determines the lowest possible energy scale of polaritons at the roton minimum. However, we found out that the polaritons at q_r , which contribute most to superconductivity, have an effective mass that is roughly 2 orders of magnitude lighter than the bare exciton mass (for the parameters used in Figure 8.4 and $n_0 = n_e$). As a consequence, polaritons at the roton minimum are relatively robust against broadening by static disorder.

The quantity that we are most interested in here is the critical temperature of the superconductor. In App.A.8 we provide a short review on how to correctly calculate the critical temperature of a superconductor, and argue that one should use the modified McMillan formula [114, 115]:

$$\begin{aligned} k_B T_c &= \frac{f_1 f_2 \omega_{log}}{1.2} \exp \left[-\frac{1.04(1+\lambda)}{\lambda(1-0.62\mu^*) - \mu^*} \right], \\ \mu^* &= \frac{\mu}{1 + \mu \ln(\epsilon_F/\hbar\omega_D)}. \end{aligned} \quad (8.21)$$

This formula is only meaningful if the exponent is negative, and is roughly valid for $\lambda < 10$. In the above $\omega_{log} = \exp [\langle \ln(\omega) \rangle]$, (the average is taken with respect to the weight function $\alpha^2(\omega)F(\omega)/\omega$). The screened Coulomb repulsion μ between electrons averaged over the Fermi surface, is given by:

$$\mu = \sum_{\mathbf{k}, \mathbf{k}'} \frac{V_{\mathbf{k}-\mathbf{k}'}}{\epsilon(\mathbf{k}-\mathbf{k}')} \delta(\xi_{\mathbf{k}}) \delta(\xi'_{\mathbf{k}'}) / N(0). \quad (8.22)$$

The correction factors f_1, f_2 are given in Appendix A.8.

In order to calculate the critical temperature we need to know the strength of the exciton-exciton interaction $u_{\mathbf{q}}$. Given that the exciton-exciton interaction is generally repulsive it has the effect of pushing up the polariton dispersion, stiffening the polaritons. In contrast, the electrons mediate an attractive interaction between polaritons leading to softening. The momentum dependence of the polariton-polariton interaction around q_r has not been investigated, since experiments have been limited to small momentum values of the order of the photon momentum. Theoretical calculations [24–26] seem to suggest that in our system the exciton-exciton interaction at large momenta $q \approx 1/a_B$ is about an order of magnitude smaller than the interaction at $q = 0$ and might even be attractive.

Fortunately, since we have a highly tunable system, the highest critical temperatures that we can obtain do not depend strongly on either the strength or the q-space dependence of $u_{\mathbf{q}}$, as long as the polaritons can soften at some momentum q (i.e. there is a q such that $u_{\mathbf{q}} + \chi(\mathbf{q})v_{\mathbf{q}}^2 < 0$). Therefore, given the uncertainty, we choose $u = 0.12\mu\text{eV}\mu\text{m}^2$ for our numerical simulations but emphasize that similar results can be obtained by tuning other parameters as long as $u < 0.5\mu\text{eV}\mu\text{m}^2$. Furthermore, we reemphasize that tuning the polariton-polariton interaction using Feshbach resonances has been proposed and demonstrated [27, 28].

In the upper-left panel of Figure 8.4 we plot in solid purple the critical temperatures that can be achieved in a typical TMD monolayer by tuning the polariton density n_0 in a system with 4 exciton layers (which have the effect of doubling g_0 compared to the initial value). According to our mean-field calculation in the blue region the 2DES should become superconducting whereas we cannot apply our theory in the green region due to

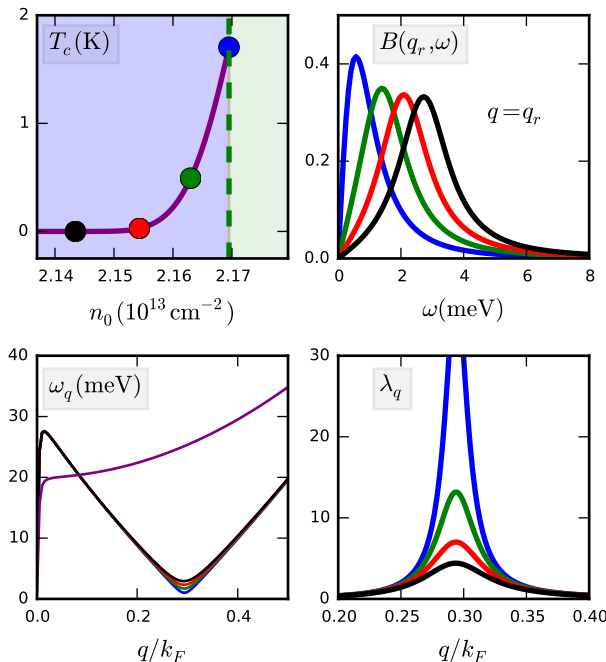


FIGURE 8.4: Upper-left panel: critical temperature (solid purple line) for a typical TMD monolayer as a function of polariton density n_0 . The dashed green line is at the critical polariton density $n_e = 2.169 \times 10^{13} \text{ cm}^{-2}$ and can be regarded as dividing the BEC (blue region) and super-solid (green region) phases of the polaritons. Upper-right panel: The polariton spectral function at the roton-minimum $B(q_r, \omega)$. Lower-left panel: polariton dispersion renormalization (in purple is the bare dispersion). Lower-right panel: λ_q . The different colors of the lines in the upper-right, lower-left and lower-right panels correspond to different values of n_0 denoted by the colored dots in the upper-left panel. Expressed in percentages of n_e these are: $n_0 = 100\%n_e$ (blue), $n_0 = 99.7\%n_e$ (green), $n_0 = 99.3\%n_e$ (red), $n_0 = 98.8\%n_e$ (black). The rest of the parameters are typical TMD monolayers parameters: $d = a_B = 1 \text{ nm}$, $L = 1.5a_B = 1.5 \text{ nm}$, $g_0 = 10\sqrt{4} \text{ meV}$ (4 exciton layers are used), $\epsilon = 4\epsilon_0$, $m_e = m_h = 0.2m_0$, $n_e = 10^{13} \text{ cm}^{-2}$, $u = 0.12 \mu\text{eV}\mu\text{m}^2$.

the breakdown of the Bogolyubov approximation. The dashed green line dividing the two regions in the phase diagram is at the critical polariton

density $n_0 = 2.169 \times 10^{13} \text{ cm}^{-2}$. At this point $\lambda \approx 1.5$, the condensate depletion is less than 5% and the roton minimum is approximately at 1 meV.

In the other three panels we investigate the polariton quasi-particles that mediate the electron pairing. Therefore we plot the polariton dispersion (lower-left), the polariton spectral function at $q = q_r$ (upper-right) and $\lambda_{\mathbf{q}}$ (lower-right), which will be defined below. The different colors of the lines in these three panels correspond to different values of n_0 denoted by the colored dots in the upper-left panel Figure 8.4. The blue line corresponds to the case of highest polariton density ($n_0 = n_e$) while the black line corresponds to the lowest polariton density ($n_0 = 98.8\%n_e$).

The polariton spectral function is defined as:

$$B(\mathbf{q}, \omega) = \frac{1}{\pi} \text{Im}[\bar{D}(\mathbf{q}, \omega)] = \frac{1}{\pi} \text{Im} \left[\frac{2\tilde{\Omega}_{\mathbf{q}}}{\omega^2 - \tilde{\Omega}_{\mathbf{q}}^2 - 2i\gamma_{\mathbf{q}}\tilde{\Omega}_{\mathbf{q}}} \right], \quad (8.23)$$

$$\gamma_{\mathbf{q}} = \frac{\Omega_{\mathbf{q}}}{\tilde{\Omega}_{\mathbf{q}}} |\text{Im}(\Sigma_{12}(\mathbf{q}, \omega))| = 2 \frac{N_0 v_{\mathbf{q}}}{\epsilon^2(\mathbf{q})} \frac{\Omega_{\mathbf{q}}}{\tilde{\Omega}_{\mathbf{q}}} \text{Im} [\chi_0(\mathbf{q}, \tilde{\Omega}_{\mathbf{q}})], \quad (8.24)$$

where $\bar{D}(\mathbf{q}, \omega)$ is the propagator of the polariton quasiparticles and $\gamma_{\mathbf{q}}$, the polariton linewidth, is proportional to the imaginary part of the polariton self-energy Σ_{12} due to interactions with the electrons (see Appendix A.8 for details).

Starting from the definitions of the EPC constant and the Eliashberg function from Eqs. 8.17 and 8.18 we can express the EPC constant as:

$$\lambda = \frac{1}{N(0)\epsilon_F} \sum_{\mathbf{q}} \lambda_{\mathbf{q}}, \quad (8.25)$$

$$\lambda_{\mathbf{q}} = \frac{\epsilon_F}{\pi} \frac{\gamma_{\mathbf{q}}}{\tilde{\Omega}_{\mathbf{q}}^2}. \quad (8.26)$$

$\lambda_{\mathbf{q}}$ simply quantifies the attraction strength between two electrons on the Fermi surface resulting from exchanging a virtual BEC excitation of momentum q .

We see from Figure 8.4 that in order to achieve critical temperatures of a few Kelvins the roton-like minimum needs to be lowered to energies of a few meV. As the polaritons soften, the momentum dependent electron-electron attraction, quantified by $\lambda_{\mathbf{q}}$, develops a strong peak at $q = q_r$. This shows that mainly the soft polaritons are responsible for the superconducting phase transition of the 2DES, because they interact most strongly with

the 2DES, for two reasons. First of all the softening of the polaritons results in a depletion of the condensate which leads to an increase in the electron polariton matrix element proportional to $\sqrt{\Omega_q/\tilde{\Omega}_q}$. Secondly, the electron-electron attraction mediated by the soft polaritons increases even more because these polaritons are closer to resonance with the electronic interactions which are confined to an energy layer of width $k_B T_c \ll \omega_D$ around the Fermi energy. Looking at the spectral function of the quasi-particles at the roton minimum, denoted by $B(q_r, \omega)$, we notice that the polaritons at the roton minimum become overdamped, similar to paramagnons near a magnetic instability. At this point McMillan's formula should still be valid but one should be careful about the broad polariton spectral function. We investigate the effects of the finite linewidth of this spectral function in Appendix A.8 and show that the electrons remain good quasi-particles and that the broad polariton spectral function will not have a significant impact on the superconducting critical temperature.

Another remarkable feature of the electron-electron attraction mediated by polaritons is that it favors p-wave pairing (or other higher symmetries) to s-wave pairing. This is easily understood if we look at the total electron-electron interaction in real space, which we present in Figure 8.3. Notice that this interaction is formed by a strongly repulsive part at the origin followed by a oscillatory part with the wavelength $2\pi/q_r$, due to the strongly peaked interaction in momentum space. Because of this shape of the interaction, the s-wave pair will feel the strongly repulsive interaction at the origin, while the p-wave pair will avoid this region due to the Pauli-exclusion principle. In accordance with this simple picture, we find p-wave critical temperatures a few times higher than the s-wave critical temperature. However, since the electrons in the p-wave pair are not time-reversal partners these pairs will be influenced by the disorder in the system. Therefore, an accurate calculation of the p-wave critical temperatures requires an estimation of the randomness in our system.

Notice the strong dependence of the critical temperature on the polariton density, which indicates that some fine tuning will be necessary in order to observe the superconducting phase. Fortunately, the polariton density is proportional to the intensity of the laser generating the condensate, and the intensity of a laser can be tuned with extreme accuracy. Laser intensities with less than 0.02% noise have been maintained relatively easily in the context of polaritons by using a feedback loop [116]. We also emphasize that we tried to be conservative in our choice of bare system parameters.

It may for example be possible to obtain higher T_c if the polariton density can be increased further without reaching the Mott transition.

8.4.2 Supersolid and Charge Density Waves

As we approach the regime of strong coupling characterized by a significant softening of the polaritons, the system becomes susceptible to other instabilities, in addition to the superconducting instability. When the polaritons soften to the degree that the polariton dispersion touches zero there will be an instability in the polariton BEC. A transition to a supersolid phase occurs in the green region in Figure 8.4 since the polariton dispersion touches zero roughly at $n_0 \approx 2.173 \times 10^{13} \text{ cm}^{-2}$. Even though such a supersolid instability was proposed for indirect excitons [106, 107], we remark that this phase transition can be more easily observed in a polariton BEC not least because the realization of an exciton BEC is still an experimental challenge. In our theoretical framework based on the Bogolyubov approximation, the onset of this instability can be observed as a dramatic increase in the BEC depletion as the polariton dispersion approaches zero. Since our analysis is only valid when the condensate depletion is small from now on we assume that the polariton dispersion never touches zero.

As the polariton system approaches its BEC instability to a supersolid, the 2DES becomes susceptible to instabilities mediated by the soft polaritons. In the previous section we analyzed the susceptibility of the 2DES towards a superconducting phase. However, the strongly peaked electron-electron attraction at $q = q_r$, as shown in the bottom-right panel of Figure 8.4 can result in a CDW state.

A CDW order can also appear due to the phase transition of the BEC into a supersolid. This transition is analogous to the case of ‘frozen phonons’ which has been proposed as an explanation for the CDW order in materials such as TMDs [117–119], where a finite-momentum phonon softening leads to a condensation resulting in a static distortion in the lattice which in turn leads to a modulation in the electron density. In our case this corresponds to the fact that the mean field $\langle b_{qr} \rangle$ becomes important (the momentum direction should be chosen spontaneously), which would require a careful extension of our Bogolyubov approximation scheme.

Remarkably, in contrast to the conventional behavior based on nesting features in the electron band structure, this type of singularity is not originating from the electronic response function but due to a singular behavior in the electron-polariton interaction at some wavevector. In both cases men-

tioned above one can tune the wavevector where the polariton dispersion touches zero and therefore can tune the nesting wavevector q_r .

We reemphasize that in order to observe a superconducting or CDW phase transition in the 2DES, the polaritons have to soften and the BEC has to be close to the super solid phase transition. More generally, despite the differences in structure and phenomenology, the phase diagram of many unconventional superconductors exhibit the common trait that superconductivity resides near the boundary of another symmetry breaking phase. Examples are the superconducting phases appearing at magnetic quantum phase transitions as found in many of the Ce-based heavy fermion compounds such as CeIn_3 [120–123], or in iron pnictides accompanying spin density wave states [124], as well as magnetic, stripe and nematic orders discussed for copper oxides [125]. Another example, similar in some respects to our system, is the TMD family, where charge density wave order competes with superconductivity and this feature has been attributed to a softening of the finite momentum phonon modes [117–119].

8.5 MATERIALS SUITABLE FOR REACHING THE STRONG COUPLING REGIME

In this section we do a systematic analysis of the materials most suitable for reaching the strong coupling regime where the 2DES becomes unstable towards a new phase. We find that materials with low dielectric constants are most suitable and conclude that semiconducting TMD monolayers are good candidates for observing polariton mediated superconductivity.

At a first sight, it may seem that there are many parameters that influence the electron-polariton interaction mediated instabilities that can change from material to material: ϵ , m_e , a_B , d , L , g_0 , k_F . However, these parameters are typically not independent. In fact, we argue that all of these material parameters scale with the dielectric constant ϵ as shown in Table 8.1.

First, we emphasize that the mass dependence in the first row is more complicated and one may even treat m_e as an independent parameter as well. For the dipole dependence d we assumed that, regardless of the mechanism, the induced dipole can be of the order of the Bohr radius but not larger. Similarly, we assumed that the distance L between the 2DES and polariton planes cannot be smaller than the exciton Bohr radius, to avoid tunneling between the two planes. We also assumed that the light-matter

m_e	\propto	ϵ^{-1}
a_B	$\propto \epsilon / m_e$	ϵ^2
d	$\propto a_B$	ϵ^2
L	$\propto a_B$	ϵ^2
g_0	$\propto a_B^{-1}$	ϵ^{-2}
k_F	$\propto L^{-1}$	ϵ^{-2}
n_0	$\propto a_B^{-2}$	ϵ^{-4}

TABLE 8.1: Parameter dependence on the dielectric constant ϵ

coupling is proportional to a_B^{-1} . It turns out that because of the large momentum cutoff due to the finite distance L between the 2DES and polariton planes we get better results with decreasing k_F . However, we cannot lower k_F arbitrarily since we still need RPA to be valid. Finally, in the last row, we assumed that the maximum value of $n_0 a_B^2$ is a material independent constant since it is set by phase space filling [126].

The strong coupling regime can be characterized by a large EPC constant λ and a small Coulomb repulsion constant μ . Therefore we need to investigate the dependence of these parameters on the dielectric constant. Introducing the variable $u \equiv q/2k_F$ and the material independent constants $\bar{L} = 2k_F L \propto \epsilon^0$ and $\bar{k}_{TF} = k_{TF}/(2k_F) \propto \epsilon^0$:

$$\begin{aligned} \lambda(\epsilon) &\propto \epsilon^{-3} \int_0^1 du \frac{e^{-2u\bar{L}}}{\sqrt{1-u^2(1+\bar{k}_{TF}/u)^2}} \cdot \frac{\Omega_{2k_F u}}{\tilde{\Omega}_{2k_F u}^2}, \\ \mu(\epsilon) &= \epsilon^0 \int_0^1 du \frac{1}{\sqrt{1-u^2(1+\bar{k}_{TF}/u)^2}}. \end{aligned} \quad (8.27)$$

Looking at the above expressions it is clear that μ remains roughly constant from material to material which is not unexpected (if we chose m_e as an independent parameter we would then get some variance in μ for different materials). However, since the electron-polariton interaction is retarded the relevant constant μ^* given in Eq. (A.127) indicates that we can decrease the effective electron-electron repulsion by choosing materials with large Fermi energies and small Debye frequency.

We also see that λ depends both on the dielectric constant ϵ and on the bare and renormalized polariton energies. All of these three parameters can be tuned independently to some extent through various methods. We notice that observation of polariton mediated superconductivity requires

materials with smaller dielectric constants, because smaller dielectric constants favor the dipole interaction over the monopole Coulomb repulsion. This explains why $\lambda \propto \epsilon^{-3}$ while $\mu \propto \epsilon^0$.

In addition to a small dielectric constant we want a large bare polariton energy and a small renormalised polariton dispersion. The dielectric constant also sets the value of g_0 which gives the energy scale of the bare polariton energy. It should be emphasized though that the bare polariton energy can also be tuned through other methods. One method is to tune the detuning between excitons and cavity and make the polaritons more excitonic or more photonic. This will also change the electron-polariton coupling, an effect which is not captured in Eq. (8.27). Another method is the use of multiple quantum wells. By using N quantum wells one can increase g_0 by \sqrt{N} while leaving the other parameters unchanged.

Another interesting quantity to investigate is what is the largest renormalization that can be obtained as a function of the dielectric constant. Looking at Eq. (8.8) and setting $u_q = 0$ we see that the largest renormalisation that can be obtained is given by $\Delta\omega = 2N_0\chi(q_r)v_{q_r}^2 \propto \epsilon^{-3}$.

To conclude, we note that under the conditions described in the preceding paragraphs, $\lambda(\epsilon) \propto \epsilon^{-6}$.

8.6 CONCLUSION

In this chapter we investigated a repulsively interacting Bose-Fermi mixture of electrons and polaritons.

We discussed the collective states that can emerge in both the electron system (superconductivity or CDW) and the polariton system (supersolidity). We found that the long-ranged electron-electron interaction resulted in similarly long-ranged electron-polariton and polariton-polariton interactions, strongly peaked at a certain wavevector. This led to a pronounced softening the polariton dispersion, which made the polariton system susceptible to a superconducting transition. Remarkably the polariton mediated electron-electron interactions increased in the proximity of the supersolid transition, increasing the robustness of the superconducting state in the electron system.

Future investigations could extend the work in this chapter by going beyond the second order in the electron-polariton interactions. It would be interesting to also investigate a similar setup but with attractive interactions between the electron and polariton that support a bound state, and

see whether the superconducting critical temperature could be increased in this way.

SUMMARY AND OUTLOOK

We provide a summary of the work in the thesis and provide an outlook to exciting possibilities that open up from our research.

In this thesis we investigated the collective phenomena that appear in hybrid Bose-Fermi mixtures formed of polaritons (or excitons) and electrons. We did this by integrating concepts from quantum optics and condensed matter physics. The outcome has been a combination of purely theoretical advances as well as important explanations of puzzling experimental observations. There are several dimensions along which we can organize the work in this thesis.

From a certain perspective, this thesis dealt with systems where the properties of photons are strongly modified due to the scattering with charged particles. For instance, we showed in Chapter 3 how photons can dress with polarization waves in their environment to form new collective states known as Fermi-polarons, that dominate the optical spectra of doped semiconductor materials. This dressing resulted in a remarkably strong enhancement of photon non-linearities, as we showed in Chapter 4. We also showed how this dressing could make photons respond to (low-frequency) electric and magnetic fields as if they were charged, effectively providing a way to create artificial gauge fields for the neutral photons. At first sight, it might seem odd that photons, the quanta of the electromagnetic field and the mediators of electromagnetic forces could in turn respond to electromagnetic fields and also interact strongly with each other.

Conversely, we also investigated the modification of the properties of charged particles in the presence of a large population of polaritons created by strong optical pumping. We looked at the dressing of electrons in Chapter 3 and their interactions in Chapter 4. Whereas the (photon mediated) Coulomb interactions between particles with charges of the same sign is repulsive, we showed how, in this scheme, it could be modified to become attractive, and we investigated how this can lead to the emergence of long-range ordered states in the electron system in Chapter 8.

From a slightly different point of view, this thesis made important contributions to the theory of the broader field of Bose-Fermi mixtures. One im-

portant aspect that differentiates our system from Bose-Fermi mixtures in ultracold atomic gases is the presence of long-ranged Coulomb interactions between electrons. In Chapter 5 we discuss a wavefunction based approach to take into account the effect of these interactions on the polaron formation. This can also induce long-ranged interactions between the bosons and the fermions as we discuss in Chapter 8, that can lead to the competition between superconductivity and polariton supersolid/CDW phases. We also discussed the effect of the motion of one type of particles on the other type of particles in Chapter 7. Using the Fermi-polaron framework we investigated a new type of zero-temperature Coulomb drag between the two species of particles which can be interpreted as an artificial gauge field created by the moving particles, not unlike moving electrons create magnetic fields.

Our work opens up exciting new possibilities for further study of many-body physics phenomena using light. For instance the role played by the long-ranged electron-electron interactions in the polaron dressing is still unclear. Another important question is whether polarons interactions would increase when these effects are properly taken into account.

Similarly, while we discuss the possibility to have polariton mediated superconductivity in a system of repulsively interacting electrons and polaritons, it would be interesting to further analyze the role that a trion bound state could play in the superconducting transition. In particular, it would be interesting to continue the investigation in Chapter 4 about the interactions of Bose-polarons, to see whether the presence of a bound state can lead to a more robust superconducting phase in the electron system.

Another exciting avenue could be the study of this Bose-Fermi mixture in the limit when polariton and electron densities are comparable. We already discussed some of the phenomena that can be observed as we approach this regime, for the case of repulsive interactions between electrons and polaritons, in Chapter 8. It would be interesting to further analyze the competition between Bose-polaron, Fermi-polaron and trion formation as the electron and polariton densities are becoming comparable.

A

APPENDIX

A.1 EFFECTIVE ATTRACTIVE POLARON PROPAGATOR

In this section we wish to show how, starting from the full Green's function $G_x(p)$ one can introduce an effective (or projected) propagator, that describes the propagation of the low energy excitations (i.e. the attractive polarons). Starting from the general Green's function

$$G_x(p) = \frac{1}{\omega - \omega_{\mathbf{p}} - \Sigma_{\text{int}}(p) + i/2\tau_x \operatorname{sgn}\omega} \quad (\text{A.1})$$

we introduce the dispersion of attractive polarons as the lowest energy pole of the above, i.e.,

$$\zeta_{\mathbf{p}} \equiv \omega_{\mathbf{p}} + \operatorname{Re}\Sigma_{\text{int}}(\mathbf{p}, \zeta_{\mathbf{p}}) \simeq \frac{\mathbf{p}^2}{2m_x^*} - \mu_x^*, \quad (\text{A.2})$$

where we introduced the polaron mass m_x^* and also introduced a new chemical potential μ_x^* , measured from the bottom of the attractive polaron dispersion. The above equation is correct for small momenta $\mathbf{p} \ll k_F$, while for larger momenta it will start to deviate from a quadratic dispersion.

Expanding the self energy $\Sigma(\mathbf{p}, \omega)$ to linear order in ω we can write:

$$\begin{aligned} G_x(p) &\simeq 1 / [\omega - \omega_{\mathbf{p}} - \operatorname{Re}\Sigma_{\text{int}}(\mathbf{p}, \zeta_{\mathbf{p}}) - i\operatorname{Im}\Sigma_{\text{int}}(\mathbf{p}, \zeta_{\mathbf{p}}) + \\ &\quad (\omega - \zeta_{\mathbf{p}}) \partial_{\omega}\Sigma_{\text{int}}(\mathbf{p}, \omega)|_{\omega=\zeta_{\mathbf{p}}} + i/2\tau_x \operatorname{sgn}(\omega)] \\ &= 1 / [\omega - \zeta_{\mathbf{p}} + (\omega - \zeta_{\mathbf{p}}) \partial_{\omega}\Sigma_{\text{int}}(\mathbf{p}, \omega)|_{\omega=\zeta_{\mathbf{p}}} + i/2\tau_x \operatorname{sgn}(\omega) \\ &\quad - i\operatorname{Im}\Sigma_{\text{int}}(\mathbf{p}, \zeta_{\mathbf{p}})] \\ &= \frac{Z_{\mathbf{p}}}{\omega - \zeta_{\mathbf{p}} + iZ_{\mathbf{p}}/2\tau_x \operatorname{sgn}(\omega) - iZ_{\mathbf{p}}\operatorname{Im}\Sigma_{\text{int}}(\mathbf{p}, \zeta_{\mathbf{p}})} \end{aligned} \quad (\text{A.3})$$

where we introduced the renormalization factor $Z_{\mathbf{p}}^{-1} \equiv 1 - \partial_{\omega}\Sigma_{\text{int}}(\mathbf{p}, \omega)|_{\omega=\zeta_{\mathbf{p}}}$. It clear from this definition that in general the renormalization factor $Z_{\mathbf{p}}$ is complex ($|Z_{\mathbf{p}}|$ denotes the quasiparticle weight) since the self energy is complex. However as long as

$$\partial_{\omega}\operatorname{Im}\Sigma_{\text{int}}(\mathbf{p}, \omega)|_{\omega=\zeta_{\mathbf{p}}} \ll \operatorname{Im}\Sigma_{\text{int}}(\mathbf{p}, \zeta_{\mathbf{p}}) \quad (\text{A.4})$$

we can neglect the complex part of $Z_{\mathbf{p}}$. We prove that the above condition is satisfied for small momenta $|\mathbf{p}| \ll k_F$ in App. (A.4) where we explicitly evaluate the imaginary part of the self energy. In this limit we can approximate the quasiparticle weight by a constant:

$$Z_{\mathbf{p}}^{-1} \simeq 1 - \partial_{\omega} \text{Re}\Sigma_{\text{int}}(\mathbf{p}, \omega)|_{\omega=\zeta_{\mathbf{p}}} \simeq 1 - \partial_{\omega} \text{Re}\Sigma_{\text{int}}(\mathbf{p}_F, \omega)|_{\omega=0} \equiv Z^{-1} \quad (\text{A.5})$$

We can also introduce the lifetime of the attractive polaron as:

$$1/2\tau_x^*(\mathbf{p}) = iZ/2\tau_x + iZ|\text{Im}\Sigma_{\text{int}}(\mathbf{p}, \zeta_{\mathbf{p}})| \quad (\text{A.6})$$

where we introduced the absolute value of the imaginary part of the self energy, which changes sign at $\omega = 0$. Using the above we can rewrite the exciton propagator for low momenta as:

$$G_x(p) \simeq \frac{Z}{\omega - \zeta_{\mathbf{p}} + i\tau_x^*(\mathbf{p}) \text{sgn}(\omega)} \equiv Z\bar{G}_x(p) \quad (\text{A.7})$$

which defines the projected operator $\bar{G}_x(p)$.

In the main text we sometimes need to evaluate the partial derivatives of $\Sigma(\mathbf{p})$ on shell,i.e. at $p = (\mathbf{p}, \zeta_{\mathbf{p}})$. From Eq. (A.5) we immediately have:

$$\partial_{\omega} \Sigma_{\text{int}}(\mathbf{p}, \omega)|_{\omega=\zeta_{\mathbf{p}}} \simeq 1 - Z^{-1} \quad (\text{A.8})$$

To evaluate the momentum derivative we derivate Eq. (A.2) to obtain:

$$\begin{aligned} \frac{d\zeta_{\mathbf{p}}}{d\mathbf{p}} &= \frac{\mathbf{p}}{m_x^*} = \frac{d\omega_{\mathbf{p}}}{d\mathbf{p}} + \frac{d(\text{Re}\Sigma_{\text{int}}(\mathbf{p}, \zeta_{\mathbf{p}}))}{d\mathbf{p}} = \frac{\mathbf{p}}{m_x} - \partial_{\mathbf{p}} \text{Re}\Sigma_{\text{int}}(\mathbf{p}, \zeta_{\mathbf{p}}) \\ &\quad + \frac{d\zeta_{\mathbf{p}}}{d\mathbf{p}} \partial_{\omega} \text{Re}\Sigma_{\text{int}}(\mathbf{p}, \omega)|_{\omega=\zeta_{\mathbf{p}}} \end{aligned} \quad (\text{A.9})$$

From the above we immediately obtain:

$$\partial_{\mathbf{p}} \text{Re}\Sigma_{\text{int}}(\mathbf{p}, \zeta_{\mathbf{p}}) = Z^{-1} \frac{\mathbf{p}}{m_x^*} - \frac{\mathbf{p}}{m_x} \quad (\text{A.10})$$

It is useful to obtain an explicit expression for the polaron dispersion $\zeta_{\mathbf{p}}$ with respect to the value (and derivatives) of the self energy at the Fermi surface $\mathbf{p} = \mathbf{p}_F$, by expanding the self energy in a Taylor series with respect to these points:

$$\begin{aligned} \text{Re}\Sigma_{\text{int}}(\mathbf{p}, \omega) &\simeq \text{Re}\Sigma_{\text{int}}(\mathbf{p}_F, 0) + \mathbf{p} \partial_{\mathbf{p}} \text{Re}\Sigma_{\text{int}}(\mathbf{p}, 0)|_{\mathbf{p}=\mathbf{p}_F} \\ &\quad + \frac{\mathbf{p}^2}{2} \partial_{\mathbf{p}}^2 \text{Re}\Sigma_{\text{int}}(\mathbf{p}, 0)|_{\mathbf{p}=\mathbf{p}_F} + \omega \partial_{\omega} \text{Re}\Sigma_{\text{int}}(\mathbf{p}_F, 0)|_{\omega=0} \end{aligned} \quad (\text{A.11})$$

The pole ω of Eq. (A.1), which yields ζ_p therefore satisfies the equation:

$$\begin{aligned} \omega - \omega_p - \text{Re}\Sigma_{\text{int}}(\mathbf{p}_F, 0) - \mathbf{p} \partial_{\mathbf{p}} \text{Re}\Sigma_{\text{int}}(\mathbf{p}, 0)|_{\mathbf{p}=\mathbf{p}_F} \\ - \frac{\mathbf{p}^2}{2} \partial_{\mathbf{p}}^2 \text{Re}\Sigma_{\text{int}}(\mathbf{p}, 0)|_{\mathbf{p}=\mathbf{p}_F} - \omega \partial_{\omega} \text{Re}\Sigma_{\text{int}}(\mathbf{p}_F, 0)|_{\omega=0} = 0 \end{aligned} \quad (\text{A.12})$$

which can be solved to obtain:

$$\begin{aligned} \zeta_p &= Z \left(\omega_p + \text{Re}\Sigma_{\text{int}}(\mathbf{p}_F, 0) + \frac{\mathbf{p}^2}{2m_x} - \mathbf{p} \partial_{\mathbf{p}} \text{Re}\Sigma_{\text{int}}(\mathbf{p}, 0)|_{\mathbf{p}=\mathbf{p}_F} \right. \\ &\quad \left. - \frac{\mathbf{p}^2}{2} \partial_{\mathbf{p}}^2 \text{Re}\Sigma_{\text{int}}(\mathbf{p}, 0)|_{\mathbf{p}=\mathbf{p}_F} \right) \end{aligned} \quad (\text{A.13})$$

where we introduced ζ_0 . From the above it is clear that the renormalized mass of the polaron can be written as:

$$\frac{1}{m_x^*} = Z \left(\frac{1}{m_x} + \partial_{\mathbf{p}}^2 \text{Re}\Sigma_{\text{int}}(\mathbf{p}, 0)|_{\mathbf{p}=\mathbf{p}_F} \right) \quad (\text{A.14})$$

A.2 POLARON DISPERSION FOR A DRIFTING FERMI SEA

Here, we determine the polaron dispersion, when the electrons are drifting at velocity v_e . For simplicity, we restrict ourselves to the case of zero polaron density, $\mu_x^* = 0$. Moreover, we focus on sufficiently low energies (i.e., below the trion energy) such that we can represent the exciton Green's function by the effective polaron Green's function

$$\bar{G}_x^R(p) = \frac{1}{\omega - \zeta_p + iZ/2\tau_x - iZ\text{Im}\Sigma_{\text{int}}(p)}, \quad (\text{A.15})$$

where $\zeta_p = \mathbf{p}^2/2m_x^*$ is the polaron dispersion at zero density, when the electron Fermi sea is at rest. According to Eq. (4.49), we can write the self energy in the absence of a drift as

$$\Sigma_{\text{int}}^{(0)}(\omega, \mathbf{p}) = \int \frac{d\mathbf{k}}{(2\pi)^2} n_F(\epsilon_{\mathbf{k}}) T^{(0)}(\omega + \epsilon_{\mathbf{k}}, \mathbf{k} + \mathbf{p}). \quad (\text{A.16})$$

The T matrix in Eq. (4.50) can be expressed as

$$\begin{aligned} T^{-1}(\omega, \mathbf{p}) &= v^{-1} \\ &+ \int \frac{d\mathbf{q}}{(2\pi)^2} \frac{n_F(\epsilon_{\mathbf{q}}) - 1}{\omega - \epsilon_{\mathbf{q}} - \zeta_{\mathbf{p}-\mathbf{q}} + iZ/2\tau_x - iZ\text{Im}\Sigma_{\text{int}}(\omega - \epsilon_{\mathbf{q}}, \mathbf{p} - \mathbf{q})}, \end{aligned} \quad (\text{A.17})$$

where we have substituted the exciton Green's function by Eq. (A.15). This is justified because in the domain of integration the energy argument of G_x always remains smaller than ω , and hence Eq. (A.15) is a good approximation. We can now simply introduce a drift velocity of the Fermi surface of electrons by shifting the distribution function $n_F(\epsilon_{\mathbf{k}}) \rightarrow n_F(\epsilon_{\mathbf{k}-\mathbf{A}})$ with $\mathbf{A} = \mathbf{v}_e m_e$. We denote the self energy with a shifted Fermi surface as $\tilde{\Sigma}$ and find

$$\tilde{\Sigma}_{\text{int}}^{(0)}(\omega, \mathbf{p}, \mathbf{A}) = \int \frac{d\mathbf{k}}{(2\pi)^2} n_F(\epsilon_{\mathbf{k}-\mathbf{A}}) \tilde{T}(\omega + \epsilon_{\mathbf{k}}, \mathbf{k} + \mathbf{p}, \mathbf{A}). \quad (\text{A.18})$$

The self-consistent T matrix needs to be changed accordingly

$$\begin{aligned} \tilde{T}^{-1}(\omega, \mathbf{p}, \mathbf{A}) &= v^{-1} \\ &+ \int \frac{d\mathbf{q}}{(2\pi)^2} \frac{n_F(\epsilon_{\mathbf{q}-\mathbf{A}}) - 1}{\omega - \epsilon_{\mathbf{q}} - \tilde{\zeta}_{\mathbf{p}-\mathbf{q}} + iZ/2\tau_x - iZ\text{Im}\tilde{\Sigma}_{\text{int}}(\omega - \epsilon_{\mathbf{q}}, \mathbf{p} - \mathbf{q}, \mathbf{A})}, \end{aligned} \quad (\text{A.19})$$

where we have defined the polaron dispersion in the presence of a Fermi sea $\tilde{\zeta}_{\mathbf{p}}$ that we seek to obtain. Shifting the variable of integration the self energy reads

$$\tilde{\Sigma}_{\text{int}}^{(0)}(\omega, \mathbf{p}, \mathbf{A}) = \int \frac{d\mathbf{k}}{(2\pi)^2} n_F(\epsilon_{\mathbf{k}}) \tilde{T}(\omega + \epsilon_{\mathbf{k}+\mathbf{A}}, \mathbf{k} + \mathbf{A} + \mathbf{p}, \mathbf{A}) \quad (\text{A.20})$$

with

$$\begin{aligned} \tilde{T}^{-1}(\omega + \epsilon_{\mathbf{k}+\mathbf{A}}, \mathbf{k} + \mathbf{A} + \mathbf{p}, \mathbf{A}) &= v^{-1} + \int \frac{d\mathbf{q}}{(2\pi)^2} (n_F(\epsilon_{\mathbf{q}}) - 1) / \\ &(\omega + \epsilon_{\mathbf{k}+\mathbf{A}} - \epsilon_{\mathbf{q}+\mathbf{A}} - \tilde{\zeta}_{\mathbf{k}+\mathbf{p}-\mathbf{q}} + iZ/2\tau_x \\ &- iZ\text{Im}\tilde{\Sigma}_{\text{int}}(\omega + \epsilon_{\mathbf{k}+\mathbf{A}} - \epsilon_{\mathbf{q}+\mathbf{A}}, \mathbf{k} + \mathbf{p} - \mathbf{q}, \mathbf{A})). \end{aligned} \quad (\text{A.21})$$

We make the following general ansatz for the new polaron dispersion

$$\tilde{\zeta}_{\mathbf{p}} = \frac{(\mathbf{p} + \delta\mathbf{p})^2}{2m_x^*} + \delta E, \quad (\text{A.22})$$

where $\delta\mathbf{p}$ and δE are constants to be determined. It is straightforward to rewrite the real part of the denominator of Eq. (A.21) as

$$\omega + \epsilon_{\mathbf{k}+\mathbf{A}} - \epsilon_{\mathbf{q}+\mathbf{A}} - \tilde{\zeta}_{\mathbf{k}+\mathbf{p}-\mathbf{q}} = \omega' + \epsilon_{\mathbf{k}} - \epsilon_{\mathbf{q}} - \tilde{\zeta}_{\mathbf{k}+\mathbf{p}'-\mathbf{q}'}, \quad (\text{A.23})$$

where we have introduced

$$\mathbf{p}' = \mathbf{p} + \delta\mathbf{p} - \mathbf{A}m_x^*/m_e. \quad (\text{A.24})$$

$$\omega' = \omega - \frac{(\mathbf{p} + \delta\mathbf{p})\mathbf{A}}{m_e} + \frac{A^2 m_x^*}{2m_e^2} - \delta E. \quad (\text{A.25})$$

Notice that the right-hand side of Eq. (A.23) involves the bare polaron dispersion at zero electron drift velocity. Using this relation, we can express the T matrix in the presence of an electron drift by the bare T matrix at shifted energy and momentum arguments, $\tilde{T}(\omega + \epsilon_{\mathbf{k}+\mathbf{A}}, \mathbf{k} + \mathbf{A} + \mathbf{p}, \mathbf{A}) = T(\omega' + \epsilon_{\mathbf{k}}, \mathbf{k} + \mathbf{p}')$. Similarly the self energy can be expressed as

$$\tilde{\Sigma}_{\text{int}}^{(0)}(\omega, \mathbf{p}, \mathbf{A}) = \Sigma_{\text{int}}^{(0)}(\omega', \mathbf{p}'). \quad (\text{A.26})$$

Here we have used the relation

$$\text{Im}\tilde{\Sigma}_{\text{int}}(\omega + \epsilon_{\mathbf{k}+\mathbf{A}} - \epsilon_{\mathbf{q}+\mathbf{A}}, \mathbf{k} + \mathbf{p} - \mathbf{q}, \mathbf{A}) = \text{Im}\Sigma_{\text{int}}(\omega + \epsilon_{\mathbf{k}} - \epsilon_{\mathbf{q}}, \mathbf{k} + \mathbf{p} - \mathbf{q}), \quad (\text{A.27})$$

which can be verified straightforwardly using Eqs. (A.20) and (A.21). We can now determine the polaron dispersion in Eq. (A.22) from the pole of the Green's function

$$\left[\omega - \frac{p^2}{2m_x} + \mu_x - \text{Re}\tilde{\Sigma}(\omega, \mathbf{p}, \mathbf{A}) \right]_{\omega=\tilde{\zeta}_p} = 0. \quad (\text{A.28})$$

Near the polaron pole we can write

$$\text{Re}\tilde{\Sigma}_{\text{int}}^{(0)}(\omega, \mathbf{p}, \mathbf{A}) = \text{Re}\Sigma_{\text{int}}^{(0)}(\omega', \mathbf{p}') \simeq (1 - Z^{-1})\omega' + Z^{-1}\zeta_{p'} - \frac{p'^2}{2m_x} + \mu_x. \quad (\text{A.29})$$

Substituting $\mathbf{A} = m_e \mathbf{v}_e$ we find after some straightforward manipulations

$$\delta \mathbf{p} = \mathbf{v}_e(m_x^* - m_x) \quad (\text{A.30})$$

$$\delta E = -\frac{\mathbf{v}_e^2(m_x^* - m_x)}{2} \quad (\text{A.31})$$

and hence the polaron dispersion when the electrons are drifting at a constant velocity reads

$$\tilde{\zeta}_p = \frac{(\mathbf{p} + \mathbf{v}_e(m_x^* - m_x))^2}{2m_x^*} - \frac{\mathbf{v}_e^2(m_x^* - m_x)}{2}. \quad (\text{A.32})$$

A complementary way to show the emergence of this force is using a variational approach. To do this we start from the following Hamiltonian that

incorporates the interaction between excitons and electrons in the presence of an electric field. We will use the Coulomb gauge, such that the effect of the electric field is to shift the electron dispersion, and therefore preserve translational invariance. We obtain:

$$H(t) = \sum_{\mathbf{k}} \epsilon_{\mathbf{k}+m_e \mathbf{v}_e(t)} c_{\mathbf{k}}^\dagger c_{\mathbf{k}} + \sum_{\mathbf{k}} \omega_{\mathbf{k}} x_{\mathbf{k}}^\dagger x_{\mathbf{k}} + \sum_{\mathbf{k}, \mathbf{k}', \mathbf{q}} \frac{v}{A} x_{\mathbf{k}+\mathbf{q}}^\dagger c_{\mathbf{k}'-\mathbf{q}}^\dagger c_{\mathbf{k}'} x_{\mathbf{k}}$$
(A.33)

where c^\dagger is the electron creation operator, while x^\dagger denotes the creation of an excitonic impurity. Furthermore, $\epsilon_{\mathbf{k}} = \frac{\mathbf{k}^2}{2m_e} - \mu_e$ is the electron dispersion, while $\omega_{\mathbf{k}} = \frac{\mathbf{k}^2}{2m_x} - \mu_x$ denotes the impurity dispersion. Notice that we investigate only the case of vanishing exciton density, i.e. $\mu_x < 0$. We remark that the total conjugate momentum $\hat{\mathbf{p}}_T \equiv \sum_{\mathbf{k}} \mathbf{k} (x_{\mathbf{k}}^\dagger x_{\mathbf{k}} + c_{\mathbf{k}}^\dagger c_{\mathbf{k}})$ is an integral of motion and we can simply replace it by its eigenvalue \mathbf{p}_T .

Strictly speaking the above Hamiltonian is valid only when disorder can be neglected and in this case $\mathbf{v}_e(t)$ is the velocity acquired by electrons due to the acceleration by the electric field: $\mathbf{v}_e(t) = \text{Re} \frac{e}{i\Omega m_e} \mathbf{E} e^{-i\Omega t}$. However, we can also include the effect of disorder on the electron system, heuristically, by assuming that the velocity $\mathbf{v}_e(t)$ is the steady state electron velocity in the presence of an electric field and disorder (as calculated in Eq. 7.5).

It is instructive to first solve the problem in the absence of an electric field. To do this we introduce a Chevy-ansatz, which is completely equivalent to a non-self-consistent T-matrix approach:

$$|\Psi_{\mathbf{p}}\rangle = a_{\mathbf{p}}^\dagger |0\rangle = \left(\phi_{\mathbf{p}} x_{\mathbf{p}}^\dagger + \sum_{\mathbf{k}, \mathbf{q}} \phi_{\mathbf{p}, \mathbf{k}, \mathbf{q}} x_{\mathbf{p}+\mathbf{q}-\mathbf{k}}^\dagger c_{\mathbf{k}}^\dagger c_{\mathbf{q}} \right) |0\rangle$$
(A.34)

To obtain the ground state energy we have to minimize $\langle \Psi_{\mathbf{p}} | H - E | \Psi_{\mathbf{p}} \rangle$, where the energy E is the Langrange multiplier ensuring the normalization of the wavefunction. The minimization will yield, the dispersion of the polarons $\zeta_{\mathbf{p}}(t) = \zeta_0 + \mathbf{p}^2/(2m_x^*)$ (see Ref. [2, 3] for details regarding the minimization procedure; the mass m_x^* might not be the same as the m_x^* obtained self-consistently, since this is a non-self-consistent derivation).

Having solved the problem in the absence of the electric field, we now find a mapping from the instantenous eigenstates of the Hamiltonian in the presence of an electric field to the states in the absence of any field. To show this mapping we firtly go to a frame that is co-moving with the electrons with the unitary $U(t) = e^{iS(t)}$ where $S(t) = \mathbf{r}_e(t) \hat{\mathbf{p}}_T$, where $\mathbf{r}_e(t) = \int_0^t dt' \mathbf{v}_e(t')$. Since $U(t)x_{\mathbf{k}}U^\dagger(t) = x_{\mathbf{k}} e^{-i\mathbf{k}\mathbf{r}_e(t)}$, the conservation

of total conjugate momentum implies that $U(t)HU^\dagger(t) = H$, so the only contribution to the Hamiltonian comes from the time dependence of the transformation $-iU(t)\frac{\partial U^\dagger(t)}{\partial t} = \frac{\partial S(t)}{\partial t} = \frac{e}{m_e}\mathbf{A}(t)\hat{\mathbf{p}}_T$. The new Hamiltonian becomes:

$$H(t) = \sum_{\mathbf{k}} \epsilon_{\mathbf{k}} c_{\mathbf{k}}^\dagger c_{\mathbf{k}} + \sum_{\mathbf{k}} \omega_{\mathbf{k}-m_x \mathbf{v}_e(t)} x_{\mathbf{k}}^\dagger x_{\mathbf{k}} + \sum_{\mathbf{k}, \mathbf{k}', \mathbf{q}} \frac{V}{A} x_{\mathbf{k}+\mathbf{q}}^\dagger e_{\mathbf{k}'-\mathbf{q}}^\dagger e_{\mathbf{k}'} x_{\mathbf{k}} \quad (\text{A.35})$$

where now the exciton dispersion is shifted by an amount $-m_x \mathbf{v}_e(t)$. Assuming that the electric field is small enough, the system will remain in the many-body ground state, according to the adiabatic theorem. To determine the instantenous groundstate of $H(t)$ we have to minimize $\langle \Psi_{\mathbf{p}}(t) | H(t) - E | \Psi_{\mathbf{p}}(t) \rangle$, where the Chevy ansatz is given by:

$$|\Psi_{\mathbf{p}}(t)\rangle = a_{\mathbf{p}}^\dagger |0\rangle = \left(\phi_{\mathbf{p}}(t) x_{\mathbf{p}}^\dagger + \sum_{\mathbf{k}, \mathbf{q}} \phi_{\mathbf{p}, \mathbf{k}, \mathbf{q}}(t) x_{\mathbf{p}+\mathbf{q}-\mathbf{k}}^\dagger c_{\mathbf{k}}^\dagger c_{\mathbf{q}} \right) |0\rangle \quad . \quad (\text{A.36})$$

One can check that, up to some irrelevant constants $\langle \Psi_{\mathbf{p}}(t) | H(t) | \Psi_{\mathbf{p}}(t) \rangle = \langle \Psi_{\mathbf{p}-m_x \mathbf{v}_e(t)} | H | \Psi_{\mathbf{p}-m_x \mathbf{v}_e(t)} \rangle$ (one way to see this is to explicitly expand these terms and compare them) which illustrates the mapping to the states in the absence of an electric field. From the above we immediately see that:

$$\tilde{\zeta}_{\mathbf{p}}(t) = \zeta_{\mathbf{p}-m_x \mathbf{v}_e(t)} = \frac{(\mathbf{p} - m_x \mathbf{v}_e(t))^2}{2m_x^*} - \mu_x^* \quad (\text{A.37})$$

where we used a tilde to denote the dispersion in the frame co-moving with the electrons. We remark that polarons acquire a backward velocity $-m_x/m_x^* \mathbf{v}_e(t)$, which is smaller than the electron velocity due to the mass remormalization. Moving back to the lab frame, the dispersion will become:

$$\zeta_{\mathbf{p}}(t) = \frac{(\mathbf{p} + (m_x^* - m_x) \mathbf{v}_e(t))^2}{2m_x^*} - \mu_x^* \quad (\text{A.38})$$

Assuming that the electric field is small enough the evolution is adiabatic and we can focus only on the attractive-polaron states and ignore all the

other higher lying states and therefore we can write down an effective Hamiltonian in terms of attractive polarons:

$$H(t) = \sum_{\mathbf{p}} \left(\frac{[\mathbf{p} + (m_x^* - m_x)\mathbf{v}_e(t)]^2}{2m_x^*} - \mu_x^* \right) a_{\mathbf{p}}^\dagger a_{\mathbf{p}} \quad (\text{A.39})$$

which is similar to the Hamiltonian introduced in Sec. (7.3.5).

A.4 POLARON LIFETIME

In this Appendix we investigate the residual interactions between polarons and the Fermi sea and calculate the corresponding scattering rates associated with these processes. We first calculate the scattering lifetime using Fermi's Golden Rule, since it is more transparent, but then we show that the same result can be obtained by explicitly evaluating $\text{Im}\Sigma(\mathbf{p}, \epsilon_{\mathbf{p}})$. In the following we are interested in the case of only one polaron in the system with momentum $|\mathbf{p}| \ll k_F$ and therefore we choose $\mu_x^* < 0$.

A.4.1 *Interaction between polarons and electrons*

The interaction between this polaron and an electron of momentum \mathbf{k} is given by:

$$U(\mathbf{p}, \mathbf{k}) = ZT(\mathbf{p} + \mathbf{k}, \zeta_{\mathbf{p}} + \epsilon_{\mathbf{k}}) \quad (\text{A.40})$$

where Z is the quasiparticle weight of the polaron. Since, by assumption, the polaron has a small energy $\zeta_{\mathbf{p}} \ll e_F$, the polaron will only be able to scatter electrons in a thin shell around the Fermi surface, and therefore, for our purposes we have $\mathbf{k} \simeq \mathbf{k}_F$ and therefore:

$$U \simeq ZT(\mathbf{k}_F, 0) \quad (\text{A.41})$$

In the above T denotes the self-consistent T-matrix. We know that the T-matrix has a simple pole at the trion-resonance $\omega_T(k)$. Therefore, for energies in the vicinity of the trion resonance we can approximate the T-matrix by:

$$T(\mathbf{k}, \omega) \simeq \frac{C}{\omega - \omega_T(k) + i\gamma_T} \quad (\text{A.42})$$

where $\omega_T(\mathbf{k})$ is the trion energy measured from the exciton chemical potential μ_x , and γ_T denotes the lifetime of the trion-state.

Since it is not immediately obvious how to calculate C for the self-consistent T-matrix, we proceed to estimate it. Since the self-consistent T-matrix cannot be too much different than the non-self-consistent T-matrix T_0 (which we know how to calculate exactly) we use the analytical expression of T_0 to obtain an order of magnitude estimation for T . Considering, for simplicity the case $m_x = m_e$ we know that [5]:

$$T_0(0, \omega) = \frac{2}{\rho_e \left(\ln \left(\frac{\epsilon_T}{\omega + \mu_x} \right) + i\pi \right)} = \frac{2\epsilon_T}{\rho_e} \frac{1}{\omega + \epsilon_T + \mu_x} + \mathcal{O} \left(\left(\frac{\omega + \epsilon_T + \mu_x}{\epsilon_T} \right)^2 \right) \quad (\text{A.43})$$

which shows that $C \simeq 2\epsilon_T / \rho_e$. Denoting the energy difference between the trion of momentum \mathbf{k}_F and the attractive polaron of momentum \mathbf{p} with Δ we can approximate the interaction U as:

$$U \simeq -\frac{2Z\epsilon_T}{\rho_e \Delta} \quad (\text{A.44})$$

A.4.2 Polaron lifetime using Fermi's Golden Rule

According to Fermi's Golden rule, the scattering rate from a state of momentum \mathbf{p} is given by:

$$\Gamma = 2\pi U^2 \sum_{|\mathbf{p}'| < |\mathbf{p}|, \mathbf{k}} \delta(\zeta_{\mathbf{p}} - \zeta_{\mathbf{p}'} - \epsilon_{\mathbf{k}+\mathbf{p}-\mathbf{p}'} + \epsilon_{\mathbf{k}}) [n_F(\epsilon_{\mathbf{k}}) - n_F(\epsilon_{\mathbf{k}+\mathbf{p}-\mathbf{p}'}))] \quad (\text{A.45})$$

where we used the fact that a polaron can scatter by creating electron-hole pairs in the Fermi sea. We can write the above more compactly by introducing the electron response function:

$$\chi(\mathbf{q}, \omega) \equiv -\sum_{\mathbf{k}} \frac{n_F(\epsilon_{\mathbf{k}}) - n_F(\epsilon_{\mathbf{k}+\mathbf{q}})}{\omega - \epsilon_{\mathbf{k}+\mathbf{q}} + \epsilon_{\mathbf{k}} + i0^+} \quad (\text{A.46})$$

which allows us to rewrite Γ as:

$$\begin{aligned} \Gamma &= 2U^2 \sum_{|\mathbf{p}'| < |\mathbf{p}|} \text{Im}\chi(\mathbf{p} - \mathbf{p}', \zeta_{\mathbf{p}} - \zeta_{\mathbf{p}'}) \\ &= 2U^2 \sum_{|\mathbf{q}| < |\mathbf{p}|} \text{Im}\chi(\mathbf{q}, \zeta_{\mathbf{p}} - \zeta_{\mathbf{p}-\mathbf{q}}) \theta(\zeta_{\mathbf{p}} - \zeta_{\mathbf{p}-\mathbf{q}}) \end{aligned} \quad (\text{A.47})$$

Since $|\mathbf{q}| < |\mathbf{p}| \ll k_F$ and therefore $\zeta_{\mathbf{p}} - \zeta_{\mathbf{p}-\mathbf{q}} \ll \mu_e$ we can use the low frequency expansion:

$$\text{Im}\chi(\mathbf{q}, \omega) \simeq 2\rho_e \frac{\omega}{\mu_e} \frac{k_F}{|\mathbf{q}|} \quad (\text{A.48})$$

which in our case means that:

$$\begin{aligned} \Gamma &\simeq 4\rho_e U^2 \int_0^p dq q \int_0^{2\pi} d\phi \text{Im} 2\rho_e \frac{2pq \cos \phi - q^2}{2m_x^* \mu_e} \frac{k_F}{|\mathbf{q}|} \theta(2pq \cos \phi - q^2) \\ &= 4\rho_e U^2 \frac{p^3 k_F}{2m_x^* \mu_e} \int_0^1 dq \int_0^{2\pi} d\phi (2q \cos \phi - q^2) \theta(2q \cos \phi - q^2) \end{aligned} \quad (\text{A.49})$$

The integral is easy to evaluate and is $\simeq 1$. Since $Z \simeq \sqrt{\mu_e/\epsilon_T}$ we finally obtain

$$\Gamma \sim \frac{\epsilon_T}{\Delta^2} \frac{p^3 k_F}{m_e m_x^*}. \quad (\text{A.50})$$

A.4.3 Polaron lifetime from self energy

The same expression can be derived by explicitly evaluating the imaginary part of the self energy. To evaluate the imaginary part one can use the optical theorem. In our case it is just as simple to directly evaluate the imaginary part of the self energy. The polaron broadening due to interaction with the Fermi sea is related to the self energy by:

$$\Gamma = Z \text{Im} \Sigma(\mathbf{p}, \zeta_{\mathbf{p}}) \quad (\text{A.51})$$

where:

$$\Sigma(\mathbf{p}, \omega) = \int \frac{d^2 \mathbf{k}}{(2\pi)^2} n_F(\epsilon_{\mathbf{k}}) T(\mathbf{p} + \mathbf{k}, \omega + \epsilon_{\mathbf{k}}) \quad (\text{A.52})$$

where the T matrix is given by:

$$T(\mathbf{p}, \omega)^{-1} = V^{-1} - \int \frac{d^2 \mathbf{k}}{(2\pi)^2} (1 - n_F(\epsilon_{\mathbf{k}})) G_x^R(\mathbf{p} - \mathbf{k}, \omega - \epsilon_{\mathbf{k}}) \quad (\text{A.53})$$

From the above we conclude that:

$$\text{Im}T(\mathbf{p}, \omega)^{-1} = \int \frac{d^2 \mathbf{k}}{(2\pi)^2} (1 - n_F(\epsilon_{\mathbf{k}})) \text{Im}G_x^A(\mathbf{p} - \mathbf{k}, \omega - \epsilon_{\mathbf{k}}) \quad (\text{A.54})$$

$$\begin{aligned} \text{Im}T(\mathbf{p}, \omega) &= |T(\mathbf{p}, \omega)|^2 \text{Im}T(\mathbf{p}, \omega)^{-1} \simeq T(\mathbf{p}, \omega)^2 \text{Im}T(\mathbf{p}, \omega)^{-1} \\ \text{Im}\Sigma(\mathbf{p}, \omega) &= \int \frac{d^2 \mathbf{k}}{(2\pi)^2} \frac{d^2 \mathbf{k}'}{(2\pi)^2} T(\mathbf{p} + \mathbf{k}, \omega + \epsilon_{\mathbf{k}})^2 (1 - n_F(\epsilon'_{\mathbf{k}})) n_F(\epsilon_{\mathbf{k}}) \\ &\quad \cdot \text{Im}G_x^A(\mathbf{p} + \mathbf{k} - \mathbf{k}', \omega + \epsilon_{\mathbf{k}} - \epsilon_{\mathbf{k}'}) \end{aligned} \quad (\text{A.55})$$

$$\begin{aligned} &= \int \frac{d^2 \mathbf{k}}{(2\pi)^2} \frac{d^2 \mathbf{k}'}{(2\pi)^2} T(\mathbf{p} + \mathbf{k}, \omega + \epsilon_{\mathbf{k}})^2 (1 - n_F(\epsilon'_{\mathbf{k}})) n_F(\epsilon_{\mathbf{k}}) \\ &\quad \cdot \pi Z \delta(\omega - \zeta_{\mathbf{p} + \mathbf{k} - \mathbf{k}'} + \epsilon_{\mathbf{k}} - \epsilon_{\mathbf{k}'}) \end{aligned} \quad (\text{A.56})$$

From the above we see that the polaron broadening will be:

$$\begin{aligned} \Gamma &= Z \text{Im}\Sigma(\mathbf{p}, \zeta_{\mathbf{p}}) = Z^2 \pi \int \frac{d^2 \mathbf{k}}{(2\pi)^2} \frac{d^2 \mathbf{k}'}{(2\pi)^2} T(\mathbf{p} + \mathbf{k}, \zeta_{\mathbf{p}} + \epsilon_{\mathbf{k}})^2 (\text{A.57}) \\ &\quad (1 - n_F(\epsilon'_{\mathbf{k}})) n_F(\epsilon_{\mathbf{k}}) \delta(\zeta_{\mathbf{p}} - \zeta_{\mathbf{p} + \mathbf{k} - \mathbf{k}'} + \epsilon_{\mathbf{k}} - \epsilon_{\mathbf{k}'}) \end{aligned}$$

which, is can be directly related to Eq. (A.45) through the change of coordinates $\mathbf{k}' \rightarrow -\mathbf{p}' + \mathbf{k} + \mathbf{p}$ and using the approximation $T(\mathbf{p} + \mathbf{k}, \zeta_{\mathbf{p}} + \epsilon_{\mathbf{k}}) \simeq T(\mathbf{k}_F, 0)$ which is valid for $|\mathbf{p}| \ll k_F$.

A.4.4 Polaron lifetime at finite exciton density

The above calculation was performed in the limit of vanishing exciton density, but we can use the same method to calculate the lifetime in the presence of a finite density of excitons. We therefore calculate the imaginary part of the interaction self energy for a polaron of frequency $\omega < 0$ and momentum $|\mathbf{p}| < |\mathbf{p}_F|$. This corresponds to a hole of energy $-\omega$ and momentum $-\mathbf{p}$, which can scatter into states with momenta \mathbf{p}' obeying the condition $0 \geq \zeta_{\mathbf{p}'} \geq \omega$ by creating electron-hole pairs.

Using similar arguments as in Sec. (A.4.2) the scattering rate can be calculated using Fermi's Golden Rule:

$$\begin{aligned} \Gamma(\mathbf{p}, \omega) &= 2U^2 \sum_{\mathbf{p}', |\mathbf{p}'| < |\mathbf{p}_F|} \text{Im}\chi(\mathbf{p} - \mathbf{p}', \omega - \zeta_{\mathbf{p}'}) \theta(\zeta_{\mathbf{p}'} - \omega) \quad (\text{A.58}) \\ &\simeq \Gamma(\mathbf{p}, \zeta_{\mathbf{p}}) + (\omega - \zeta_{\mathbf{p}}) \partial_{\omega} \Gamma(\mathbf{p}, \omega)_{\omega=\zeta_{\mathbf{p}}} \end{aligned}$$

where we expanded Γ in a Taylor series in frequency around $\zeta_{\mathbf{p}}$ and kept only the first term:

$$\Gamma(\mathbf{p}, \zeta_{\mathbf{p}}) = 2U^2 \sum_{\mathbf{p}', |\mathbf{p}'| < |\mathbf{p}_F|} \text{Im}\chi(\mathbf{p} - \mathbf{p}', \zeta_{\mathbf{p}} - \zeta_{\mathbf{p}'}) \theta(\zeta_{\mathbf{p}'} - \zeta_{\mathbf{p}}) \quad (\text{A.59})$$

$$\partial_{\omega}\Gamma(\mathbf{p}, \omega)_{\omega=\zeta_{\mathbf{p}}} = 2U^2 \partial_{\omega} \left[\sum_{\substack{\mathbf{p}' \\ |\mathbf{p}'| < |\mathbf{p}_F|}} \text{Im}\chi(\mathbf{p} - \mathbf{p}', \omega - \zeta_{\mathbf{p}'}) \theta(\zeta_{\mathbf{p}'} - \omega) \right]_{\omega=\zeta_{\mathbf{p}}} \quad (\text{A.60})$$

Introducing $\mathbf{q} = \mathbf{p} - \mathbf{p}'$ and using the low frequency and momentum expansion of the response function χ , as given in Eq. (A.48) we obtain:

$$\Gamma(\mathbf{p}, \zeta_{\mathbf{p}}) \simeq \frac{4U^2 \rho_e k_F}{\mu_e} \sum_{\mathbf{q}, |\mathbf{p}-\mathbf{q}| < p_F} \frac{\zeta_{\mathbf{p}} - \zeta_{\mathbf{p}-\mathbf{q}}}{|\mathbf{q}|} \theta(\zeta_{\mathbf{p}-\mathbf{q}} - \zeta_{\mathbf{p}}) \quad (\text{A.61})$$

$$= \frac{U^2 \rho_e k_F}{\mu_e \pi^2} \int_0^{2p_F} dq q \int_0^{2\pi} d\phi \frac{q^2 - 2pq \cos \phi}{2m_x^*} \frac{1}{q} \cdot \theta(q^2 - 2pq \cos \phi) \theta(p_F^2 + 2pq \cos \phi - p^2 - q^2) \quad (\text{A.62})$$

$$= \frac{U^2 \rho_e k_F}{\mu_e \pi^2} \frac{p_F^3}{2m_x^*} I_0(p/p_F) \quad (\text{A.63})$$

where we introduced the integral of order 1:

$$I_0(u) \equiv \int_0^2 dq \int_0^{2\pi} d\phi (q^2 - 2qu \cos \phi) \theta(q^2 - 2qu \cos \phi) \theta(1 + 2uq \cos \phi - u^2 - q^2) \quad (\text{A.64})$$

In the above, one of the theta functions ensures that $\zeta_{\mathbf{p}'} \geq \omega$ while the other theta function ensures that $|\mathbf{p}'| < p_F$. It is useful to investigate the energy of hole quasiparticles with $-\omega = \zeta_{\mathbf{p}} \ll \mu_x^*$. For these particles $p/p_F \simeq 1 - \omega/2\mu_x^*$. Introducing $\delta = \omega/\mu_x^*$ one can easily check that $I_0(1 - \delta/2) = C\delta^2 + \mathcal{O}(\delta^3)$. This proves that, in analogy to Fermi Liquid theory, the polaron excitations are well defined quasiparticles, with lifetime proportional to ω^2 .

The derivative of Γ can be evaluated similarly using Eq. (A.48) :

$$\begin{aligned}\partial_\omega \Gamma(\mathbf{p}, \omega)_{\omega=\zeta_p} &= \frac{4U^2\rho_e k_F}{\mu_e} \partial_\omega \left[\sum_{\mathbf{q}, |\mathbf{p}-\mathbf{q}| < p_F} \frac{\omega - \zeta_{\mathbf{p}-\mathbf{q}}}{|\mathbf{q}|} \theta(\zeta_{\mathbf{p}-\mathbf{q}} - \omega) \right]_{\omega=\zeta_p} \\ &= \frac{4U^2\rho_e k_F}{\mu_e} \left[\sum_{\mathbf{q}, |\mathbf{p}-\mathbf{q}| < p_F} \frac{1}{|\mathbf{q}|} \theta(\zeta_{\mathbf{p}-\mathbf{q}} - \zeta_p) - \right. \\ &\quad \left. \frac{\zeta_p - \zeta_{\mathbf{p}-\mathbf{q}}}{|\mathbf{q}|} \delta(\zeta_{\mathbf{p}-\mathbf{q}} - \zeta_p) \right]\end{aligned}\quad (\text{A.65})$$

Similar to the evaluation of Γ we can evaluate the above by turning the sum into integrals. We immediately see that the last term in the brackets vanishes and we are left with

$$\partial_\omega \Gamma(\mathbf{p}, \omega)_{\omega=\zeta_p} = \frac{U^2 \rho_e k_F}{\mu_e \pi^2} p_F I_1(p/p_F) \quad (\text{A.66})$$

where we introduced the integral of order 1:

$$I_1(u) \equiv \int_0^2 dq \int_0^{2\pi} d\phi \theta(q^2 - 2qu \cos \phi) \theta(1 + 2uq \cos \phi - u^2 - q^2) \quad (\text{A.67})$$

A.5 RELATION BETWEEN $\text{Im}\Sigma_{\text{int}}$ AND $\text{Im}G_x$

In Sec. 7.3.4 of the main text, we encounter an expression of the type

$$\int dp A[G_x^R(p)] \text{Im}\Sigma_{\text{int}}(p) \theta(-\omega) \quad (\text{A.68})$$

where A is a functional of G_x^R . In this appendix, we show that this expression can alternatively be written as

$$\begin{aligned}\mathcal{I} &\equiv \int dp A[G_x^R(p)] \text{Im}\Sigma_{\text{int}}(p) \theta(-\omega) \\ &= \int dp dk A[G_x^R(p)] \text{Im}G_x^A(k) w^{(0)}(k, p) \theta(-\epsilon) \\ &= \int dp dk dk' A[G_x^R(p)] \text{Im}G_x^A(k) G_e(k') G_e(p + k' - k) [T^R(p + k')]^2 \theta(-\epsilon)\end{aligned}\quad (\text{A.69})$$

where A is a functional of G_x^R . We first derive an expression for the imaginary part of the self energy. Using $G_e(k) = G_e^R(k) + 2i\text{Im}G_e(k)\theta(-\epsilon)$ and a similar relation for the T matrix we can write the self energy as

$$\Sigma_{\text{int}}(p)\theta(-\omega) = -i\theta(-\omega) \int dk \left[G_e^R(k)T^R(k+p) \right. \quad (\text{A.70})$$

$$+ G_e^R(k)2i\text{Im}T^A(k+p)\theta(-\omega-\epsilon) + 2i\text{Im}G_e^A(k)\theta(-\epsilon)T^R(k+p) \\ - 4\text{Im}G_e^A(k)\text{Im}T^A(k+p)\theta(-\omega-\epsilon)\theta(-\epsilon) \Big]$$

$$= 2\theta(-\omega) \int dk \left\{ \text{Re}G_e(k)\text{Im}T^A(k+p)\theta(-\omega-\epsilon) \right. \quad (\text{A.71})$$

$$+ \text{Im}G_e^A(k)\text{Re}T(k+p)\theta(-\epsilon)$$

$$+ i\text{Im}G_e^A(k)\text{Im}T^A(k+p)[\theta(-\omega-\epsilon) - \theta(-\epsilon)]$$

section

The imaginary part of the T matrix is

$$\text{Im}T(k+p) = 2|T(k+p)|^2 \int dk' \text{Im}G_e^A(k')\text{Im}G_x^A(k+p-k') \quad (\text{A.72})$$

$$\theta(-\epsilon')\theta(\epsilon' - \omega - \epsilon).$$

With this we can express the imaginary part of the self energy as

$$\text{Im}\Sigma_{\text{int}}(p)\theta(-\omega) = 4\theta(-\omega) \int dk dk' |T(k+p)|^2 \text{Im}G_e^A(k) \quad (\text{A.73})$$

$$\cdot \text{Im}G_e^A(k')\text{Im}G_x^A(p+k-k')\theta(-\epsilon')[\theta(-\omega-\epsilon) - \theta(-\epsilon)]\theta(\epsilon' - \epsilon - \omega).$$

To prove Eq (A.70), we make the replacement $G_e(p+k'-k) = G_e^R(p+k'-k) + 2i\text{Im}G_e^A(p+k'-k)\theta(\epsilon - \omega - \epsilon')$. The first term is canceled by the integral over ω since all poles are located in the same complex half plane and hence after shifting $k' \rightarrow k' - p$, we find

$$\mathcal{I} = 2i \int dp dk dk' A[G_x^R(p)]\text{Im}G_x^A(k)G_e(k'-p)\text{Im}G_e^A(k'-k) \quad (\text{A.74})$$

$$[T^R(k')]^2\theta(-\epsilon)\theta(\epsilon - \omega)$$

The shift of variables conveniently allows us to repeat the same trick writing $G_e(k'-p) = G_e^A(k'-p) - 2i\text{Im}G_e^A(k'-p)\theta(\epsilon' - \omega)$. The first term is again canceled by the ω integration and we find after returning to the original integration variables

$$\mathcal{I} = 4 \int dp dk dk' A[G_x^R(p)]\text{Im}G_x^A(k)\text{Im}G_e^A(k')\text{Im}G_e^A(p+k'-k) \quad (\text{A.75})$$

$$[T^R(k'+p)]^2\theta(-\epsilon)\theta(\epsilon')\theta(\epsilon - \epsilon' - \omega)$$

By comparison with Eq. (A.73) and using the simple identity

$$\theta(-\epsilon)\theta(\epsilon')\theta(\epsilon - \epsilon' - \omega) = \theta(-\epsilon')[\theta(-\omega - \epsilon) - \theta(-\epsilon)] \\ \theta(\epsilon' - \epsilon - \omega)\theta(-\omega), \quad (\text{A.76})$$

we arrive at

$$\int dp A[G_x^R(p)]\text{Im}\Sigma_{\text{int}}^{(0)}(p)\theta(-\omega) = \int dp dk A[G_x^R(p)]\text{Im}G_x^A(k) \\ w^{(0)}(k, p)\theta(-\epsilon). \quad (\text{A.77})$$

A.5.1 Exciton density

We now show that the integral $-i \int dp G_x(p)$ over the exciton Green's function indeed yields the correct polaron density

$$n_x \equiv \langle \sum_{\mathbf{p}} x_{\mathbf{p}}^\dagger(t)x_{\mathbf{p}}(t) \rangle = \sum_p n_x(\mathbf{p}) = \sum_{\mathbf{p}} \langle T[x_{\mathbf{p}}(t)x_{\mathbf{p}}^\dagger(t + 0^+)] \rangle \\ = -i \sum_{\mathbf{p}} \int \frac{d\omega}{2\pi} G_x(\mathbf{p}, \omega) e^{i\omega 0^+} \quad (\text{A.78})$$

where the infinitesimal $\omega 0^+$ originates from time-ordering and ensures that the contour is closed in the upper-half plane. Using the decomposition $G(p) = G^R(p) + 2i\text{Im}G^A(p)\theta(-\omega)$ we find

$$-i \int dp G_x(p) = 2 \int dp \text{Im}G_x^A(p)\theta(-\omega) \\ = \int dp \frac{1}{\tau_x^*} |G_x^R(p)|^2 \theta(-\omega) + 2 \int dp \text{Im}\Sigma_{\text{int}}^{(0)}(p)\theta(-\omega) [G_x^R(p)]^2 \quad (\text{A.79})$$

where we have expanded the second term to lowest order in n_x . As $1/\tau_x^*$ is a small parameter, the first term is dominated by on-shell contributions $\omega \simeq \zeta_p$ and we can write

$$\frac{1}{\tau_x^*} |G_x^R(p)|^2 \theta(-\omega) \simeq 2\pi Z \frac{1/2\tau_x^*}{1/2\tau_x^* + \text{Im}\Sigma_{\text{int}}(p)} \delta(\omega - \zeta_p) \theta(-\omega) \\ \simeq 2\pi Z \theta(-\omega) \delta(\omega - \zeta_p), \quad (\text{A.80})$$

where the last line follows from $\text{Im}\Sigma_{\text{int}}(p) \ll 1/\tau_x^*$ for onshell energies $\zeta_p \simeq \omega \leq 0$ consistent with the assumptions made in Sec. 7.3.4. The second term can be replaced by Eq. (A.77), which yields

$$-i \int dp G_x(p) = Z n_x + 2 \int dp \text{Im}G_x^A(k)\theta(-\epsilon) W^{(0)}(k, p) [G_x^R(p)]^2, \quad (\text{A.81})$$

where the density is $n_x = \mu_x^* v_x^*$. We have $\int dp W^{(0)}(k, p) [G_x^R(p)]^2 = -Z\partial_\omega \Sigma(p) = 1 - Z$ and, hence,

$$-i \int dp G_x(p) = n_x. \quad (\text{A.82})$$

A.6 PROOF OF EQ. (7.33) IN MAIN TEXT

We now demonstrate Eq. (7.33) of the main text, which reads

$$\frac{\mathbf{k}}{m_e} G_e(k) G_e(k + \Omega) \simeq \frac{\left(i\tau_e \Omega \frac{\mathbf{k}}{m_e} \partial_\epsilon + \partial_{\mathbf{k}} \right) G_e(k)}{1 - i\tau_e \Omega} \quad (\text{A.83})$$

to leading order in Ω and $1/\tau_e$, where $G_e = [\epsilon - \epsilon_{\mathbf{k}} + i(1/2\tau_e)\text{sgn}\epsilon]^{-1}$. We start by writing $G_e(k) = G_e^R(k) + 2i\text{Im}G_e^A(k)\theta(-\epsilon)$ and we obtain

$$\begin{aligned} G_e(k) G_e(k + \Omega) &= G_e^R(k) G_e^R(k + \Omega) \\ &+ \text{Re}G_e^R(k) 2i\text{Im}G_e^A(k + \Omega)\theta(-\epsilon - \Omega) + \text{Re}G_e^R(k + \Omega) 2i\text{Im}G_e^A(k)\theta(-\epsilon) \\ &+ 2\text{Im}G_e^A(k)\text{Im}G_e^A(k + \Omega)[\theta(-\epsilon) - \theta(-\epsilon - \Omega)] \end{aligned} \quad (\text{A.84})$$

We are interested in a result to zeroth order in Ω and $1/\tau_e$. At this order, all but the first term vanish everywhere except when $\epsilon = \epsilon_{\mathbf{k}}$. Our strategy is to expand these expressions in terms of δ functions around the resonance, for instance, we write

$$\text{Re}G_e^R(k)\text{Im}G_e^A(k + \Omega) = \alpha_0 \delta(\epsilon - \epsilon_{\mathbf{k}}) + \alpha_1 \delta'(\epsilon - \epsilon_{\mathbf{k}}) + \alpha_2 \delta''(\epsilon - \epsilon_{\mathbf{k}}) + \dots \quad (\text{A.85})$$

We can obtain the coefficients from the following integrals

$$\alpha_0 = \int d\epsilon \text{Re}G_e^R(k)\text{Im}G_e^A(k + \Omega) = \frac{-\pi\Omega}{\tau_e^{-2} + \Omega^2}, \quad (\text{A.86})$$

$$\alpha_1 = - \int d\epsilon (\epsilon - \epsilon_{\mathbf{k}}) \text{Re}G_e^R(k)\text{Im}G_e^A(k + \Omega) = -\frac{\pi[2(2\tau_e)^{-2} + \Omega^2]}{\tau_e^{-2} + \Omega^2}, \quad (\text{A.87})$$

$$\alpha_2 = \int d\epsilon (\epsilon - \epsilon_{\mathbf{k}})^2 \text{Re}G_e^R(k)\text{Im}G_e^A(k + \Omega) = -\frac{\pi\Omega[3(2\tau_e)^{-2} + \Omega^2]}{\tau_e^{-2} + \Omega^2}. \quad (\text{A.88})$$

The second order is already linear in the small parameters and can hence be ignored. The expansion then reads

$$\begin{aligned} \text{Re}G_e^R(k)\text{Im}G_e^A(k+\Omega) &\simeq \frac{\pi}{\tau_e^{-2} + \Omega^2} \left[-\Omega\delta(\epsilon - \epsilon_{\mathbf{k}}) - \right. \\ &\quad \left. \left(\frac{1}{2\tau_e^2} + \Omega^2 \right) \delta'(\epsilon - \epsilon_{\mathbf{k}}) \right]. \end{aligned} \quad (\text{A.89})$$

Similar considerations yield

$$\text{Re}G_e^R(k+\Omega)\text{Im}G_e^A(k) \simeq \frac{\pi}{\tau_e^{-2} + \Omega^2} \left[\Omega\delta(\epsilon - \epsilon_{\mathbf{k}}) - \frac{1}{2\tau_e^2} \delta'(\epsilon - \epsilon_{\mathbf{k}}) \right] \quad (\text{A.90})$$

$$\text{Im}G_e^A(k)\text{Im}G_e^A(k+\Omega) \simeq \frac{\pi}{\tau_e^{-2} + \Omega^2} \left[\frac{1}{\tau_e}\delta(\epsilon - \epsilon_{\mathbf{k}}) + \frac{\Omega}{2\tau_e} \delta'(\epsilon - \epsilon_{\mathbf{k}}) \right] \quad (\text{A.91})$$

Substituting these relations in Eq. (A.84) we find

$$G_e(k)G_e(k+\Omega) \simeq G_e^R(k)^2 - 2i\pi\delta'(\epsilon - \epsilon_{\mathbf{k}})\theta(-\epsilon) + \frac{2\pi\Omega\tau_e}{1-i\Omega\tau_e} \delta(\epsilon - \epsilon_{\mathbf{k}})\delta(\epsilon) \quad (\text{A.92})$$

where we have expanded the step function $\theta(-\epsilon - \Omega) \simeq \theta(-\epsilon) - \Omega\delta(\epsilon)$. The right-hand side of Eq. (A.83) can be evaluated explicitly using $G_e(k) = G_e^R(k) + 2\pi i\delta(\epsilon - \epsilon_{\mathbf{k}})\theta(-\epsilon)$. We obtain

$$\begin{aligned} \left(i\tau_e\Omega \frac{\mathbf{k}}{m_e} \partial_{\epsilon} + \partial_{\mathbf{k}} \right) G_e(k) &= (1 - i\tau_e\Omega) \frac{\mathbf{k}}{m_e} \left\{ G_e^R(k)^2 - 2\pi i\delta'(\epsilon - \epsilon_{\mathbf{k}})\theta(-\epsilon) \right. \\ &\quad \left. + \frac{2\pi\tau_e\Omega}{1-i\Omega\tau_e} \delta(\epsilon - \epsilon_{\mathbf{k}})\delta(\epsilon) \right\} \end{aligned} \quad (\text{A.93})$$

which concludes the proof.

A.7 MIGDAL-ELIASHBERG THEORY

To tackle the many-body problem we use a Green's functions approach. After doing a mean field approximation the electron-polariton Hamiltonian has a similar structure to the well understood electron-phonon Hamiltonian. Therefore, we will use Migdal-Eliashberg theory to analyze this system theoretically.

We start from the initial Hamiltonian in Eq. (8.1). When most of the polaritons are in the BEC ground state at $k = 0$ we can simplify this Hamiltonian using the Bogolyubov prescription [127], which is equivalent to mak-

ing the following replacement: $a_0 = a_0^\dagger = \sqrt{N_0}$ (N_0 is the number of polaritons in the condensate). This is followed by a Bogolyubov approximation which consists in ignoring terms of lower order in N_0 .

The resulting Hamiltonian is given in Eq. (8.4), which we reproduce here to keep the derivation self-consistent:

$$\begin{aligned} H &= \sum_{\mathbf{k}} \xi_{\mathbf{k}} e_{\mathbf{k}}^\dagger e_{\mathbf{k}} + \sum_{\mathbf{k} \neq 0} \Omega_{\mathbf{k}} a_{\mathbf{k}}^\dagger a_{\mathbf{k}} + \frac{1}{2A} \sum_{\mathbf{k}\mathbf{k}'\mathbf{q}} e_{\mathbf{k}+\mathbf{q}}^\dagger e_{\mathbf{k}'-\mathbf{q}}^\dagger e_{\mathbf{k}} e_{\mathbf{k}} \\ &\quad + \sum_{\mathbf{k} \neq 0} \frac{n_0 u_{\mathbf{k}}}{2} \left(a_{\mathbf{k}}^\dagger a_{-\mathbf{k}}^\dagger + a_{\mathbf{k}} a_{-\mathbf{k}} + 2a_{\mathbf{k}}^\dagger a_{\mathbf{k}} \right) + n_0 u_0 \sum_{\mathbf{k} \neq 0} a_{\mathbf{k}}^\dagger a_{\mathbf{k}} \\ &\quad + \sum_{\mathbf{k}\mathbf{k}'\mathbf{q}} \sqrt{\frac{n_0}{A}} v_{\mathbf{q}} e_{\mathbf{k}'+\mathbf{q}}^\dagger e_{\mathbf{k}'} \left(a_{\mathbf{q}}^\dagger - a_{\mathbf{q}} \right) \end{aligned} \quad (\text{A.94})$$

After the mean-field Bogolyubov approximation the electron-polariton interaction has the same structure as the electron-phonon interaction and therefore we can analyze it in analogy with the Migdal-Eliashberg theory, which is controlled by the small parameter $\hbar\omega_D/\epsilon_F$, the ratio of the characteristic phonon/electron energy scales. Although in doing the many body theory we treated all interactions simultaneously in order to avoid double counting, we choose to present our results in a more intuitive order.

We define the bare electron propagator in imaginary time as

$$\mathcal{G}_e^{(0)}(p) = -\langle T_\tau e_{\mathbf{k}}(\tau) e_{\mathbf{k}}^\dagger(0) \rangle = \frac{1}{i\omega_n - \xi_{\mathbf{k}}}, \quad (\text{A.95})$$

where $p = (i\omega_n, \mathbf{k})$ and $e_{\mathbf{k}}(\tau) \equiv e^{H\tau} e_{\mathbf{k}} e^{-H\tau}$. Notice that in this appendix we will work with Green's functions in imaginary time, which we will denote by \mathcal{G} , although a very similar derivation could be done in terms of the time-ordered Green's functions that we have used in the rest of this thesis.

In light of the following analysis we define the bare polariton propagator as

$$\mathcal{G}_{11}^{(0)}(p) = -\langle T_\tau a_{\mathbf{k}}(\tau) a_{\mathbf{k}}^\dagger(0) \rangle = \frac{1}{i\omega_n - \Omega_{\mathbf{k}}}. \quad (\text{A.96})$$

The analogy with phonons is made by introducing a phonon-like operator and propagator:

$$\begin{aligned} A_{\mathbf{q}} &\equiv a_{\mathbf{q}} + a_{-\mathbf{q}}^\dagger, \\ \mathcal{D}(\mathbf{q}, \tau) &\equiv -\langle T_\tau A_{\mathbf{q}}(\tau) A_{-\mathbf{q}}(0) \rangle. \end{aligned} \quad (\text{A.97})$$

In the absence of interactions we have:

$$\mathcal{D}^{(0)}(p) = \mathcal{G}_{11}^{(0)}(p) + \mathcal{G}_{11}^{(0)}(-p) = \frac{2\Omega_{\mathbf{k}}}{(i\omega_n)^2 - \Omega_{\mathbf{k}}^2}. \quad (\text{A.98})$$

As mentioned above we will understand the electron-polariton interaction in terms of the Migdal Eliashberg theory of the electron-phonon interaction. To make any progress, we need to make a Born-Oppenheimer approximation, which in the many-body physics language means that we ignore the electron-phonon vertex corrections due to phonons. This approach is justified by Migdal's theorem [128]. We give a brief argument, based on a phase space analysis, that summarizes Migdal's theorem as it applies to our system. For a more rigorous proof one should check Refs. [111, 128].

As we will show in the following sections most of the polaritons that interact with the electrons on the Fermi surface are found in a narrow energy interval. Therefore, we can associate an energy scale to the polaritons which we will denote by ω_D , in analogy with the Debye energy in the phonon case. We will define this energy quantitatively below but for now we will assume that such an energy scale can be associated to the polaritons and furthermore we make the assumption that $\hbar\omega_D \ll \epsilon_F$.

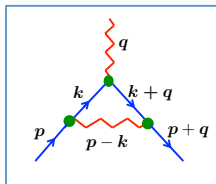


FIGURE A.1: First vertex correction diagram. In blue are the electron propagators while in red are the polariton propagator.

Let us consider the first correction to the electron-polariton vertex, with the corresponding Feynman diagram presented in Figure A.1. If this correction can be ignored than we can certainly ignore the higher order corrections. Suppose a polariton of momentum \mathbf{q} decays and forms an electron-hole pair of momenta $\mathbf{k} + \mathbf{q}$ and \mathbf{k} respectively. This pair will be coherent for a distance of $1/|\mathbf{q}|$. Since the electrons move at roughly the Fermi velocity this gives us a coherence timescale of $1/|\mathbf{q}|v_F$. Only in this timescale electrons can be scattered again. Since the polaritons take much longer to respond we expect this vertex correction to be of order $\omega_D/|\mathbf{q}|v_F$. The average momentum of the phonon is of the order of k_F so we expect the vertex

correction to depend on the small parameter $\hbar\omega_D/\epsilon_F$. (If we wish to be more accurate the first vertex correction is of the order of $\lambda\hbar\omega_D/\epsilon_F$, where λ is the electron-polariton coupling constant to be defined below). Thus, we can safely conclude that vertex corrections can be ignored.

The only nontrivial effect of many-body interactions between electrons is the renormalisation of interaction between quasiparticles, i.e. screening [110]. In the following we will explore the screening of both the electron-electron and the electron-polariton interactions in the random phase approximation (RPA). This effect appears as a renormalisation of the photon propagator, where, according to the RPA approximation, the photon proper self-energy is approximated by the simplest polarisation bubble.

In the RPA framework, the screened electron-electron and electron-polariton interaction is expressed in terms of the dielectric function $\epsilon(\mathbf{q}, i\omega_n)$, which has the following analytical form:

$$\begin{aligned}\epsilon(\mathbf{k}, i\omega_n) &= 1 - V_{\mathbf{k}}\chi_0(\mathbf{k}, i\omega_n), \\ \chi_0(\mathbf{k}, i\omega_n) &= \frac{1}{\beta} \sum_{\mathbf{k}, ik_n} \mathcal{G}^{(0)}(\mathbf{k} + \mathbf{q}, i\omega_n + ik_n) \mathcal{G}^{(0)}(\mathbf{k}, ik_n) \\ &= \sum_{\mathbf{k}} \frac{n_F(\xi_{\mathbf{k}}) - n_F(\xi_{\mathbf{k}+\mathbf{q}})}{i\omega_n + \xi_{\mathbf{k}} - \xi_{\mathbf{k}+\mathbf{q}}}, \\ \chi(\mathbf{k}, i\omega_n) &= \frac{\chi_0(\mathbf{k}, i\omega_n)}{\epsilon(\mathbf{k}, i\omega_n)}.\end{aligned}\tag{A.99}$$

In the above, $n_F(\epsilon)$ is the Fermi distribution function. The polarisation bubble χ_0 is the Lindhard function and denotes the linear response to a perturbation when electron-electron interactions are neglected. In this case the perturbation disturbs the electron system and creates electron-hole pairs and thus polarising the system. In contrast, the screened polarisation bubble χ is the response function when electron-electron interactions have been taken into account in the RPA.

The dielectric function for a 2D system at zero temperature has been calculated for the first time in Ref. [129]. The poles of the dielectric function give us the collective excitations of the electron system, the plasmons. Unless otherwise indicated, for the rest of the paper we will take the static limit, (a.k.a. the Thomas-Fermi limit) because it is easier to handle. This limit is accurate as long as the frequencies involved are much smaller than

the plasma frequency (in 2D, the only regime where this limit is not satisfied is at very small momenta). In the static limit we have:

$$\epsilon(\mathbf{k}, \omega) \approx \epsilon(\mathbf{k}, 0) = \frac{1}{1 + \frac{k_{TF}}{|\mathbf{k}|}}, \quad (\text{A.100})$$

where $k_{TF} = m_e e^2 / (2\pi\epsilon\hbar^2) = 2/a_B$ is the Thomas-Fermi wavevector.

In terms of this dielectric function, the screened electron-electron and electron-polariton interaction is given by:

$$\begin{aligned} \tilde{V}_{\mathbf{k}} &= \frac{V_{\mathbf{k}}}{\epsilon(\mathbf{k})}, \\ \tilde{v}_{\mathbf{k}} &= \frac{v_{\mathbf{k}}}{\epsilon(\mathbf{k})}. \end{aligned} \quad (\text{A.101})$$

The dilute Bose-condensed gas is another one of the few many body systems that are well understood. In this case the small parameter which allows a controlled expansion is given by $n_0 a^2$, where n_0 is the polariton density and a is the scattering length of the bosonic repulsion. The field theoretical treatment of the problem was first developed by Beliaev [130]. A more accessible exposition of this formalism is presented in Ref. [131].

In addition to the normal polariton propagator introduced above, when interactions are turned on there is an additional anomalous propagator that must be considered. Together, these propagators satisfy the Dyson-Beliaev equations. These equations can be written more compactly by introducing two additional propagators, which are, however, not independent of these two. In the end, the 4 propagators that need to be considered are:

$$\begin{aligned} \mathcal{G}_{11}(\mathbf{k}, \tau) &= -\langle T_{\tau} a_{\mathbf{k}}(\tau) a_{\mathbf{k}}^\dagger(0) \rangle, \\ \mathcal{G}_{12}(\mathbf{k}, \tau) &= -\langle T_{\tau} a_{\mathbf{k}}(\tau) a_{+\mathbf{k}}(0) \rangle, \\ \mathcal{G}_{21}(\mathbf{k}, \tau) &= -\langle T_{\tau} a_{-\mathbf{k}}^\dagger(\tau) a_{\mathbf{k}}^\dagger(0) \rangle, \\ \mathcal{G}_{22}(\mathbf{k}, \tau) &= -\langle T_{\tau} a_{-\mathbf{k}}^\dagger(\tau) a_{-\mathbf{k}}(0) \rangle. \end{aligned} \quad (\text{A.102})$$

These propagators and the associated self energies are not independent but satisfy the following identities:

$$\begin{aligned} \mathcal{G}_{22}(p) &= \mathcal{G}_{11}(-p), & \mathcal{G}_{12}(p) &= \mathcal{G}_{21}(-p), \\ \Sigma_{22}(p) &= \Sigma_{11}(-p), & \Sigma_{12}(p) &= \Sigma_{21}(-p).. \end{aligned} \quad (\text{A.103})$$

Solving the Dyson-Beliaev equations in the Bogolyubov approximation and making the RPA approximation we obtain the renormalised propagators:

$$\begin{aligned}\mathcal{G}_{11}(p) &= \frac{i\omega_n + \Omega_{\mathbf{k}} + \Sigma_{12}(p)}{(i\omega_n)^2 - \Omega_{\mathbf{k}}^2 - 2\Omega_{\mathbf{k}}\Sigma_{12}(p)}, \\ \mathcal{G}_{12}(p) &= \frac{-\Sigma_{12}(p)}{(i\omega_n)^2 - \Omega_{\mathbf{k}}^2 - 2\Omega_{\mathbf{k}}\Sigma_{12}(p)}, \\ \Sigma_{12}(p) &= N_0 \left[u_{\mathbf{k}} + \chi(\mathbf{k}, i\omega_n) v_{\mathbf{k}}^2 \right].\end{aligned}\quad (\text{A.104})$$

The dispersion of the renormalised polaritons, denoted by $\tilde{\Omega}_{\mathbf{k}}$, is obtained from the zeros of the real part of the denominator, therefore:

$$\tilde{\Omega}_{\mathbf{k}} = \sqrt{\Omega_{\mathbf{k}}^2 + 2\Omega_{\mathbf{k}}N_0 [u_{\mathbf{k}} + \chi(\mathbf{k})v_{\mathbf{k}}^2]}, \quad (\text{A.105})$$

where we made the approximation $\text{Re}[\chi(\mathbf{k}, i\omega_n)] \approx \chi(\mathbf{k})$. Notice that the effect of electron-polariton interaction is to renormalise the polariton-polariton interaction. Because this is a second order interaction the effect is proportional to the square of the bare electron-polariton interaction and the response function χ which also contains the effects due to screening.

The polariton spectral function linewidth comes from the imaginary part of the response function, which is zero in the static limit, so we need to use the frequency dependent response function to calculate the polariton linewidth. Using $\Omega_{\mathbf{k}} |\text{Im}[\Sigma_{12}(\mathbf{k}, \omega)]| = \tilde{\Omega}_{\mathbf{k}} \gamma_{\mathbf{k}}$ ($\gamma_{\mathbf{k}}$ is the polariton linewidth) we obtain, in the limit $|\text{Im}[\epsilon(\mathbf{k}, \omega)]| \ll |\text{Re}[\epsilon(\mathbf{k}, \omega)]|$, the following expression for the polariton linewidth:

$$\begin{aligned}\gamma_{\mathbf{q}} &= 2 \frac{N_0 v_{\mathbf{q}}^2}{\epsilon^2(\mathbf{q})} \frac{\Omega_{\mathbf{q}}}{\tilde{\Omega}_{\mathbf{q}}} \text{Im} [\chi_0(q, \tilde{\Omega}_{\mathbf{q}})] \\ &= 2\pi \frac{N_0 v_{\mathbf{q}}^2}{\epsilon^2(\mathbf{q})} \frac{\Omega_{\mathbf{q}}}{\tilde{\Omega}_{\mathbf{q}}} \sum_{\mathbf{k}} (n_F(\xi_{\mathbf{k}}) - n_F(\xi_{\mathbf{k}+\mathbf{q}})) \\ &\quad \cdot \delta(\tilde{\Omega}_{\mathbf{q}} - \xi_{\mathbf{k}} + \xi_{\mathbf{k}+\mathbf{q}}).\end{aligned}\quad (\text{A.106})$$

As mentioned above, the polarisation bubble has been evaluated exactly in Ref. [129] but to get a simpler analytical formula we make the following approximation. At low temperatures the Fermi factors restrict the k integration to a narrow region about the Fermi surface of width $\tilde{\Omega}_{\mathbf{q}}$, so for

reasonably well behaved Fermi surfaces we can replace these factors with $\tilde{\Omega}_{\mathbf{q}}\delta(\xi_{\mathbf{k}})$ to obtain:

$$\gamma_{\mathbf{q}} \approx 2\pi \frac{N_0 v_{\mathbf{q}}^2}{\epsilon^2(\mathbf{q})} \frac{\Omega_{\mathbf{q}}}{\tilde{\Omega}_{\mathbf{q}}} \tilde{\Omega}_{\mathbf{q}} \sum_{\mathbf{k}} \delta(\xi_{\mathbf{k}}) \delta(\xi_{\mathbf{k}+\mathbf{q}}). \quad (\text{A.107})$$

We remark that the same result can be obtained using Fermi's golden rule if we consider the renormalised electron polariton interactions to be given by $\tilde{M}_{\mathbf{q}} = \sqrt{\frac{N_0 v_{\mathbf{q}}^2}{\epsilon^2(\mathbf{q})} \frac{\Omega_{\mathbf{q}}}{\tilde{\Omega}_{\mathbf{q}}}}$ as shown in Refs. [132, 133]. We will find out below that this is indeed the proper renormalised electron-polariton interaction.

Evaluating the sum we obtain:

$$\frac{\gamma_{\mathbf{q}}}{\tilde{\Omega}_{\mathbf{q}}} \approx \frac{\tilde{M}_{\mathbf{q}}^2 N(0)}{\epsilon_F} \frac{2k_F}{|\mathbf{q}| \sqrt{1 - (|\mathbf{q}|/2k_F)^2}}, \quad (\text{A.108})$$

where $N(0)$ is the electron density of states at the the Fermi surface. In order to have long lived quasi-particles we need to satisfy $\gamma_{\mathbf{q}}/\tilde{\Omega}_{\mathbf{q}} \ll 1$.

Having discussed the condensate properties in a field theoretical formalism, we investigate the effect of the condensate on the electrons and we see that polariton excitations can mediate an attractive interaction between electrons.

In the presence of interactions, the phonon like propagator introduced in Eq. (A.97) has the form:

$$\begin{aligned} \mathcal{D}(p) &= \mathcal{G}_{11}(p) + \mathcal{G}_{22}(p) + \mathcal{G}_{12}(p) + \mathcal{G}_{21}(p) \\ &= \frac{2\Omega_{\mathbf{k}}}{(i\omega_n)^2 - \tilde{\Omega}_{\mathbf{k}}^2 - 2i\gamma_{\mathbf{q}}\tilde{\Omega}_{\mathbf{q}}}. \end{aligned} \quad (\text{A.109})$$

Notice that the propagator depends on both the bare and the renormalised polariton spectrum. As usual [110], we define a *reduced* propagator $\bar{\mathcal{D}}$ which corresponds to the propagation of the new polariton quasi-particles and therefore depends only on the renormalized quasi-particles' spectrum:

$$\mathcal{D}(p) = \frac{\Omega_{\mathbf{k}}}{\tilde{\Omega}_{\mathbf{k}}} \bar{\mathcal{D}}(p). \quad (\text{A.110})$$

The polariton mediated electron-electron attraction can be expressed in terms of this propagator:

$$\begin{aligned} V_{e-e}^{(eff)}(p) &= \frac{V_{\mathbf{k}}}{\epsilon(\mathbf{k})} + \frac{N_0 v_{\mathbf{k}}^2}{\epsilon^2(\mathbf{k})} \mathcal{D}(p) \\ &= \frac{V_{\mathbf{k}}}{\epsilon(\mathbf{k})} + \tilde{M}_{\mathbf{k}}^2 \bar{\mathcal{D}}(p), \end{aligned} \quad (\text{A.111})$$

where we have introduced the renormalised electron-polariton matrix element

$$\tilde{M}_{\mathbf{q}} = \sqrt{\frac{N_0 v_{\mathbf{q}}^2}{\epsilon^2(\mathbf{q})} \frac{\Omega_{\mathbf{q}}}{\tilde{\Omega}_{\mathbf{q}}}}. \quad (\text{A.112})$$

Notice that the term $\Omega_{\mathbf{k}}/\tilde{\Omega}_{\mathbf{k}}$ from the initial propagator $\mathcal{D}(p)$ has been absorbed in the electron-polariton matrix element. In the previous section we noticed that this is necessary in order to obtain the same polariton linewidth as the one calculated using Fermi's golden rule and now we have seen why.

We also investigate the electron self energy acquired through interactions with polaritons. This contribution is small but its derivative with respect to energy is large within ω_D of the Fermi surface. Therefore it will strongly affect the electrons within ω_D of the Fermi surface. The main effects are a renormalised mass and a finite quasi particle linewidth.

The contribution of the polaritons to the electron self-energy has the following analytical form:

$$\begin{aligned} \Sigma(\mathbf{k}, i\omega_n) &= -\frac{1}{\beta} \sum_{iq_n} \int \frac{d^2 \mathbf{q}}{(2\pi)^2} \tilde{M}_{\mathbf{q}} \bar{\mathcal{D}}(\mathbf{q}, iq_n) \\ &\quad \cdot \mathcal{G}^{(0)}(\mathbf{k} + \mathbf{q}, i\omega_n + iq_n). \end{aligned} \quad (\text{A.113})$$

The resulting effects are conventionally expressed in terms of the Eliashberg function $\alpha^2 F(\omega)$. This function is closely related to the polariton density of states:

$$F(\omega) = \sum_{\mathbf{q}} \delta(\omega - \tilde{\Omega}_{\mathbf{q}}). \quad (\text{A.114})$$

However, the connection is somewhat obscured in the usual definition:

$$\alpha^2 F(\omega) = \sum_{\mathbf{k}, \mathbf{k}'} |\tilde{M}_{\mathbf{k}-\mathbf{k}'}|^2 \delta(\omega - \tilde{\Omega}_{\mathbf{k}-\mathbf{k}'}) \delta(\xi_{\mathbf{k}}) \delta(\xi_{\mathbf{k}'}) / N(0). \quad (\text{A.115})$$

The above function can be expressed in terms of the previously investigated polariton linewidth $\gamma_{\mathbf{q}}$:

$$\alpha^2 F(\omega) = \frac{2}{\pi} N(0) \omega \sum_{\mathbf{q}} \gamma_{\mathbf{q}} \delta(\omega - \tilde{\Omega}_{\mathbf{q}}). \quad (\text{A.116})$$

Most properties of the electron-polariton interaction can be expressed in terms of the EPC (electron-polariton coupling in our case) constant λ and averages $\langle \omega^n \rangle$, where n are integers and the average is taken with respect to the weight function $\alpha^2 F(\omega)$. For example, the Debye frequency that we defined above can be expressed quantitatively as:

$$\omega_D \equiv \langle \omega \rangle = 2 \int_0^\infty d\omega \alpha^2 F(\omega) / \lambda. \quad (\text{A.117})$$

The definition of the EPC constant is:

$$\lambda = 2 \int \frac{d\omega \alpha^2 F(\omega)}{\omega}. \quad (\text{A.118})$$

This constant can also be expressed in terms of the $\lambda_{\mathbf{q}}$ which makes explicit the contribution of polaritons with different momenta:

$$\lambda = \frac{1}{N} \sum_{\mathbf{q}} \lambda_{\mathbf{q}} = \frac{1}{\pi N(0)} \sum_{\mathbf{q}} \frac{\gamma_{\mathbf{q}}}{\tilde{\Omega}_{\mathbf{q}}^2}, \quad (\text{A.119})$$

where N is the total number of electrons, which in $2D$ is given by $N = N(0)\epsilon_F$.

Returning to the electron self energy due to interactions with polaritons, the real part results in a mass renormalisation of the electron quasi particle given by:

$$m_e^* = m_e(1 + \lambda) \rightarrow \xi_k = \frac{\xi_k}{1 + \lambda}. \quad (\text{A.120})$$

The imaginary part of the self energy gives the electron quasi particle linewidth Γ . At zero temperature [134]:

$$\Gamma(\omega) = \pi \int_0^\omega d\omega' \alpha^2 F(\omega'). \quad (\text{A.121})$$

Clearly, the electron quasi-particles with energies close to the polariton energy scale ω_D will be short lived because electrons will be able to lose their energy to excite polaritons. For these electrons, the quasi particle picture fails. However, in our system, we have the following energy scale $k_B T_c \ll \omega_D$. Therefore, we expect that the superconducting electrons will not be affected by dissipation due to polaritons, so we can still use the quasi particle picture.

A.7.0.1 Finite polariton spectral function linewidth

In the previous discussion we have treated the polaritons as perfect quasi-particles. When the linewidth of the polariton spectral function becomes significant the Eliashberg function needs to be modified and is broadened:

$$\begin{aligned}\alpha^2 F(\omega) &= \sum_{\mathbf{k}, \mathbf{k}'} |\tilde{M}_{\mathbf{k}-\mathbf{k}'}|^2 B(\mathbf{k}-\mathbf{k}', \omega) \delta(\xi_{\mathbf{k}}) \delta(\xi'_{\mathbf{k}'}) / N(0), \\ B(\mathbf{q}, \omega) &= \frac{1}{\pi} \text{Im}[\bar{D}(\mathbf{q}, \omega)] = \frac{1}{\pi} \text{Im} \left[\frac{2\tilde{\Omega}_{\mathbf{q}}}{\omega^2 - \tilde{\Omega}_{\mathbf{q}}^2 - 2i\gamma_{\mathbf{q}}\tilde{\Omega}_{\mathbf{q}}} \right],\end{aligned}\quad (\text{A.122})$$

where the Lorentzian $B(\mathbf{q}, \omega)$ is the polariton spectral function. We are interested in how the finite-polariton lie width will influence the superconducting properties of the electron system.

The first question that we need to ask is whether the electrons remain good quasi-particles. As shown in Refs. [132, 133], when the finite polariton - linewidth is included the electron lifetime scales as ε^2 close to the Fermi surface. Therefore electrons close to the Fermi surface are well-defined quasi-particles. In all our numerical simulations we checked that electrons are well defined quasiparticles in a shell of the order of $k_B T_c$, where T_c is the superconducting critical temperature.

According to McMillan's formula in Eq. (A.127) the superconducting critical temperature can be expressed in terms of 4 constants: $\mu^*, \lambda, \omega_{log} = \exp[\langle \ln(\omega) \rangle]$, $\bar{\omega}_2 = \langle \omega^2 \rangle^{1/2}$ (the averages are taken with respect to the weight function $\alpha^2(\omega)F(\omega)/\omega$). Only the last 3 constants will be affected by the broadening of the Eliashberg function. Furthermore, for large λ the critical temperature $T_c \propto \sqrt{\lambda}\bar{\omega}_2$, therefore we will only investigate how these constants are modified.

We can rewrite λ as:

$$\lambda = 2 \sum_{\mathbf{k}, \mathbf{q}} |\tilde{M}_{\mathbf{q}}|^2 \delta(\xi_{\mathbf{k}}) \delta(\xi_{\mathbf{k}+\mathbf{q}}) \frac{1}{N(0)} \int_0^\infty d\omega \frac{B(\mathbf{q}, \omega)}{\omega}. \quad (\text{A.123})$$

However, by definition:

$$\bar{D}(\mathbf{q}, \omega) = \int_{-\infty}^{\infty} d\omega' \frac{B(\mathbf{q}, \omega')}{\omega' - \omega + i\delta}. \quad (\text{A.124})$$

Using the oddness of $B(\mathbf{q}, \omega)$ we obtain:

$$\int_0^\infty d\omega \frac{B(\mathbf{q}, \omega)}{\omega} = -\frac{\bar{D}(\mathbf{q}, 0)}{2} = \frac{\tilde{\Omega}_{\mathbf{q}}}{\tilde{\Omega}_{\mathbf{q}}^2(0)}, \quad (\text{A.125})$$

where $\tilde{\Omega}_{\mathbf{q}}(0)$ denotes renormalised polariton energy obtained by using the static (Thomas-Fermi) dielectric function. Thus, when the finite polariton lifetime is taken into account, λ should be calculated using the polariton energies obtained from the static limit for the polarisation bubble (which is actually what we already did to simplify calculations).

We now investigate the effect of the broadened Eliashberg function on $\lambda\langle\omega^2\rangle$:

$$\begin{aligned} \lambda\langle\omega^2\rangle &= 2 \sum_{\mathbf{k}, \mathbf{q}} |\tilde{M}_{\mathbf{q}}|^2 \delta(\xi_{\mathbf{k}}) \delta(\xi_{\mathbf{k}+\mathbf{q}}) \frac{1}{N(0)} \int_0^\infty d\omega \omega B(\mathbf{q}, \omega) \\ &= 2 \sum_{\mathbf{k}, \mathbf{q}} |\tilde{M}_{\mathbf{q}}|^2 \tilde{\Omega}_{\mathbf{q}} \delta(\xi_{\mathbf{k}}) \delta(\xi_{\mathbf{k}+\mathbf{q}}) \frac{1}{N(0)}, \end{aligned} \quad (\text{A.126})$$

where we used the well known [133] sum rule $\tilde{\Omega}_{\mathbf{q}} = \int_0^\infty d\omega \omega B(\mathbf{q}, \omega)$. Therefore $\lambda\langle\omega^2\rangle$ is not affected at all by the broadening of the Eliashberg function.

In conclusion we can safely neglect the effect of the polariton linewidth on the superconducting properties of the 2DES.

A.8 SUPERCONDUCTIVITY

In this section we briefly review the methods that can be used to calculate the critical temperature of a polariton-mediated superconductor. This discussion is necessary in the polariton community in order to make clear the connection to superconductivity and to see in which ways our system behaves as a conventional/unconventional superconductor.

We mention that it is notoriously difficult to make quantitative theoretical predictions of the superconducting properties of a new material. However, this limitation is due to the lack of knowledge of the normal state of the material and not due to the accuracy of the BCS theory. In metals, many complications arise which do not concern us, i.e. the choice of the bare pseudopotential describing electron-ion interaction, phonon polarisation vectors, Umklapp processes, distortions of the Fermi surface, etc. However, in our system the normal state can be more readily investigated,

because the bosons and the fermions can be separated and investigated separately. In this respect, this type of superconductivity is most similar to the superconductivity in doped semiconductors, which are, in this sense, the best understood superconductors [135].

In previous work on polariton mediated superconductivity, not only renormalisation effects have been ignored, but also the method used to calculate the critical temperature is not valid. Therefore, in this section we review the methods that can be used to make reliable predictions about a new superconductor given that the normal state is known and we point out the reason why the predictions made in previous work cannot be taken seriously.

In Section A.8.1 we present McMillan's equation, which is the simplest method to obtain the critical temperature of a superconductor given some system parameters¹. Then, in Section A.8.2 we introduce the BCS gap equation, which was initially used by Bardeen, Cooper, and Schrieffer to theoretically explain superconductivity, in order to explain the discrepancy between our results and the results obtained in previous work [103] in Section A.8.3.

A.8.1 *McMillan equation*

The state of the art in the theory of superconductivity are the Eliashberg equations, obtained in a Green's Function formalism. In certain limits they can be reduced to a set of two coupled integral equations which must be solved self-consistently. In some limits, which we will present below, these equations can be solved analytically to obtain the critical temperature of the superconductor [114]. Further correction factors can be introduced by fitting to the exact results obtained by numerically solving the Eliashberg equations, to obtain, as shown in Ref. [115]:

$$\begin{aligned}
 k_B T_c &= \frac{f_1 f_2 \omega_{log}}{1.2} \exp \left[-\frac{1.04(1+\lambda)}{\lambda(1-0.62\mu^*) - \mu^*} \right] \\
 f_1 &= \left[1 + (\lambda/\Lambda_1)^{3/2} \right]^{1/3}, f_2 = 1 + \frac{(\bar{\omega}_2/\omega_{log} - 1) \lambda^2}{\lambda^2 + \Lambda_2^2} \\
 \Lambda_1 &= 2.46(1+3.8\mu^*), \Lambda_2 = 1.82(1+6.3\mu^*)(\bar{\omega}_2/\omega_{log}) \\
 \mu^* &= \frac{\mu}{1 + \mu \ln(\epsilon_F/\hbar\omega_D)}
 \end{aligned} \tag{A.127}$$

¹ Usually, the McMillan formula is used the other way around: given a critical temperature, system parameters like the EPC constant λ can be calculated

In the above $\omega_{log} = \exp [\langle \ln(\omega) \rangle]$, $\bar{\omega}_2 = \langle \omega^2 \rangle^{1/2}$ (the averages are taken with respect to the weight function $\alpha^2(\omega)F(\omega)/\omega$), and μ , the screened Coulomb repulsion between electrons averaged over the Fermi surface, is given by:

$$\mu = \sum_{\mathbf{k}, \mathbf{k}'} \frac{V_{\mathbf{k}-\mathbf{k}'}}{\epsilon(\mathbf{k}-\mathbf{k}')} \delta(\xi_{\mathbf{k}}) \delta(\xi'_{\mathbf{k}'}) / N(0). \quad (\text{A.128})$$

According to Ref. [115], the above formula, known as McMillan's formula, is accurate for μ^* ranging between $0 < \mu^* < 0.2$ and $0.3 < \lambda < 10$. Therefore, in order to know the critical temperature of a superconductor, we need to know four material constants $\lambda, \omega_{log}, \bar{\omega}_2$ and μ^* . The difficulty lies in accurately determining these parameters. In our case, due to the simplicity of our system, we expect these parameters to be close to the theoretical predictions.

It is useful to express the parameters λ and μ as momentum integrals, rather than frequency integrals. In this case simple analytical expressions can be obtained:

$$\begin{aligned} \lambda &= \frac{2N(0)}{\pi k_F} \int_0^{2k_F} dq \frac{\tilde{M}_q^2}{\tilde{\Omega}_q} \left[1 - \left(\frac{q}{2k_F} \right)^2 \right]^{-1/2}, \\ \mu &= \frac{N(0)}{\pi k_F} \int_0^{2k_F} dq V_q \left[1 - \left(\frac{q}{2k_F} \right)^2 \right]^{-1/2}. \end{aligned} \quad (\text{A.129})$$

A.8.2 Superconducting gap equation

We wish to compare our method to the method used in previous work on polariton-mediated superconductivity. In order to make this comparison, we show how the superconducting critical temperature can be obtained from a Hamiltonian formalism. Since this section is only meant for comparison we do not consider any renormalisation effects, or the Coulomb repulsion. Therefore, our starting Hamiltonian will be:

$$\begin{aligned} H &= \sum_{\mathbf{k}} \xi_{\mathbf{k}} e_{\mathbf{k}}^\dagger e_{\mathbf{k}} + \sum_{\mathbf{q}} \tilde{\Omega}_{\mathbf{q}} a_{\mathbf{q}}^\dagger a_{\mathbf{q}} \\ &\quad + \sum_{\mathbf{k}, \mathbf{q}} \tilde{M}_{\mathbf{q}} \left(a_{\mathbf{q}} + a_{-\mathbf{q}}^\dagger \right) e_{\mathbf{k}+\mathbf{q}}^\dagger e_{\mathbf{k}}. \end{aligned} \quad (\text{A.130})$$

In a Hamiltonian formalism one can obtain an integral equation for the gap function, provided one can trace out the polaritons to obtain an electron-electron attractive interaction between Cooper pairs such that:

$$H_{eff} = V(\mathbf{k}, \mathbf{k}') e_{\mathbf{k}'}^\dagger e_{-\mathbf{k}'}^\dagger e_{\mathbf{k}} e_{-\mathbf{k}}. \quad (\text{A.131})$$

Supposing that this Hamiltonian can be obtained, then one can apply the methods first introduced by Bardeen, Cooper and Schrieffer [136] to obtain the following BCS gap equation (at zero temperature):

$$\Delta(\mathbf{k}) = \sum_{\mathbf{k}'} V(\mathbf{k}, \mathbf{k}') \frac{\Delta(\mathbf{k}')}{2\sqrt{\Delta(\mathbf{k}')^2 + \xi_{\mathbf{k}'}}}. \quad (\text{A.132})$$

Going to a continuum and changing variables from k to ε, θ we obtain the above equation in a more convenient form:

$$\Delta(\varepsilon) = \int_{-\epsilon_F}^{\epsilon_F} d\varepsilon' \frac{\Delta(\varepsilon')}{2\sqrt{\Delta(\varepsilon')^2 + \varepsilon'}} V(\varepsilon - \varepsilon'). \quad (\text{A.133})$$

It is not at all obvious how to correctly trace out the polaritons to obtain an electron-electron effective interaction, mainly due to the retarded nature of this interaction [137]. We briefly present three methods and comment on their validity:

$$\begin{aligned} V^F(\mathbf{k}, \mathbf{k}') &= \frac{2|\tilde{M}_{\mathbf{q}}|^2 \tilde{\Omega}_{\mathbf{q}}}{\Delta\varepsilon^2 - \tilde{\Omega}_{\mathbf{q}}^2}, \\ V^{BCS}(\mathbf{k}, \mathbf{k}') &= \begin{cases} -\frac{2|\tilde{M}_{\mathbf{q}}|^2}{\tilde{\Omega}_{\mathbf{q}}} & , \text{if } |\Delta\varepsilon| < \omega_D \\ 0 & , \text{otherwise} \end{cases}, \\ V^S(\mathbf{k}, \mathbf{k}') &= -\frac{2|\tilde{M}_{\mathbf{q}}|^2}{|\Delta\varepsilon| + \tilde{\Omega}_{\mathbf{q}}}, \end{aligned} \quad (\text{A.134})$$

where $\mathbf{q} = \mathbf{k} - \mathbf{k}'$ and $\Delta\varepsilon = \xi_{\mathbf{k}'} - \xi_{\mathbf{k}}$.

The first effective potential V^F was initially derived by Fröhlich [113] through a Schrieffer-Wolff transformation to leading order in the electron-phonon coupling. Notice that it has a resonance singularity, which means that at that point higher order terms in the Schrieffer-Wolff transformation become important. However, the singularity is eliminated when performing the (principal value) angular integral which appears from changing variables in going from Eq. (A.132) to Eq. (A.133).

To eliminate the singularity of the Fröhlich potential, Bardeen et.al. approximated the Fröhlich Hamiltonian by a box potential V^{BCS} . Such a simplification is possible because the potential is integrated over in the gap equation, making the details of the potential insignificant. However, the price to be paid is the introduction of a fitting parameter ω_D . This means, that the BCS potential can be used to explain superconductivity but not to predict it, because of the unknown ω_D .

The last approach involves a more suitable renormalization procedure, which involves continuous unitary transformations. In this regard we mention the similarity renormalization first introduced by Glazek and Wilson [138] and the flow equations introduced by Wegner [139]. It has been shown [140] that the potential obtained through similarity renormalisation techniques V^S can predict accurately the superconducting critical temperature.

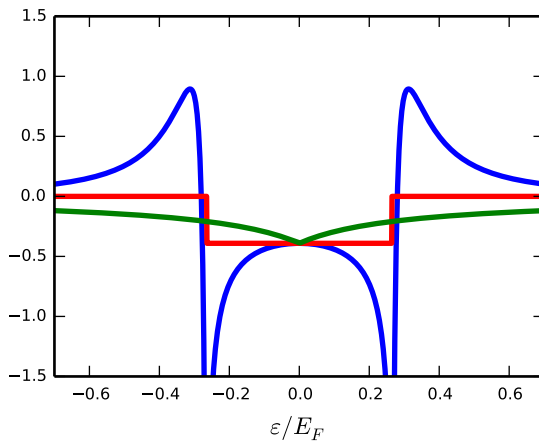


FIGURE A.2: Comparison between $V^F(\varepsilon)$ (blue), $V^{BCS}(\varepsilon)$ (red) and $V^S(\varepsilon)$ (green).

For the BCS potential we choose $\omega_D = g_0$. For simulations we used typical GaAs parameters, the same parameters used for the solid lines in Figure 8.2.

To compare the different approaches we plot the three potentials $V(\varepsilon)$ on top of each other in Figure A.2. Notice that at the FS (i.e. $\varepsilon = 0$) all the potentials agree with each other, as they should since at this point the potential corresponds to real processes.

A.8.3 Comparison to previous work

In the previous work on polariton-mediated superconductivity [46, 103, 104], the authors used the Fröhlich potential $V^F(\varepsilon)$. Notice that, although this potential is non-singular after being integrated, it still develops two large shoulders close to the Debye energy. The dependence of the critical temperature on the size and width of the shoulders has been investigated in Ref. [46] and they have been used to predict a large critical temperatures obtainable in polariton-mediated superconductivity. As we discussed in the main text, we find much smaller T_c for similar system parameters. Another consequence of the use of the Fröhlich potential is the appearance of an oscillatory gap, which again has been treated as a peculiarity of polariton-mediated superconductivity. We argue on the other hand that the peculiarities mentioned above are by no means unique to polariton-mediated superconductivity. Instead, their appearance is due to the use of the Fröhlich potential.

BIBLIOGRAPHY

1. Carusotto, I. & Ciuti, C. Quantum fluids of light. *Reviews of Modern Physics* **85**, 299 (2013).
2. Sidler, M., Back, P., Cotlet, O., Srivastava, A., Fink, T., Kroner, M., Demler, E. & Imamoglu, A. Fermi polaron-polaritons in charge-tunable atomically thin semiconductors. *Nature Physics* **13**, 255 (2017).
3. Chevy, F. Universal phase diagram of a strongly interacting Fermi gas with unbalanced spin populations. *Physical Review A* **74**, 063628 (2006).
4. Schirotzek, A., Wu, C.-H., Sommer, A. & Zwierlein, M. W. Observation of Fermi polarons in a tunable Fermi liquid of ultracold atoms. *Physical review letters* **102**, 230402 (2009).
5. Schmidt, R., Enss, T., Pietilä, V. & Demler, E. Fermi polarons in two dimensions. *Physical Review A* **85**, 021602 (2012).
6. Landau, L. & Pekar, S. Effective mass of a polaron. *Zh. Eksp. Teor. Fiz.* **18**, 419 (1948).
7. Jørgensen, N. B., Wacker, L., Skalmstang, K. T., Parish, M. M., Levinson, J., Christensen, R. S., Bruun, G. M. & Arlt, J. J. Observation of attractive and repulsive polarons in a Bose-Einstein condensate. *Physical review letters* **117**, 055302 (2016).
8. Hu, M.-G., Van de Graaff, M. J., Kedar, D., Corson, J. P., Cornell, E. A. & Jin, D. S. Bose polarons in the strongly interacting regime. *Physical review letters* **117**, 055301 (2016).
9. Rath, S. P. & Schmidt, R. Field-theoretical study of the Bose polaron. *Physical Review A* **88**, 053632 (2013).
10. Mahan, G. D. *Many-particle physics* (Springer Science & Business Media, 2013).
11. Baym, G. & Kadanoff, L. P. Conservation laws and correlation functions. *Physical Review* **124**, 287 (1961).
12. Tan, L. B., Cotlet, O., Bergschneider, A., Schmidt, R., Back, P., Shimazaki, Y., Kroner, M. & İmamou, A. Interacting polaron-polaritons. *Physical Review X* **10**, 021011 (2020).

Bibliography

13. Cotlet, O., Wild, D. S., Lukin, M. D. & Imamoglu, A. Rotons in optical excitation spectra of monolayer semiconductors. *Physical Review B* **101**, 205409 (2020).
14. Landau, L. Theory of the Superfluidity of Helium II. *Phys. Rev.* **60**, 356 (1941).
15. Cotlet, O., Pientka, F., Schmidt, R., Zarand, G., Demler, E. & Imamoglu, A. Transport of neutral optical excitations using electric fields. *Physical Review X* **9**, 041019 (2019).
16. Narozhny, B. & Levchenko, A. Coulomb drag. *Reviews of Modern Physics* **88**, 025003 (2016).
17. Geim, A. K. & Grigorieva, I. V. Van der Waals heterostructures. *Nature* **499**, 419 (2013).
18. Raja, A., Chaves, A., Yu, J., Arefe, G., Hill, H. M., Rigosi, A. F., Berkelbach, T. C., Nagler, P., Schüller, C., Korn, T., Nuckolls, C., Hone, J., Brus, L. E., Heinz, T. F., Reichman, D. R. & Chernikov, A. Coulomb engineering of the bandgap and excitons in two-dimensional materials. *Nat. Commun.* **8**, 15251 (2017).
19. Liu, G.-B., Shan, W.-Y., Yao, Y., Yao, W. & Xiao, D. Three-band tight-binding model for monolayers of group-VIB transition metal dichalcogenides. *Physical Review B* **88**, 085433 (2013).
20. Liu, G.-B., Xiao, D., Yao, Y., Xu, X. & Yao, W. Electronic structures and theoretical modelling of two-dimensional group-VIB transition metal dichalcogenides. *Chemical Society Reviews* **44**, 2643 (2015).
21. Kośmider, K., González, J. W. & Fernández-Rossier, J. Large spin splitting in the conduction band of transition metal dichalcogenide monolayers. *Physical Review B* **88**, 245436 (2013).
22. Berkelbach, T. C., Hybertsen, M. S. & Reichman, D. R. Theory of neutral and charged excitons in monolayer transition metal dichalcogenides. *Physical Review B* **88**, 045318 (2013).
23. Sidler, M. *Many-Body Effects in Optical Excitations of Transition Metal Dichalcogenides* PhD thesis (ETH Zurich, 2018).
24. Ciuti, C., Savona, V., Piermarocchi, C., Quattropani, A. & Schwendemann, P. Role of the exchange of carriers in elastic exciton-exciton scattering in quantum wells. *Physical Review B* **58**, 7926 (1998).
25. Byrnes, T., Recher, P. & Yamamoto, Y. Mott transitions of exciton polaritons and indirect excitons in a periodic potential. *Physical Review B* **81**, 205312 (2010).

26. Byrnes, T., Kolmakov, G. V., Kezerashvili, R. Y. & Yamamoto, Y. Effective interaction and condensation of dipolaritons in coupled quantum wells. *Physical Review B* **90**, 125314 (2014).
27. Carusotto, I., Volz, T. & Imamou, A. Feshbach blockade: Single-photon nonlinear optics using resonantly enhanced cavity polariton scattering from biexciton states. *EPL (Europhysics Letters)* **90**, 37001 (2010).
28. Takemura, N., Trebaol, S., Wouters, M., Portella-Oberli, M. T. & Deveaud, B. Polaritonic Feshbach resonance. *Nature Physics* (2014).
29. Koschorreck, M., Pertot, D., Vogt, E., Fröhlich, B., Feld, M. & Köhl, M. Attractive and repulsive Fermi polarons in two dimensions. *Nature* **485**, 619 (2012).
30. Kohstall, C., Zaccanti, M., Jag, M., Trenkwalder, A., Massignan, P., Bruun, G. M., Schreck, F. & Grimm, R. Metastability and coherence of repulsive polarons in a strongly interacting Fermi mixture. *Nature* **485**, 615 (2012).
31. Cetina, M., Jag, M., Lous, R. S., Fritzsche, I., Walraven, J. T., Grimm, R., Levinsen, J., Parish, M. M., Schmidt, R., Knap, M., *et al.* Ultrafast many-body interferometry of impurities coupled to a Fermi sea. *Science* **354**, 96 (2016).
32. Ross, J. S., Wu, S., Yu, H., Ghimire, N. J., Jones, A. M., Aivazian, G., Yan, J., Mandrus, D. G., Xiao, D., Yao, W. & Xu, X. Electrical control of neutral and charged excitons in a monolayer semiconductor. *Nat. Commun.* **4**, 1474 (2013).
33. Punk, M., Dumitrescu, P. & Zwerger, W. Polaron-to-molecule transition in a strongly imbalanced Fermi gas. *Physical Review A* **80**, 053605 (2009).
34. Parish, M. M. Polaron-molecule transitions in a two-dimensional Fermi gas. *Physical Review A* **83**, 051603 (2011).
35. Suris, R., Kochereshko, V., Astakhov, G., Yakovlev, D., Ossau, W., Nürnberger, J., Faschinger, W., Landwehr, G., Wojtowicz, T., Karczewski, G., *et al.* Excitons and Trions Modified by Interaction with a Two-Dimensional Electron Gas. *physica status solidi (b)* **227**, 343 (2001).
36. Levinsen, J., Marchetti, F. M., Keeling, J. & Parish, M. M. Spectroscopic probes of quantum many-body correlations in polariton microcavities. *arXiv preprint arXiv:1806.10835* (2018).

Bibliography

37. Bruus, H. & Flensberg, K. *Many-body quantum theory in condensed matter physics: an introduction* (Oxford university press, 2004).
38. Baym, G. & Kadanoff, L. P. Conservation Laws and Correlation Functions. *Phys. Rev.* **124**, 287 (2 1961).
39. Stefanucci, G. & van Leeuwen, R. *Nonequilibrium Many-Body Theory of Quantum Systems* (Cambridge University Press, 2013).
40. Mora, C. & Chevy, F. Normal phase of an imbalanced fermi gas. *Physical review letters* **104**, 230402 (2010).
41. Yu, Z., Zöllner, S. & Pethick, C. Comment on “normal phase of an imbalanced fermi gas”. *Physical review letters* **105**, 188901 (2010).
42. Camacho-Guardian, A. & Bruun, G. M. Landau effective interaction between quasiparticles in a Bose-Einstein condensate. *Physical Review X* **8**, 031042 (2018).
43. Hu, H., Mulkerin, B. C., Wang, J. & Liu, X.-J. Attractive Fermi polarons at nonzero temperatures with a finite impurity concentration. *Physical Review A* **98**, 013626 (2018).
44. Tajima, H. & Uchino, S. Many Fermi polarons at nonzero temperature. *New Journal of Physics* **20**, 073048 (2018).
45. Cotlet, O., Zeytinoğlu, S., Sigrist, M., Demler, E. & Imamoğlu, A. Superconductivity and other collective phenomena in a hybrid Bose-Fermi mixture formed by a polariton condensate and an electron system in two dimensions. *Physical Review B* **93**, 054510 (2016).
46. Laussy, F. P., Taylor, T., Shelykh, I. A. & Kavokin, A. V. Superconductivity with excitons and polaritons: review and extension. *Journal of Nanophotonics* **6**, 064502 (2012).
47. Henshaw, D. G. & Woods, A. D. B. Modes of Atomic Motions in Liquid Helium by Inelastic Scattering of Neutrons. *Phys. Rev.* **121**, 1266 (1961).
48. Mottl, R., Brennecke, F., Baumann, K., Landig, R., Donner, T. & Esslinger, T. Roton-Type Mode Softening in a Quantum Gas with Cavity-Mediated Long-Range Interactions. *Science* **336**, 1570 (2012).
49. Chomaz, L., van Bijnen, R. M. W., Petter, D., Faraoni, G., Baier, S., Becher, J. H., Mark, M. J., Wächtler, F., Santos, L. & Ferlaino, F. Observation of roton mode population in a dipolar quantum gas. *Nat. Phys.* **14**, 442 (2018).

50. Khamehchi, M. A., Zhang, Y., Hamner, C., Busch, T. & Engels, P. Measurement of collective excitations in a spin-orbit-coupled Bose-Einstein condensate. *Phys. Rev. A* **90**, 063624 (2014).
51. Ji, S.-C., Zhang, L., Xu, X.-T., Wu, Z., Deng, Y., Chen, S. & Pan, J.-W. Softening of Roton and Phonon Modes in a Bose-Einstein Condensate with Spin-Orbit Coupling. *Phys. Rev. Lett.* **114**, 105301 (2015).
52. Ha, L.-C., Clark, L. W., Parker, C. V., Anderson, B. M. & Chin, C. Roton-Maxon Excitation Spectrum of Bose Condensates in a Shaken Optical Lattice. *Phys. Rev. Lett.* **114**, 055301 (2015).
53. Massignan, P., Zaccanti, M. & Bruun, G. M. Polarons, dressed molecules and itinerant ferromagnetism in ultracold Fermi gases. *Reports on Progress in Physics* **77**, 034401 (2014).
54. Parish, M. M. & Levinsen, J. Highly polarized Fermi gases in two dimensions. *Phys. Rev. A* **87**, 033616 (2013).
55. Yamashita, K., Asano, K. & Ohashi, T. Quantum Condensation in Electron–Hole Bilayers with Density Imbalance. *J. Phys. Soc. Jpn.* **79**, 033001 (2010).
56. Parish, M. M., Marchetti, F. M. & Littlewood, P. B. Supersolidity in electron-hole bilayers with a large density imbalance. *EPL* **95**, 27007 (2011).
57. Fedorov, A. K., Kurbakov, I. L. & Lozovik, Y. E. Roton-maxon spectrum and instability for weakly interacting dipolar excitons in a semiconductor layer. *Phys. Rev. B* **90**, 165430 (2014).
58. Back, P., Sidler, M., Cotlet, O., Srivastava, A., Takemura, N., Kroner, M. & Imamou, A. Giant paramagnetism-induced valley polarization of electrons in charge-tunable monolayer mose 2. *Physical review letters* **118**, 237404 (2017).
59. Wang, Z., Mak, K. F. & Shan, J. Strongly Interaction-Enhanced Valley Magnetic Response in Monolayer WSe₂. *Phys. Rev. Lett.* **120**, 066402 (2018).
60. Zhong, D., Seyler, K. L., Linpeng, X., Cheng, R., Sivadas, N., Huang, B., Schmidgall, E., Taniguchi, T., Watanabe, K., McGuire, M. A., Yao, W., Xiao, D., Fu, K.-M. C. & Xu, X. Van der Waals engineering of ferromagnetic semiconductor heterostructures for spin and valleytronics. *Sci. Adv.* **3**, e1603113 (2017).

Bibliography

61. Kormányos, A., Burkard, G., Gmitra, M., Fabian, J., Zólyomi, V., Drummond, N. D. & Fal'ko, V. K. · P Theory for Two-Dimensional Transition Metal Dichalcogenide Semiconductors. *2D Mater.* **2**, 022001 (2015).
62. Feynman, R. P. & Cohen, M. Energy Spectrum of the Excitations in Liquid Helium. *Phys. Rev.* **102**, 1189 (1956).
63. Parish, M. M. Polaron-molecule transitions in a two-dimensional Fermi gas. *Phys. Rev. A* **83**, 051603 (2011).
64. Gao, S., Liang, Y., Spataru, C. D. & Yang, L. Dynamical Excitonic Effects in Doped Two-Dimensional Semiconductors. *Nano Lett.* **16**, 5568 (2016).
65. Van Tuan, D., Scharf, B., Žutić, I. & Dery, H. Marrying Excitons and Plasmons in Monolayer Transition-Metal Dichalcogenides. *Phys. Rev. X* **7**, 041040 (2017).
66. Sidler, M., Back, P., Cotlet, O., Srivastava, A., Fink, T., Kroner, M., Demler, E. & Imamoglu, A. Fermi polaron-polaritons in charge-tunable atomically thin semiconductors. *Nat. Phys.* **13**, 255 (2016).
67. Yao, K., Yan, A., Kahn, S., Suslu, A., Liang, Y., Barnard, E. S., Tongay, S., Zettl, A., Borys, N. J. & Schuck, P. J. Optically Discriminating Carrier-Induced Quasiparticle Band Gap and Exciton Energy Renormalization in Monolayer MoS₂. *Phys. Rev. Lett.* **119**, 087401 (2017).
68. Efimkin, D. K. & MacDonald, A. H. Many-body theory of trion absorption features in two-dimensional semiconductors. *Phys. Rev. B* **95**, 035417 (2017).
69. See Supplemental Material, which includes references [22, 61, 141], for computational details and for explicit expressions of the decay rates $\Gamma_{1,2,3,4}$.
70. Robert, C., Lagarde, D., Cadiz, F., Wang, G., Lassagne, B., Amand, T., Balocchi, A., Renucci, P., Tongay, S., Urbaszek, B. & Marie, X. Exciton radiative lifetime in transition metal dichalcogenide monolayers. *Phys. Rev. B* **93**, 205423 (2016).
71. Wang, Z., Zhao, L., Mak, K. F. & Shan, J. Probing the spin-polarized electronic band structure in monolayer transition metal dichalcogenides by optical spectroscopy. *Nano letters* **17**, 740 (2017).
72. Dunn, R. C. Near-Field Scanning Optical Microscopy. *Chem. Rev.* **99**, 2891 (1999).

73. Schiefele, J., Pedrós, J., Sols, F., Calle, F. & Guinea, F. Coupling Light into Graphene Plasmons through Surface Acoustic Waves. *Phys. Rev. Lett.* **111**, 237405 (2013).
74. Henkel, N., Nath, R. & Pohl, T. Three-Dimensional Roton Excitations and Supersolid Formation in Rydberg-Excited Bose-Einstein Condensates. *Phys. Rev. Lett.* **104**, 195302 (2010).
75. Sedrakyan, T. A., Glazman, L. I. & Kamenev, A. Spontaneous Formation of a Nonuniform Chiral Spin Liquid in a Moat-Band Lattice. *Phys. Rev. Lett.* **114**, 037203 (2015).
76. Ozawa, T., Price, H. M., Amo, A., Goldman, N., Hafezi, M., Lu, L., Rechtsman, M. C., Schuster, D., Simon, J., Zilberberg, O., *et al.* Topological photonics. *Reviews of Modern Physics* **91**, 015006 (2019).
77. St-Jean, P., Goblot, V., Galopin, E., Lemaître, A., Ozawa, T., Le Gratiet, L., Sagnes, I., Bloch, J. & Amo, A. Lasing in topological edge states of a one-dimensional lattice. *Nature Photonics* **11**, 651 (2017).
78. Klembt, S., Harder, T., Egorov, O., Winkler, K., Ge, R., Bandres, M., Emmerling, M., Worschech, L., Liew, T., Segev, M., *et al.* Exciton-polariton topological insulator. *Nature* **562**, 552 (2018).
79. Zheng, L. & MacDonald, A. H. Coulomb drag between disordered two-dimensional electron-gas layers. *Phys. Rev. B* **48**, 8203 (11 1993).
80. Kamenev, A. & Oreg, Y. Coulomb drag in normal metals and superconductors: Diagrammatic approach. *Phys. Rev. B* **52**, 7516 (10 1995).
81. Flensberg, K., Hu, B. Y.-K., Jauho, A.-P. & Kinaret, J. M. Linear-response theory of Coulomb drag in coupled electron systems. *Phys. Rev. B* **52**, 14761 (20 1995).
82. Guidini, A., Bertaina, G., Galli, D. E. & Pieri, P. Condensed phase of Bose-Fermi mixtures with a pairing interaction. *Physical Review A* **91**, 023603 (2015).
83. Nandi, D., Finck, A., Eisenstein, J., Pfeiffer, L. & West, K. Exciton condensation and perfect Coulomb drag. *Nature* **488**, 481 (2012).
84. Sie, E. J., Lui, C. H., Lee, Y.-H., Fu, L., Kong, J. & Gedik, N. Large, valley-exclusive Bloch-Siegert shift in monolayer WS₂. *Science* **355**, 1066 (2017).
85. Gantsevich, S., Gurevich, V. & Katilyus, R. Fluctuations in Semiconductors in a Strong Electric Field and the Scattering of Light by "Hot" Electrons. *Soviet Physics JETP* **30** (1970).

Bibliography

86. Matulionis, A., Ramonas, M., Katilius, R. & Gantsevich, S. *Theory of fluctuations in non-equilibrium electron?hot-phonon system in Noise and Fluctuations (ICNF), 2011 21st International Conference on* (2011), 196.
87. Efimkin, D. & MacDonald, A. H. Many-body theory of trion absorption in a strong magnetic field. *arXiv:1707.05845* (2017).
88. Ravets, S., Knüppel, P., Faelt, S., Cotlet, O., Kroner, M., Wegscheider, W. & Imamoglu, A. Polaron polaritons in the integer and fractional quantum Hall regimes. *Physical review letters* **120**, 057401 (2018).
89. Vlietinck, J., Ryckebusch, J. & Van Houcke, K. Diagrammatic Monte Carlo study of the Fermi polaron in two dimensions. *Phys. Rev. B* **89**, 085119 (8 2014).
90. Kroiss, P. & Pollet, L. Diagrammatic Monte Carlo study of quasi-two-dimensional Fermi polarons. *Phys. Rev. B* **90**, 104510 (10 2014).
91. Schmidt, R. & Enss, T. Excitation spectra and rf response near the polaron-to-molecule transition from the functional renormalization group. *83*, 063620 (2011).
92. Pimenov, D., von Delft, J., Glazman, L. & Goldstein, M. Fermi-edge exciton-polaritons in doped semiconductor microcavities with finite hole mass. *Physical Review B* **96**, 155310 (2017).
93. Liu, X., Galfsky, T., Sun, Z., Xia, F., Lin, E.-c., Lee, Y.-H., Kéna-Cohen, S. & Menon, V. M. Strong light–matter coupling in two-dimensional atomic crystals. *Nature Photonics* **9**, 30 (2015).
94. Dufferwiel, S., Lyons, T., Solnyshkov, D., Trichet, A., Withers, F., Schwarz, S., Malpuech, G., Smith, J., Novoselov, K., Skolnick, M., *et al.* Valley-addressable polaritons in atomically thin semiconductors. *Nature Photonics* **11**, 497 (2017).
95. Hu, F., Luan, Y., Scott, M., Yan, J., Mandrus, D., Xu, X. & Fei, Z. Imaging exciton–polariton transport in MoSe₂ waveguides. *Nature Photonics* **11**, 356 (2017).
96. Whittaker, D., Kinsler, P., Fisher, T., Skolnick, M., Armitage, A., Afshar, A., Sturge, M. & Roberts, J. Motional narrowing in semiconductor microcavities. *Physical review letters* **77**, 4792 (1996).
97. Savona, V., Piermarocchi, C., Quattropani, A., Tassone, F. & Schwendimann, P. Microscopic theory of motional narrowing of microcavity polaritons in a disordered potential. *Physical Review Letters* **78**, 4470 (1997).

98. Larentis, S., Movva, H. C., Fallahazad, B., Kim, K., Behroozi, A., Taniguchi, T., Watanabe, K., Banerjee, S. K. & Tutuc, E. Large effective mass and interaction-enhanced Zeeman splitting of K-valley electrons in MoSe₂. *Physical Review B* **97**, 201407 (2018).
99. Pisoni, R., Kormányos, A., Brooks, M., Lei, Z., Back, P., Eich, M., Overweg, H., Lee, Y., Rickhaus, P., Watanabe, K., *et al.* Interactions and magnetotransport through spin-valley coupled Landau levels in monolayer MoS₂. *arXiv preprint arXiv:1806.06402* (2018).
100. Lim, H.-T., Togan, E., Kroner, M., Miguel-Sánchez, J. & Imamou, A. Electrically tunable artificial gauge potential for polaritons. *Nature communications* **8**, 14540 (2017).
101. Nelsen, B., Liu, G., Steger, M., Snoke, D. W., Balili, R., West, K. & Pfeiffer, L. Dissipationless flow and sharp threshold of a polariton condensate with long lifetime. *Physical Review X* **3**, 041015 (2013).
102. Alexandrov, A. S. & Devreese, J. T. *Advances in Polaron Physics* (Springer, 2010).
103. Laussy, F. P., Kavokin, A. V. & Shelykh, I. A. Exciton-polariton mediated superconductivity. *Physical review letters* **104**, 106402 (2010).
104. Cherotchenko, E., Espinosa-Ortega, T., Nalitov, A., Shelykh, I. & Kavokin, A. Superconductivity in Semiconductor Structures: the Excitonic Mechanism. *arXiv preprint arXiv:1410.3532* (2014).
105. Ginzburg, V. On surface superconductivity. *Physics Letters* **13**, 101 (1964).
106. Shelykh, I. A., Taylor, T. & Kavokin, A. V. Rotons in a hybrid Bose-Fermi system. *Physical review letters* **105**, 140402 (2010).
107. Matuszewski, M., Taylor, T. & Kavokin, A. V. Exciton supersolidity in hybrid Bose-Fermi systems. *Physical review letters* **108**, 060401 (2012).
108. Cristofolini, P., Christmann, G., Tsintzos, S. I., Deligeorgis, G., Konstantinidis, G., Hatzopoulos, Z., Savvidis, P. G. & Baumberg, J. J. Coupling quantum tunneling with cavity photons. *Science* **336**, 704 (2012).
109. Leavitt, R. & Little, J. Excitonic effects in the optical spectra of superlattices in an electric field. *Physical Review B* **42**, 11784 (1990).
110. Mahan, G. D. *Many-particle physics* (Springer Science & Business Media, 2000).

Bibliography

111. Scalapino, D. J. *The electron-phonon interaction and strong-coupling superconductors* (Marcel Dekker, New York, 1969).
112. Zeytinou, S., İmamou, A. & Huber, S. Engineering matter interactions using squeezed vacuum. *Physical Review X* **7**, 021041 (2017).
113. Frohlich, H. Interaction of electrons with lattice vibrations. *Proceedings of the Royal Society of London. Series A. Mathematical and Physical Sciences* **215**, 291 (1952).
114. McMillan, W. Transition temperature of strong-coupled superconductors. *Physical Review* **167**, 331 (1968).
115. Allen, P. B. & Dynes, R. Transition temperature of strong-coupled superconductors reanalyzed. *Physical Review B* **12**, 905 (1975).
116. Abbaspour, H., Sallen, G., Trebaol, S., Morier-Genoud, F., Portella-Oberli, M. & Deveaud, B. The Effect of a Noisy Driving Field on a Bistable Polariton System. *arXiv preprint arXiv:1505.00932* (2015).
117. Weber, F., Rosenkranz, S., Castellan, J.-P., Osborn, R., Karapetrov, G., Hott, R., Heid, R., Bohnen, K.-P. & Alatas, A. Electron-phonon coupling and the soft phonon mode in TiSe₂. *Physical review letters* **107**, 266401 (2011).
118. Calandra, M. & Mauri, F. Charge-density wave and superconducting dome in TiSe₂ from electron-phonon interaction. *Physical review letters* **106**, 196406 (2011).
119. Joe, Y. I., Chen, X., Ghaemi, P., Finkelstein, K., de La Peña, G., Gan, Y., Lee, J., Yuan, S., Geck, J., MacDougall, G., et al. Emergence of charge density wave domain walls above the superconducting dome in 1T-TiSe₂. *Nature Physics* **10**, 421 (2014).
120. Mathur, N., Grosche, F., Julian, S., Walker, I., Freye, D., Haselwimmer, R. & Lonzarich, G. Magnetically mediated superconductivity in heavy fermion compounds. *Nature* **394**, 39 (1998).
121. Monthoux, P. & Lonzarich, G. p-Wave and d-wave superconductivity in quasi-two-dimensional metals. *Physical Review B* **59**, 14598 (1999).
122. Monthoux, P. & Lonzarich, G. Magnetically mediated superconductivity in quasi-two and three dimensions. *Physical Review B* **63**, 054529 (2001).
123. Monthoux, P. & Lonzarich, G. Magnetic interactions in a single-band model for the cuprates and ruthenates. *Physical Review B* **71**, 054504 (2005).

124. Canfield, P. C. & Bud'Ko, S. L. FeAs-based superconductivity: a case study of the effects of transition metal doping on BaFe₂As₂. *arXiv preprint arXiv:1002.0858* (2010).
125. Tranquada, J., Sternlieb, B., Axe, J., Nakamura, Y. & Uchida, S. Evidence for stripe correlations of spins and holes in copper oxide superconductors. *Nature* **375**, 561 (1995).
126. Rochat, G., Ciuti, C., Savona, V., Piermarocchi, C., Quattropani, A. & Schwendimann, P. Excitonic Bloch equations for a two-dimensional system of interacting excitons. *Physical Review B* **61**, 13856 (2000).
127. Pitaevskii, L. & Stringari, S. *Bose-Einstein Condensation* (Clarendon Press, 2003).
128. Migdal, A. Interaction between electrons and lattice vibrations in a normal metal. *Sov. Phys. JETP* **7**, 996 (1958).
129. Stern, F. Polarizability of a two-dimensional electron gas. *Physical Review Letters* **18**, 546 (1967).
130. Beliaev, S. Application of the methods of quantum field theory to a system of bosons. *SOVIET PHYSICS JETP-USSR* **7**, 289 (1958).
131. Shi, H. & Griffin, A. Finite-temperature excitations in a dilute Bose-condensed gas. *Physics Reports* **304**, 1 (1998).
132. Allen, P. B. Neutron spectroscopy of superconductors. *Physical Review B* **6**, 2577 (1972).
133. Allen, P. B. Effect of soft phonons on superconductivity: A re-evaluation and a positive case for Nb₃Sn. *Solid State Communications* **14**, 937 (1974).
134. Grimvall, G. *The electron-phonon interaction in metals* **9** (North-Holland Amsterdam, 1981).
135. Cohen, M. L. Superconductivity in modified semiconductors and the path to higher transition temperatures. *Superconductor Science and Technology* **28**, 43001 (2015).
136. Bardeen, J., Cooper, L. N. & Schrieffer, J. R. Theory of superconductivity. *Physical Review* **108**, 1175 (1957).
137. Allen, P. & Mitrović, B. *Solid State Physics*, Vol. 37. Academic, New York, 1 (1982).
138. Glazek, S. D. & Wilson, K. G. Perturbative renormalization group for Hamiltonians. *Physical Review-Section D-Particles and Fields* **49**, 4214 (1994).

Bibliography

139. Wegner, F. Flow-equations for Hamiltonians. *Annalen der physik* **506**, 77 (1994).
140. Mielke, A. Calculating critical temperatures of superconductivity from a renormalized Hamiltonian. *EPL (Europhysics Letters)* **40**, 195 (1997).
141. Haug, H. & Koch, S. W. *Quantum Theory of the Optical and Electronic Properties of Semiconductors* Fifth (World Scientific, Singapore, 2009).

Ovidiu Cotlet

Riedthofstrasse 7, 8105 Regensdorf,
14.06.1990, Romanian, B Permit
+41 78 629 29 55
ocotlet@phys.ethz.ch



Education

09.2014 - Present	ETH Zurich, Switzerland	PhD in Physics
	– Bypassed Master's degree based on 5 Qualifying Exams (GPA: 5.5/6)	
	– Relevant coursework: Mathematical Finance, Corporate Finance, Introduction to Management, Leadership and Power, Machine Learning, Neural Networks	
09.2009 - 06.2013	Princeton University, USA	B.A. in Physics, <i>cum laude</i> , (GPA: 3.6/4)
	– Certificate of Proficiency in Engineering Physics	
09.2005 - 06.2009	Filadelfia Theoretical High school, Romania	Math & Computer Sc. Diploma (GPA: 10/10)
	– Valedictorian; captain of varsity soccer and ping-pong teams	

Professional Experience

09.2014 - Present	ETH Zurich, Switzerland	
	Doctoral researcher in the Quantum Photonics Group	
	– Initiated and led collaborations with approximately 30 researchers from Harvard and 7 other major institutions in the US, Switzerland, Germany, Italy and Japan	
	– Published 8 articles in high-impact journals; 3 more in writing process	
	– Attended workshops in the <i>Aspen Center for Physics</i> and <i>Kavli Institute for Theoretical Physics</i>	
	– Supervised 2 master students during their thesis work	
	– Coordinated and taught several classes of up to 100 students	
01.2014-04.2014	University of St. Andrews, UK	
	Research assistant	
	– Collaborated with researchers in the field of quantum optics and published results	
09.2009-06.2013	Princeton University, USA	
	Research assistant	
	– Published senior thesis work on the theory of a novel microwave laser	
	– Summer research assistant in the fields of biophysics, cosmology and quantum optics	

Extracurricular Relevant Experience

09.2018-12.2018	Graduate Consulting Club of ETH Zurich	
	Associate in a Consulting Team	
	– As a member of a team, executed a pro bono consulting project for a student association at ETH Zurich on how to improve the well-being of PhD students and postdocs	
	– The team's full results became the basis of several research proposals and initiatives at ETH	

Skills & Interests

Languages:	English (fluent), German (intermediate), Romanian (native)
Technical:	Python, C/C++, Mathematica, Microsoft Office
Interests:	Football, Poker, Hiking, History podcasts, Russian Literature

Awards & Honors

2013	Allen G. Shenstone Prize in Physics , Princeton University
2012	Kusaka Memorial Prize in Physics , Princeton University
2009	International Physics Olympiad , silver medal
2008	International Olympiad in Informatics , member of the enlarged Romanian team, formed of the <i>top 20 high-school students</i> in the country

PUBLICATIONS

Articles in peer-reviewed journals:

1. Sidler, M., Back, P., Cotlet, O., Srivastava, A., Fink, T., Kroner, M., Demler, E. & Imamoglu, A. Fermi polaron-polaritons in charge-tunable atomically thin semiconductors. *Nature Physics* **13**, 255 (2017).
2. Cotlet, O., Zeytinoğlu, S., Sigrist, M., Demler, E. & Imamoglu, A. Superconductivity and other collective phenomena in a hybrid Bose-Fermi mixture formed by a polariton condensate and an electron system in two dimensions. *Physical Review B* **93**, 054510 (2016).
3. Kulkarni, M., Cotlet, O. & Türeci, H. E. Cavity-coupled double-quantum dot at finite bias: Analogy with lasers and beyond. *Physical Review B* **90**, 125402 (2014).
4. Back, P., Sidler, M., Cotlet, O., Srivastava, A., Takemura, N., Kroner, M. & Imamou, A. Giant paramagnetism-induced valley polarization of electrons in charge-tunable monolayer mose 2. *Physical review letters* **118**, 237404 (2017).
5. Ravets, S., Knüppel, P., Faelt, S., Cotlet, O., Kroner, M., Wegscheider, W. & Imamoglu, A. Polaron polaritons in the integer and fractional quantum Hall regimes. *Physical review letters* **120**, 057401 (2018).
6. Cotlet, O., Pientka, F., Schmidt, R., Zarand, G., Demler, E. & Imamoglu, A. Transport of neutral optical excitations using electric fields. *Physical Review X* **9**, 041019 (2019).
7. Cotlet, O., Wild, D. S., Lukin, M. D. & Imamoglu, A. Rotons in optical excitation spectra of monolayer semiconductors. *Physical Review B* **101**, 205409 (2020).
8. Tan, L. B., Cotlet, O., Bergschneider, A., Schmidt, R., Back, P., Shimazaki, Y., Kroner, M. & Imamou, A. Interacting polaron-polaritons. *Physical Review X* **10**, 021011 (2020).